Wayne State University

January 2020

Computational Analysis Of Oxidative Stress In Endothelial Dysfunction: Insights On The Role Of Tetrahydrobiopterin, Ascorbate And Glutathione

Sheetal Kedar Panday
Wayne State University

COMPUTATIONAL ANALYSIS OF OXIDATIVE STRESS IN ENDOTHELIAL DYSFUNCTION: INSIGHTS ON THE ROLE OF TETRAHYDROBIOPTERIN, ASCORBATE AND GLUTATHIONE

by

SHEETAL KEDAR PANDAY

DISSERTATION

Submitted to the Graduate School

of Wayne State University,

Detroit, Michigan

in partial fulfillment of the requirements

for the degree of

DOCTOR OF PHILOSOPHY

2020

MAJOR: BIOMEDICAL ENGINEERING

Approved by:

_____

Advisor   Date

_____

_____

_____

DEDICATION

I dedicate this dissertation to my parents,
my husband, Kedar and my loving son, Shlok.
Your unyielding love, support and encouragement have constantly inspired me to pursue and
complete this research.

ACKNOWLEDGMENTS

I would like to thank my advisor, Prof. Mahendra Kavdia, for his guidance, for his support, for his eagerness, and mostly for his patience. I would like to thank all my committee members for providing their expertise and encouragement. I would like to thank the members of the Kavdia lab, past and present, for their camaraderie. I would like to acknowledge the Department of Biomedical Engineering and the Graduate School of the Wayne State University for the funding of this degree.

Needless to say, none of this would have been possible without the love and support from my family. My parents, Aai and Baba who have always been a source of my confidence, for continually believing in me and for keeping me motivated. My husband, Kedar; my loving son, Shlok; my brother, Ketan and my in-laws for their unconditional love, support and keeping me sane during this whole process. I am very fortunate to have amazing friends whose presence made this journey enjoyable.

TABLE OF CONTENTS

LIST OF TABLES

LIST OF FIGURES

LIST OF ABBREVIATIONS

ASC: Ascorbate

BH_4:   (6R-)5,6,7,8-tetrahydrobiopterin

CVD: Cardiovascular diseases

eNOS: Endothelial nitric oxide synthase

G6PD: Glucose 6 phosphate dehydrogenase

GPX: Glutathione peroxidase

GSH: Glutathione

GSNO: S-nitrosoglutathion

GSSG: Glutathione disulfide

GTPCH: Guanosine triphosphate cyclohydrolase 1

H_2O_2:   Hydrogen peroxide

N_2O_3:   Dinitrogen trioxide

NO: Nitric oxide

NOX: Nicotinamide adenine dinucleotide phosphate (NADPH) oxidases

$O_2^{\bullet-}$:   Superoxide

ODE: Ordinary differential equations

$ONOO^-$:   Peroxynitrite

Prx: Peroxiredoxin

Q_{BH4}:   Rate of BH_4 synthesis

$Q_{supcell}$:   Rate of $O_2^{\bullet-}$ production from non-eNOS based sources

RNS: Reactive nitrogen species

ROS: Reactive oxygen species

SOD: Superoxide dismutase

TBP: Total biopterin levels

XO: Xanthine oxidases

CHAPTER I

INTRODUCTION AND MOTIVATION

1.1. Introduction

Cardiovascular diseases (CVD) are the leading cause of morbidity and mortality in the world [1]. Oxidative stress and endothelial dysfunction are reported as hallmarks for onset and progression of CVD such as diabetes, atherosclerosis, hypertension, etc [2-5]. Endothelial dysfunction is integral to the pathogenesis of CVDs and is mainly characterized by limited bioavailability of nitric oxide (NO) [6]. Increase in the levels of reactive oxygen (ROS) and nitrogen species (RNS) occur in oxidative stress [7]. ROS and RNS directly inactivate NO, act as signaling molecules and promote protein dysfunction. Such events contribute to the initiation and progression of endothelial dysfunction [8]. Further, in oxidative stress, the capacity of antioxidant defense systems is hampered [9]. The therapeutic potential of the antioxidants in circumventing the oxidative stress to improve endothelial dysfunction have reported mixed results. The relative importance of the underlying mechanisms of oxidative stress mediated endothelial dysfunction remain to be determined. The primary focus of this dissertation is to quantitatively understand the interactions of ROS/RNS with the antioxidants and provide mechanistic basis for endothelial dysfunction.

1.2. Motivation

ROS are the intermediates of molecular oxygen (O_2) that are formed during cellular physiological processes [10]. At physiological concentrations, ROS act as important secondary messengers that transduce intracellular signals involved in various biological process [11, 12]. The levels of ROS are kept in check by the antioxidant defense system of the cell such as enzymatic

antioxidants including superoxide dismutase (SOD), glutathione peroxidase (GPX), catalase, peroxiredoxin (Prx) and thioredoxin etc. or the nonenzymatic antioxidants including ascorbate (ASC) and glutathione (GSH) [13, 14]. When an aberrant production of ROS exceeds the buffering capacity of these antioxidants, oxidative stress occurs [13]. Figure 1 below provides the general impression of oxidative stress.
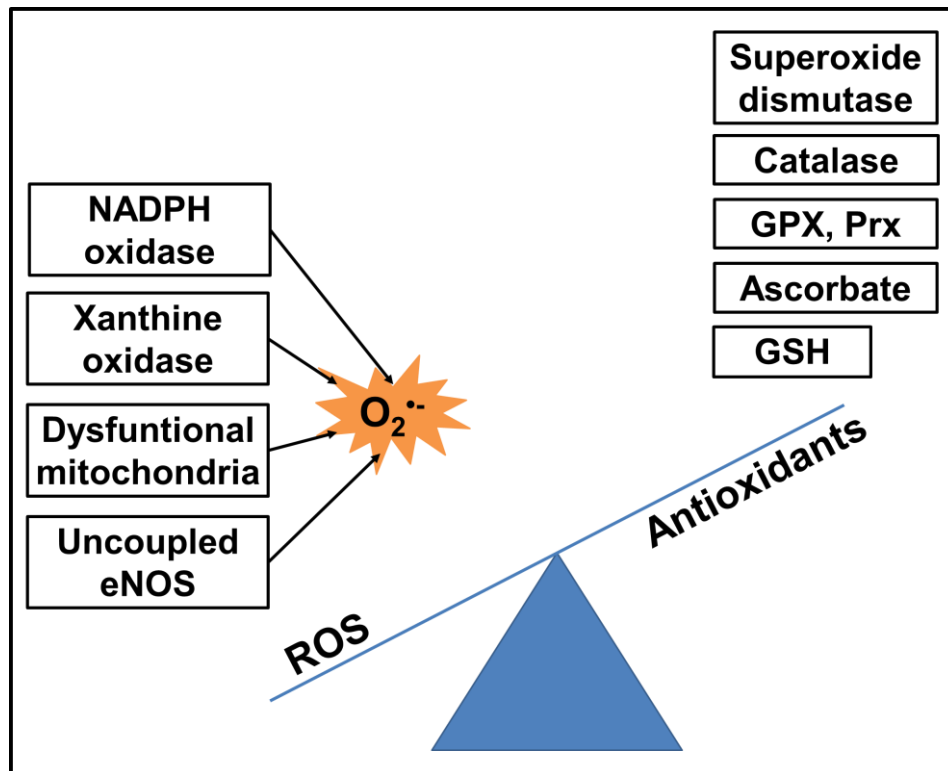
Figure 1: Oxidative stress overview

Endothelium is a single layer of cells that lines the lumen of blood vessels and plays an important physiological role in vascular homeostasis [15]. The endothelial cells are also known to mediate several other functions, including modulation of vascular tone, maintenance of blood fluidity, regulation of inflammation and immune response, and neovascularization [15]. In endothelial cells a major vasodilator, NO, is synthesized by a constitutive enzyme, endothelial

nitric oxide synthase (eNOS). eNOS requires an essential cofactor (6R-)5,6,7,8-tetrahydrobiopterin (BH$_4$) for producing NO [16].

The increase in oxidative stress leads to a cascade of events that hampers the endothelial cell functionality. These include decreased NO bioavailability [17]; increased $O_2^{\bullet-}$ production from ROS producing enzymes [8]; reduction in the activity of antioxidant enzyme including ASC and GSH enzyme system [18]; oxidation of BH$_4$ [19]; reduction in expression and activity of eNOS [20]; increased expression and enzymatic activity of arginase that break down eNOS substrate L-Arginine; decrease in the guanosine triphosphate cyclohydrolase 1 (GTPCH) activity which leads to reduction in *de novo* synthesis of BH$_4$; production of ONOO$^-$ which leads to increased oxidation of BH$_4$, decrease in SOD activity, tyrosine nitration and apoptosis [7]. Although studies have recognized the association of endothelial dysfunction with oxidative stress, the underlying mechanisms are still unclear.

The therapeutic potential of the antioxidants in circumventing the oxidative stress and/or improve endothelial dysfunction has been studied largely. However, years of clinical research on oxidative stress in animal models of cardiovascular disease and dysfunction reported inconsistent results on the effective of antioxidants therapies in treating CVDs [7]. Putative reasons for these inconsistencies could be due to; (i) relatively weak nature of the antioxidants used in clinical trials, (ii) an incomplete understanding of the complex molecular mechanisms whereby ROS cause pathological changes, (iii) the difficulty in extrapolating findings from experimental models to clinical scenarios, and (iv) the methodological challenges relating to accurate measurement of ROS in the cardiovascular system [21]. Computational modeling, which involves the use of mathematical models, can be used as an effective method to identify the underlying principles of operation in biological systems [22]. The work presented in this dissertation uses computational

modeling-based approaches to circumvent the limitation of using experimental methods such as simultaneous measurement of reactive species involved in oxidative stress. In this context, computational modeling is used as a valuable tool to provide insights on the dynamics of the complex interactions amongst reactive species in oxidative stress.

This work presented in this dissertation addresses the lack of systems level understanding of oxidative stress mediated endothelial dysfunction and helps establish the mechanistic basis of the role of cofactors and antioxidants in endothelial dysfunction. The improved quantitative understanding of the role of oxidative stress in the progression of CVDs may allow for effective treatment as well as earlier intervention in treating vascular diseases.

1.3. Research objectives and specific aims

There is a substantial evidence for the presence of complex interactions of ROS/RNS in oxidative stress mediated endothelial dysfunction. However, we lack quantitative understanding of these interactions due to technical limitations in experimental work. Thus, the overall *objective* of this dissertation is to provide quantitative analyses of oxidative stress in endothelial cells and deepen the understanding of the mechanistic basis of endothelial dysfunction. We used computational modeling approaches to tackle the experimental complexities in analyzing reactive species by simulating the concurrent dynamics of many variables. The *central hypothesis* of this dissertation is oxidative stress can lead to uncoupling of eNOS and presence of BH_4 and antioxidants can improve NO bioavailability in endothelial cells. To test this hypothesis, we developed following specific aims.

1.3.1. AIM 1: Develop a detailed mathematical model for biopterin dependent eNOS biochemical pathway

Oxidative stress levels can dynamically change the biopterin ratio (ratio of BH_4 to the total biopterin levels, (TBP)) by oxidative depletion of BH_4 and causes uncoupling of eNOS. The uncoupling of eNOS shifts the eNOS production of NO to $O_2^{\bullet-}$ [23, 24]. The extent of eNOS uncoupling is predominantly determined by the availability of BH_4, an essential cofactor of eNOS that plays an important role in maintaining normal endothelial function [25-27]. The enhancement of BH_4 bioavailability holds therapeutic potential for improvement of endothelial dysfunction [16, 28, 29], whereas other studies have shown limited [30] or no improvement [31, 32] in endothelial function. Our understanding of the complex interactions of eNOS uncoupling, oxidative stress and BH_4 availability are not complete and a quantitative understanding of these interactions is required. To study this, we have developed a computational model for eNOS uncoupling that considers the temporal changes in biopterin ratio in the oxidative stress conditions. Using the model, we have studied the effects of cellular oxidative stress and BH_4 synthesis on the eNOS NO production and biopterin ratio.

1.3.2. AIM 2: Develop mathematical model to analyze the role of ascorbate in oxidative stress mediated endothelial dysfunction

ASC, the reduced form of vitamin C, is an essential intracellular and circulatory antioxidant which has been suggested to play an important role in maintaining endothelial function. ASC deficiency has been associated with an increased risk of CVD [33]. The synthesis and bioavailability of NO are sensitive to cellular antioxidant status and redox balance. ASC plays an important role in maintaining this redox balance. Exogenous treatment with ASC is considered to be of therapeutic potential [34, 35], however the potential mechanism of ASC in the mitigation of

endothelial dysfunction is not clear [36]. In this study, we extended our computational model of eNOS uncoupling developed in AIM 1 and studied the interactions of oxidative stress and biopterin ratio in the presence of ASC and GSH. This model provides important quantitative insights on the protective role of ASC in endothelial dysfunction.

1.3.3. AIM 3: Develop a mathematical model to analyze the interactions of ROS/RNS with glutathione enzyme system

GSH and GPX enzyme system is essential for normal intracellular homeostasis and gets disturbed under several pathophysiological conditions including endothelial dysfunction [37, 38]. The GSH/GPX system plays an important role in eliminating ROS/RNS. Studies have provided important information regarding the interactions of ROS/RNS with the GSH/GPX in biological systems. However, it is not clear how this cross talk affects these reactive species and GSH/GPX enzyme system, under physiologic and oxidative/nitrosative stress conditions [39, 40]. In this study, we developed a detailed endothelial cell kinetic model to understand the relationship amongst the key enzyme systems including GSH, GPX, Prx and reactive species, such as H_2O_2, $ONOO^-$, and dinitrogen trioxide (N_2O_3). The analysis presented in this study would help us interpret the complex interactions amongst reactive species and enzyme systems under physiologic and oxidative/nitrosative stress conditions.

CHAPTER II

LITERATURE REVIEW

CVDs are regarded as the number one cause of deaths globally according to the World Health Organization (WHO) fact sheet for September 2016 [1]. An estimated 17.5 million people died from CVDs in 2012, which represents 31% of all global deaths [1]. According to the American Heart Association and American Stroke Association, the cost estimates for all aspects of CVD totaled $318 billion in 2015 and spending for all cardiovascular conditions is projected to continue to rise with just the indirect cost projected to $368 billion by 2035 [41]. Although the mortality rate of the disease has been brought down tremendously, we still lack the mechanistic basis behind the onset and progression of the CVDs, despite of decades of research in this area. The different forms of CVDs are complex in their etiology, however, risk factors common to all forms include smoking, diabetes, hypertension, hypercholesteremia, obesity and aging [42]. The risk factors for CVDs are associated with significant increases in ROS in the vascular wall [9, 43]. High level of ROS can dynamically change the redox homeostasis of the endothelial cell. Cardiovascular risk factors also negatively influence the bioavailability of NO and cause endothelial dysfunction [6].

2.1. Oxidative stress and cardiovascular diseases

Oxidative stress has been associated with the pathogenesis of several diseases including vascular diseases, neurodegenerative diseases, diabetes, atherosclerosis, cancer, aging and obesity [4, 44-49]. The term 'oxidative stress' is frequently used in redox biology and medicine. It was first formulated in 1985 and as of today, approximately 219,225 PubMed entries show this term [50]. Oxidative stress has been defined as an imbalance between generation of reactive oxygen species (ROS) and their elimination by antioxidant defense capacity of the cell. This imbalance is

caused due to elevated levels of ROS or reduced levels of antioxidants [51]. The ROS produced include free oxygen radicals such as $O_2^{\bullet-}$, oxygen ions, and peroxides [9]. The ROS-producing enzymes contributing to vascular oxidative stress include, nicotinamide adenine dinucleotide phosphate oxidase (NADPH) oxidase, xanthine oxidase (XO), enzymes of the mitochondrial respiratory chain, and dysfunctional enzyme endothelial nitric oxide synthase (eNOS) that produce vasodilator, nitric oxide (NO) [52]. The antioxidant defense that gets hampered in oxidative stress include including SOD, GPX, catalase, Prx and thioredoxin etc. or the non-enzymatic one including ASC and GSH [13, 53]

In endothelial cells reduced NO bioavailability because of increased NO degradation by ROS marks the onset of endothelial dysfunction. For instance, $O_2^{\bullet-}$ reacts with NO to form peroxynitrite ($ONOO^-$). Formation of $ONOO^-$ promotes protein nitration and has deleterious consequences on endothelial cells [54]. Studies on animal experimental models to analyze the effect of genetic deletion or overexpression of ROS producing enzymes and the antioxidant enzymes on the disease phenotype, provides the molecular proof for the involvement of oxidative stress in CVDs. The extent of cells/tissue exposed to and the severity of the oxidative stress determines the consequences of oxidative stress [55].

2.2. Endothelial dysfunction as an early detector of cardiovascular diseases

Endothelium forms a semipermeable barrier between the vascular wall and the blood stream, which is both mechanical and biological in nature. It not only regulates the transport of macromolecules between the vascular lumen and vascular smooth muscle but can also secret relaxing and contracting molecules. The important functions of the endothelium are vasodilation and modulating vascular tone by synthesizing and releasing vasoactive substances. In addition,

endothelium is involved in regulation of platelet function, inflammatory responses, vascular smooth muscle cell growth and migration. The maintenance of vascular tone is done by endothelial derived relaxing factor, nitric oxide (NO). In endothelial cells, NO is synthesized by a constitutive enzyme eNOS and NO can diffuse freely across biological membranes. It stimulates soluble guanynyl cyclase in the smooth muscle cells that leads to increase in intracellular cyclic guanosine monophosphate levels and results in vasodilation [15, 56].

The term endothelial dysfunction refers to several pathological conditions, including altered anticoagulant and anti-inflammatory properties of the endothelium, impaired modulation of vascular growth, and dysregulation of vascular remodeling [3]. In literature this term is most often used to characterize impairment in vasorelaxation caused due to reduction in NO bioavailability [3, 42, 57]. Accumulating evidence has demonstrated that endothelial functions are essential to ensure proper maintenance of vascular homeostasis [15]. The pathogenesis of the vascular disease is attributed to the alterations in the vascular endothelium [58]. The endothelium lining the arteries is especially subjected to harmful stimuli including oscillatory shear stress, disturbed turbulent flow and oxidative stress among others [59]. Endothelial dysfunction is the hallmark of a wide range of CVDs including atherosclerosis, diabetes, smoking, aging, obesity, hyperhomocysteinemia, hypertension and others. [56, 57, 60-64]. The general schematic for the development and progression of cardiovascular diseases from the risk factors has been summarized in Figure 2 (modified from [42]) below.
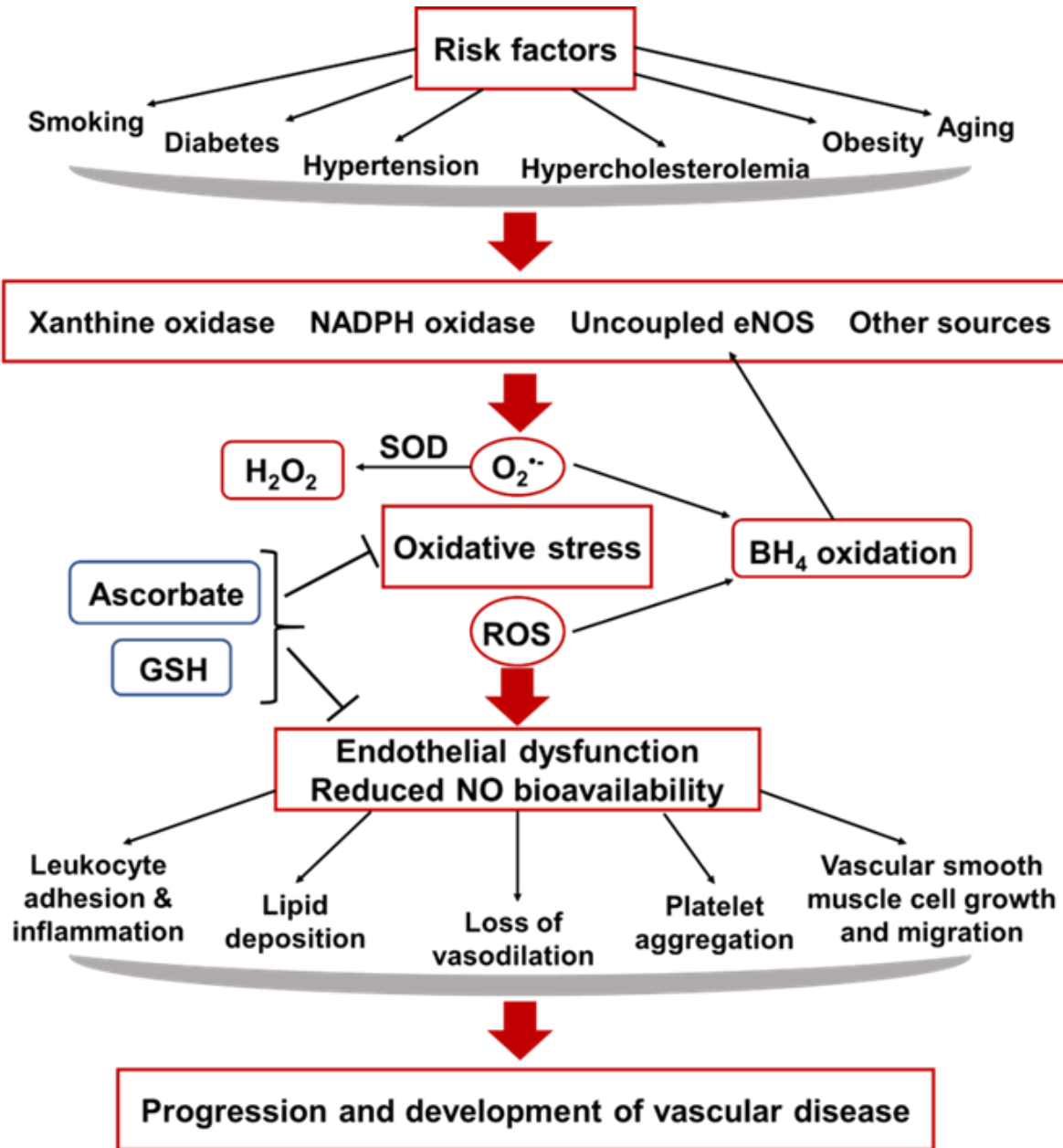
Figure 2: General schematic of development and progression of vascular diseases

2.3. Intracellular sources of reactive oxygen species

Mammalian cells utilize aerobic respiration, which requires molecular oxygen (O_2) for biochemical conversion, to produce adenosine triphosphate (ATP) from food. As a side effect of this process, ROS are generated [10]. These ROS have unpaired electrons and are considered as

free radicals such as superoxide ion ($O_2^{\bullet-}$) and hydroxyl radical ($\bullet OH$), which are unstable and have short biological half-lives. As well as, nonradical oxidizing ROS such as hydrogen peroxide (H_2O_2), NO etc. These are comparatively stable and have longer half-lives [65, 66]. The one electron reduction of O_2 generates $O_2^{\bullet-}$, which is a highly reactive radical with rapid spontaneous (8×10^4 $M^{-1}\cdot s^{-1}$) or enzymatic (2×10^9 $M^{-1}\cdot s^{-1}$) dismutation rates. $O_2^{\bullet-}$ is also considered as a precursor for converting to other forms of ROS/RNS through a series of reactions [67]. $O_2^{\bullet-}$ is mainly produced in the inner mitochondrial membrane space as it is rich in O_2 and electrons. $O_2^{\bullet-}$ is ineffective at permeating through lipid membranes, hence considered as poor signaling molecule [68]. The majority of $O_2^{\bullet-}$ generated is rapidly converted to H_2O_2. H_2O_2 can diffuse through organelle as well as cell membranes and is considered as more stable ROS, than $O_2^{\bullet-}$. H_2O_2 is also considered as an ideal secondary messenger for mediating downstream cell signaling mechanisms [69]. H_2O_2 decomposition produces highly reactive $\bullet OH$ radical, which is associated with oxidative damage due to its mostly nonselective and irreversible reactivity [70]. In addition to ROS, RNS such as NO, nitrogen dioxide ($NO_2^{\bullet}$), $ONOO^-$, dinitrogen trioxide (N_2O_3), and nitrous acid (HNO_2) also contribute to the oxidative stress [71]. These RNS have deleterious effects on the cell mostly due to oxidative damage to proteins and DNA [72].

2.3.1. NADPH oxidase (NOX)

Nicotinamide adenine dinucleotide phosphate (NADPH) oxidases are the family enzymes whose primary function is ROS production and are considered as re critical mediators of cardiovascular physiology and pathophysiology [73, 74]. NOX has two membrane bound subunits (gp91phox and p22phox) and several cytoplasmic subunits (p47phox, p67phox, p40phox and G protein) [75, 76]. There are seven isoforms of NOX in mammals, amongst which the NOX1, NOX2, NOX4 and NOX5. are variably expressed in the endothelial cells [73-75]. The various

NOX isoforms are differentiated based on their specific type of ROS generation. NOX1 and NOX2 primarily produce $O_2^{\bullet-}$ from O_2; NOX4 has been reported to generate H_2O_2 rather than $O_2^{\bullet-}$; and NOX5 produces both $O_2^{\bullet-}$ and H_2O_2 [77, 78]. NOX1 expression is residual under basal conditions and after stimuli increases considerably. NOX2 affects both NO bioavailability as well as contractile properties of vasculature [79]. NOX4 expression exerts vasoprotective effects [80] as well as detrimental effect [81], depending on the stimuli. NOX5 is calcium sensitive isoform important in redox-sensitive contractions. Recent study has described a novel function for vascular NOX5 that links calcium and ROS to the pro-contractile molecular machinery in vasculature [82]. Various risk factors including hypertension, obesity, hypercholesterolaemia, atherosclerosis, diabetes mellitus and dementia, can activate NOX, resulting in an enhanced production of ROS [45, 46, 83-85].

2.3.2. Xanthine oxidase (XO)

XO is another enzyme largely concentrated in endothelial cells that mediates oxidation of hypoxanthine and xanthine and produces $O_2^{\bullet-}$ and H_2O_2 as by-products. In humans, unstimulated cells have a relatively low basal expression of XO, yet upon cellular activation by cytokines, the transcription of XO is rapidly upregulated and its activity increased [86]. Endothelial dysfunction is linked with increment in endothelial XO [51]. Conditions like hypoxia or hyperoxia, which have changes in the intracellular or extracellular O_2 content can also alter the transcriptional regulation of XO and lead to the intracellular accumulation of $O_2^{\bullet-}$ [86, 87]. The activity of XO is increased in patients with coronary artery disease [88] and inhibitors of this enzyme reduce endothelial dysfunction in both humans and animal models [89-91].

2.3.3. Endothelial nitric oxide synthase (eNOS)

NO is produced by three different isoforms of nitric oxide synthases (NOS), NOS1 are neuronal NOS (nNOS), NOS2 are inducible NOS (iNOS) and NOS3 are endothelial NOS isoform. They all utilize L-arginine and molecular O_2 as substrates and require cofactors such as; reduced nicotinamide-adenine-dinucleotide phosphate (NADPH), flavin adenine dinucleotide (FAD), flavin mononucleotide (FMN), and (6R-)5,6,7,8-tetrahydrobiopterin (BH$_4$) for producing NO. The central and peripheral neurons and some other cell types constitutively express nNOS. Important functions of nNOS include, maintaining synaptic plasticity in the central nervous system, regulating blood pressure in CNS, smooth muscle relaxation, and vasodilatation via peripheral nitrergic nerves. iNOS is expressed in many cell types in response to stimuli from lipopolysaccharide, cytokines, or other agents. Large concentration of NO is generated from iNOS compared to nNOS and eNOS that have cytostatic effects on parasitic target cells. iNOS contributes to the pathophysiology of inflammatory diseases and septic shock. eNOS is mostly expressed in endothelial cells. Under physiological conditions, eNOS produces NO and exerts vasoprotective effects on the endothelium [92]. However, under pathological conditions, uncoupling of eNOS occurs which produces $O_2^{\bullet-}$, instead of NO. This further aggravates oxidative stress [9, 92]. Particularly, ONOO$^-$ promote eNOS uncoupling [52].

2.3.3.1. eNOS catalyzed NO and $O_2^{\bullet-}$ production

The catalysis of eNOS is shown in Figure 3. In the endothelial cells, the active form of eNOS exists as a dimer with two domains, oxygenase and reductase. The reductase domain has the binding sites for the flavin co-factors FAD, FMN; the substrate NADPH and; calcium (Ca^{2+}) and calmodulin which is required for the electron flow through the reductase domain and to keep the two domains bound to each other [24]. The oxygenase domain has the binding sites for heme,

the co-factor tetrahydrobiopterin (BH_4) and the substrate L-Arginine (L-Arg) [24]. In the reductase domain NADPH oxidizes to $NADP^+$ and the electrons (e^-) donated proceed via FAD and FMN redox carriers to the oxygenase domain. In the oxygenase domain the e^- interact with the heme and BH_4 at the active site to catalyse the reaction of oxygen (O_2) with L-Arg to generate citrulline and NO as products through a series of biochemical reactions. An increase in the production of ROS (including $O_2^{\bullet-}$, $\bullet OH$ and $CO_3^{\bullet-}$) and RNS (including $ONOO^-$ and $\bullet NO_2$) leads to oxidation of BH_4 to dihydrobiopterin (BH_2) [93, 94]. Both BH_2 and BH_4 can compete with similar affinity for binding to eNOS [95]. The binding of BH_2 to eNOS leads to the uncoupling of eNOS resulting in $O_2^{\bullet-}$ production [93, 94, 96, 97].
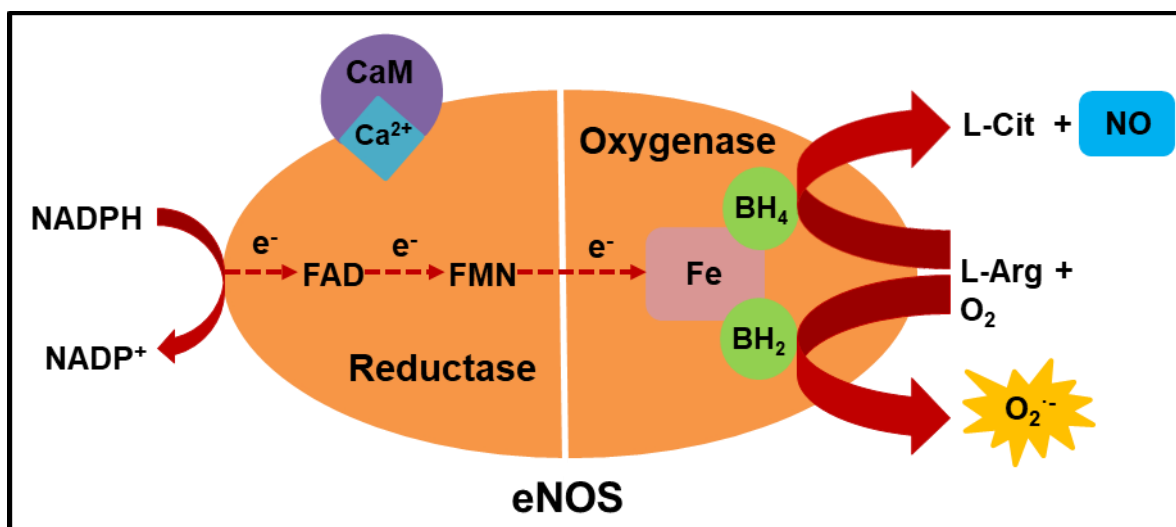
Figure 3: Reaction catalyzed by eNOS and the production of NO and $O_2^{\bullet-}$

2.3.4. Mitochondrial electron transport chain

Mitochondria utilize molecular O_2 for energy production and oxidative phosphorylation. During this process, consumed O_2 is converted to $O_2^{\bullet-}$, predominantly at complexes I, II and III. Mitochondrial respiratory chain has been considered as the main source of ROS in vascular cells [98, 99]. In addition to leak from respiratory chain, the mitochondrial growth factor adaptor Shc

and monoamine oxidases are also responsible for ROS production in the vascular system [100]. Importantly, the overproduction of ROS in mitochondria results in changed mitochondrial permeability, phenomenon called 'ROS-induced ROS release' that triggers ROS burst and has a pathological impact [101].

2.4. Antioxidant defense system

Antioxidants can counteract ROS/RNS and neutralize oxidants. The general endogenous antioxidants system consists of (i) enzymatic antioxidants including superoxide dismutase (SOD), catalase, glutathione peroxidase (GPX), peroxiredoxin (Prx) and thioredoxin (Trx); (ii) hydrophilic antioxidants including urate, ASC, GSH and flavonoids and (iii) lipophilic anitioxidants including tocopherol, carotenoid and ubiquinol [13, 14, 102].

2.4.1. Superoxide dismutase (SOD)

SOD is one of the most potent intracellular enzymatic antioxidants responsible for catalyzing the dismutation of $O_2^{\bullet-}$ into H_2O_2 as shown below:

$$O_2^{\bullet-} + O_2^{\bullet-} + 2H^+ \rightarrow H_2O_2 + O_2$$

There are three different isoforms of SOD localized in different cellular compartments: a cytosolic copper-zinc superoxide dismutase (SOD1 or CuZnSOD), a predominantly mitochondrial manganese superoxide dismutase (SOD2 or MnSOD), and an extracellular CuZnSOD (SOD3) with affinity for cell surface heparin sulfate proteoglycans. In endothelial cells, under physiological conditions, SOD1-derived H_2O_2 has been shown to act as an endothelium-dependent hyperpolarization factor in vivo and SOD2 derived H_2O_2 promoted endothelial cells sprouting and new blood vessel formation. The reduced levels of SOD were associated with increased $O_2^{\bullet-}$ levels, inhibited angiogenesis and impaired relaxation to acetylcholine. Deficiency of SOD has also been

found in pulmonary hypertension, diabetes. Also, overexpression of SOD has been shown to improve endothelial function in rate models of hypertension and heart failure [4]. The H_2O_2 is reduced to molecular O_2 and water by antioxidant enzymes, catalase, peroxidases.

2.4.2. Catalase

Catalase was the first antioxidant enzyme to be characterized and catalyzes conversion of H_2O_2 to water and O_2 as below:

$$2H_2O_2 \rightarrow 2H_2O + O_2$$
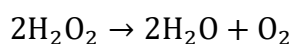
Catalase consists of four subunits each containing is a heme- group and NADPH molecule. The rate constant for the reactions described above is extremely high ($\sim 10^7$ M.s^{-1}). Catalase also has one of the highest turnover rates of all enzymes, where one molecule of catalase can convert approximately 6 million molecules of H_2O_2 to water and O_2 each minute [103]. Catalases are exclusively located in the peroxisome of cells. It is abundantly expressed in liver, lungs, and kidneys. Catalase is known to efficiently clear exogenous H_2O_2 [102]. The role of catalase in endothelial is uncertain, as under normal conditions, its activity seems to be not essential. However, under oxidative stress, catalase activity increases in endothelial cells [4].

2.4.3. Glutathione peroxidase (GPX)

GPX catalyze the oxidation of GSH at direction of a hydroperoxide, which may be H_2O_2, ONOO$^-$ or another species such as a lipid hydroperoxide as below:

$$ROOH + 2GSH \rightarrow GSSG + H_2O + ROH$$

GPX is the selenium-dependent protein antioxidant that catalyzes the reduction of H_2O_2 to molecular O_2 and water by using GSH as a reducing equivalent. GPX is known to clear endogenous

H_2O_2 [102]. In mammals eight different isoforms of GPX has been identified. Five of these isoforms (GPX1, GPX2, GPX3, GPX4 and GPX6) contain selenocysteine residue in their active site and three isoforms (GPX5, GPX7 and GPX8) have cysteine residues [104]. GPX-1 isoform is most abundantly expressed in endothelial cells. GPX-1 is located both in the mitochondria and cytoplasm of endothelial cells. Increased GPX-1 expressions have been reported to protect endothelial cells from H_2O_2 induced apoptosis. While GPX-1 gene knockout was found to augment leukocyte adhesion to endothelial cells, induce pro-inflammatory phenotype in aging, impair vasodilation through decreased NO levels and increase oxidative stress [4]. GPX is also involved in clearing $ONOO^-$ and are known to protect cells from $ONOO^-$ mediated cytotoxicity [105]. Cellular GPX deficiency has been implicated in endothelial dysfunction and pro-inflammation [38, 106, 107].

2.4.4. Peroxiredoxin (Prx)

Prx are thiol-specific enzymes that use cysteine residues for inactivating H_2O_2 to water. In mammals six isoforms of Prx has been identified. Prx1-5 isoforms require two cysteine residues whereas Prx6 requires one cysteine residue for their catalytic activity. These isoforms are distributed across various cellular sites of ROS production, such as cytosol, mitochondria and peroxisomes. Prx1-5 uses thioredoxin as reducing equivalent, while Prx6 does not use thioredoxin [108]. As like GPX, Prx can also inactivate $ONOO^-$ [109, 110]. Increased expression of Prx6 has been observed under conditions of increased ROS generation in various models of injury, as well as patients with peripheral arterial disease show marked increase in circulating levels of Prx1, 2, 4, and 6 [108]. Prx1 is reported to protect mice against excessive endothelial activation and atherosclerosis, and the Prdx1$^{-/-}$ mice are reported susceptible to chronic inflammation [111].

2.4.5. Ascorbate (ASC) – reduced form of Vitamin C

Vitamin C, also known as ascorbic acid or ascorbate (ASC), is a water-soluble molecule that cannot be synthesized endogenously in humans, monkeys, guinea pigs, and several other animal species. Humans normally acquire vitamin C from dietary sources through a substrate-saturable transporting mechanism. Two sodium-dependent transporters are specific for ASC, and its oxidation product dehydroascorbic acid (DHA) is transported by glucose transporters [112]. Ascorbic acid is differentially accumulated by most tissues and body fluids. Plasma and tissue vitamin C concentrations are dependent on amount consumed, bioavailability, renal excretion, and utilization [113]. Low levels of plasma ASC are associated several diseases including cancer, diabetes, HIV, sepsis and cardiovascular diseases [53, 114-116]. The systemic or localized cellular ASC deficiency has been reported as a cause for endothelial dysfunction in cardiovascular disease [117]. For instance, supplementation of ASC has shown improvement in patients with obstructive sleep apnea which is a condition associated with oxidative stress, endothelial dysfunction and increased cardiovascular morbidity and mortality [35].

2.4.6. Glutathione (GSH) antioxidant system

GSH is the most thiol antioxidant, abundant in cytosol, nuclei and mitochondria is a major soluble antioxidant found in cells. Because of its high intracellular concentration (1 – 10 mM), GSH is considered as a major thiol-disulfide redox buffer of the cell. GSH is mostly present in its reduced form, when oxidized it forms glutathione disulfide (GSSG). The ratio of GSH/GSSG is a good measure of oxidative stress of an organism. GSSG is reduced by the NADPH-dependent flavoenzyme glutathione reductase (GR), and this enzyme is critical to the maintenance of a proper GSH redox potential in mammalian cells [118]. The protective roles of GSH against oxidative/nitrosative stress includes, GSH acting as a cofactor or reducing equivalent for enzymes,

participate in amino acid transport across plasma membrane, scavenge reactive species and regenerate vitamins C and E. Depletion in GSH has been implicated in several diseases including arthritis, AIDS, Parkinson's disease, alcoholic liver diseases, cancer, cardiovascular and brain disorders [103].

2.5. Oxidative stress mediated endothelial dysfunction as a therapeutic target for treating cardiovascular diseases

In CVDs, the increase in oxidative stress leads to a cascade of events that hampers the endothelial cell functionality. Table 1 summarizes the recent literature that establishes the association of oxidative stress in endothelial dysfunction. Researchers have been studying different ways to treat endothelial dysfunction for long time. Potentiation of the antioxidant pathways has been suggested as an effective strategy to improve endothelial dysfunction and a potential target to reduce the cardiovascular risk [119]. For instance, studies reported therapeutic potential of replenishing BH_4 bioavailability to increase NO bioavailability [25] or supplementing antioxidants [117] such as SOD and ASC to reduce the oxidative stress. Although being known for having therapeutic potential, studies using BH_4 and ASC have shown mixed results [33, 120]. In fact, most of the clinical trials on antioxidant therapy have hardly shown positive clinical outcome [5]. Further, the GSH/GPX enzyme system is known to participate in numerous physiological and pathophysiological processes including endothelial cell function and dysfunction [37, 38, 107, 121]. Supplementation of GSH and selenium compound, known to improve GPX expression and activity, has been shown to protect endothelial cells and improve endothelial dysfunction *in vivo*, *in vitro* as well as *clinical studies* [122-124]. In the present dissertation, the dynamic interactions of ROS/RNS with cofactors, substrates and antioxidants has been analyzed as shown in Figure 4

below. Specifically, the role of BH$_4$, ASC and GSH/GPX in oxidative stress and cardiovascular

health and disease are presented.

Table 1: Association of oxidative stress and endothelial dysfunction

Causes	Implications	References
Decrease in NO bioavailability	Endothelial dysfunction	Incalza *et al.* [4], Chen et al. [125], Satitthummanid *et al.* [126]
Increase O$_2$$^{\bullet-}$ production	Oxidative stress	Daiber *et al.* [7], Sena *et al.* [51], Di Meo *et al.* [8]
Decrease in SOD, ASC, GSH and GPX	Oxidative stress	He *et al.* [13], Kurutas *et al.* [103], Gabryel *et al.* [127], Likidlilid *et al.* [128]
Increase in eNOS activity/expression	eNOS uncoupling	Santhanam *et al.* [27], Karbach *et al.* [2],
Decrease in BH$_4$ bioavailability	eNOS uncoupling	Wang *et al.* [28], Chen and Ding *et al.* [129]
Increase in ONOO$^-$ levels	Tyrosine nitration and apoptosis	Radi *et al.* [130], Ferrer-Sueta *et al.* [54] Pacher *et al.* [131]
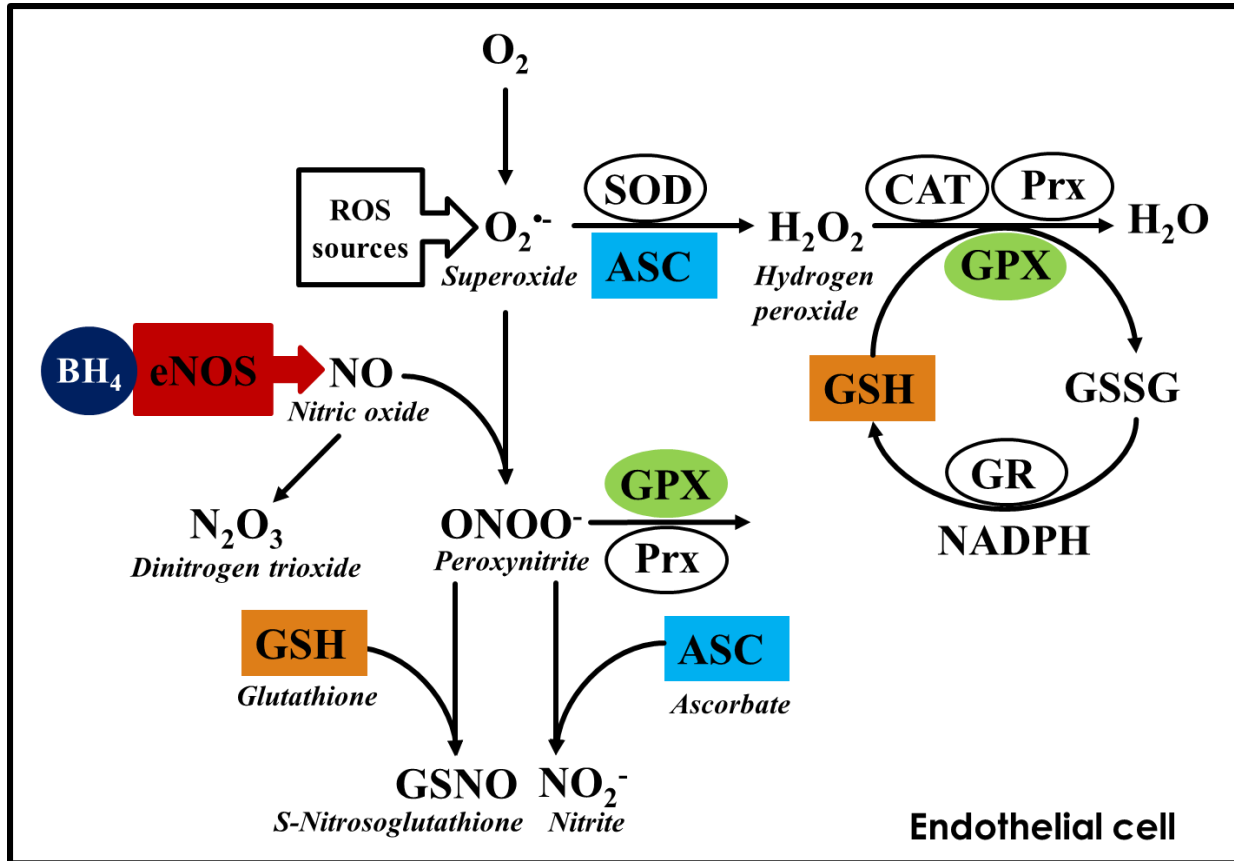
Figure 4: Overview of interactions of ROS/RNS with cofactors, substrates and antioxidants presented in the dissertation

2.5.1. Role of tetrahydrobiopterin in endothelial dysfunction

In endothelial cells, biopterin is primarily present in reduced form ($6R$-)5,6,7,8-tetrahydrobiopterin (BH_4) because of low levels of oxidative stress under normal physiologic conditions [132]. BH_4 is considered as an essential cofactor of eNOS that plays an important role in maintaining normal endothelial function. Increase in oxidative stress can cause uncoupling of the eNOS. The uncoupling of eNOS shifts the eNOS production of NO to superoxide ($O_2^{\bullet-}$) [23, 24]. The extent of eNOS uncoupling is predominantly determined by the availability of BH_4, [25, 26]. However, more recently it has been determined that the extent of oxidative stress is dependent on the biopterin ratio which is the ratio of BH_4 to the total biopterin levels (TBP) [93, 95].

In addition, oxidative stress can alter the activity of GTPCH. GTPCH is a key enzyme in *de novo* synthesis pathway for the endogenous production of BH_4 [94, 133]. The activity of GTPCH is reported to increase [134, 135] or reduce [136] in oxidative stress conditions. Shimizu *et al.* [134, 135] reported that the long exposures of endothelial cells to H_2O_2, •OH and $ONOO^-$ induced GTPCH mRNA expression and resulted in an increase of only BH_4 levels and not the oxidized forms of biopterin. The GTPCH inhibitor reduced the BH_4 levels in ROS and RNS exposed vascular endothelial cells. Meininger *et al.* [136] reported a decrease in GTPCH activity with a proportional decrease in the BH_4 levels in diabetic rats. The endothelial cell NO synthesis from the diabetic rats was only 18% compared to that of normal animals.

Several experimental studies have reported changes in biopterin ratio and NO levels because of BH_4 enhancement in endothelial dysfunction [95, 137, 138]. Crabtree *et al.* [95] reported a decrease in the biopterin ratio from 1:1 (BH_4:BH_2) in non-supplemented cells to 1:6 in 10 μM BH_4 supplemented hyperglycemic endothelial cells. They also reported a 40% decrease in NO production for BH_4 supplemented hyperglycemic endothelial cells. Alp *et al.* [138] reported that BH_4 comprised only 10% of the total biopterin content in diabetic-GTPCH overexpressing transgenic mice as compared to 80% in control GTPCH overexpressing transgenic mice. This decrease in the biopterin ratio was attributed to a 2 to 3–fold increase in $O_2^{\bullet-}$ production in diabetic-GTPCH overexpressing transgenic mice. Sasaki *et al.* [137] reported that $O_2^{\bullet-}$ production increased 1.6-fold in diabetic mice as compared to non-diabetic control mice and BH_4 supplementation suppressed $O_2^{\bullet-}$ production in diabetic mice. These studies demonstrate the presence of complex biochemical interactions between BH_4, oxidized biopterins, ROS and RNS that ultimately modulate eNOS uncoupling in endothelial dysfunction. In Chapter III the analysis of these interactions is elucidated.

2.5.2. Ascorbate and endothelial dysfunction

Low levels of ascorbate (ASC, reduced form of vitamin C) are associated with diseases such as cancer, diabetes, HIV, sepsis and cardiovascular diseases [53, 114-116]. The systemic or localized cellular ASC deficiency has been reported as a cause for endothelial dysfunction in cardiovascular disease [117]. It is well established that endothelial dysfunction is primarily caused due to a reduction in NO and an increase in oxidative stress [20, 55, 139, 140]. The synthesis and bioavailability of NO are sensitive to cellular antioxidant status and redox balance. ASC plays an important role in maintaining this redox balance [35, 116, 117, 141, 142]. Exogenous treatment with ASC is considered to be of therapeutic potential [34], however the potential mechanism of ASC in the mitigation of endothelial dysfunction is not clear [36].

Individual experimental studies have reported several putative mechanisms by which ASC may improve endothelial dysfunction. These mechanisms include: i) increasing or maintaining intracellular levels of BH_4 bioavailability in the reduced form [143, 144]; ii) scavenging of ROS/RNS including $O_2^{\bullet-}$ and $ONOO^-$ [145]; and iii) increasing eNOS activity through promoting eNOS phosphorytion [116] or reducing eNOS S-nitrosylation [146]. To better decipher the role of ASC in improving endothelial dysfunction, a quantitative understating of intracellular ASC interactions in endothelial cells is needed.

Many clinical and experimental studies provide evidence for the therapeutic potential of ASC. Akolkar *et al.* [147] reported that doxorubicin-induced oxidative and nitrosative stress in cardiac tissues was mitigated by the supplementation of ASC. Mullan *et al*. [148] showed an improvement in the arterial- blood pressure and stiffness in patients with type 2 diabetes after 1 month of oral dose of ASC. Studies also reported a reversal of NO-dependent endothelial dysfunction in coronary or peripheral arteries of atherosclerotic patients following the

supplementation of ASC [149, 150]. However, other studies reported ASC as pro-oxidant and increased oxidative stress. Varadhraj *et al.* [151] showed that the pharmacological ASC concentrations in the range of 10 mM or higher induced oxidative stress and led to a loss of redox-dependent cell viability in microvascular endothelial cells. It is evident that we lack the understanding of how ASC attenuates oxidative stress in health and disease. In chapter IV, the analysis the role of ASC in endothelial dysfunction is provided by integrating these potential mechanisms.

2.5.3. Role of glutathione and glutathione peroxidase in alleviating oxidative stress

GSH acts as a reducing agent in biological processes such as antioxidant defense, detoxification, signal transduction regulation, and cell apoptosis and proliferation [40, 152, 153]. GSH/GPX enzyme system removes ROS and RNS [39]. Deleterious consequences of excess ROS/RNS include, increased oxidative/nitrosative stress, NO degradation, protein nitration, DNA damage, lipid and protein structure modification, and mitochondria failure [4, 154]. GSH depletion can lead to an increase in ROS and RNS generation, an increase in mitochondrial complex I activity and NADPH oxidation, a decrease in cell viability, and an impairment of ATP generation [155-157]. The GPX catalyzes reduction of many oxidative species including H_2O_2 and $ONOO^-$ and uses GSH as a substrate [105, 158]. GPX depletion potentiates oxidative stress and leads to endothelial dysfunction [38] and apoptosis [159].

Several studies have reported the importance of GSH in alleviating oxidative stress. Ehrhart *et al.* [160] reported that GSH played a more important role than catalase in oxidative stress defense. Canals *et al.* [161] reported that NO changed from being anti-apoptotic to pro-apoptotic agent upon GSH depletion. GSH gets oxidized to glutathione disulfide (GSSG) and regenerated by the action of glutathione reductase and NADPH system. Yeh *et al.* [162] reported that GSH and

GSSG levels were significantly associated with increased oxidative stress in patients receiving hemodialysis treatment. Prasai *et al.* [163] reported that a reduction in [GSH]/[GSSG] ratio led to an increase in ROS and activated vascular endothelial growth factor receptor (VEGFR2).

GSH and GPX play an important role in modulating ROS and RNS levels in biological systems. GSH participates in recycling of GPX. GPX can deplete or maintain H_2O_2 as well as $ONOO^-$ at base level [104, 106]. Marc *et al.* [38] reported that GPX detoxifies nearly 70% H_2O_2 in endothelial cells. Gabryel *et al.* [127] reported that GPX and SOD activity increase protected ischemic endothelial cells. Fu *et al.* [164] showed that GPX removed ROS and protected against lipid peroxidation and protein oxidation from injuries mediated by only ROS, but not RNS. Maraldi *et al.* [165] showed that an increase in GPX activity was not sufficient to scavenge RNS-induced oxidative stress. In addition to the GSH/GPX system, studies have reported a role of Prx in the removal of H_2O_2 and $ONOO^-$ in many cell types [109, 166-168]. All these studies suggest that there is a cross talk of ROS and RNS with GSH/GPX system. In chapter V the interactions of ROS/RNS with GSH/GPX system are analyzed.

2.6. Use of computational modeling analysis

Extensive literature points that oxidative stress mediated endothelial dysfunction plays a central role in the pathogenesis of various CVDs and neurovascular diseases. Even though the therapeutic potential of essential eNOS cofactor and antioxidants including BH_4, ASC and GSH and its related enzyme system has been shown in experimental studies, the clinical outcomes are not reflected. The reason for this being we lack the quantitative understanding at the molecular level inside the endothelial cells in health and disease. The experimental studies mostly provide the qualitative data for the mechanisms involving reactive species in health and diseases. However,

the endothelial cell is a dynamic system and a delicate balance is present amongst many processes inside which are disrupted in the disease state. Several challenges are involved for evaluating the quantitative assessment of reactive species in experimental settings. These include i) free radical are short-lived intermediate species making them difficult to quantify, ii) different species have complex roles in different processes, thus multiple species analysis is required, iii) difficult to develop cellular models that mimic *in vivo* conditions, iv) there exists spatial heterogeneity between different chemical species amongst the different compartments of the cell.

Most of these challenges could be overcome by mathematical modeling approaches, which can help to elucidate behavior of these interactions for a particular system. Computational systems biology uses mathematical and computational methods to understand how biological systems work, with a secondary goal of manipulating and optimizing biomedical systems, guided by mathematics. Development of mathematical models, using mass action and reaction kinetics that are deterministic in nature, can provide ample information about the system under study. Such a study is important it is difficult to gather dynamics interactions of short lived reactive species using traditional experimental approaches. Also, implementation of computational model is perceived as a necessary methodological step for systems biologists. Such a model would be used to provide an *in silico* numerical evaluation of hypotheses, guidelines for designing future experiments, as well as avoid the use of complex analytical methods. This would considerably reduce the costs of expensive *in vivo* or *in vitro* experiments [169].

Mathematical modeling has proven insightful in providing mechanistic roles of ROS/RNS as well as antioxidants previously. Endothelial cell based computational model were developed to investigate eNOS uncoupling related NO and $O_2^{\bullet-}$ production. These models showed that the extent of eNOS uncoupling is dependent on the biopterin ratio [93, 170]. Computational modeling was

used to gain mechanistic insights on the role of ASC. Kuiper *et al.* [171] developed the pharmacokinetic model of ASC diffusion through tumor tissue to study the penetration of ASC through tissues. Their model predicted cellular ASC levels are dependent on the plasma supply. Ponte *et al.* [172] provided insights in the mechanism of ASC activation of anticancer drugs. Hu *et al.* [173] developed a dynamic system of coexisting NO and $O_2^{\bullet-}$ and studied the effect of ASC on the nitrosation kinetics of the model system by including the reactions of ASC on free radical scavenging and repairing in the model.

Several computational modeling studies investigated quantitative and mechanistic roles of GSH/GPX system in oxidative stress [174-176]. Keszler *et al.* [177] proposed various pathways for the reaction amongst GSH, NO and oxygen (O_2) and reported the reaction between GSH with N_2O_3 as a potential mechanisms of S-nitrosothiol (GSNO) formation. Hu *et al.* [175] and Bagci *et al.* [178] reported that GSH depletion resulted in an increased levels of ROS and RNS including, dinitrogen trioxide (N_2O_3) and $ONOO^-$. Ng *et al.* [176] examined the removal rate of H_2O_2 with respect to the kinetic behavior of GSH and GPX and reported H_2O_2 removal is a function of both GSH and GPX. While, Adimora *et al.* [179] modeled intracellular H_2O_2 clearance pathways including Prx and GSH/GPX and reported that the Prx was one of the major H_2O_2 clearance pathway.

The results from both experimental and modeling studies provide evidence for the presence of complex interactions amongst oxidative stress and endothelial dysfunction. This also establishes the need for the quantitative understanding of these interactions which will help in identifying intricate molecular determinants governing endothelial function and dysfunction. Identification of the underlying mechanisms is essential to develop novel clinical breakthroughs and improve knowledge [5].

CHAPTER III

COMPUTATIONAL ANALYSIS OF INTERACTIONS OF OXIDATIVE STRESS AND TETRAHYDROBIOPTERIN SYNTHESIS[1] IN ENOS COUPLING

3.1. Introduction

An increase in oxidative stress causes endothelial dysfunction in several CVDs. Increase in oxidative stress results in the reduction in BH_4 and eNOS uncoupling. Several experimental studies have examined the interactions of oxidative stress and BH_4 enhancement on the biopterin ratio and endothelial dysfunction [95, 137, 138]. The results from these studies demonstrates the presence of complex biochemical interactions between BH_4, oxidized biopterins, ROS and RNS that modulates eNOS uncoupling. Our understanding of the complex interactions of eNOS uncoupling, oxidative stress and BH_4 availability is not complete and a quantitative understanding of these interactions is required. In the present study, we developed a computational model for eNOS uncoupling that considers the temporal changes in biopterin ratio in the oxidative stress conditions. Using the model, we studied the effects of cellular oxidative stress ($Q_{supcell}$) representing the non-eNOS based oxidative stress sources and BH_4 synthesis (Q_{BH4}) on eNOS NO production and biopterin ratio (BH_4/total biopterins (TBP)). The results from the present study will be helpful in guiding the experimentation in this high priority area of cardiovascular research. In order to do so, the first step is to develop the computational model for eNOS uncoupling that considers the temporal changes in biopterin ratio in the cellular oxidative stress conditions.

---

[1] This work has been published: **Joshi, S.**, S. Kar, and M. Kavdia, *Computational analysis of interactions of oxidative stress and tetrahydrobiopterin reveals instability in eNOS coupling.* Microvasc Res, 2017. **114**: p. 114-128.

3.2. Materials and methods

3.2.1. Model Description

Figure 5 shows an endothelial cell computational model for the eNOS biochemical pathways that includes interactions of the cellular oxidative stress and BH_4 synthesis. The eNOS biochemical pathway related NO and $O_2^{\bullet-}$ production depends on the relative availability of BH_4 and BH_2, respectively, which is a function of the biopterin ratio. In this study, the biopterin ratio is defined as the ratio of reduced biopterin to total biopterin ($[BH_4]/[TBP]$). The concentration of BH_4 and BH_2 depends on the rate of synthesis and oxidation of BH_4 [180]. The sources of oxidative stress in endothelial cells include NADPH oxidase, xanthine oxidase and mitochondrial electron transport chain [181, 182]. Each of these distinctive oxidative stress sources produces $O_2^{\bullet-}$ at different rates [183-185] and results in enhanced ROS and RNS production in endothelial cells [181, 186]. Figure 6 represents the downstream reactions involving the products of eNOS biochemical pathway, NO and $O_2^{\bullet-}$ with other ROS, RNS and biopterins (BH_4, BH_3 and BH_2).

The eNOS biochemical pathway produces NO and $O_2^{\bullet-}$, when eNOS is coupled (left) and uncoupled (right), respectively. The enzymes-substrate complexes are denoted by orange rectangle and respective rate constants for the reactions involved are indicated. Q_{BH4} and $Q_{supcell}$ are the rates of biopterin synthesis and cellular oxidative stress, respectively. Shows the downstream reaction of NO and $O_2^{\bullet-}$ and their mutual reaction product $ONOO^-$. BH_4 can be oxidized to BH_3 by free radicals including $O_2^{\bullet-}$, $ONOO^-$, $\bullet OH$, $\bullet NO_2$ and NO_3^- to form BH_3. The BH_3 further oxidizes to BH_2 by molecular O_2 (k36).
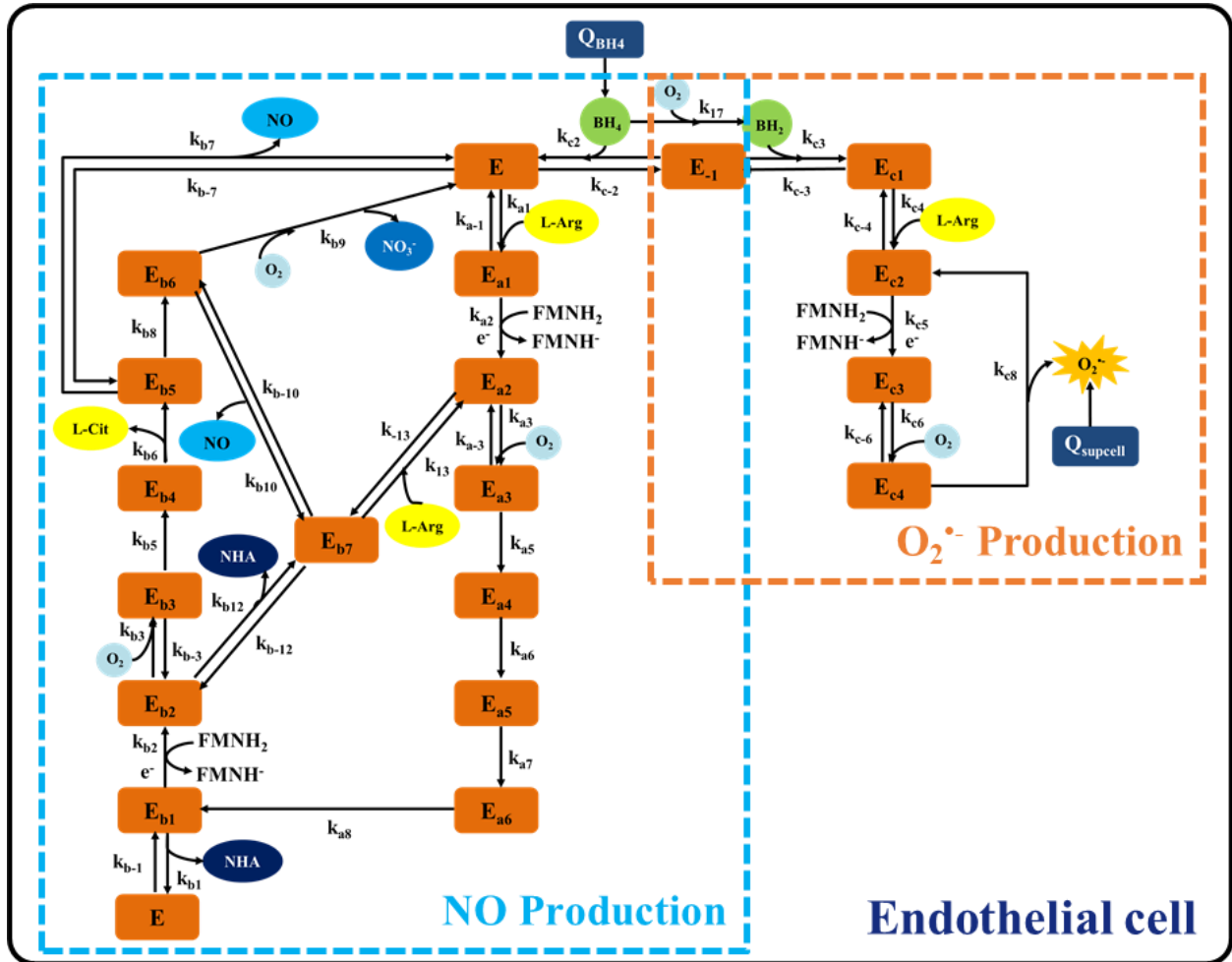
Figure 5: Schematics of reaction pathway for computational model for interactions of eNOS biochemical pathway, cellular oxidative stress and tetrahydrobiopterin synthesis.
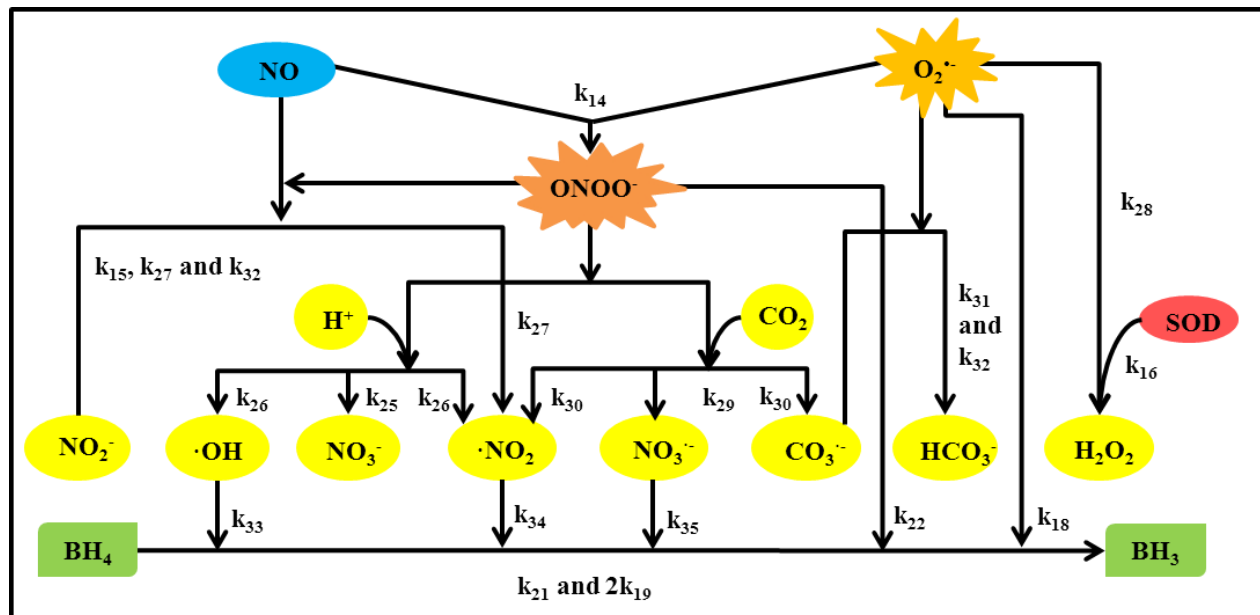
Figure 6: Schematic for interactions of NO and $O_2^{\bullet-}$ and their downstream reactions leading to oxidation of BH_4 to BH_3 and ultimately to BH_2.

The eNOS biochemical pathway and downstream reactions with the respective rate constants modeled in this study are presented in Table 2 and Table 3. The nomenclature of enzyme-substrate complex involved in eNOS biochemical pathway denoted in Figure 5 can be found in the parenthesis under species in Table 3. In brief, the key reactions from the eNOS biochemical pathway for NO production include; (i) the binding of the co-factor BH_4 and substrates (L-arginine and O_2) to eNOS, (ii) the oxidation of L-arginine to N-hydroxyl-L-arginine (NHA) through enzyme substrate complexes (from eNOS-[Fe^{III}-O_2^-]-BH_4-Arg, E1 to eNOS-(Fe^{III})-BH_4-NHA, E2) and (iii) the oxidation of NHA to form NO and citrulline through enzyme substrate complexes (from eNOS-(Fe^{III})-BH_4-NHA, E2 to eNOS-(Fe^{III})-NO-BH_4, E4) [93, 187]. The eNOS biochemical pathway for $O_2^{\bullet-}$ production involves the binding of co-factor BH_2 and substrates (L-arginine and O_2) to eNOS [188-191]. However, the inability of BH_2 to transfer electron to the

eNOS heme results in the dissociation of the eNOS-substrate complex eNOS-[Fe^{III}-O_2^-]-BH_2-Arg, E5 to form $O_2^{\bullet -}$ [97, 190].

Table 2: Chemical reactions and rate constants involved in the eNOS biochemical pathway for NO and $O_2^{\bullet -}$ production and their downstream reactions involving NO, ROS, RNS and biopterins.

Reactions	Rate Constants	References
$eNOS - (Fe^{III}) + BH_4 \xrightarrow{k_{c2}} eNOS - (Fe^{III}) - BH_4$	$k_{c2} = 2.20 \times 10^4\ M^{-1}.s^{-1}$	[188]
$eNOS - (Fe^{III}) - BH_4 \xrightarrow{k_{c-2}} eNOS - (Fe^{III}) + BH_4$	$k_{c-2} = 0.005\ s^{-1}$	[188]
$eNOS - (Fe^{III}) - BH_4 + L - Arg \xrightarrow{k_{a1}} eNOS - (Fe^{III}) - BH_4 - Arg$	$k_{a1} = 1.19 \times 10^6\ M^{-1}.s^{-1}$	[191]
$eNOS - (Fe^{III}) - BH_4 - Arg \xrightarrow{k_{a-1}} eNOS - (Fe^{III}) - BH_4 + L - Arg$	$k_{a-1} = 3.77\ s^{-1}$	[191]
$eNOS - (Fe^{III}) - BH_4 - Arg + FMNH_2 + e^- \xrightarrow{k_{a2}} eNOS - (Fe^{II}) - BH_4 - Arg + FMNH^-$	$k_{a2} = 0.474\ s^{-1}$	[192]
$eNOS - (Fe^{II}) - BH_4 - Arg + O_2 \xrightarrow{k_{a3}} eNOS - [Fe^{III} - O_2^-] - BH_4 - Arg$	$k_{a3} = 8.20 \times 10^5\ M^{-1}.s^{-1}$	[97]
$eNOS - [Fe^{III} - O_2^-] - BH_4 - Arg \xrightarrow{k_{a-3}} eNOS - (Fe^{II}) - BH_4 - Arg + O_2$	$k_{a-3} = 48.3\ s^{-1}$	[97]
$eNOS - (Fe^{II}) - BH_4 - Arg + O_2 + e^- \xrightarrow{k_{a5}} eNOS - [Fe^{III} - OOH] - BH_3 - Arg$	$k_{a5} = 7.68\ s^{-1}$	[97]
$eNOS - [Fe^{III} - OOH] - BH_3 - Arg \xrightarrow{k_{a6}} eNOS - [Fe^{IV} - O] - BH_3 - Arg$	$k_{a6} = 7.68\ s^{-1}$	[193]

$eNOS - [Fe^{IV} - O] - BH_3 - Arg \xrightarrow{k_{a7}} eNOS - (Fe^{III}) - BH_3 - NHA$	$k_{a7} = 6.85 \text{ s}^{-1}$	[194]
$eNOS - (Fe^{III}) - BH_3 - NHA \xrightarrow{k_{a8}} eNOS - (Fe^{III}) - BH_4 - NHA$	$k_{a8} = 3.62 \text{ s}^{-1}$	[195]
$eNOS - (Fe^{III}) - BH_4 - NHA \xrightarrow{k_{b1}} eNOS - (Fe^{III}) - BH_4 + NHA$	$k_{b1} = 0.1 \text{ s}^{-1}$	[191]
$eNOS - (Fe^{III}) - BH_4 + NHA \xrightarrow{k_{b-1}} eNOS - (Fe^{III}) - BH_4 - NHA$	$k_{b-1} = 1 \times 10^5 \text{ M}^{-1}.\text{s}^{-1}$	[191]
$eNOS - (Fe^{III}) - BH_4 - NHA + FMNH_2 + e^- \xrightarrow{k_{b2}} eNOS - (Fe^{II}) - BH_4 - NHA + FMNH^-$	$k_{b2} = 0.474 \text{ s}^{-1}$	[192]
$eNOS - (Fe^{II}) - BH_4 - NHA + O_2 \xrightarrow{k_{b3}} eNOS - [Fe^{III} - O_2^-] - BH_4 - NHA$	$k_{b3} = 9.19 \times 10^5 \text{ M}^{-1}.\text{s}^{-1}$	[97]
$eNOS - [Fe^{III} - O_2^-] - BH_4 - NHA \xrightarrow{k_{b-3}} eNOS - (Fe^{II}) - BH_4 - NHA + O_2$	$k_{b-3} = 40.5 \text{ s}^{-1}$	[97]
$eNOS - [Fe^{III} - O_2^-] - BH_4 - NHA + e^- \xrightarrow{k_{b5}} eNOS - [Fe^{III} - OOH] - BH_3 - NHA$	$k_{b5} = 36.6 \text{ s}^{-1}$	[196]
$eNOS - [Fe^{III} - OOH] - BH_3 - NHA \xrightarrow{k_{b6}} eNOS - (Fe^{III}) - NO - BH_4 + L - Cit + H_2O$	$k_{b6} = 9.45 \text{ s}^{-1}$	[196]
$eNOS - (Fe^{III}) - NO - BH_4 \xrightarrow{k_{b7}} eNOS - (Fe^{III}) - BH_4 + NO$	$k_{b7} = 11.5 \text{ s}^{-1}$	[192]
$eNOS - (Fe^{III}) - BH_4 + NO \xrightarrow{k_{b-7}} eNOS - (Fe^{III}) - NO - BH_4$	$k_{b-7} = 1.7 \times 10^6 \text{ M}^{-1}.\text{s}^{-1}$	[197]

$eNOS - (Fe^{III}) - NO - BH_4 + e^- \xrightarrow{k_{b8}} eNOS - (Fe^{II}) - NO - BH_4$	$k_{b8} = 7.8 \times 10^{-3} \, s^{-1}$	[192]
$eNOS - (Fe^{II}) - NO - BH_4 + O_2 \xrightarrow{k_{b9}} eNOS - (Fe^{III}) - BH_4 + ONOO^-$	$k_{b9} = 1.76 \, s^{-1}$	[192]
$eNOS - (Fe^{II}) - NO - BH_4 + NO \xrightarrow{k_{b10}} eNOS - (Fe^{II}) - BH_4$	$k_{b10} = 1.76 \times 10^{-3} \, s^{-1}$	[192]
$eNOS - (Fe^{II}) - BH_4 \xrightarrow{k_{b-10}} eNOS - (Fe^{II}) - NO - BH_4 + NO$	$k_{b-10} = 3.07 \times 10^6 \, M^{-1}.s^{-1}$	[197]
$eNOS - (Fe^{II}) - BH_4 - NHA \xrightarrow{k_{b12}} eNOS - (Fe^{II}) - BH_4 + NHA$	$k_{b12} = 3.66 \, s^{-1}$	[191]
$eNOS - (Fe^{II}) - BH_4 + NHA \xrightarrow{k_{b-12}} eNOS - (Fe^{II}) - BH_4 - NHA$	$k_{b-12} = 1.09 \times 10^6 \, M^{-1}.s^{-1}$	[191]
$eNOS - (Fe^{II}) - BH_4 + L - Arg \xrightarrow{k_{13}} eNOS - (Fe^{II}) - BH_4 - Arg$	$k_{13} = 1.19 \times 10^6 \, M^{-1}.s^{-1}$	[191]
$eNOS - (Fe^{II}) - BH_4 - Arg \xrightarrow{k_{-13}} eNOS - (Fe^{II}) - BH_4 + L - Arg$	$k_{-13} = 3.77 \, s^{-1}$	[191]
$eNOS - (Fe^{III}) + BH_2 \xrightarrow{k_{c3}} eNOS - (Fe^{III}) - BH_2$	$k_{c3} = 2.20 \times 10^4 \, M^{-1}.s^{-1}$	[188]
$eNOS - (Fe^{III}) - BH_2 \xrightarrow{k_{c-3}} eNOS - (Fe^{III}) + BH_2$	$k_{c-3} = 0.047 \, s^{-1}$	[188]
$eNOS - (Fe^{III}) - BH_2 + L - Arg \xrightarrow{k_{c4}} eNOS - (Fe^{III}) - BH_2 - Arg$	$k_{c4} = 1.19 \times 10^6 \, M^{-1}.s^{-1}$	[191]
$eNOS - (Fe^{III}) - BH_2 - Arg \xrightarrow{k_{c-4}} eNOS - (Fe^{III}) - BH_2 + L - Arg$	$k_{c-4} = 3.77 \, s^{-1}$	[191]

Reaction	Rate constant	Ref
$eNOS - (Fe^{III}) - BH_2 - Arg + FMNH_2 + e^- \xrightarrow{k_{c5}} eNOS - (Fe^{II}) - BH_2 - Arg + FMNH^-$	$k_{c5} = 0.474 \text{ s}^{-1}$	[198]
$eNOS - (Fe^{II}) - BH_2 - Arg + O_2 \xrightarrow{k_{c6}} eNOS - [Fe^{III} - O_2^-] - BH_2 - Arg$	$k_{c6} = 1.73 \times 10^6 \text{ M}^{-1}.\text{s}^{-1}$	[190]
$eNOS - [Fe^{III} - O_2^-] - BH_2 - Arg \xrightarrow{k_{c-6}} eNOS - (Fe^{II}) - BH_2 - Arg + O_2$	$k_{c-6} = 14.2 \text{ s}^{-1}$	[190]
$eNOS - [Fe^{III} - O_2^-] - BH_2 - Arg \xrightarrow{k_{c8}} eNOS - (Fe^{III}) - BH_2 - Arg + O_2^-$	$k_{c8} = 0.375 \text{ s}^{-1}$	[190]
$NO + O_2^{\bullet-} \xrightarrow{k_{14}} ONOO^- \leftrightarrow ONOOH$	$k_{14} = 6.7 \times 10^9 \text{ M}^{-1}.\text{s}^{-1}$	[199]
$4NO + O_2 + 2H_2O \xrightarrow{k_{15}} 4NO_2^- + 2H^+$	$k_{15} = 2.4 \times 10^6 \text{ M}^{-2}.\text{s}^{-1}$	[200]
$O_2^{\bullet-} + H_2O \xrightarrow{SOD, k_{16}} 0.5O_2 + 0.5H_2O_2 + OH^-$	$k_{16} = 3.85 \times 10^9 \text{ M}^{-1}.\text{s}^{-1}$	[199]
$2BH_4 + O_2 \xrightarrow{k_{17}} 2BH_2 + 2H_2O$	$k_{17} = 0.6 \text{ M}^{-1}.\text{s}^{-1}$	[201]
$BH_4 + O_2^{\bullet-} + H^+ \xrightarrow{k_{18}} BH_3 + H_2O_2$	$k_{18} = 3.9 \times 10^5 \text{ M}^{-1}.\text{s}^{-1}$	[201]
$2BH_3 \xrightarrow{k_{19}} BH_4 + BH_2$	$k_{19} = 4.65 \times 10^4 \text{ M}^{-1}.\text{s}^{-1}$	[201]
$BH_4 + ONOO^- \xrightarrow{k_{22}} BH_3$	$k_{22} = 6 \times 10^3 \text{ M}^{-1}.\text{s}^{-1}$	[202]
$ONOOH \xrightarrow{k_{25}} NO_3^- + H^+$	$k_{25} = 0.981 \text{ s}^{-1}$	[200]
$ONOOH \xrightarrow{k_{26}} \bullet NO_2 + \bullet OH$	$k_{26} = 0.401 \text{ s}^{-1}$	[200]
$ONOO^- (ONOOH) + NO \xrightarrow{k_{27}} \bullet NO_2 + NO_2^-$	$k_{27} = 9.1 \times 10^4 \text{ M}^{-1}.\text{s}^{-1}$	[199]
$HO_2 + O_2^{\bullet-} + H_2O \xrightarrow{k_{28}} O_2 + H_2O_2 + OH^-$	$k_{28} = 3.57 \times 10^5 \text{ M}^{-1}.\text{s}^{-1}$	[200]

$ONOO^- + CO_2 \xrightarrow{k_{29}} NO_3^- + CO_2$	$k_{29} = 3.886 \times 10^4 \, M^{-1}.s^{-1}$	[200]
$ONOO^- + CO_2 \xrightarrow{k_{30}} \bullet NO_2 + CO_3^{\bullet -}$	$k_{30} = 1.915 \times 10^4 \, M^{-1}.s^{-1}$	[200]
$CO_3^{\bullet -} + O_2^{\bullet -} + H^+ \xrightarrow{k_{31}} HCO_3^- + O_2$	$k_{31} = 6.65 \times 10^8 \, M^{-1}.s^{-1}$	[200]
$CO_3^{\bullet -} + NO + OH^- \xrightarrow{k_{32}} HCO_3^- + NO_2^-$	$k_{32} = 5.82 \times 10^9 \, M^{-1}.s^{-1}$	[200]
$BH_4 + \bullet OH \xrightarrow{k_{33}} OH^- + H^+ + BH_3$	$k_{33} = 8.8 \times 10^9 \, M^{-1}.s^{-1}$	[144]
$BH_4 + \bullet NO_2 \xrightarrow{k_{34}} NO_2^- + H^+ + BH_3$	$k_{34} = 9.4 \times 10^8 \, M^{-1}.s^{-1}$	[144]
$BH_4 + CO_3^{\bullet -} \xrightarrow{k_{35}} CO_3^{2-} + H^+ + BH_3$	$k_{35} = 4.6 \times 10^9 \, M^{-1}.s^{-1}$	[144]
$BH_3 + O_2 \xrightarrow{k_{36}} BH_2 + HO_2^{\bullet}$	$k_{36} = 3.2 \times 10^3 \, M^{-1}.s^{-1}$	[201]
BH_2 (Diffusion out of cell)	$k_{38} = 152.5 \, s^{-1}$	Text; [203-205]
$GTPCH \xrightarrow{Q_{BH4}} BH_4$	$Q_{BH4} = 0.5 \, nM.s^{-1}$	[206]
$O_2 + e^- (\text{NADPH oxidase/Mitochondria}) \xrightarrow{Q_{supcell}} O_2^{\bullet -}$	$Q_{supcell} = 0.01, 0.1, 1, 10, 100, 1000, 10000 \, nM.s^{-1}$	Text; [183, 184, 207, 208]

Table 3: Rate expression of various species involved in the eNOS biochemical pathway for NO and $O_2^{\bullet -}$ production and their downstream reactions.

Species	v_i (M.s^{-1})
eNOS-(Fe^{III}) (E$_{-1}$)	$k_{c-3}[eNOS - (Fe^{III}) - BH_2] - k_{c-2}[eNOS - (Fe^{III}) - BH_4]$ $- k_{c3}[BH_2][eNOS - (Fe^{III})] - k_{c2}[eNOS - (Fe^{III})][BH_4]$
eNOS-(Fe^{III})-BH$_2$ (E$_{c1}$)	$k_{c-4}[eNOS - (Fe^{III}) - BH_2 - Arg] + k_{c3}[BH_2][eNOS - (Fe^{III})] - k_{c4}[eNOS - (Fe^{III}) - BH_2][Arg]$ $- k_{c-3}[eNOS - (Fe^{III}) - BH_2]$

eNOS-(Fe^{III})-BH$_2$-Arg (E$_{c2}$)	$k_{c4}[eNOS - (Fe^{III}) - BH_2][Arg] + k_{c8}[eNOS - [Fe^{III} - O_2^-]$ $- BH_2 - Arg] - k_{c-4}[eNOS - (Fe^{III}) - BH_2$ $- Arg] - k_{c5}[eNOS - (Fe^{III}) - BH_2 - Arg]$
eNOS-(Fe^{II})-BH$_2$-Arg (E$_{c3}$)	$k_{c5}[eNOS - (Fe^{III}) - BH_2 - Arg] + k_{c-6}[eNOS - [Fe^{III}$ $- O_2^-] - BH_2 - Arg] - k_{c6}[eNOS - (Fe^{II})$ $- BH_2 - Arg][O_2]$
eNOS-[Fe^{III}-O$_2^-$]-BH$_2$-Arg or eNOS-[Fe^{II}-O$_2$]-BH$_2$-Arg (E$_{c4}$)	$k_{c6}[eNOS - (Fe^{II}) - BH_2 - Arg][O_2] - k_{c8}[eNOS - [Fe^{III}$ $- O_2^-] - BH_2 - Arg] - k_{c-6}[eNOS - [Fe^{III}$ $- O_2^-] - BH_2 - Arg]$
eNOS-(Fe^{III})-BH$_4$ (E)	$k_{c2}[eNOS - (Fe^{III})][BH_4] + k_{a-1}[eNOS - (Fe^{III}) - BH_4$ $- Arg] + k_{b1}[eNOS - (Fe^{III}) - BH_4 - NHA]$ $+ k_{b7}[eNOS - (Fe^{III}) - NO - BH_4]$ $+ k_{b9}[eNOS - (Fe^{III}) - NO - BH_4]$ $+ k_{b9}[eNOS - (Fe^{II}) - NO - BH_4]$ $- k_{c-2}[eNOS - (Fe^{III}) - BH_4] - k_{a1}[eNOS$ $- (Fe^{III}) - BH_4][Arg] - k_{b-1}[NHA][eNOS$ $- (Fe^{III}) - BH_4] - k_{b-7}[eNOS - (Fe^{III})$ $- BH_4][NO]$
eNOS-(Fe^{III})-BH$_4$-Arg (E$_{a1}$)	$k_{a1}[eNOS - (Fe^{III}) - BH_4][Arg] - k_{a-1}[eNOS - (Fe^{III})$ $- BH_4 - Arg] - k_{a2}[eNOS - (Fe^{III}) - BH_4$ $- Arg]$
eNOS-(Fe^{II})-BH$_4$-Arg (E$_{a2}$)	$k_{a2}[eNOS - (Fe^{III}) - BH_4 - Arg]$ $+ k_{a-3}[eNOS - [Fe^{III} - O_2^-] - BH_4 - Arg]$ $+ k_{13}[Arg][eNOS - (Fe^{II}) - BH_4]$ $- k_{-13}[eNOS - (Fe^{II}) - BH_4 - Arg]$ $- k_{a3}[eNOS - (Fe^{II}) - BH_4 - Arg][O_2]$
eNOS-[Fe^{III}-O$_2^-$]-BH$_4$-Arg or eNOS-[Fe^{II}-O$_2$]-BH$_4$-Arg (E$_{a3}$)	$k_{a3}[eNOS - (Fe^{II}) - BH_4 - Arg][O_2] - k_{a5}[eNOS - [Fe^{III}$ $- O_2^-] - BH_4 - Arg] - k_{a-3}[eNOS - [Fe^{III}$ $- O_2^-] - BH_4 - Arg]$
eNOS-[Fe^{III}-OOH]-BH$_3$-Arg (E$_{a4}$)	$k_{a5}[eNOS - [Fe^{III} - O_2^-] - BH_4 - Arg] - k_{a6}[eNOS - [Fe^{III}$ $- OOH] - BH_3 - Arg]$

eNOS-[Fe^{IV}-O]-BH$_3$-Arg (E$_{a5}$)	$[eNOS - (Fe^{III})] + [eNOS - (Fe^{III}) - BH_2]$ $+ [eNOS - (Fe^{III}) - BH_2 - Arg]$ $+ [eNOS - (Fe^{II}) - BH_2 - Arg]$ $+ [eNOS - [Fe^{III} - 0_2^-] - BH_2 - Arg]$ $+ [eNOS - (Fe^{III}) - BH_4]$ $+ [eNOS - (Fe^{III}) - BH_4 - Arg]$ $+ [eNOS - (Fe^{II}) - BH_4 - Arg] + [eNOS$ $- [Fe^{III} - 0_2^-] - BH_4 - Arg] + [eNOS - [Fe^{III}$ $- OOH] - BH_3 - Arg] + [eNOS - [Fe^{IV} - 0]$ $- BH_3 - Arg] + [eNOS - (Fe^{III}) - BH_3$ $- NHA] + [eNOS - (Fe^{III}) - BH_4 - NHA]$ $+ [eNOS - (Fe^{II}) - BH_4 - NHA] + [eNOS$ $- [Fe^{III} - 0_2^-] - BH_4 - NHA] + [eNOS$ $- [Fe^{III} - OOH] - BH_3 - NHA] + [eNOS$ $- (Fe^{III}) - NO - BH_4] + [eNOS - (Fe^{II})$ $- NO - BH_4] + [eNOS - (Fe^{II}) - BH_4]$ $- [eNOS]$
eNOS-(Fe^{III})-BH$_3$-NHA (E$_{a6}$)	$k_{a7}[eNOS - [Fe^{IV} - 0] - BH_3 - Arg] - k_{a8}[eNOS - (Fe^{III})$ $- BH_3 - NHA]$
eNOS-(Fe^{III})-BH$_4$-NHA (E$_{b1}$)	$k_{a8}[eNOS - (Fe^{III}) - BH_3 - NHA] + k_{b-1}[NHA][eNOS$ $- (Fe^{III}) - BH_4] - k_{b2}[eNOS - (Fe^{III}) - BH_4$ $- NHA] - k_{b1}[eNOS - (Fe^{III}) - BH_4 - NHA]$
eNOS-(Fe^{II})-BH$_4$-NHA (E$_{b2}$)	$k_{b2}[eNOS - (Fe^{III}) - BH_4 - NHA] + k_{b-3}[eNOS - [Fe^{III}$ $- 0_2^-] - BH_4 - NHA] + k_{b-12}[eNOS - (Fe^{II})$ $- BH_4][NHA] - k_{b3}[eNOS - (Fe^{II}) - BH_4$ $- NHA][0_2] - k_{b12}[eNOS - (Fe^{II}) - BH_4$ $- NHA]$
eNOS-[Fe^{III}-O$_2^-$]-BH$_4$-NHA or eNOS-[Fe^{II}-O$_2$]-BH$_4$-NHA (E$_{b3}$)	$k_{b3}[eNOS - (Fe^{II}) - BH_4 - NHA][0_2] - k_{b-3}[eNOS$ $- [Fe^{III} - 0_2^-] - BH_4 - NHA] - k_{b5}[eNOS$ $- [Fe^{III} - 0_2^-] - BH_4 - NHA]$
eNOS-[Fe^{III}-OOH]-BH$_3$-NHA (E$_{b4}$)	$k_{b5}[eNOS - [Fe^{III} - 0_2^-] - BH_4 - NHA] - k_{b6}[eNOS$ $- [Fe^{III} - OOH] - BH_3 - NHA]$
eNOS-(Fe^{III})-NO-BH$_4$ (E$_{b5}$)	$k_{b6}[eNOS - [Fe^{III} - OOH] - BH_3 - NHA] + k_{b-7}[eNOS$ $- (Fe^{III}) - BH_4][NO] - k_{b8}[eNOS - (Fe^{III})$ $- NO - BH_4] - k_{b7}[eNOS - (Fe^{III}) - NO$ $- BH_4]$

eNOS-(Fe^{II})-NO-BH$_4$ (E$_{b6}$)	$k_{b8}[eNOS - (Fe^{III}) - NO - BH_4] + k_{b-10}[NO][eNOS - (Fe^{II}) - BH_4] - k_{b10}[eNOS - (Fe^{II}) - NO - BH_4] - k_{b9}[eNOS - (Fe^{II}) - NO - BH_4]$
eNOS-(Fe^{II})-BH$_4$ (E$_{b7}$)	$k_{b10}[eNOS - (Fe^{II}) - NO - BH_4] + k_{-13}[eNOS - (Fe^{II}) - BH_4 - Arg] + k_{b12}[eNOS - (Fe^{II}) - BH_4 - NHA] - k_{b-10}[NO][eNOS - (Fe^{II}) - BH_4] - k_{b-12}[eNOS - (Fe^{II}) - BH_4][NHA] - k_{13}[eNOS - (Fe^{II}) - BH_4][Arg]$
NO	$k_{b7}[eNOS - (Fe^{III}) - NO - BH_4] + k_{b10}[eNOS - (Fe^{II}) - NO - BH_4] - k_{b-7}[NO][eNOS - (Fe^{III}) - BH_4] - k_{b-10}[eNOS - (Fe^{II}) - BH_4][NO] - 4k_{15}[NO]^2[O_2] - k_{14}[NO][O_2^{\bullet-}] - 0.22k_{27}[ONOO^-][NO] - k_{32}[NO][CO_3^{\bullet-}]$
Citrulline	$k_{b6}[eNOS - [Fe^{III} - OOH] - BH_3 - NHA]$
NHA	$k_{b1}[eNOS - (Fe^{III}) - BH_4 - NHA] + k_{b12}[eNOS - (Fe^{II}) - BH_4 - NHA] - k_{b-1}[NHA][eNOS - (Fe^{III}) - BH_4] - k_{b-12}[NHA][eNOS - (Fe^{II}) - BH_4]$
NO$_3^-$	$k_{b9}[eNOS - (Fe^{II}) - NO - BH_4] + k_{25}[ONOO^-] + k_{29}[ONOO^-][CO_2]$
O$_2^{\bullet-}$	$k_{c8}[eNOS - [Fe^{III} - O_2^-] - BH_2 - Arg] - k_{14}[NO][O_2^{\bullet-}] - k_{16}[SOD][O_2^{\bullet-}] - 0.0025k_{28}[O_2^{\bullet-}]^2 - k_{31}[O_2^{\bullet-}][CO_3^{\bullet-}] - k_{18}[BH_4][O_2^{\bullet-}]$
H$_2$O$_2$	$k_{16}[SOD][O_2^{\bullet-}] + 0.0025k_{28}[O_2^{\bullet-}]^2 + k_{18}[BH_4][O_2^{\bullet-}]$
BH$_4$	$Q_{BH_4} + 2k_{19}[BH_3]^2 + k_{20}[BH_3] + k_{c-2}[eNOS - (Fe^{III}) - BH_4] - k_{c2}[eNOS - (Fe^{III})][BH_4] - k_{33}[\bullet OH][BH_4] - k_{34}[\bullet NO_2][BH_4] - k_{35}[CO_3^{\bullet-}][BH_4] - k_{22}[BH_4][ONOO^-] - k_{17}[BH_4][O_2] - k_{18}[BH_4][O_2^{\bullet-}]$
BH$_3$	$k_{33}[\bullet OH][BH_4] + k_{34}[\bullet NO_2][BH_4] + k_{35}[CO_3^{\bullet-}][BH_4] + k_{22}[BH_4][ONOO^-] + k_{18}[BH_4][O_2^{\bullet-}] - 2k_{19}[BH_3]^2 - k_{36}[BH_3][O_2]$
BH$_2$	$k_{17}[BH_4][O_2] + k_{36}[BH_3][O_2] - k_{c-3}[eNOS - (Fe^{III}) - BH_2] - k_{c-3}[eNOS - (Fe^{III}) - BH_2] - k_{38}[BH_2]$
ONOO$^-$	$k_{14}[NO][O_2^{\bullet-}] - k_{25}[ONOO^-] - k_{26}[ONOO^-] - k_{29}[ONOO^-][CO_2] - k_{30}[ONOO^-][CO_2] - 0.22k_{27}[ONOO^-][NO] - k_{22}[BH_4][ONOO^-]$

NO_2^-	$4k_{15}[NO]^2[O_2] + 0.22k_{27}[NO][ONOO^-] + k_{32}[CO_3^{\bullet-}][NO]$ $+ k_{34}[\bullet NO_2][BH_4]$
$\bullet OH$	$k_{26}[ONOO^-] - k_{33}[\bullet OH][BH_4]$
$\bullet NO_2$	$k_{26}[ONOO^-] + k_{30}[ONOO^-][CO_2] + 0.22k_{27}[ONOO^-][NO]$ $- k_{34}[\bullet NO_2][BH_4]$
$CO_3^{\bullet-}$	$k_{30}[ONOO^-][CO_2] - k_{31}[CO_3^{\bullet-}][O_2^{\bullet-}] - k_{32}[CO_3^{\bullet-}][NO]$ $- k_{35}[CO_3^{\bullet-}][BH_4]$
R_{NO} (NO Production)	$k_{b7}[eNOS - (Fe^{III}) - NO - BH_4] + k_{b10}[eNOS - (Fe^{II})$ $- NO - BH_4]$
$R_{O_2^{\bullet-}}$ (Superoxide Production)	$k_{c8}[eNOS - [Fe^{III} - O_2^-] - BH_2 - Arg]$

The cellular oxidative stress and BH_4 synthesis are represented by production rate terms for $O_2^{\bullet-}$ ($Q_{supcell}$) and BH_4 (Q_{BH_4}). $Q_{supcell}$ ($M.s^{-1}$) represent the sum of $O_2^{\bullet-}$ production rate from non-eNOS based sources including NADPH and xanthine oxidase, and mitochondria, while Q_{BH_4} ($M.s^{-1}$) represent the rate of BH_4 synthesis by guanosine triphosphate cyclohydrolase I (GTPCH). GTPCH is a key enzyme in *de novo* synthesis pathway for the endogenous production of BH_4 [94, 133]. The activity of GTPCH is reported to increase [134, 135] or reduce [136] in oxidative stress conditions. We have accounted for the extracellular diffusion of BH_2 (k_{38}) since BH_4 is reported to have very low permeability across the endothelial cell membrane [209] and BH_3 has an extremely short half-life [144]. The main downstream reactions include (i) the reaction between NO and $O_2^{\bullet-}$ to form $ONOO^-$, which is in an acid-base equilibrium with peroxynitrous acid (ONOOH), (ii) the formation of RNS ($\bullet NO_2$) and ROS ($\bullet OH$ and $CO_3^{\bullet-}$) from the interaction of $ONOO^-$ with CO_2 and NO, respectively and by dissociation of ONOOH, (iii) the self and SOD-catalyzed dismutation of $O_2^{\bullet-}$ to form H_2O_2 , (iv) the oxidation of BH_4 to biopterin radical (BH_3) by ROS ($O_2^{\bullet-}$, $\bullet OH$ and $CO_3^{\bullet-}$) and RNS ($ONOO^-$ and $\bullet NO_2$), and (v) the oxidation of BH_4 and BH_3 to BH_2 by O_2.

3.2.2. Model Assumptions

The current model is developed for dimeric eNOS since $O_2^{\cdot-}$ generated from monomeric eNOS is negligible compared to dimeric eNOS [23, 210].

1) The NO production rate is assumed to be independent of the geometrical location of eNOS within the endothelial cell based on an earlier eNOS catalysis modeling study [187].

2) All chemical species involved in the eNOS biochemical pathways and downstream reactions are assumed to have uniform concentration within the endothelial cell similar to earlier modeling studies of eNOS catalysis [93, 170, 187].

3) The model accounts for eNOS uncoupling due to oxidative depletion of BH_4 and binding of BH_2 to eNOS. Other molecular mechanisms for eNOS uncoupling including protein phosphorylation, S-glutathionylation requires eNOS modification and are not considered in this study [211].

3.2.3. Computational Model

The model equations are formulated by applying the law of mass action kinetics to the chemical species involved in the eNOS biochemical pathways and the downstream reactions. A total of 33 distinct chemical species are involved in the eNOS biochemical pathways and downstream reactions. We have used 33 rate equations to model the temporal changes in concentration of these species. Mathematically, the rate equations for 32 of these chemical species including BH_4 and BH_2 can be represented as:

$$\frac{d[S_i]}{dt} = V_i \tag{1}$$

In equation (1), $[S_i]$ (in M) represents the concentration of the ith chemical species. V_i (in $M.s^{-1}$) represents the rate expression of the ith chemical species. Mathematically, V_i represents the

summation of the generation rates subtracted by the consumption rates of species i from its participating reactions. To account for the mass conservation of eNOS, the rate equation of an intermediate eNOS-substrate complex (33rd species) was set in the form of an algebraic equation as follows:

$$[eNOS] = [E] + [E_{-1}] + \sum[E_{ai}] + \sum[E_{bi}] + \sum[E_{ci}] \tag{2}$$

In equation (2), [E] and [E$_{-1}$] represent the different forms of native eNOS. [E$_{ai}$], [E$_{bi}$] and [E$_{ci}$] represent the different forms of the eNOS-substrate complex while [eNOS] represents the total eNOS concentration. In addition to the 33 rate equations described above, 2 other rate equations were used to represent NO and O$_2^{\bullet-}$ production rates, respectively. The rate equations of NO and O$_2^{\bullet-}$ production includes the summation of the generation terms for the respective species. The expressions of V$_i$ for the 35 different rate equations are shown in Table 2.

3.2.4. Model Parameters

The key model parameters in this study are the rate constants for the different reactions involved, enzyme concentration, substrate concentration, co-factor concentration, rate of extracellular diffusion of BH$_2$ (k$_{38}$), BH$_4$ synthesis rate by GTPCH (Q$_{BH_4}$) and O$_2^{\bullet-}$ production rate from non-eNOS based sources (Q$_{supcell}$). The model parameters involving eNOS biochemical pathway related NO and O$_2^{\bullet-}$ production and their downstream reactions are listed in Table 4. Most of these parameters and reaction rate constants were adopted from literature based on the previous computational modeling work on eNOS catalysis [93, 170]. The rate constants that were measured at different temperatures were scaled up to the physiologically relevant temperature of 37ºC using the Arrhenius equation as detailed in Kar and Kavdia [93]. Some of the rate constants used in our model, as detailed in Table 1, were obtained from neuronal NOS (k$_{c2}$, k$_{c-2}$, k$_{c3}$, k$_{c-3}$) and inducible NOS (kc$_5$) isoforms. The [TBP] at t=0 minute was set at an initial value of 7 µM based on reported

BH_4 concentration of 2.6 pmol/10^6 cells in endothelial cells [212] and oxidized biopterin represents

a small amount (~5–10%) of total biopterin under normal physiologic conditions [95].

Table 4: Kinetic parameters related to eNOS biochemical pathways for NO and $O_2^{\cdot-}$ production

Variable/Constant	Values and Units	References
[eNOS]	0.097 μM	[93, 170, 187]
V_{max} (eNOS)	0.585 μmol min^{-1}.mg^{-1}	[187, 213]
[NADPH]	166-295 μM	[214]
[CaM]	5 μM	[215]
[Ca^{2+}]	0.013-0.280 μM	[214, 216]
[L-Arginine]	100 μM	[93, 170]
[O_2]	140 μM	[93, 170]
[CO_2]	1.1 mM	[93, 170]
[SOD]	10 μM	[93, 170]
K_m (NADPH)	0.65 μM	[213]
K_m (O_2)	7.7 μM	[217]
K_m (L-Arginine)	2.9-5 μM	[187, 213]
EC_{50} (Ca^{2+})	0.11 μM	[187, 213]
EC_{50} (CaM)	0.009 μM	[187, 213]
Endothelial cell volume	400 μm^3	[187]
Endothelial cell radius	10-20 μm	[187]
Endothelial cell thickness	0.5-1.0 μm	[187]
BH_2 diffusion coefficient	1×10^{-9} m^2.s^{-1}	[205, 209]

Under physiologic conditions, the reported activity of GTPCH was 7 pmoles.mg protein^{-1}.hr^{-1} [206]. This corresponds to Q_{BH_4} of 0.5 nM.s^{-1} based on reported values of endothelial cell dimensions and total protein content [93, 187]. Hasegawa and co-workers [204, 205, 218]

measured the transport parameters (diffusion coefficient and permeability) related to extracellular diffusion of BH_2. Based on their reported values and endothelial cell dimensions [93, 187], the apparent first order rate constant [203] for extracellular BH_2 diffusion (k_{38}) was estimated to be 152.5 s^{-1}. To assess the role of oxidative stress on eNOS catalysis, we used $Q_{supcell}$ values of 0.01, 0.1, 1, 10, 100, 1000 and 10000 $nM.s^{-1}$. This range was established based on the reported endothelial $O_2^{\bullet-}$ production rates of 0.016 $nM.s^{-1}$ to 6000 $nM.s^{-1}$ under normal and oxidative stress experimental conditions [93, 183, 199, 207, 219, 220]. To represent initial state of eNOS coupling or uncoupling, we used a biopterin ratio ($[BH_4]/[TBP]$) of 0.99, 0.7, 0.25 and 0.05 at t=0 minute [170, 221].

3.2.5. Numerical Solution

The rate equations in the form of equation (1) or (2) as listed in Table 2 were solved numerically with the appropriate initial conditions using the MATLAB (Mathworks Inc, Natick, MA) ordinary differential equation solver *ode15s*. The relative and absolute error tolerance values were set at 1×10^{-10} and 1×10^{-15} respectively. The simulations were run for 5×10^5 s (8333 minutes) such that all the chemical species participating in the eNOS biochemical pathways and downstream reactions attain steady state.

3.3. Results

3.3.1. NO production rate is independent of the initial state of eNOS coupling for $Q_{supcell} \leq 1$ $nM.s^{-1}$

We analyzed the temporal changes in the eNOS related NO and $O_2^{\bullet-}$ production rates, biopterin ratio and TBP levels at the $Q_{supcell}$ of 0.01, 0.1, and 1 $nM.s^{-1}$. These $Q_{supcell}$ values represent the normal physiological or basal $O_2^{\bullet-}$ production from endothelial cells [199, 207, 220]. The $[BH_4]/[TBP]$ @ t=0 minute was set at 0.99, 0.7, 0.25 and 0.05. The BH_4 synthesis was set at Q_{BH4}

$= 0.5$ nM.s^{-1}. For all simulations, the intracellular concentration of eNOS, L-arginine, O_2, CO_2 and initial [TBP] were maintained at 0.097 µM, 100 µM, 140 µM, 1.1 mM and 7 µM, respectively.

The steady state eNOS NO production is independent of initial biopterin ratio and is constant for $Q_{supcell}$ between 0.01 and 1 nM.s^{-1}. Figure 7A and C shows the temporal variation in the eNOS based NO and $O_2^{\bullet-}$ production rates at the $Q_{supcell}$ of 0.01 and 1 nM.s^{-1}. The data for 0.1 nM.s^{-1} $Q_{supcell}$ is not shown as the data was similar to that of at the $Q_{supcell}=0.01$ nM.s^{-1}. For $Q_{supcell}$ at 0.01 and 1 nM.s^{-1}, the NO production rate profiles did not change and reached a steady state value of 26.5 and 26.4 nM.s^{-1}, respectively. These NO production rate profiles were irrespective of [BH$_4$]/[TBP] @ t=0 minute set at 0.99, 0.7, 0.25 and 0.05, respectively. However, the $O_2^{\bullet-}$ production rate initially increased to reach a peak value in less than 9 minutes and later reached a steady state value equal to the respective $Q_{supcell}$.

This temporal change was dependent on the [BH$_4$]/[TBP] @ t=0 minute and reflect the eNOS related $O_2^{\bullet-}$ production above the respective $Q_{supcell}$. The peak value of eNOS related $O_2^{\bullet-}$ production rate was 12 pM.s^{-1} for the [BH$_4$]/[TBP] @ t=0 minute of 0.05 and $Q_{supcell}$ between 0.01 and 1 nM.s^{-1}. For $Q_{supcell}$ between 0.01 and 1 nM.s^{-1}, the [BH$_4$]/[TBP] at steady state was 0.99 (Figure 7B and D). The steady state [TBP] decreased with increasing $Q_{supcell}$. The steady state [TBP] were 5.9, 5.7 and 3.8 µM at the $Q_{supcell}$ of 0.01, 0.1, and 1 nM.s^{-1}, respectively.
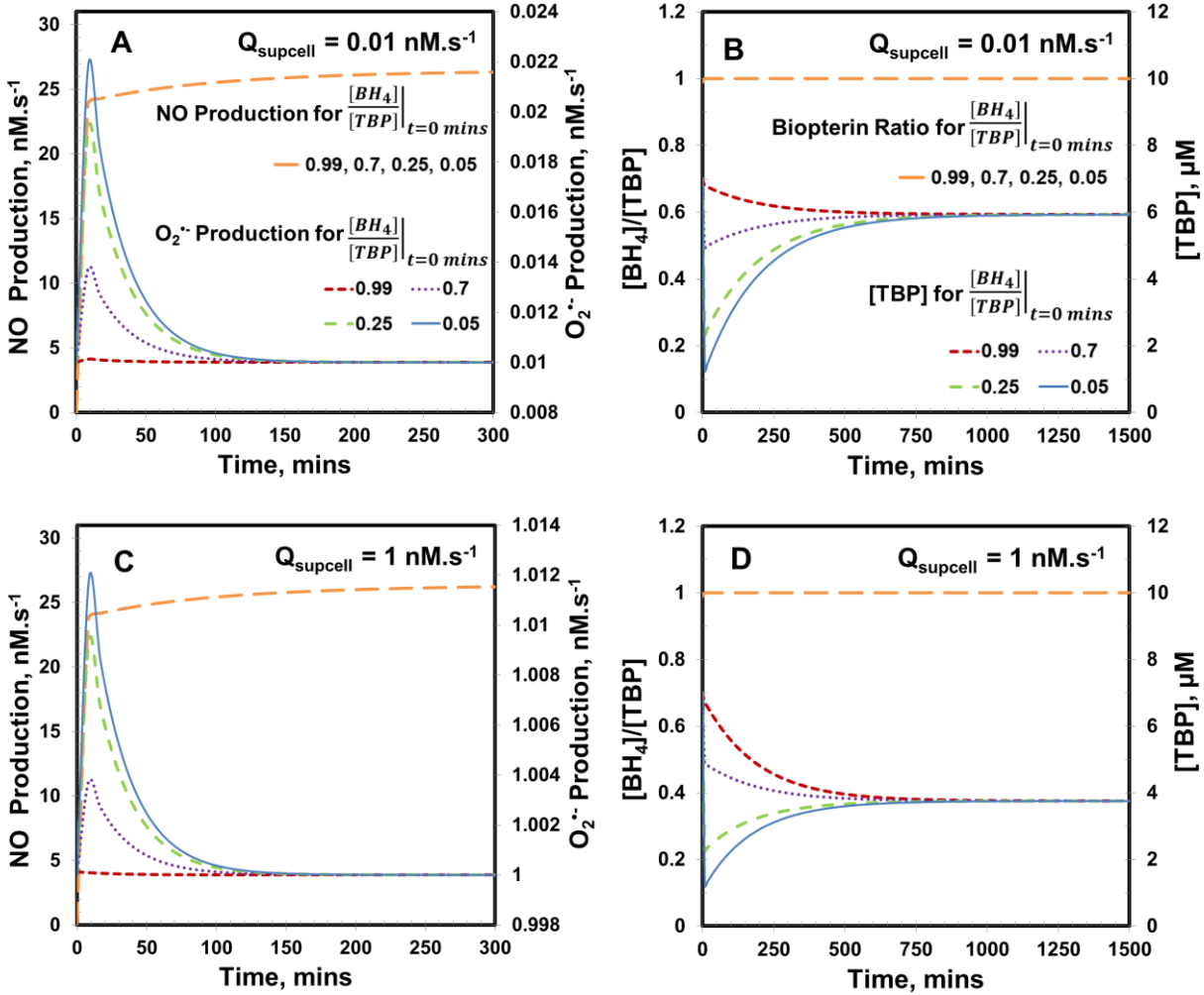
Figure 7: Temporal variations in eNOS NO and $O_2^{\bullet-}$ production rates, $[BH_4]/[TBP]$ and $[TBP]$ for normal physiologic conditions. Panel A and C shows the time dependent variation in NO and $O_2^{\bullet-}$ production rates at Qsupcell = 0.01 and 1 $nM.s^{-1}$, respectively. Panel B and D represents the temporal variation in the $[BH_4]/[TBP]$ and $[TBP]$ at Qsupcell = 0.01 and 1 $nM.s^{-1}$, respectively. The $[BH_4]/[TBP]$ @ t=0 minute were set at 0.99, 0.7, 0.25 and 0.05, respectively. The concentrations of L-arginine, O2, SOD, CO2 and eNOS were set at 100 µM, 140 µM, 10 µM, 1.1 mM and 0.097 µM, respectively. The Q_{BH4} was set at 0.5 $nM.s^{-1}$. The $[TBP]$ @ t=0 minute was set at 7 µM for all the cases simulated. The profiles for Qsupcell = 0.1 $nM.s^{-1}$, which are similar to that of at 0.01 $nM.s^{-1}$, are not shown.

3.3.2. Extent of oxidative stress determines eNOS uncoupling in endothelial cells

Persisting oxidative stress renders eNOS uncoupled that can further potentiate cellular oxidative stress [140]. To understand the effect of cellular oxidative stress levels on eNOS related

NO and $O_2^{\bullet-}$ production, $Q_{supcell}$ was increased to 10, 100, 1000 and 10000 nM.s^{-1}. The results show that variation in endothelial cell oxidative stress level increases the extent of eNOS uncoupling and introduces instabilities in the eNOS based NO production rate. Figure 8A-D shows the temporal profile of eNOS catalyzed NO production rate. For $Q_{supcell}$ of 10 nM.s^{-1} (Figure 8A), the NO production rate reached a peak value of 23.0-24.0 nM.s^{-1} in 17-75 minutes for the [BH$_4$]/[TBP] @ t=0 minute of 0.05-0.99, respectively. The NO production rates subsequently reduced with time to reach a minimum of 0.45-0.43 nM.s^{-1} in 876-959 minutes for the [BH$_4$]/[TBP] @ t=0 minute of 0.05-0.99, respectively. Thereafter, the NO production rates exhibited an oscillatory profile with 6.4 nM.s^{-1} amplitude of the oscillations.

For $Q_{supcell}$ 100 nM.s^{-1} (Figure 8B), the NO production rates initially increased to reach maximum values ranging from 17.0-18.0 nM.s^{-1} in 8 minutes. The NO production rates subsequently reduced to a minimum value of 0.005 nM.s^{-1} within 1893-1952 minutes. Thereafter, the NO production rates exhibited an oscillatory profile in the time range of 1893-2519 minutes. After 2519 minutes, the oscillations damped out to reach a new steady state value of 2.0 nM.s^{-1}.

For $Q_{supcell}$ 1000 and 10000 nM.s^{-1} (Figure 8C and D), the NO production rate increased to reach a peak followed by a reduction to a minimum and then demonstrated a step change increase \to reach a new steady state value. The peak NO production rate ranged from 14.4-16.6 nM.s^{-1} for $Q_{supcell}$ of 1000 nM.s^{-1} and 13.9-16 nM.s^{-1} for $Q_{supcell}$ of 10000 nM.s^{-1}. A minimum NO production rate of 0.004 nM.s^{-1} was reached for both the $Q_{supcell}$. The steady-state NO production rate of 1.9 nM.s^{-1} was reached within 1851-2044 minutes for $Q_{supcell}$ 1000 nM.s^{-1} and 1.5 nM.s^{-1} was reached within 1900-2135 minutes for $Q_{supcell}$ of 10000 nM.s^{-1}.
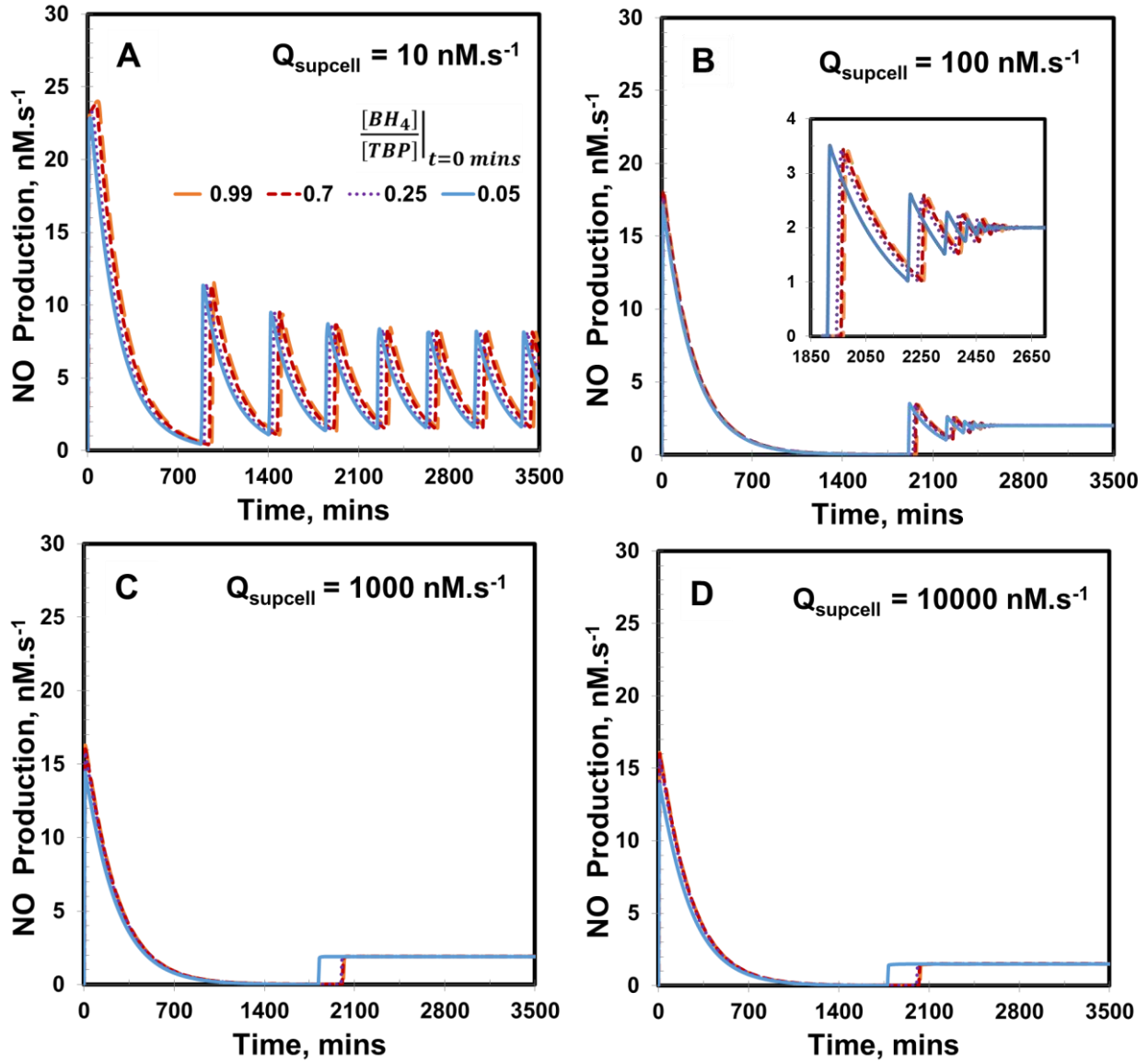
Figure 8: Cellular oxidative stress and eNOS NO production rate. Panels A-D show the temporal variation in eNOS NO production rate for increase in $Q_{supcell}$ from 10, 100, 1000 and 10000 nM.s^{-1}, respectively. The concentrations of L-arginine, O_2, SOD, CO_2 and eNOS were 100 µM, 140 µM, 10 µM, 1.1 mM and 0.097 µM, respectively. Q_{BH4} was 0.5 nM.s^{-1}. The [TBP] @ t=0 minute was 7 µM. The [BH4]/[TBP] @ t=0 minute was 0.99, 0.7, 0.25 and 0.05, respectively. The inset in Panel B shows the magnified view of the oscillations in the temporal profile of eNOS NO production rate in the time range of 1850-2650 minutes at Qsupcell = 100 nM.s^{-1}.

The overall endothelial cell $O_2^{\bullet-}$ production rates remained the same as the respective $Q_{supcell}$ (results not shown). The eNOS based $O_2^{\bullet-}$ production ranged from 0.0-0.012 nM.s^{-1} for the

oxidative stress conditions simulated in this study. Thus, eNOS uncoupling had minimal effect on the endothelial cell $O_2^{\bullet-}$ production at higher $Q_{supcell}$.

3.3.3. Oxidative stress induces temporal perturbations in the biopterin ratio

To understand the oxidative stress dependent variation of the eNOS based NO and $O_2^{\bullet-}$ production rates, Figure 9A-D shows the temporal variation in [BH4]/[TBP] for $Q_{supcell}$ 10, 100, 1000 and 10000 $nM.s^{-1}$, respectively for all values of [BH4]/[TBP] @ t=0 minute.

For $Q_{supcell}$ of 10 $nM.s^{-1}$ (Figure 9A), the [BH4]/[TBP] showed oscillatory profile with similar amplitude and frequency for all values of [BH4]/[TBP] @ t=0 minute. However, there was a time delay in the oscillation which increased with increasing [BH4]/[TBP] @ t=0 minute values. The oscillation did not dampen with time. For $Q_{supcell}$ of 100 $nM.s^{-1}$ (Figure 9B), the [BH4]/[TBP] showed an oscillatory behavior that damped with time to reach a steady state value of 0.26 for all initial [BH4]/[TBP] @ t=0 minute values. However, the oscillation-amplitude were lower and frequency were higher for $Q_{supcell}$ at 100 $nM.s^{-1}$ compared to the oscillation-amplitude and frequency for $Q_{supcell}$ at 10 $nM.s^{-1}$. For $Q_{supcell}$ of 1000 and 10000 $nM.s^{-1}$ (Figure 9C and D), we observed a pulse in the [BH4]/[TBP] profile before reaching a steady state value of 0.25 and 0.2, respectively for all initial values of [BH4]/[TBP] @ t=0 minute. There was a delay in the pulse with increasing initial [BH4]/[TBP] @ t=0 minute values.

The [BH4]/[TBP] profiles clearly demonstrates that oxidative stress renders an imbalance between BH4 synthesis and oxidation and induces temporal perturbations in the biopterin ratio. The perturbations in the biopterin ratio causes pertubations in eNOS NO production rate (as shown in Figure 8) and thus leads to eNOS uncoupling.
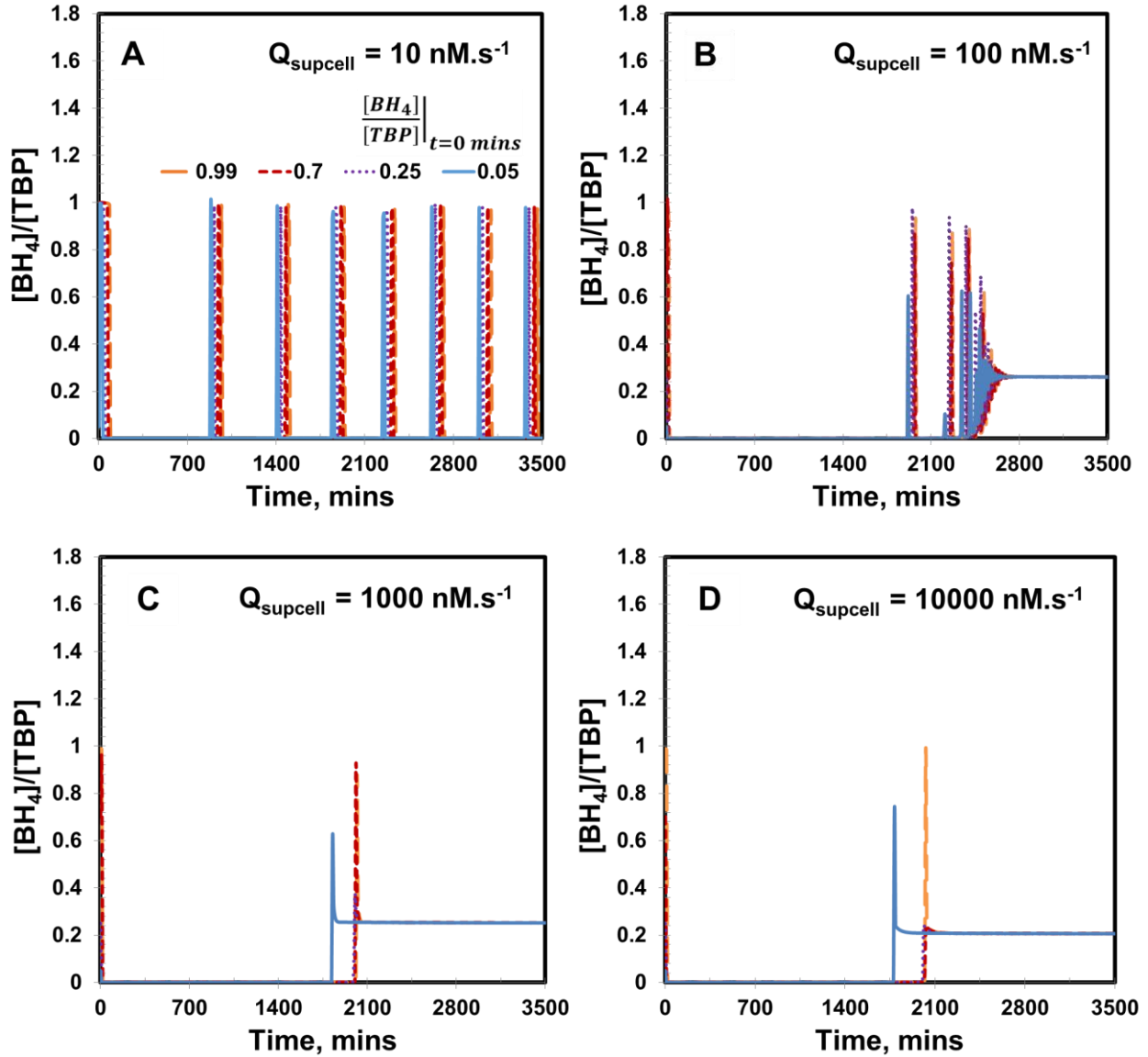
Figure 9: Cellular oxidative stress and biopterin ratio ([BH4]/[TBP]). Panels A-D show the temporal variation in the [BH4]/[TBP] corresponding to $Q_{supcell}$ values of 10, 100, 1000 and 10000 nM.s⁻¹, respectively. The [BH4]/[TBP] @ t=0 minute were 0.99, 0.7, 0.25 and 0.05, respectively. The concentrations of L-arginine, O_2, SOD, CO_2 and eNOS were set at 100 µM, 140 µM, 10 µM, 1.1 mM and 0.097 µM, respectively. The Q_{BH4} was 0.5 nM.s⁻¹ and [TBP] @ t=0 minute was 7 µM.

3.3.4. Enhancement of BH₄ synthesis may restore eNOS coupling under oxidative stress conditions

In addition to altered expression of GTPCH during oxidative stress condition, *de novo* synthesis of BH$_4$ has been targeted as a novel therapeutic approach for the treatment of endothelial dysfunction [26, 222]. To understand the effect of enhanced BH$_4$ synthesis on eNOS coupling under oxidative stress conditions, we simulated eNOS based NO production in endothelial cells at Q_{BH4} values of 0.5, 1, 1.5 and 5 nM.s^{-1} for increase in $Q_{supcell}$ from 0.01 to 10000 nM.s^{-1}. For these simulations, we used initial [BH$_4$]/[TBP] @ t=0 minute of 0.05. For an increase in the Q_{BH4}, the eNOS NO production and biopterin ratio increased at oxidative stress levels above 1 nM.s^{-1} and [TBP] increased at all oxidative stress levels (Figure 10 and 6). In addition, the time required for eNOS NO production to reach steady state reduced in all simulation above $Q_{supcell}$ of 1 nM.s^{-1}. For increase in $Q_{supcell}$ from 0.01 to 1 nM.s^{-1} (results not shown), the NO production remained constant at 26.5 nM.s^{-1} for all Q_{BH4} rates simulated.

For $Q_{supcell}$ of 10 nM.s^{-1} (Figure 10A), at Q_{BH4}=1.5 nM.s^{-1} and above, the eNOS NO production was 25.3 nM.s^{-1}, similar to normal physiologic predictions of eNOS NO production. In addition, there were oscillations in eNOS NO production at Q_{BH4}=0.5 and 1 nM.s^{-1} that disappeared at $Q_{BH4} \geq 1.5$ nM.s^{-1}. For $Q_{supcell}$ of 100 nM.s^{-1} (Figure 10B), the steady state eNOS NO production rates were 2.0, 4.1, 6.2 and 20.0 nM.s^{-1} at Q_{BH4}=0.5, 1, 1.5 and 5 nM.s^{-1}, respectively. This represents a 10-fold increase in eNOS NO production for a 10-fold increase in Q_{BH4}. At Q_{BH4} of 0.5, 1, 1.5 and 5 nM.s^{-1}, the steady state eNOS NO production rates were 1.9, 3.8, 5.6 and 16.0 nM.s^{-1}, respectively for $Q_{supcell}$ of 1000 nM.s^{-1} (Figure 10C) and were 1.5, 3.0, 4.4 and 12.2 nM.s^{-1}, respectively for $Q_{supcell}$ of 10000 nM.s^{-1} (Figure 10D). This represents a maximum of 8-fold increase in NO production for a 10-fold increase in Q_{BH4} at higher $Q_{supcell}$ (1000-10000 nM.s^{-1}).
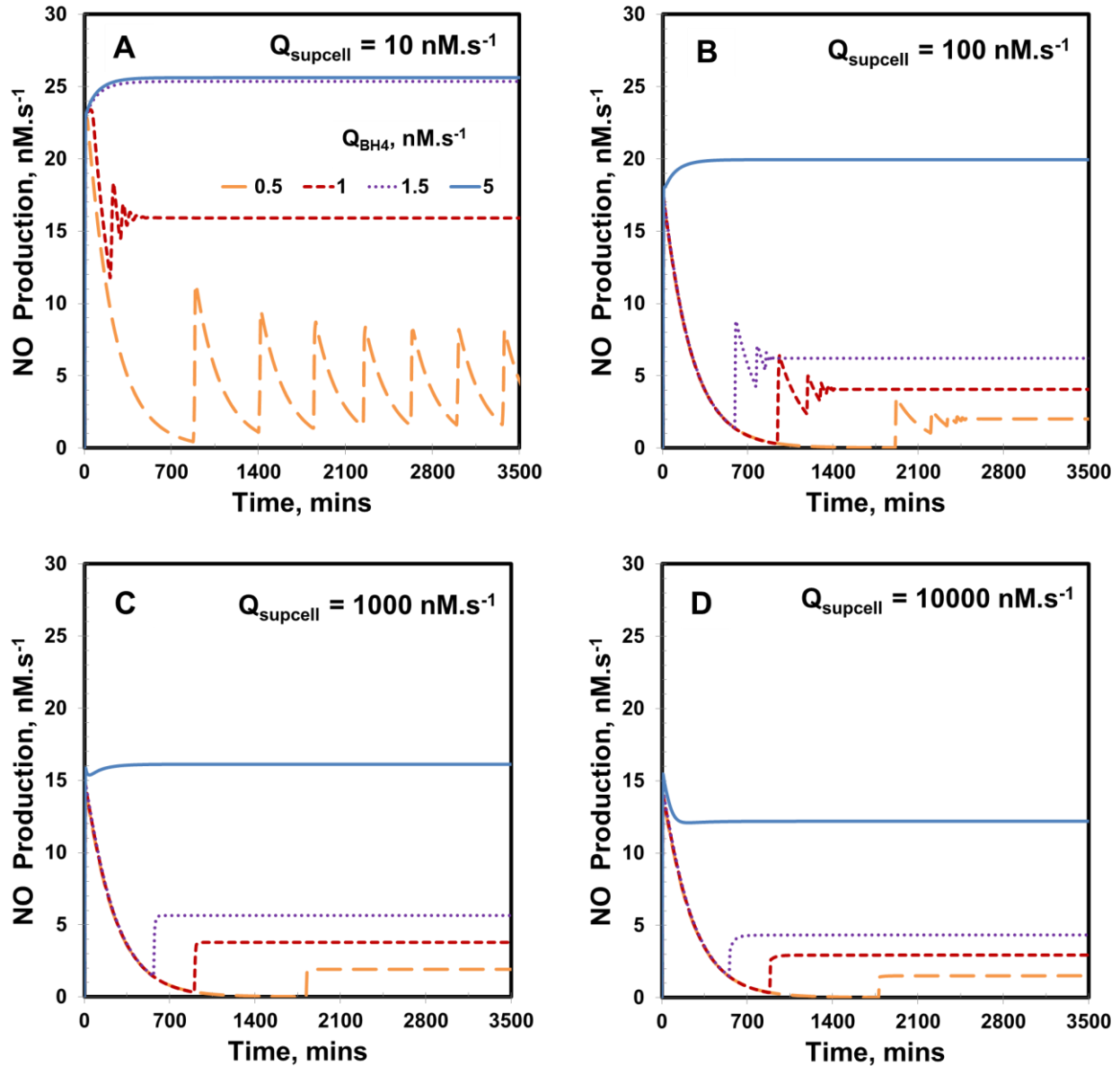
Figure 10: Effect of increased BH₄ synthesis and cellular oxidative stress on eNOS NO production rate. Panels A-D show the temporal variation in the eNOS NO production rate with increasing Q_{BH4} corresponding to $Q_{supcell}$ of 10, 100, 1000 and 10000 $nM.s^{-1}$, respectively. The increase in Q_{BH4} were set at 0.5, 1, 1.5 and 5 $nM.s^{-1}$. The [BH₄]/[TBP] @ t=0 minute was 0.05 and [TBP] @ t=0 minute was 7 µM. The concentrations of L-arginine, O₂, SOD, CO₂ and eNOS were set at 100 µM, 140 µM, 10 µM, 1.1 mM and 0.097 µM, respectively.

Even though the [TBP] increased with Q_{BH4}, the [TBP] was affected from cellular oxidative

stress (Figure 11A). The [TBP] did not reach to normal levels and remained below 1 µM under

oxidative stress conditions except for Q_{BH4} 5 $nM.s^{-1}$ at $Q_{supcell}$=10 $nM.s^{-1}$. For increase in Q_{BH4} from 0.5 to 5 $nM.s^{-1}$, the [TBP] increased from 5.9 to 59.5 µM for $Q_{supcell}$=0.01 $nM.s^{-1}$; 5.7 to 59.2 µM for $Q_{supcell}$=0.1 $nM.s^{-1}$; 3.75 to 56.6 µM for $Q_{supcell}$=1 $nM.s^{-1}$; 0.002 to 32.8 µM for $Q_{supcell}$=10 $nM.s^{-1}$; 0.002 to 0.02 µM for $Q_{supcell}$=100 $nM.s^{-1}$; 0.001 to 0.03 µM for $Q_{supcell}$=1000 $nM.s^{-1}$ and 0.001 to 0.02 µM for $Q_{supcell}$=10000 $nM.s^{-1}$.

The steady state biopterin ratio remained 0.99 for all simulated Q_{BH4} rates for $Q_{supcell} \leq 1$ $nM.s^{-1}$ (Figure 11B). For $Q_{supcell}$ of 10 $nM.s^{-1}$, the [BH$_4$]/[TBP] were 0.4, 0.7, 0.99, and 0.99 for Q_{BH4} of 0.5, 1, 1.5 and 5 $nM.s^{-1}$, respectively. For $Q_{supcell}$ of 100, 1000 and 10000 $nM.s^{-1}$, the [BH$_4$]/[TBP] increased from 0.26 to 0.94, 0.25 to 0.66, and 0.2 to 0.36, respectively for increase in Q_{BH4} from 0.5 to 5 $nM.s^{-1}$. For oxidative stress above 100 $nM.s^{-1}$, the biopterin ratio improved significantly for 10-fold increase in BH$_4$ synthesis.
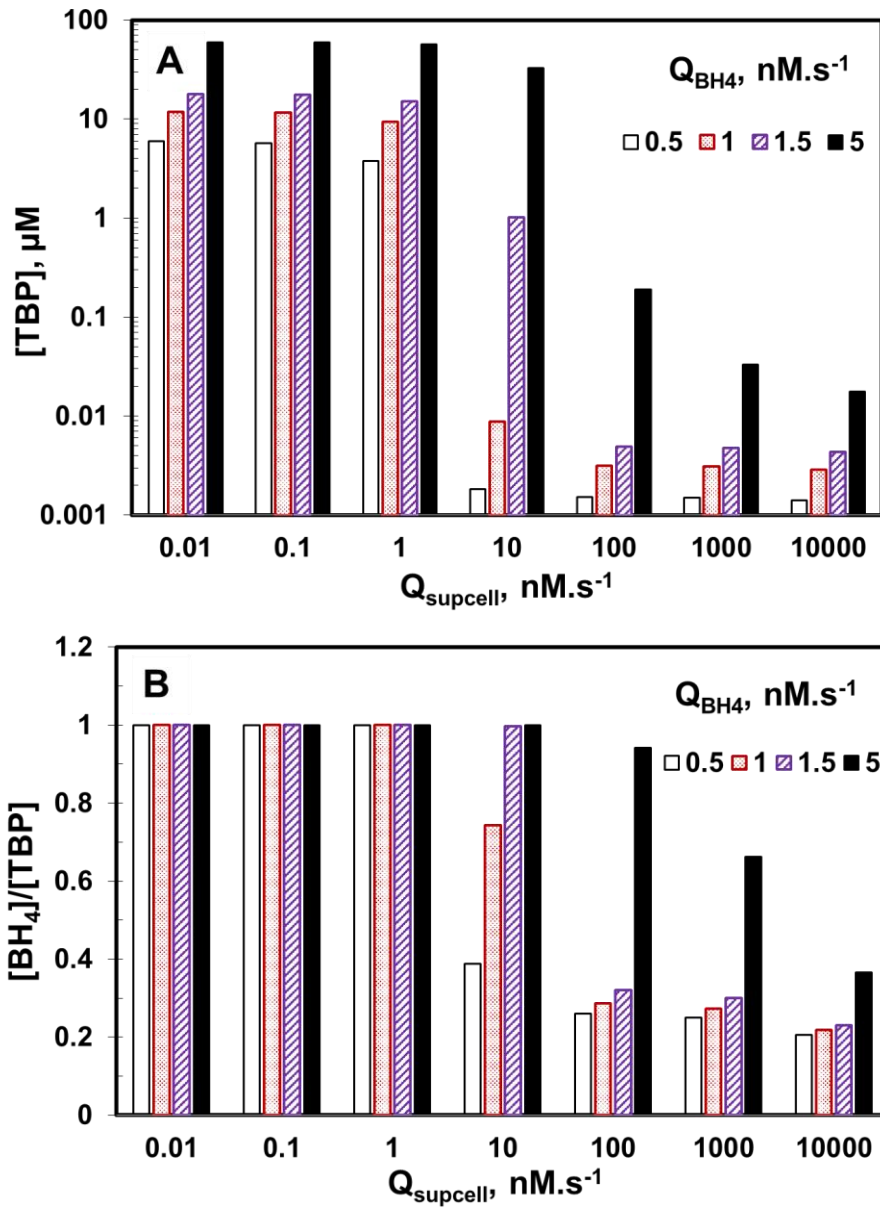
Figure 11: Effect of increased BH₄ synthesis and cellular oxidative stress on [TBP] and biopterin ratio. Panel A shows temporal variation in the [TBP] and Panel B shows temporal variation in the [BH₄]/[TBP] corresponding to the Q_{BH4} of 0.5, 1, 1.5 and 5 nM.s^{-1} @ t=0 minute in oxidative stress condition. The $Q_{supcell}$ were set at 0.01, 0.1, 1, 10, 100, 1000 and 10000 nM.s^{-1}. The [BH₄]/[TBP] @ t=0 minute were set at 0.99, 0.7, 0.25 and 0.05 respectively. The concentrations of L-arginine, O_2, SOD, CO_2 and eNOS were set at 100 µM, 140 µM, 10 µM, 1.1 mM and 0.097 µM, respectively. The [TBP] @ t=0 minute was set at 7 µM for all the simulated cases.

3.3.5. Sensitivity analysis for eNOS related $O_2^{\bullet-}$ production

The maximum eNOS $O_2^{\bullet-}$ production rate at $Q_{supcell}$ of 0.01, 0.1, 1, 10, 100, 1000 and 10000 $nM.s^{-1}$ were 11.769, 11.770, 11.772, 11.793, 11.960 and 12.245 $pM.s^{-1}$ respectively. As the $O_2^{\bullet-}$ production rate due to eNOS uncoupling stayed near 12 $pM.s^{-1}$, even though we increased non-eNOS based cellular oxidative stress, we inferred that eNOS uncoupling contributes negligibly towards endothelial cell oxidative stress. A sensitivity analysis for the rate constants involved in eNOS $O_2^{\bullet-}$ production was performed. The sensitivity analysis was performed mainly on the forward rate constants involved in the eNOS uncoupling pathway leading to $O_2^{\bullet-}$ production. The rate constants analyzed were k_{c3}, k_{c4}, k_{c5}, k_{c6}, k_{c8}, k_{38}, k_{17} and k_{36} at $Q_{supcell}$ of 1 and 100 $nM.s^{-1}$ at initial biopterin ratio of 0.05 and Q_{BH4} of 0.5 $nM.s^{-1}$ at t=0 minute. The sensitivity analysis for these rate constants was performed in the range of 50 to 200 % where, 100% indicates the control value of the respective rate constant. The results from the sensitivity analysis showed that the decrease in diffusion rate of BH_2 (k_{38}) increases the eNOS $O_2^{\bullet-}$ production rate at physiologic and oxidative stress condition (Figure 12). The increase in rate constant k_{c3}, k_{c4} and k_{c5} increases the eNOS $O_2^{\bullet-}$ production rate. The rate constants k_{c6}, k_{c8} and k_{36} does not affect the eNOS $O_2^{\bullet-}$ production rate. The increase in the oxidation rate of BH_4 (k_{17}) increases the eNOS $O_2^{\bullet-}$ production at $Q_{supcell}$ of 1 $nM.s^{-1}$ but is insensitive at $Q_{supcell}$ of 100 $nM.s^{-1}$. The range in which the eNOS $O_2^{\bullet-}$ production rate changed was 0.5 to 4 $x10^{-6}$ $nM.s^{-1}$ for $Q_{supcell}$ of 1 $nM.s^{-1}$. This eNOS $O_2^{\bullet-}$ production rate further decreased by three orders of magnitude when $Q_{supcell}$ increased to 100 $nM.s^{-1}$.
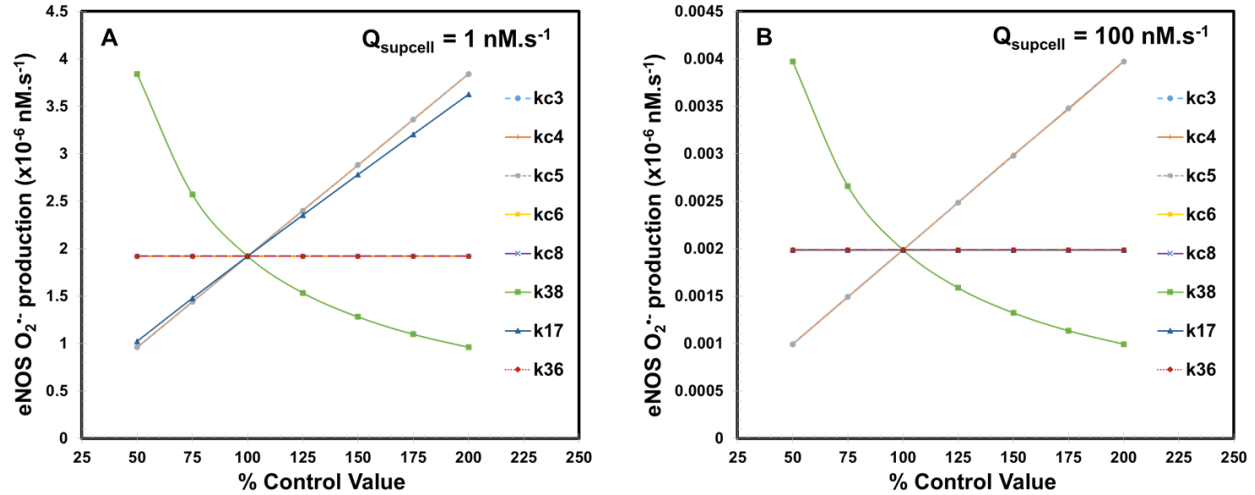
Figure 12: Sensitivity analysis for eNOS related $O_2^{•-}$ production. Panel A and B represents the steady state eNOS $O_2^{•-}$ production rate for $Q_{supcell}$ of 1 and 100 $nM.s^{-1}$, respectively. The % control values at 100 represents the base value of respective rate constant. The rate constant k_{c3}, k_{c4}, k_{c5}, k_{c6} and k_{c8} are involved in eNOS biochemical pathway for $O_2^{•-}$ production. The rate constants k_{17} and k_{36} are oxidation rates of BH_4 and BH_3 respectively and k_{38} is the diffusion rate of BH_2 out of the cell. The $[BH_4]/[TBP]$ was 0.05, Q_{BH4} was 0.5 $nM.s^{-1}$ and $[TBP]$ was 7 μM @ t=0 minute. The concentrations of L-arginine, O_2, SOD, CO_2 and eNOS were set at 100 μM, 140 μM, 10 μM, 1.1 mM and 0.097 μM, respectively.

3.4. Discussions

In this study, we investigated the impact of cellular oxidative stress and BH_4 on eNOS NO production and the biopterin ratio in endothelial cells. We found that oxidative stress reduces eNOS NO production and sets an oscillatory profile in endothelial NO production and biopterin ratio. Furthermore, the enhancement of BH_4 synthesis may improve eNOS coupling and NO production under oxidative stress condition.

3.4.1. eNOS remains coupled under normal physiologic conditions with small perturbations in oxidative stress

Vascular endothelial cells maintains basal levels of BH_4 synthesis [180, 223] and ROS production [27, 181, 223] under normal physiologic conditions. The redox homeostasis of

endothelial cells is maintained by a low amount of ROS production [224-226] and the presence of antioxidant enzymes [170, 227] and/or reducing agents including ASC and GSH [142, 228]. Under physiologic conditions, endothelial cells maintain its functions such as sustained NO production rate, BH_4 levels, and eNOS remains coupled [25, 229]. Similar observations were found in the present study. Oxidative stress in the range of 0.01 to 1 $nM.s^{-1}$ did not affect steady state NO production rate (~26.5 $nM.s^{-1}$). The model predicted that the steady state eNOS NO production and biopterin ratio are independent of the initial-biopterin ratio or state of eNOS coupling for $Q_{supcell}$ of 0.01 to 1 $nM.s^{-1}$. In addition, this NO production rate is in agreement with the experimental measurements from purified coupled eNOS at 1 µM concentration [221] and from previous computational models for coupled eNOS catalysis [93, 170, 187]. We can interpret that 0.01 to 1 $nM.s^{-1}$ represents the physiologic oxidative stress level and small changes in this range do not affect eNOS NO production. Thus, eNOS remains in coupled state under physiologic conditions. However, when the cellular oxidative stress was increased above 1 $nM.s^{-1}$, the eNOS coupling and NO production transitioned to an oscillatory state.

3.4.2. eNOS uncoupling contributes negligibly towards cellular oxidative stress

Studies have proposed that eNOS uncoupling related transition from NO to $O_2^{\bullet-}$ production may contribute significantly towards cellular oxidative stress [2, 27, 230]. On the other hand, some studies reported that the eNOS uncoupling does not contribute significantly to cellular oxidative stress [19, 185]. The major sources of $O_2^{\bullet-}$ generation are NADPH oxidase, xanthine oxidase and mitochondrial electron transport chain in diseases including hypertension, hypercholesterolemia and diabetes [9]. According to the 'kindling radical' hypothesis reactive oxygen and nitrogen species from ROS sources (e.g. NADPH oxidase) can trigger formation of additional reactive species including eNOS uncoupling related $O_2^{\bullet-}$ formation [2]. Further, the uncoupling of eNOS

from oxidative depletion of BH_4 is proposed [25]. Santhanam *et al.* [27] reported that an uncoupled eNOS is the major source of $O_2^{\bullet-}$ whereas Landmesser *et al.* [19] showed that ROS from NADPH oxidase oxidizes BH_4 and leads to eNOS uncoupling.

Our model predictions support the 'kindling radical' hypothesis that ROS sources may contribute to eNOS uncoupling through the oxidative depletion of BH_4. The endothelial cell NO production, TBP levels and biopterin ratio decreased significantly in our study when cellular oxidative stress was changed from 1 to 100 $nM.s^{-1}$. The endothelial cell NO production, TBP levels and biopterin ratio reduced from 26.5 to 2 $nM.s^{-1}$, 3.8 to 0.002 $\square M$ and 0.99 to 0.25, respectively when the $Q_{supcell}$ increased from 1 to 100 $nM.s^{-1}$. The NO production and the biopterin ratio exhibited an oscillatory profile indicating a transition to eNOS uncoupling at higher cellular oxidative stress. From the sensitivity analysis at $Q_{supcell}$ from 1 and 100 $nM.s^{-1}$, we found that the diffusion rate of BH_2 (k_{38}) is important for the eNOS related $O_2^{\bullet-}$ production and cellular BH_2 levels may affect eNOS related $O_2^{\bullet-}$ production. However, the magnitude of eNOS based $O_2^{\bullet-}$ production was very low (in the range of 10^{-6} $nM.s^{-1}$). Furthermore, the eNOS uncoupling related $O_2^{\bullet-}$ production was at least two orders of magnitude lower than the $O_2^{\bullet-}$ production from other sources at all cellular oxidative stress levels.

This indicates that eNOS uncoupling alone may not contribute towards cellular oxidative stress. However, the ROS generated from other sources may cause eNOS uncoupling, thus increasing overall oxidative stress.

3.4.3. Cellular biopterin concentration and biopetrin ratio reduces under oxidative stress conditions

BH_4 deficiency is a major cause for eNOS uncoupling in oxidative stress conditions, which may be a result of increased oxidation of BH_4 [190, 231]. Our model results showed that the total

[TBP] ranged from 3.8 to 5.9 µM and the biopterin ratio was 0.99 under normal physiologic conditions. Our model predictions are consistent with the reported [BH$_4$] of 3.9 ± 0.5 pmol/10^6 cells (i.e. 3.9 µM based on endothelial cell volume of 400 µm^3) in human endothelial cells under normal physiologic conditions by Werner *et al.* [212]. Our model predicted that the [TBP] and biopterin ratio reduced under oxidative stress conditions. The [TBP] reduced from 3.8 to 0.0015 µM and the biopterin ratio reduced from 0.99 to 0.25 when oxidative stress increased from 1 to 100 nM.s^{-1}. Jian Xu *et al.* [232] reported a similar observation of simultaneous decrease in [TBP] and biopterin ratio in hyperglycemic endothelial cells. They reported [TBP] and [BH$_4$] reduced from 30 to 25 and 20 to 15 pmol/mg protein, respectively in endothelial cells treated with normal glucose and high glucose conditions for short period of 2 hours. This corresponds to a decrease in biopterin ratio from 0.66 to 0.6 in normal to high glucose treated endothelial cells.

3.4.4. Extent of oxidative stress determines the efficacy of BH$_4$ in treating endothelial dysfunction

In addition to the oxidative depletion of BH$_4$, other mechanisms for the BH$_4$ deficiency include the downregulation/inhibition of GTPCH [232-234] and the downregulation of enzyme di-hydro folate reductase (DHFR), which is responsible for recycling of BH$_2$ back to BH$_4$ [234]. Studies have shown potential for the use of BH$_4$ in cardiovascular therapy [25, 26, 235]. However, the results from these studies are not consistent for improving the endothelial dysfunction under oxidative stress [25, 95, 236]. Experimental studies on BH$_4$ supplementation reported a 40-58% reduction in NO levels, a decrease in biopterin ratio while overall increase in [TBP] levels [95, 237, 238]. Other studies have reported significant (75% and 3 fold) increase in NO production and an improvement in biopterin ratio ([BH$_4$/BH$_2$]) following the BH$_4$ therapy [236, 239, 240]. Cai *et al.* [239] reported a [TBP] of 57 µM under BH$_4$ augmentation through increase in GTPCH

expression in physiologic conditions, which is similar to our predicted steady state [TBP] range of 32.8 to 59 µM in physiologic conditions with enhanced BH_4 synthesis.

Our model predictions suggest that enhancing BH_4 synthesis can improve intracellular BH_4 levels ($[BH_4]$) in oxidative stress conditions. The $[BH_4]$ increased with improved BH_4 synthesis at a given oxidative stress, however $[BH_4]$ decreased with the increase in cellular oxidative stress. At physiological conditions, the intracellular $[BH_4]$ was in the range of 3.75 to 5.93 µM, which increased to 56.6-59.5 µM for a 10 fold increase in BH_4 synthesis. For 3-fold increase in BH_4 synthesis the $[BH_4]$ was 15.18, 1.01, 0.002 µM, while that for 10-fold increase in BH_4 synthesis was 56.61, 32.87 and 0.18 µM, at Qsupcell of 1, 10 and 100 $nM.s^{-1}$ respectively. The $[BH_4]$ remained below 22 nM for all values of BH_4 synthesis at oxidative stress of 1000 and 10000 $nM.s^{-1}$. This indicates that BH_4 oxidizes at higher oxidative stress and supplementation may not increase intracellular BH_4 concentration.

In addition, the NO production rate increased with an increase in BH_4 synthesis. The increase in the NO production like BH_4, was also dependent on the extent of cellular oxidative stress. The NO production and biopterin ratio were less for a 10 fold increase in BH_4 synthesis at $Q_{supcell}$ of 100 to 10000 $nM.s^{-1}$ than the corresponding values at the 3 fold increase in BH_4 synthesis at $Q_{supcell}$ of 10 $nM.s^{-1}$. At $Q_{supcell}$ of 10 $nM.s^{-1}$, a 3-fold increase in BH_4 synthesis resulted in 25.3 $nM.s^{-1}$ NO production rate and 0.99 biopterin ratio, which were similar to the normal physiologic predictions of 26.4 $nM.s^{-1}$ NO production rate and 0.99 biopterin ratio at $Q_{supcell}$ of 0.01-1 $nM.s^{-1}$. For the 10-fold increase in BH_4 synthesis, the NO-production rates were 20, 16.1 and 12.2 $nM.s^{-1}$ and the biopterin ratio were 0.94, 0.66 and 0.36 for $Q_{supcell}$ of 100, 1000 and 10000 $nM.s^{-1}$, respectively.

The [TBP] increased with improved BH_4 synthesis at a given oxidative stress, however [TBP] decreased with the increase in cellular oxidative stress. The reduction in [TBP] at higher oxidative stress conditions is attributed to the relative ease with which BH_2 can diffuse out of the endothelial cell [204, 241]. This indicates that at higher oxidative stress conditions, improving BH_4 may not restore endothelial cell function.

3.4.5. A combination of BH_4 therapy and improvement in oxidative stress condition may improve endothelial dysfunction

Studies that reported improvement in the endothelial dysfunction have targeted either at the eNOS biochemical pathway (for improving BH_4 levels) [29, 242, 243] or reduction in oxidative stress by the action of antioxidants [244, 245]. Recently studies have used combination therapy that targets the eNOS biochemical pathway for increased BH_4 synthesis or NO production and antioxidants to reduce the oxidative stress [246, 247]. Baumgardt *et al.* [246] reported that the co-administration of the stable precursors of eNOS substrates- sepiapterin (a precursor of BH_4) and L-citrulline, significantly improved BH_4 concentrations, eNOS dimerization (thus eNOS activity) and NO production in the diabetic mice. However, this study targets only the eNOS biochemical pathway. Coronel *et al.* [247] reported the protective NO mechanism on the vasoconstrictor effects of phenylephrine in the kidney is lost in diabetes due to an increase in ROS and a decrease in BH_4. The restoration of this protective NO mechanism was achieved in an efficient manner with the supplementation of L-arginine which targeted stimulation of NO synthesis and a combination of antioxidants vitamin C and E, which prevented BH_4 oxidation simultaneously.

Our model results indicate that the reduction in cellular oxidative stress along with enhanced BH_4 synthesis is important for restoring eNOS coupling. At $Q_{supcell}$ of 100 $nM.s^{-1}$, a 3 fold increase in BH_4 synthesis resulted in a 3-fold increase in the NO production rate and 20%

improvement in the biopterin ratio. But, when the $Q_{supcell}$ decreased from 100 to 10 nM.s^{-1}, a 3-fold increase in BH$_4$ synthesis resulted in a 10 fold increase in NO production rate and 100% improvement in the biopterin ratio (levels comparable with the normal physiology). [TBP] also increased as the cellular oxidative stress was reduced at each Q_{BH4}. Thus, a combination of enhanced tetrahydrobiopterin synthesis with a reduction in oxidative stress may result in significant improvement in endothelial dysfunction and requires further experimental investigation.

3.4.6. Oscillations in NO production rates under oxidative stress in our simulations corresponds to unstable eNOS coupling

In many of our results, oscillations in NO production rates and biopterin ratio are observed, especially at $Q_{supcell}$ of 10 nM.s^{-1} and above. As the present study is mathematical study trying to find solution to a biological problem, the oscillations represented in our results depict the unstable state of eNOS coupling caused especially due to the instability in biopterin ratio. As seen in Figure 8, the biopterin ratio at start is in completely coupled state, which reduces back to uncoupled state and there after again increases to higher value and starts to oscillate and where these oscillations dampen towards the end of the simulation. Depending on the availability of BH$_4$ or BH$_2$, the eNOS coupling/uncoupling and production NO or O$_2^{\bullet-}$ is determined. The oscillations that are seen in the biopterin ratio are reflected in our other simulations for NO production rate as well as O$_2^{\bullet-}$ production rates (results not shown).

3.5. Conclusion

In this study, we investigated the interactions of endothelial cell oxidative stress, tetrahydrobiopterin synthesis and biopterin ratio on the extent of eNOS uncoupling. The model results indicate that eNOS remains coupled under normal physiologic conditions because of a

minimal amount of oxidative stress. The eNOS coupling is independent of the initial state of coupling/uncoupling under normal physiologic conditions. The eNOS uncoupling alone contributes negligibly towards the cellular oxidative stress. The ROS coming from sources such as NADPH oxidases, xanthine oxidases and mitochondrial electron transport chain may lead to eNOS uncoupling. This results in the reduction in NO production rate and biopterin ratio. The oxidative stress switches eNOS from a coupled state to an uncoupled state by initiating oscillations in the biopterin ratio and eNOS NO production. These oscillations are initiated due to an imbalance between BH_4 synthesis and oxidation. Furthermore, enhanced BH_4 synthesis improves eNOS coupling. However, the magnitude of improvement in eNOS coupling is determined by the extent of oxidative stress and BH_4 synthesis. We propose a combination therapy of BH_4 with a reduction in oxidative stress for significant improvement in endothelial dysfunction.

CHAPTER IV

COMPUTATIONAL INSIGHTS ON THE ROLE OF ASCORBATE IN TETRAHYDROBIOPTERIN RELATED ENDOTHELIAL DYSFUNCTION[2]

4.1. Introduction

Vitamin C is an essential dietary nutrient required as a co-factor for many enzymes in low concentrations. The reduced form of the vitamin C, L-ascorbic acid or ascorbate (ASC), is considered an effective intracellular circulatory antioxidant due to its high electron-donating power and converting back to its active reduced form readily [248]. Deficiency in ASC has been associated with an increased risk of CVDs [33, 249]. Low levels of ASC are observed in several diseases linked to increased oxidative stress, such as cancer, diabetes mellitus, cataract, sepsis and in smokers [116]. Endothelium is the most affected organ by ASC deficiency, since it regulates the distribution of ASC throughout the body [117]. The important functions of ASC in endothelial cells include increasing the synthesis and deposition of type IV collagen in the basement membrane, stimulating endothelial proliferation, inhibiting apoptosis, scavenging radical species, and sparing endothelial cell-derived nitric oxide to help modulate blood flow [117]. Of these, the role of ASC in increasing the endothelial NO bioavailability is of importance to our study of endothelial dysfunction in microcirculation. Figure 13 show the putative mechanisms of how ASC improves vascular health in CVDs as reported in several studies. These includes; (i) ASC maintaining cofactor BH_4 in reduced state [142, 250, 251]; (ii) scavenging of free radicals such as $O_2^{\bullet-}$, $ONOO^-$ by ASC [145] and (iii) increasing eNOS activity by increasing eNOS phosphorylation

---

[2] Manuscript is under preparation

[116] and decreasing eNOS S-nitrosylation [252]. However, very little quantitative information about the interactions of ASC in BH_4-dependent endothelial dysfunction is available.
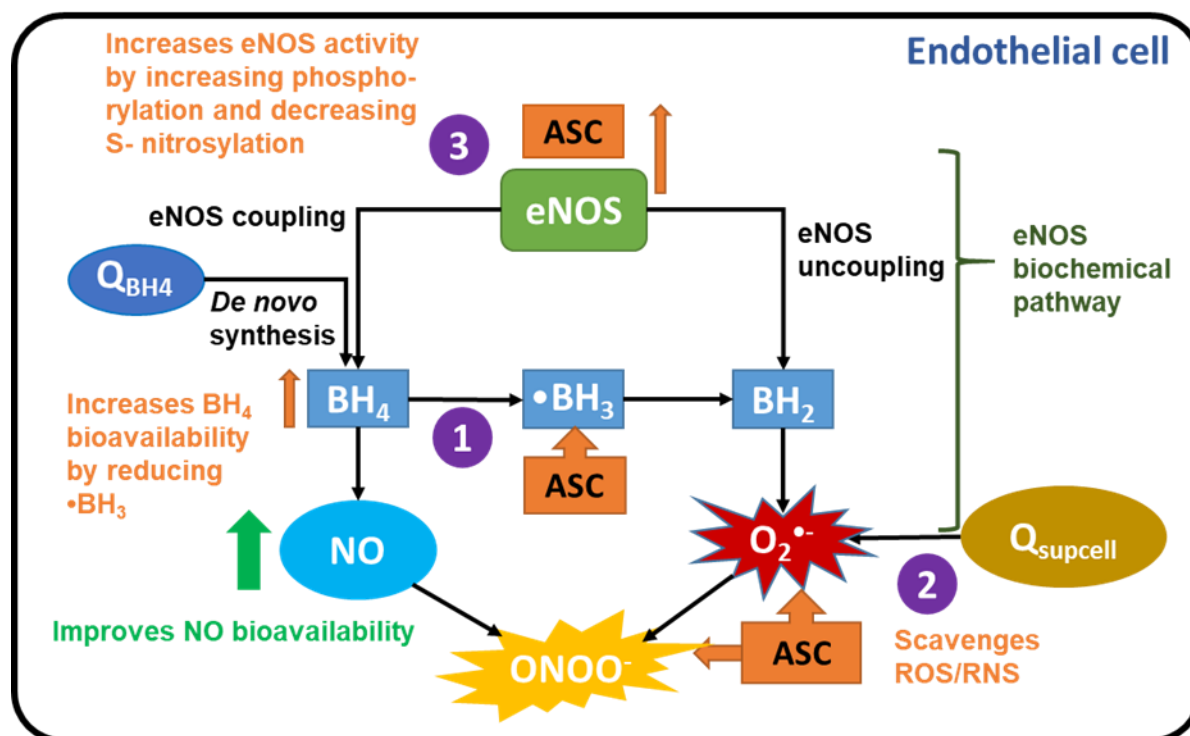
Figure 13: Putative mechanisms of ASC for improving NO bioavailability modeled in the present paper. The three mechanisms by which ASC improves NO bioavailability, modeled in this work are depicted as numerics. These includes; 1. ASC reduces oxidized trihydrobiopterin ($\bullet BH_3$) to BH_4, increasing BH_4 bioavailability. 2. ASC scavenges $O_2^{\bullet-}$ and $ONOO^-$ 3. ASC increases eNOS activity by increasing phosphorylation and decreasing S-nitrosylation. eNOS biochemical pathway produces NO and $O_2^{\bullet-}$ when coupled (left) and uncoupled (right) respectively. $Q_{supcell}$ and Q_{BH4} are the rates for non-eNOS based cellular oxidative stress and BH_4 synthesis from *de novo* synthesis pathway respectively. NO and $O_2^{\bullet-}$ forms $ONOO^-$ and other downstream reactions. (Intermediate steps in the eNOS biochemical pathway as well as downstream reactions are not shown in this figure.)

The purpose of the present study was to analyze the role of intracellular ASC in improving the NO bioavailability under oxidative stress in endothelial cell. We developed a computational model of interactions of eNOS biochemical pathway and downstream reactions of the products, biopterin, ASC and GSH, and oxidative stress in endothelial cell. We used this model to analyze

the biopterin synthesis, level of oxidative stress and ASC on the rate of production of endothelial NO and $O_2^{\bullet-}$ as well as $ONOO^-$. In addition, the model accounts for the interactions of ASC with total biopterin levels and biopterin ratio. We present results for the effects supplementation of ASC on i) the eNOS NO and $O_2^{\bullet-}$ production rates, $ONOO^-$, total biopterin and biopterin ratio; ii) and impact of biopterin synthesis on eNOS NO production rate iii) and eNOS protein concentration on the eNOS NO and $O_2^{\bullet-}$ production rate and biopterin ratio. The present work will provide insights on the protective mechanism of ASC in endothelial dysfunction.

4.2. Materials and Methods

4.2.1. Model Description

We developed an endothelial cell computational model using the known biochemical pathway of eNOS for NO and $O_2^{\bullet-}$ production [187, 190]. We modeled the eNOS biochemical pathway product and interactions of cellular oxidative stress, BH_4 synthesis, ASC, GSH and reactive species NO, $O_2^{\bullet-}$, $ONOO^-$, H_2O_2, N_2O_3, $\bullet OH$, $\bullet NO_2$, NO_2^- and others. Figure 1 summarizes the putative mechanisms of ASC for improving endothelial dysfunction as mentioned in literature. The eNOS can produce NO and $O_2^{\bullet-}$ depending on the availability and oxidative state of its cofactor BH_4 [253]. BH_4 is constitutively formed by *de novo* synthesis pathway [254], which is represented as $Q_{BH4}(M.s^{-1})$. Apart from the $O_2^{\bullet-}$ production from eNOS uncoupling, the significant amount of cellular oxidative stress comes from the non-eNOS based $O_2^{\bullet-}$ sources including NADPH and xanthine oxidase, and mitochondrial electron transport chain [255]. This is represented by a $O_2^{\bullet-}$ production rate term, $Q_{supcell}(M.s^{-1})$. Following ASC interactions are modeled in our current work and shown in Figure 13. ASC can regenerate BH_4 from its oxidized form of trihydrobiopterin ($\bullet BH_3$) radical, and promote eNOS coupling [144]. ASC is also known to scavenge the $O_2^{\bullet-}$ [256] and $ONOO^-$ [257] radicals. ASC is reported to increase eNOS activity by increasing eNOS

phosphorylation [116] and decreasing eNOS S-nitrosylation [252]. The detailed biochemical reactions for the eNOS biochemical pathway for the eNOS NO and $O_2^{\bullet-}$ production are described in our previous study Table 2 of Chapter II [255] and summarized in Table 5. These reactions are classified into two major biochemical pathways of;

i) NO production through eNOS oxidation of L arginine to N-hydroxyl-L-arginine (NHA), when bound to BH_4 and subsequent oxidation of NHA to NO and citrulline.

ii) $O_2^{\bullet-}$ production through the inability of BH_2 to transfer electron to the eNOS heme, when bound to L-arginine and O_2, results in the dissociation of the eNOS-substrate complex to form $O_2^{\bullet-}$. The detailed eNOS biochemical pathway for NO and $O_2^{\bullet-}$ production was modeled in our previous work and is not described in the current paper. Please refer to Table 1 from materials and methods section and reactions from rate constants k_{c2} to k_{b-12} from Joshi *et. al* [255] for more details.

Table 5: Summary of overall reactions involved in the eNOS biochemical pathway for NO and $O_2^{\bullet-}$ production. Please see references [255] for detailed chemical reactions and rate constants involved in eNOS biochemical pathway.

Overall reactions in eNOS biochemical pathway	
NO production	$eNOS - (Fe^{III}) + L - Arginine + BH_4 + O_2 + 2e^-$ $\rightarrow eNOS - (Fe^{III}) - BH_4 - NHA$
	$eNOS - (Fe^{III}) - BH_4 - NHA + O_2 + 3e^-$ $\rightarrow \mathbf{NO} + Citrulline + eNOS - (Fe^{III}) - BH_4 + eNOS - (Fe^{II}) - BH_4$
$O_2^{\bullet-}$ production	$eNOS - (Fe^{III}) + L - Arginine + BH_2 + O_2 + e^-$ $\rightarrow eNOS - (Fe^{III}) - BH_2 - Arginine + \mathbf{O_2^{\bullet-}}$

NO and $O_2^{\bullet-}$ production from eNOS is dependent on the biopterin ratio ([BH_4]/[TBP]) which is defined as the ratio of BH_4 to the total biopterins (TBP = BH_4 + BH_3 + BH_2) [93, 95, 255]. The downstream reactions of interactions amongst NO, $O_2^{\bullet-}$, BH_4, ASC, GSH, H_2O_2, N_2O_3,

S-Nitrosoglutathion (GSNO) and others with respective rate constants for the reactions are summarized in Table 6 along with the references.

The important downstream reactions modeled in this work (showed in Table 6) includes;

(i) the reaction between NO and $O_2^{\bullet-}$ to form $ONOO^-$ (Reaction # 1).

(ii) the oxidation of BH_4 by $O_2^{\bullet-}$, $ONOO^-$, $\bullet OH$, $\bullet NO_2$, $CO_3^{\bullet-}$ (Reactions # 4, 5, 6, 8, 19, 20, 21, 22) and subsequent diffusion of BH_2 out of the cell (Reaction # 24).

(iii) the dismutation of $O_2^{\bullet-}$, self (Reaction # 14) or SOD catalyzed (Reaction # 3) to form hydrogen peroxide (H_2O_2) which is further broken down to H_2O by catalase (Reaction # 23).

 (iv) the interaction of ASC with oxidized biopterin ($\bullet BH_3$), $ONOO^-$, $O_2^{\bullet-}$ (Reactions # 7, 9, 10).

(v) the interaction of GSH with $ONOO^-$ and N_2O_3 (Reactions # 25, 26) to form GSNO which in turn reacts with $O_2^{\bullet-}$ to generate NO (Reaction # 28)

(vi) Formation of N_2O_3 due to rapid reaction of NO and O_2 with intermediate formation of NO_2^- with reported rate constant of 2.4 to 6×10^6 $M^{-2}.s^{-1}$ [175, 258] (Reaction # 2) and hydrolysis of N_2O_3 at the rate of 1.6×10^3 s^{-1} [175, 259] (Reaction # 27).

Table 6: Downstream reactions involving NO, ROS, RNS, biopterins, ASC and GSH, rate expressions and their associated rate constants.

Reaction #	Reactions	Rate Expressions (v_i)	Rate constants $k_i(M.s^{-1})$	References
1	$NO + O_2^{\bullet-} \xrightarrow{k_{14}} ONOO^-$	$k_{14}[NO][O_2^{\bullet-}]$	6.7×10^9 $M^{-1}.s^{-1}$	[199]
2	$4NO + O_2 + 2H_2O \xrightarrow{k_{15}} 2NO_2^- + N_2O_3 + 2H^+$	$4k_{15}[NO]^2[O_2]$	2.4×10^6 $M^{-2}.s^{-1}$	[200, 255]

3	$O_2^{\bullet-} + H_2O \xrightarrow{k_{16},\text{SOD}} \frac{1}{2}O_2 + \frac{1}{2}H_2O_2 + OH^-$	$k_{16}[\text{SOD}][O_2^{\bullet-}]$	$3.85 \times 10^9\ M^{-1}.s^{-1}$	[199, 255]
4	$2BH_4 + O_2 \xrightarrow{k_{17}} 2BH_2 + 2H_2O$	$k_{17}[BH_4][O_2]$	$0.6\ M^{-1}.s^{-1}$	[201, 255]
5	$BH_4 + O_2^{\bullet-} + H^+ \xrightarrow{k_{18}} BH_3 + H_2O_2$	$k_{18}[BH_4][O_2^{\bullet-}]$	$3.9 \times 10^5\ M^{-1}.s^{-1}$	[201, 255]
6	$2BH_3 \xrightarrow{k_{19}} BH_4 + BH_2$	$2k_{19}[BH_3]^2$	$4.65 \times 10^4\ M^{-1}.s^{-1}$	[201, 255]
7	$AscH^- + BH_3 \xrightarrow{k_{20}} Asc^{\bullet-} + BH_4$	$k_{20}[BH_3][AscH^-]$	$1.7 \times 10^5\ M^{-1}.s^{-1}$ at pH=9.2	[144]
8	$BH_4 + ONOO^- \xrightarrow{k_{22}} BH_3$	$k_{22}[BH_4][ONOO^-]$	$6 \times 10^3\ M^{-1}.s^{-1}$	[202, 255]
9	$H^+ + AscH^- + ONOO^- \xrightarrow{k_{23}} DHA + NO_2^- + H_2O$	$k_{23}[ONOO^-][AscH^-]$	$361.7\ s^{-1}$	[257]
10	$H^+ + AscH^- + O_2^{\bullet-} \xrightarrow{k_{24}} Asc^{\bullet-} + H_2O_2$	$k_{24}[O_2^{\bullet-}][AscH^-]$	$5.1 \times 10^5\ M^{-1}.s^{-1}$	[256]
11	$ONOOH \xrightarrow{k_{25}} NO_3^- + H^+$	$k_{25}[ONOO^-]$	$0.981\ s^{-1}$	[93, 200]
12	$ONOOH \xrightarrow{k_{26}} \bullet NO_2 + \bullet OH$	$k_{26}[ONOO^-]$	$0.401\ s^{-1}$	[93, 200]
13	$ONOOH + NO \xrightarrow{k_{27}} \bullet NO_2 + NO_2^-$	$0.22k_{27}[ONOO^-][NO]$	$9.1 \times 10^4\ M^{-1}.s^{-1}$	[199]
14	$HO_2 + O_2^{\bullet-} + H_2O \xrightarrow{k_{28}} O_2 + H_2O_2 + OH^-$	$0.0025k_{28}[O_2^{\bullet-}]^2$	$3.57 \times 10^5\ M^{-1}.s^{-1}$	[200]
15	$ONOO^- + CO_2 \xrightarrow{k_{29}} NO_3^- + CO_2$	$k_{29}[ONOO^-][CO_2]$	$3.89 \times 10^4\ M^{-1}.s^{-1}$	[200]
16	$ONOO^- + CO_2 \xrightarrow{k_{30}} \bullet NO_2 + CO_3^{\bullet-}$	$k_{30}[ONOO^-][CO_2]$	$1.91 \times 10^4\ M^{-1}.s^{-1}$	[200]
17	$CO_3^{\bullet-} + O_2^{\bullet-} + H^+ \xrightarrow{k_{31}} HCO_3^- + O_2$	$k_{31}[CO_3^{\bullet-}][O_2^{\bullet-}]$	$6.65 \times 10^8\ M^{-1}.s^{-1}$	[200]

18	$CO_3^{\bullet-} + NO + OH^- \xrightarrow{k_{32}} HCO_3^- + NO_2^-$	$k_{32}[CO_3^{\bullet-}][NO]$	$5.82 \times 10^9 \ M^{-1}.s^{-1}$	[200]
19	$BH_4 + \bullet OH \xrightarrow{k_{33}} OH^- + H^+ + BH_3$	$k_{33}[BH_4][\bullet OH]$	$8.8 \times 10^9 \ M^{-1}.s^{-1}$	[144]
20	$BH_4 + \bullet NO_2 \xrightarrow{k_{34}} NO_2^- + H^+ + BH_3$	$k_{34}[BH_4][\bullet NO_2]$	$9.4 \times 10^8 \ M^{-1}.s^{-1}$	[144]
21	$BH_4 + CO_3^{\bullet-} \xrightarrow{k_{35}} CO_3^{2-} + H^+ + BH_3$	$k_{35}[BH_4][CO_3^{\bullet-}]$	$4.6 \times 10^9 \ M^{-1}.s^{-1}$	[144]
22	$BH_3 + O_2 \xrightarrow{k_{36}} BH_2 + HO_2^{\bullet}$	$k_{36}[BH_3][O_2]$	$3.2 \times 10^3 \ M^{-1}.s^{-1}$	[201]
23	$2H_2O_2 \xrightarrow{k_{37},CAT} 2H_2O + O_2$	$k_{37}[CAT][H_2O_2]$	$3.4 \times 10^7 \ M^{-1}.s^{-1}$	[260]
24	BH_2 (Diffusion out of cell)	$k_{38}[BH_2]$	$152.5 \ s^{-1}$	[204, 255]
25	$ONOO^- + GSH \xrightarrow{k_{39}} GSNO + GSSG$	$k_{39}[ONOO^-][GSH]$	$1.35 \times 10^3 \ M^{-1}.s^{-1}$	[175, 261]
26	$N_2O_3 + GSH \xrightarrow{k_{40}} GSNO + H^+ + NO_2^-$	$k_{40}[N_2O_3][GSH]$	$6.6 \times 10^7 \ M^{-1}.s^{-1}$	[175, 262]
27	$N_2O_3 + H_2O \xrightarrow{k_{41}} 2H^+ + NO_2^-$	$k_{41}[N_2O_3]$	$1.6 \times 10^3 \ s^{-1}$	[175, 259]
28	$O_2^{\bullet-} + 2GSNO + H_2O \xrightarrow{k_{42}} GSSG + NO_2^- + NO_3^- + 2H^+$	$k_{42}[GSNO]^2[O_2^{\bullet-}]$	$9 \times 10^8 \ M^{-2}.s^{-1}$	[263]

$AscH^- =$ Ascorbate ion

4.2.2. Model development

The NO production rate is considered independent of the geometric location of eNOS and all the chemical species involved in eNOS biochemical pathway are considered in uniform concentrations inside the endothelial cell [170, 187, 255]. By applying the law of mass action kinetics to each chemical species of interest involved in the eNOS biochemical pathways and its downstream reactions, the model equations were developed. A total of 39 chemical species were

involved in the model and their rate equations with respect to time were in the form of ordinary differential equations and mathematically represented as:

$$\frac{d[S_i]}{dt} = \sum v_i \tag{1}$$

where, $[S_i]$ (M) represents the concentration of the ith chemical species and $v_i (M. s^{-1})$ represents the production/consumption terms of the ith species.

In addition, to simplify our kinetic model we applied mass conservation eNOS protein and glutathione disulfide (GSSG), oxidized GSH. It was set in the algebraic form as follows:

$$[eNOS] = [E] + [E_{-1}] + \sum [E_{ai}] + \sum [E_{bi}] + \sum [E_{ci}] \tag{2}$$

where, $[E]$ and $[E_{-1}]$ represents different forms of native eNOS and $[E_{ai}]$, $[E_{bi}]$ and $[E_{ci}]$ represents different forms of the eNOS-substrate complexes. [eNOS] represents the total eNOS concentration.

$$[GSSG] = [GSH]_0 - [GSH] - [GSNO] \tag{3}$$

where, [GSSG] represents total GSSG concentration which is conserved always. $[GSH]_0$ represents initial GSH concentration provided in the system at time, t=0 mins, while [GSH], [GSNO] and [GSSG] vary with time. (GSNO, S-Nitrosoglutathion)

The rate equations for production of NO (R_{NO}) and $O_2^{\bullet-}$ ($R_{O2\bullet-}$) are written separately that includes summation of the generation terms for the respective species. Total of 39 rate expressions were modeled. The details of 21 rate expressions, out of total 39 rate equations used in this study, are for modeling eNOS biochemical pathway. These rate expressions including all eNOS and eNOS-substrate complexes, citrulline and NHA used in this work can be found in our previous

modeling paper Joshi *et al.* [255], Table 2. The rate expressions for the remaining 16 chemical species model equations involved in downstream reactions are illustrated in Table 7.

Table 7: Rate expression of different species for the downstream reactions involving products of eNOS biochemical pathways - NO and $O_2^{\bullet-}$, other ROS and RNS, biopterins, ASC and GSH.

Rate equations $\dfrac{d[S_i]}{dt}$	$\sum v_i$
$\dfrac{d[NO]}{dt}$	$k_{b7}[eNOS - (Fe^{III}) - NO - BH_4]$ $+ k_{b10}[eNOS - (Fe^{II}) - NO - BH_4]$ $- k_{b-7}[NO][eNOS - (Fe^{III}) - BH_4]$ $- k_{b-10}[NO][eNOS - (Fe^{II}) - BH_4] - k_{14}[NO][O_2^{\bullet-}]$ $- 4k_{15}[NO]^2[O_2] - 0.22k_{27}[ONOO^-][NO]$ $- k_{32}[CO_3^{\bullet-}][NO] + k_{42}[GSNO]^2[O_2^{\bullet-}]$
$\dfrac{d[O_2^{\bullet-}]}{dt}$	$Q_{supcell} + k_{c8}[eNOS - (Fe^{III} - O_2^-) - BH_2 - Arg] - k_{14}[NO][O_2^{\bullet-}]$ $- k_{16}[SOD][O_2^{\bullet-}] - k_{18}[BH_4][O_2^{\bullet-}]$ $- k_{24}[O_2^{\bullet-}][AscH^-] - 0.0025k_{28}[O_2^{\bullet-}]^2$ $- k_{31}[CO_3^{\bullet-}][O_2^{\bullet-}] - k_{42}[GSNO]^2[O_2^{\bullet-}]$
$\dfrac{d[ONOO^-]}{dt}$	$k_{14}[NO][O_2^{\bullet-}] - k_{22}[BH_4][ONOO^-] - k_{23}[ONOO^-][AscH^-]$ $- k_{25}[ONOO^-] - k_{26}[ONOO^-]$ $- 0.22k_{27}[ONOO^-][NO] - k_{29}[ONOO^-][CO_2]$ $- k_{30}[ONOO^-][CO_2] - k_{39}[ONOO^-][GSH]$
$\dfrac{d[BH_4]}{dt}$	$Q_{BH4} + k_{c-2}[eNOS - (Fe^{III}) - BH_4] - k_{c2}[eNOS - (Fe^{III})][BH_4]$ $- k_{17}[BH_4][O_2] - k_{18}[BH_4][O_2^{\bullet-}] + k_{19}[BH_3]^2$ $+ k_{20}[BH_3][AscH^-] - k_{22}[BH_4][ONOO^-]$ $- k_{33}[BH_4][\bullet OH] - k_{34}[BH_4][\bullet NO_2]$ $- k_{35}[BH_4][CO_3^{\bullet-}]$
$\dfrac{d[BH_3]}{dt}$	$k_{18}[BH_4][O_2^{\bullet-}] - 2k_{19}[BH_3]^2 - k_{20}[BH_3][AscH^-]$ $+ k_{22}[BH_4][ONOO^-] + k_{33}[BH_4][\bullet OH]$ $+ k_{34}[BH_4][\bullet NO_2] + k_{35}[BH_4][CO_3^{\bullet-}]$ $- k_{36}[BH_3][O_2]$
$\dfrac{d[BH_2]}{dt}$	$k_{c-3}[eNOS - (Fe^{III}) - BH_2] - k_{c3}[BH_2][eNOS - (Fe^{III})]$ $+ k_{17}[BH_4][O_2] + k_{19}[BH_3]^2 + +k_{36}[BH_3][O_2]$ $- k_{38}[BH_2]$
$\dfrac{d[H_2O_2]}{dt}$	$k_{16}[SOD][O_2^{\bullet-}] + k_{18}[BH_4][O_2^{\bullet-}] + 0.0025k_{28}[O_2^{\bullet-}]^2$ $- k_{37}[CAT][H_2O_2]$

$\dfrac{d[\bullet\,OH]}{dt}$	$k_{26}[ONOO^-] - k_{33}[BH_4][\bullet\,OH]$
$\dfrac{d[\bullet\,NO_2]}{dt}$	$k_{26}[ONOO^-] + 0.22k_{27}[ONOO^-][NO] + k_{30}[ONOO^-][CO_2]$ $- k_{34}[BH_4][\bullet\,NO_2]$
$\dfrac{d[CO_3^{\bullet-}]}{dt}$	$k_{30}[ONOO^-][CO_2] - k_{31}[CO_3^{\bullet-}][O_2^{\bullet-}] - k_{32}[CO_3^{\bullet-}][NO]$ $- k_{35}[BH_4][CO_3^{\bullet-}]$
$\dfrac{d[NO_3^-]}{dt}$	$k_{b9}[eNOS - (Fe^{II}) - NO - BH_4] + k_{25}[ONOO^-]$ $+ k_{29}[ONOO^-][CO_2]$
$\dfrac{d[NO_2^-]}{dt}$	$2k_{15}[NO]^2[O_2] + 0.22k_{27}[ONOO^-][NO] + k_{32}[CO_3^{\bullet-}][NO]$ $+ k_{34}[BH_4][\bullet\,NO_2] + k_{40}[N_2O_3][GSH] + k_{41}[N_2O_3]$
$\dfrac{d[GSH]}{dt}$	$\left[\dfrac{v_m[GSSG]}{K_m + [GSSG]}\right] - k_{39}[ONOO^-][GSH] - k_{40}[N_2O_3][GSH]$
$\dfrac{d[GSNO]}{dt}$	$k_{39}[ONOO^-][GSH] + k_{40}[N_2O_3][GSH] - k_{42}[GSNO]^2[O_2^{\bullet-}]$
$\dfrac{d[N_2O_3]}{dt}$	$4k_{15}[NO]^2[O_2] - k_{40}[N_2O_3][GSH] - k_{41}[N_2O_3]$
$\dfrac{d[GSSG]}{dt}$	$[GSH]_0 - [GSH] - [GSNO] - [GSSG]$
R_{NO} (NO production)	$k_{b7}[eNOS - (Fe^{III}) - NO - BH_4]$ $+ k_{b10}[eNOS - (Fe^{II}) - NO - BH_4]$ $+ k_{42}[GSNO]^2[O_2^{\bullet-}]$
$R_{O_2^{\bullet-}}$ ($O_2^{\bullet-}$ production)	$Q_{supcell} + k_{c8}[eNOS - (Fe^{III} - O_2^-) - BH_2 - Arg]$

4.2.3. Model parameters

The important parameters used in this study include calculating/using;

(i) the initial concentrations of; eNOS protein, TBP, L-Arginine, O_2, CO_2, superoxide dismutase (SOD) and catalase enzymes, biopterin ratio, ASC and GSH

(ii) rate constants for all the reactions, as well as calculation of Q_{BH4} and $Q_{supcell}$

(iii) calculation of rate constants for scavenging of $O_2^{\bullet-}$ and $ONOO^-$ by ASC using Arrhenius equation.

Table 8 provides the model parameters, initial concentrations and rates for Q_{BH4} and $Q_{supcell}$ used in this study. The initial condition for species is assumed zero otherwise mentioned in the figure legends. We used the eNOS protein concentration of 0.097 µM, based on experimentally reported values of eNOS protein concentration of 5137 pg/10^6 cells and single endothelial cell volume of 400 $µM^3$ for HUVEC's, [187]. The effect of ASC on eNOS activity due to increasing eNOS phosphorylation or decreasing eNOS S-nitrosylation was modeled by varying eNOS protein concentration from 0.097 µM to ± 50% [116, 252]. The role of cellular oxidative stress on endothelial cell function was assessed by using the term, $Q_{supcell}$. Various studies have been performed to report endothelial $O_2^{\bullet-}$ production rate in the range of 0.016 nM.s^{-1} to 6000 nM.s^{-1} [183, 199, 207]. In Chapter II, we used a range of 0.01 to 10000 nM.s^{-1} for $Q_{supcell}$ and determined that $Q_{supcell}$ of 1 nM.s^{-1} and below represents normal physiological state, maximum damage to the endothelial function is caused under the oxidative stress range of 1-100 nM.s^{-1} and no significant change in species was observed above $Q_{supcell}$ of 1000 nM.s^{-1} [255]. Thus, in the present study we used $Q_{supcell}$ values of 1, 10, 100 and 1000 nM.s^{-1} to represent the cellular oxidative stress conditions progressing from physiological to pathophysiological state. Under

physiological conditions, the activity for guanosine triphosphate cyclohydrolase I (GTPCH), rate limiting enzyme of *de novo* synthesis pathway was reported to be 7 pmol.mg protein[-1].h[-1] [206]. Based on endothelial cell volume of 400 μm^3 and assuming the total protein content of protein content to be 0.1 mg protein/10^6 endothelial cells [187], we calculated the Q_{BH4} of 0.5 nM.s[-1] for all simulated cases. From our previous work [255], we found that the initial state of eNOS coupling/uncoupling does not significantly contribute towards cellular oxidative stress. Also the NO production rate was independent of initial state eNOS coupling or uncoupling at higher oxidative stress conditions. Thus, the [BH4]/[TBP] was set at 0.05 at t=0 min, which represents initial state of eNOS uncoupling for all the simulated cases. We adopted the initial concentrations for $[TBP]_0$, $[L-Arginine]_0$, $[O_2]_0$, $[CO_2]_0$ and $[SOD]_0$ as 7 µM, 100 µM, 140 µM, 1.1 µM and 10 µM from our previous modeling work [255]. Based on *in vitro* studies by Aebi *et al.* [260], we used the catalase concentration of 0.9 µM and the rate constant for hydrolysis of H_2O_2 is 3.4×10^7 M^{-1}.s[-1]. To investigate the optimal concentrations of ASC required for increasing NO bioavailability, we used [ASC] in the range of 0 to 200 µM in this study. This range was based on the reported ASC levels in organs and tissues as reviewed in Li *et al.* [264], mean plasma levels of ASC between 50 and 60 µM for healthy individuals [146]; low levels of plasma ASC of 3–5 µM observed in individuals linked to diseases with increased oxidative stress [116] and concentration-dependent saturation for ASC above 100 µM reported by Heller *et al.* [250] for 24h pretreated endothelial cells with [ASC] in the range 1 µM to 1 mM. Based on the rate constants for the interaction of $O_2^{\bullet-}$ with ASC determined by chemiluminescence method measured at 25ºC and pH 7.8 is 3.3×10^5 M^{-1}.s[-1] [256] and that of $ONOO^-$ with ASC is 236 M.s^{-1} [257] respectively, we calculated the rate constants for the reaction of ASC with $O_2^{\bullet-}$ and $ONOO^-$ at 37 ºC to be 5.1×10^5 M^{-1}.s[-1] and 361.7 M.s^{-1} respectively, using Arrhenius equation, as shown in Table 2. GSH

concentration is present in the range of 0.5 to 10 mM and exceeds by one order of magnitude than ASC under physiological conditions in endothelial cells [265, 266]. The effect of GSH levels was analyzed by using [GSH] of 0.1, 1 and 10 mM in the present study. The enzymatic kinetic parameters related to the enzyme glutathione reductase including $V_{m,GR}$ and $K_{m,GR}$ were used to model GSH and are also shown in Table 8.

4.2.4. Model solution

The rate equations, coupled with appropriate initial conditions, were solved using MATLAB R2017b (Mathworks, Natick, MA, USA) ordinary differential solver *ode 15s*, which is a variable multistep solver based on the numerical differentiation formulae. The relative and absolute error tolerance values were set at 1×10^{-10} and 1×10^{-15}, respectively. However, for some simulation to get the numerical simulations the tolerance was increased to 1×10^{-4} (relative) and 1×10^{-7} (absolute). The simulations were run for 500,000s (approximately 8333 mins) to obtain the steady-state values.

Table 8: Model parameters used in ASC related endothelial dysfunction model

Variable/Constant	Values	Units	References
$[eNOS]_0$	0.048 ,0.097, 0.144	µM	Text, [93, 170, 187, 255]
$Q_{supcell}$	1, 10, 100, 1000	$nM.s^{-1}$	Text, [255]
Q_{BH4}	0.5, 1, 1.5, 5	$nM.s^{-1}$	Text, [206, 255]
$[BH_4]/[TBP]$	0.05	-	[255]
$[TBP]_0$	7	µM	[93, 255]
$[L-Arginine]_0$	100	µM	[93, 255]
$[O_2]_0$	140	µM	[93, 255, 267]
$[CO_2]_0$	1.1	mM	[93, 255, 267]

$[SOD]_0$	10	μM	[93, 255, 267]
$[CAT]_0$	0.9	μM	[260]
$[ASC]_0$	0, 5, 10, 25, 50, 100, 200	μM	Text, [53, 115, 268, 269]
$[GSH]_0$	0.01, 0.1, 1, 10, 100	mM	Text, [270]
$V_{m,GR}$	3.2×10^{-4}	$M.s^{-1}$	[93, 175]
$K_{m,GR}$	50	μM	[93, 175]

4.3. Results

4.3.1. Ascorbate supplementation improves NO production and biopterin bioavailability

To gain quantitative understanding for the role of ASC in endothelial dysfunction, we analyzed the effect of ASC supplementation, under cellular oxidative stress, on the temporal profiles of eNOS NO production rate, biopterin ratio and concentration profiles of TBP, $O_2^{\bullet-}$ an $ONOO^-$. Figure 14 show the temporal profiles of species as a function of ASC supplementation. Our model results showed that the eNOS NO production rate increased with ASC supplementation in oxidative stress conditions. Under basal oxidative stress condition ($Q_{supcell}$ of 1 nM.s^{-1}), ASC supplementation had no effect on eNOS NO production rate (Figure 2A). Increasing oxidative stress introduced instability in eNOS when no ASC was present in the system, as seen by the oscillations at $Q_{supcell}$ of 10 nM.s^{-1} (Figure 14B - control). ASC supplementation stabilized eNOS and improved the NO production level by almost 85-90%.

Under excessive oxidative stress condition, more ASC was required to maximize NO production rate (Figure 14C and D). ASC supplementation also improved TBP levels and biopterin ratio in a dose dependent manner in all simulated oxidative stress conditions (Figure 14E-H). The instability observed in eNOS can be attributed to the instability in biopterin ratio (Figure 14I-L).

ASC is involved in reducing oxidized biopterin (BH_3) back to it reduced state (BH_4). Thus, ASC supplementation is responsible for improving TBP levels as well as maintaining biopterin ratio.

We further analyzed the role of ASC in scavenging $O_2^{\bullet-}$ and $ONOO^-$ under oxidative stress conditions. ASC supplementation reduced $O_2^{\bullet-}$ concentration (Figure 14M-P) at respective $Q_{supcell}$, however, increased the $ONOO^-$ concentration by almost 90% under excessive oxidative stress as compared to when no ASC was present in the system (Figure 14S and T). The increase in $ONOO^-$ concentration can be attributed to increase in NO levels with ASC supplementation. Our results suggest that the chief mechanism by which ASC improves NO production rate is by increasing BH_4 bioavailability and stabilizing eNOS.
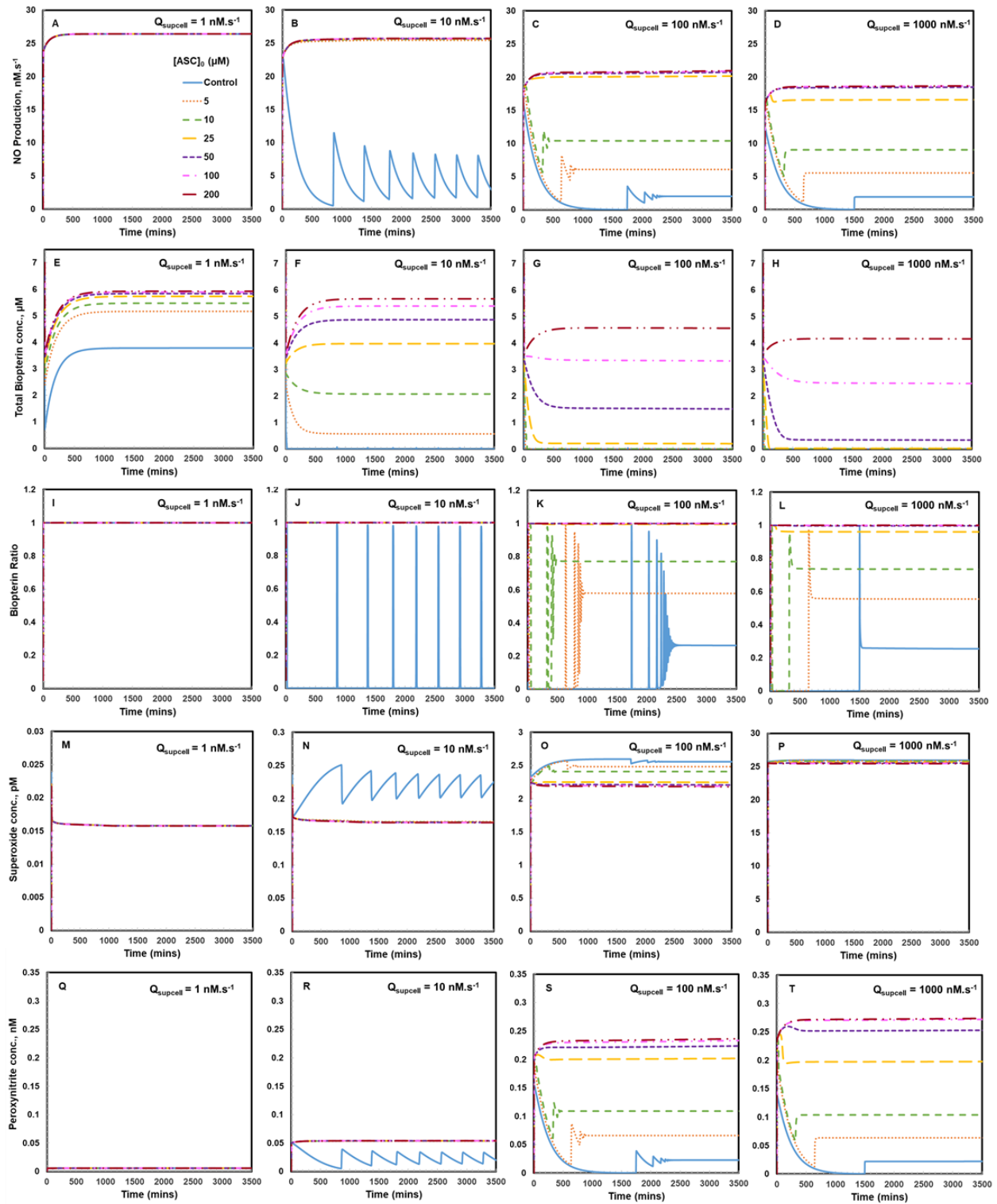
Figure 14: Temporal profile of species as a function of ASC supplementation under increasing cellular oxidative stress conditions. Panels A–T show ASC dependent the temporal variation in various species for the $Q_{supcell}$ of 1, 10, 100 and 1000 nM·s^{-1}, where $Q_{supcell}$ of 1 nM.s^{-}

[1] indicates physiological conditions. The [ASC] was varied from control, 5, 10, 25, 50, 100 and 200 µM, where control being no ASC introduced in the system. Q_{BH4} was set at 0.5 nM.s^{-1}. The [TBP] and biopterin ratio was set at 7 µM and 0.05 @ t = 0 min, respectively. The initial concentration of GSH, eNOS, L-arginine, O_2, SOD and CO_2 was 1 mM, 0.097 µM, 100 µM, 140 µM, 10 µM and 1.1 mM, respectively.

4.4.2. Effect of simultaneous increase in tetrahydrobiopterin synthesis and ascorbate on eNOS NO production

Individual studies have reported that both ASC [271] and BH$_4$ [272] supplementation can offer therapeutic potential by modulating oxidative stress and providing endothelial protection. In this study, we analyzed the effect of combination therapy of ASC and BH$_4$ supplementation, under excessive oxidative stress condition (at $Q_{supcell}$ of 100 nM.s^{-1}), on eNOS NO production rate and biopterin ratio. We augmented the Q_{BH4} from physiologic levels of 0.5 nM.s^{-1} by 2, 3 and 10 orders of magnitude, represented by Q_{BH4} of 1, 1.5 and 5 nM.s^{-1} and increased ASC supplementation from control, 10 and 50 µM in the system. Control being no ASC introduced in the system.

Our results show that increasing Q_{BH4} increased the eNOS NO production rate as well as improved the biopterin ratio. As observed in our previous results (Figure 14), ASC supplementation removed the instability in eNOS uncoupling maintained biopterin ratio. As seen from Figure 15A, when there was no ASC in the system, higher Q_{BH4} was required to maintain elevated NO production rates. However, with the introduction of ASC, even at low Q_{BH4} the higher NO production rates were attained (compare Figure 15B and C). Thus, combination therapy of ASC and BH$_4$ supplementation can considerably improve eNOS NO production rate and biopterin ratio. Our results suggest that ASC supplementation would be effective in cases of BH$_4$ deficiency or impaired BH$_4$ synthesis.
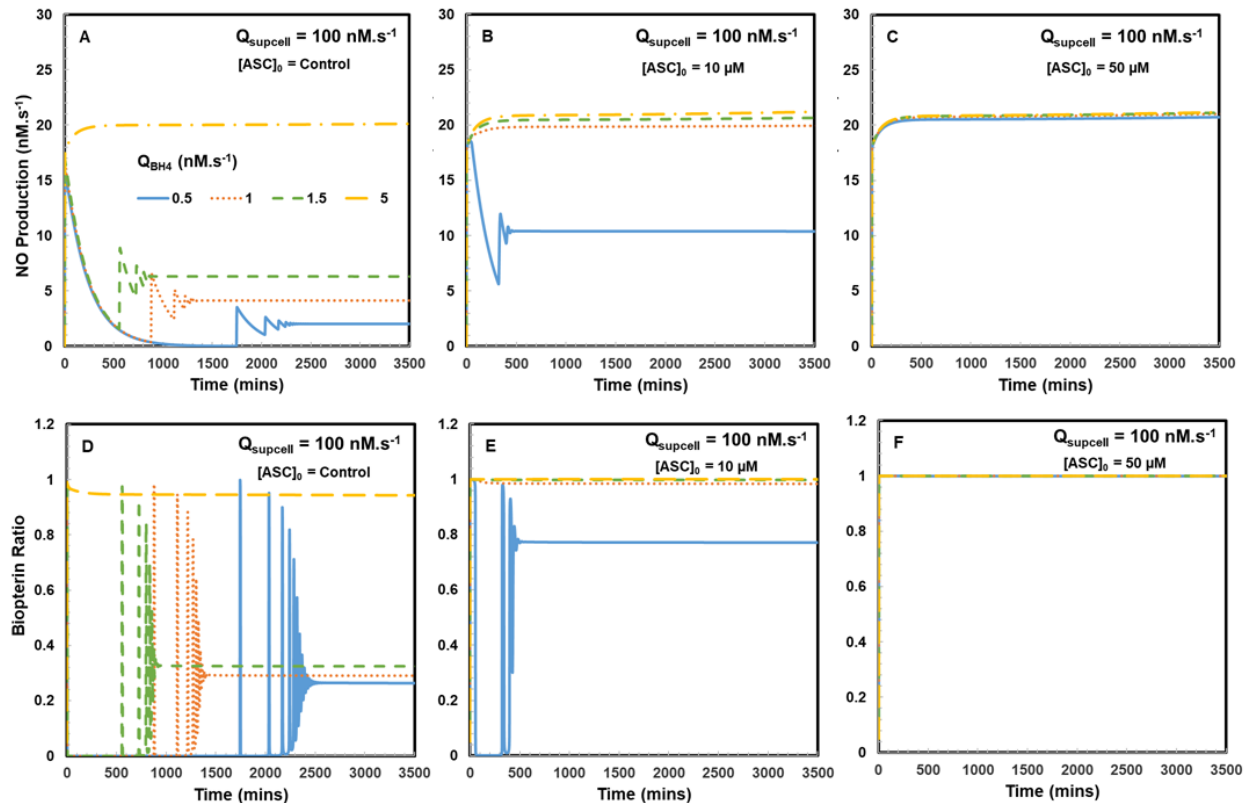
Figure 15: Effect of enhanced BH₄ synthesis and ASC supplementation on NO production rate and biopterin ratio under cellular oxidative stress. Panels A–C and Panels D-F show Q_{BH4} dependent temporal variation in eNOS NO production rate and biopterin ratio, respectively for [ASC] supplementation of control, 10 and 50 µM. The $Q_{supcell}$ was 100 nM·s⁻¹ to represent oxidative stress conditions. The BH₄ synthesis rate (Q_{BH4}) was varied from 0.5, 1, 1.5 and 5 nM.s⁻¹. The [TBP] and biopterin ratio were set at 7 µM and 0.05 @ t = 0 min. The initial concentration of GSH, L-arginine, O₂, SOD, CO₂ and eNOS was 1 Mm, 100 µM, 140 µM, 10 µM, 1.1 mM and 0.097 µM, respectively.

4.4.3. Effect of eNOS on NO production in the presence of ascorbate

In this study, we examined the effect of eNOS concentration and ASC supplementation on the NO production rate under oxidative stress conditions. Figure 16A-I show the temporal variations in NO production rate for ASC supplementation under and eNOS concentrations of 0.048, 0.097 (physiologic) and 0.144 µM and increasing oxidative stress.

As shown in Figure 16, increasing eNOS concentration increased NO production rate. However, as the oxidative stress level increased the NO production rate was lowered at respective [eNOS]. ASC supplementation helped to maintain higher NO production rate and was more effective at higher oxidative stress conditions. When there was no ASC in the system, the eNOS NO production rate decreased by 55% at physiologic conditions and by 4% under oxidative stress conditions, with the decrease in [eNOS]. After introducing ASC in the system, 75 – 90% increase in eNOS NO production rate was observed at respective [eNOS] and $Q_{supcell}$. Thus, for improving NO production rate ASC supplementation as well as increased [eNOS] is required.
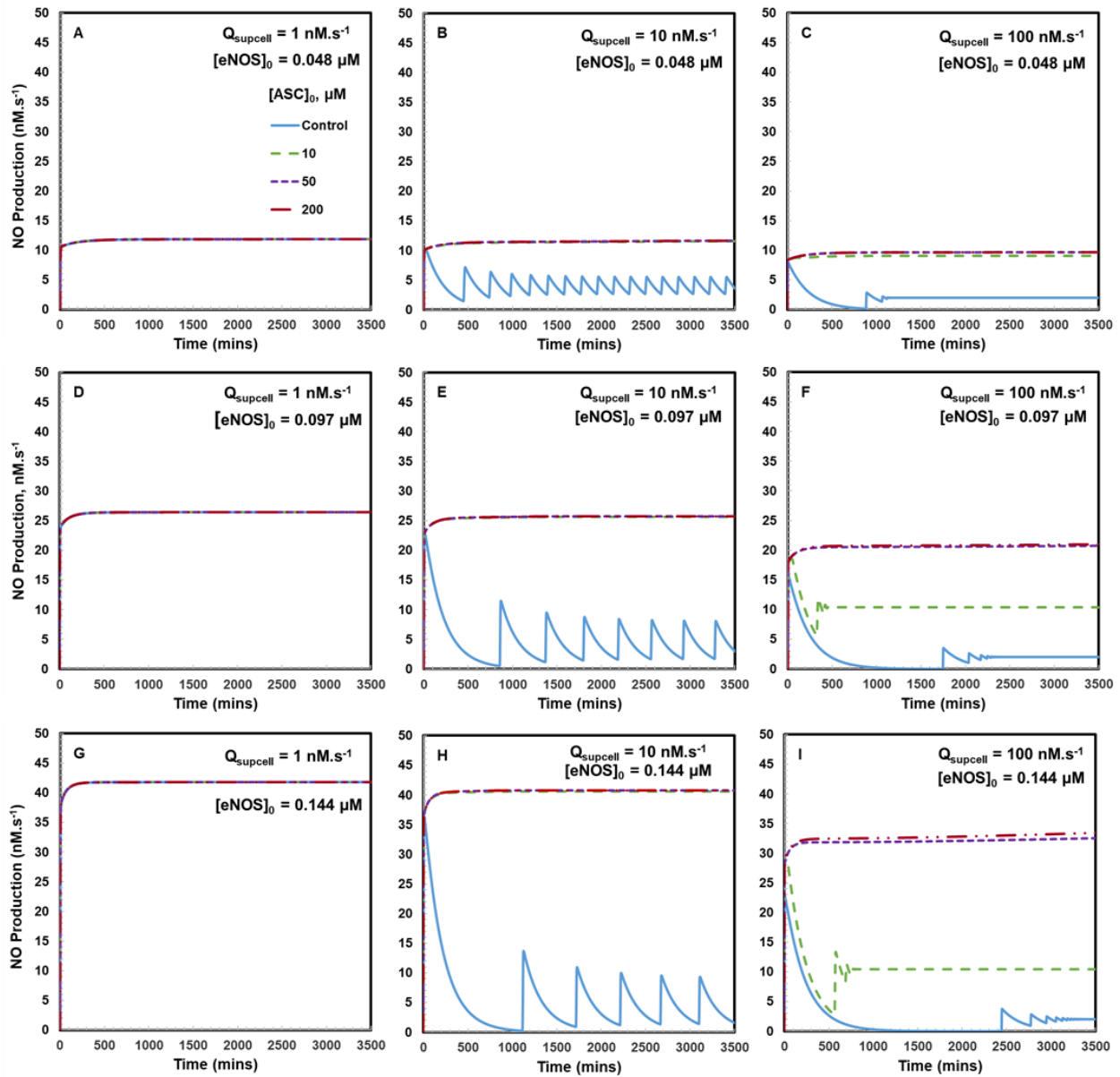
Figure 16: Effect of eNOS concentration NO production rates in the presence of ASC. Panels A–I show eNOS and ASC dependent temporal variation in in eNOS NO production rate for the $Q_{supcell}$ of 1, 10 and 100 nM·s^{-1}. The [eNOS] was set at 0.048, 0.097 and 0.144 µM @ t= 0 min. The [ASC] was varied from control, 5, 10, 25, 50, 100 and 200 µM, where control being no ASC introduced in the system. Q_{BH4} was set at 0.5 nM·s−1. The [TBP] was set at 7 µM and [BH4]/[TBP] was set at 0.05 at t = 0 min. The initial concentrations of GSH, L-arginine, O_2, SOD and CO_2 were 1 mM, 100 µM, 140 µM, 10 µM and 1.1 mM, respectively.

4.4.4. Effect of GSH and ASC on NO production

We analyzed the effect of physiological GSH concentration and ASC supplementation on the NO production rate under oxidative stress conditions. Figure 17 show that, GSH at higher millimolar concentration can slightly improve NO production rate. However, enhanced NO production rate, under oxidative stress conditions, was observed only in the presence of ASC. This slight increase in NO production rate can be attributed to the NO coming from the reaction between GSNO and $O_2^{\bullet-}$.
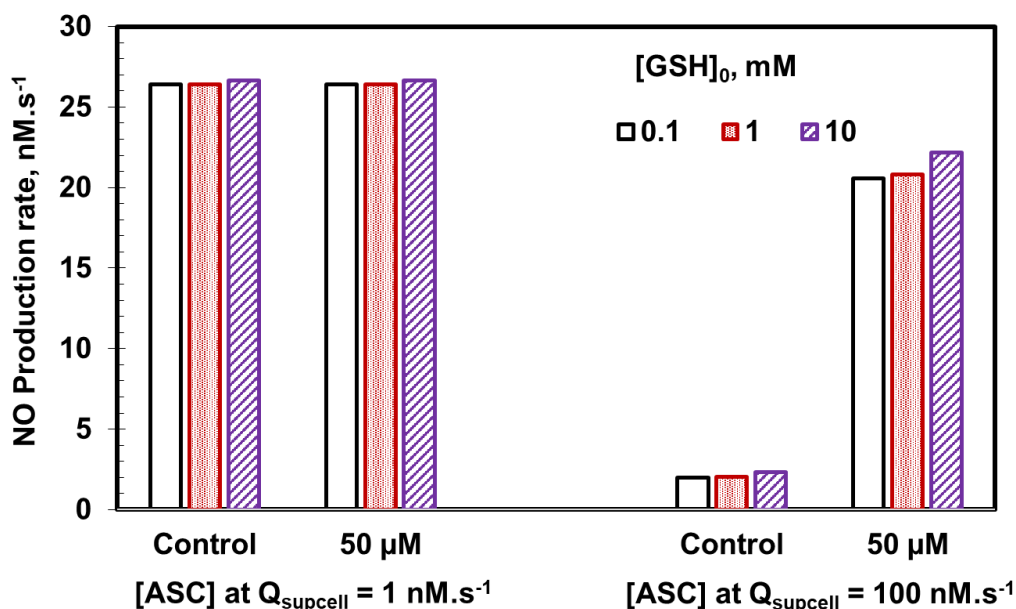
Figure 17: Steady state concentrations of NO production rate as a function of GSH and ASC. The steady state NO production rate was analyzed for varied [GSH] at t=0 min at 0.1, 1 and 10 mM. The [ASC] was control and 50 µM, where control being no ASC introduced in the system. The $Q_{supcell}$ was 1 and 100 nM·s^{-1}. Q_{BH4} was set at 0.5 nM.s^{-1}. The [TBP] and biopterin ratio was set at 7 µM and 0.05 @ t = 0 min, respectively. The initial concentration of eNOS, L-arginine, O_2, SOD and CO_2 was 0.097 µM, 100 µM, 140 µM, 10 µM and 1.1 mM, respectively.

4.4.5. Effect of GPX and Prx on the role of ASC in oxidative stress

Our earlier results in this study show that ASC supplementation although improves NO production rate, it also increased $ONOO^-$ levels. Glutathione peroxidase (GPX) and peroxiredoxins (Prx) are reported to detoxify $ONOO^-$ as well as H_2O_2 in endothelial cells [105, 109, 166, 179]. We revised our existing model by adding below 4 reactions for $ONOO^-$ and H_2O_2 clearance by reduced GPX (GPXr) and reduced Prx (Prx-SH$_2$);

$$GPXr + ONOO^- \xrightarrow{k_a} GPXo + NO_2^-$$

$$GPXr + H_2O_2 \xrightarrow{k_b} GPXo + H_2O$$

$$ONOOH + Prx\text{-}(SH_2) \xrightarrow{k_c} NO_2 + Prx\text{-}SOH + 2H^+$$

$$H_2O_2 + Prx\text{-}(SH_2) \xrightarrow{k_d} H_2O + Prx\text{-}SOH$$
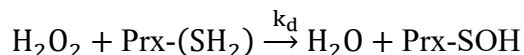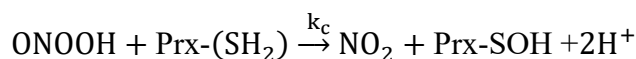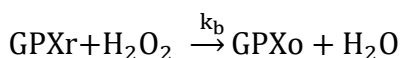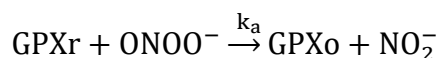
where, the rate constants k_a, k_b, k_c and k_d are 2×10^6 $M^{-1}.s^{-1}$, 2.1×10^7 $M^{-1}.s^{-1}$, 1×10^7 $M^{-1}.s^{-1}$ and 1.3×10^7 $M^{-1}.s^{-1}$, respectively. The details for these reactions and rate constants can be found in Chapter V, Table 9. We used the concentrations of GPX and Prx as 5 µM and 20 µM.

Figure 18 shows the temporal profiles of species including NO production rate, TBP, biopterin ratio and $ONOO^-$ levels as a function of GPX and Prx under oxidative stress conditions and for ASC supplementation. The presence of GPX and Prx, decreased $ONOO^-$ levels considerably (compare Figure 14S and Figure 18H) and improved NO production rate even at ASC supplementation of as low as 10 µM (compare Figure 14C and Figure 18B). The improvement in NO production rate in the presence of GPX and Prx can be attributed to the improved TBP levels and biopterin ratio. Lower $ONOO^-$ levels resulted in less oxidation of BH$_4$, thus improving BH$_4$ bioavailability.
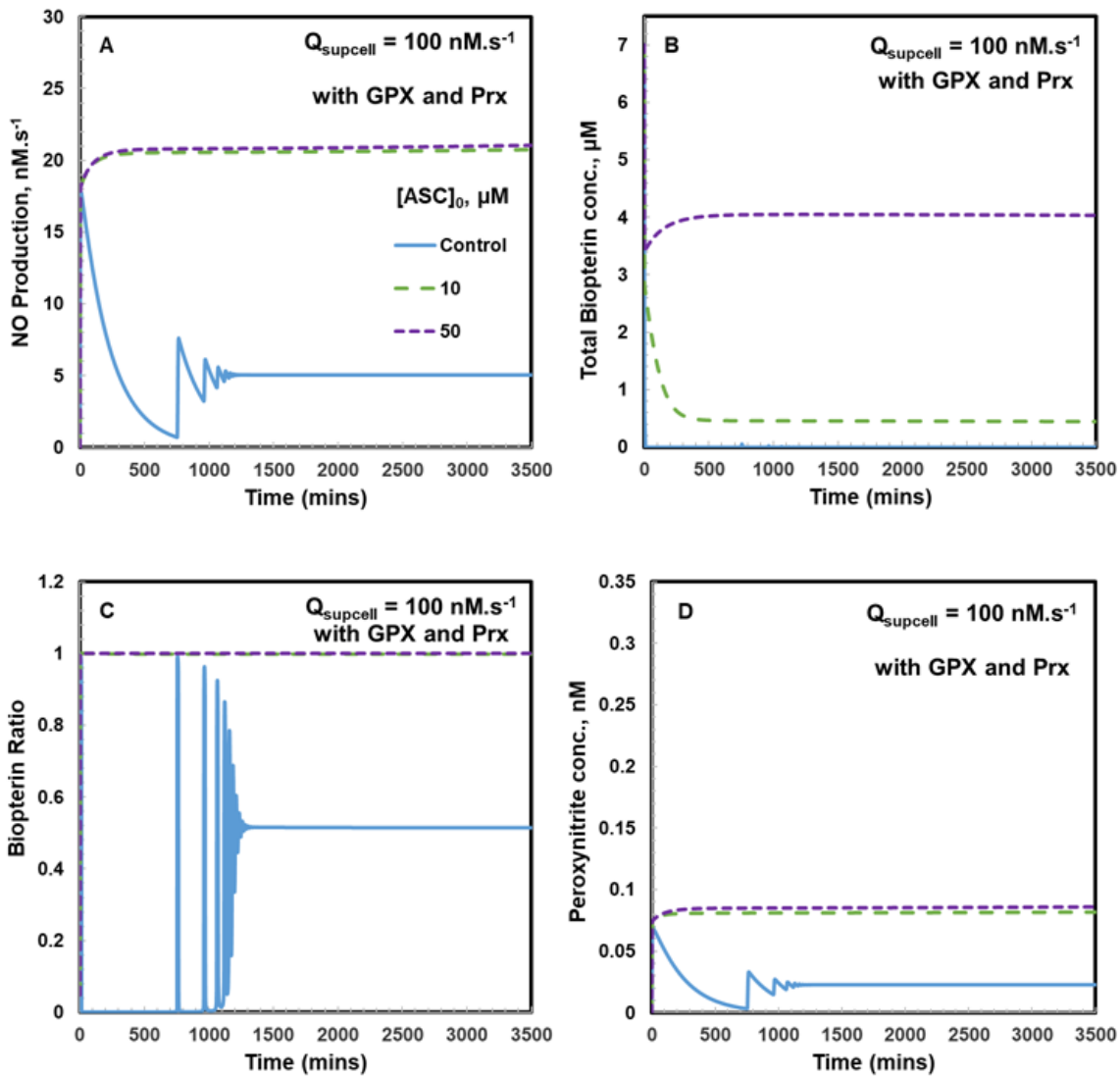
Figure 18: Temporal profile of species as a function of ASC supplementation in the presence of GPX and Prx under oxidative stress conditions. Panels A–D show ASC dependent the temporal variation in various species for the $Q_{supcell}$ of 100 nM·s^{-1}. The [ASC] was varied from control, 10 and 50 µM, where control being no ASC introduced in the system. Q_{BH4} was set at 0.5 nM.s^{-1}. The [TBP] and biopterin ratio was set at 7 µM and 0.05 @ t = 0 min, respectively. The initial concentration of GSH, eNOS, L-arginine, O_2, SOD and CO_2 was 1 mM, 0.097 µM, 100 µM, 140 µM, 10 µM and 1.1 mM, respectively.

4.4. Discussions

4.4.1. Role of ascorbate in endothelial dysfunction

ASC is shown to improve endothelial function by increasing the bioavailability of NO in diseases with increased oxidative stress such as hypertension [273], diabetes [274, 275], hyperhomocysteinemia [276]. A clinical study done by Ceriello *et al.* [274] showed that during induced acute hypoglycemia, reduction in the generation of oxidative stress and inflammation and improvement in endothelial dysfunction is observed by infusion of ASC in type 1 diabetes patients. Another clinical study done by Grebe *et al.* [35] showed that ASC supplementation increased flow-mediated dilation in patient suffering from obstructive sleep apnea, a condition of endothelial dysfunction caused due to oxidative stress. ASC supplementation is reported to prevent oxidative/nitrosative stress by decreasing $O_2^{\bullet-}$ levels in DOX-treated wistar rats [147]. Our model results agree with these *in vivo* studies. Our results showed that under oxidative stress conditions, the NO production rate from eNOS are decreased by almost 99% due to reactions with reactive species. ASC supplementation improved NO production rate by 85% (as seen in Figure 14). ASC supplementation also decreased $O_2^{\bullet-}$ levels, however it was not considerable.

4.4.2. Ascorbate improves NO bioavailability by increasing the tetrahydrobiopterin bioavailability and stabilizing eNOS

One of the proposed mechanistic roles of ASC in endothelial dysfunction is improved BH_4 bioavailability. Baker *et al.* [251] reported that ASC supplementation increased the intracellular BH_4 content in endothelial cells and subsequently enhanced eNOS activity. Heller *et al.* [277] reported, ASC pretreatment in the range of 0.1-100 µM in HUVEC's led to a 3-fold increase of the cellular production of NO, when 3 µM of BH_4 was added to the cell lysate. They further reported the effect was saturated at [ASC] of 100 µM and that ASC is involved in either enhancing

the availability of BH_4 or increasing its affinity for the eNOS. Valent *et al.* [278] in their study of spectrophotometric analysis of the protective effect of ASC against spontaneous oxidation of BH_4 in aqueous solution reported that the half-life time of BH_4 was increased by 1.4-fold in the presence of 100 μM of ASC and ASC maintained BH_4 levels. They also reported ASC did not convert oxidized BH_2 to reduced BH_4. Kinetic study by Patel *et al.* [144] reported that ASC protects BH_4 indirectly by repairing the •BH_3 radical which was determined by studying the decay of the •BH_3 radical in the absence and presence of ASC. The study on EPR-kinetic analysis and characterization of the pteridine radical also showed that ASC is not capable of reducing BH_2 to BH_4 [279]. Our model results provide evidence that ASC improves endothelial dysfunction by increasing total biopterin levels and improving biopterin ratio. ASC supplementation also stabilized eNOS due to improved biopterin ratio and hence increased NO production rate was observed in the presence of ASC in oxidative stress conditions. Our model results also showed saturation effect of ASC around 100 μM, since 90 % improvement in NO production rate, TBP levels and biopterin ratio was observed ≥ 50 μM. Increase in NO production rate was also observed at higher physiological concentrations of GSH (Figure 17). This suggests increasing levels of NO donor, such as GSNO may be a strategy to improve NO bioavailability. Details of interactions of GSH enzyme system in oxidative and nitrosative stress and the mechanisms of GSNO formation can be found in Chapter V. Further, our results for combination therapy of BH_4 and ASC confirmed that ASC is efficient for improving the NO levels by stabilizing eNOS and making more BH_4 available for eNOS coupling at higher cellular oxidative stress. Our results indicate that ASC supplementation would be effective in cases of BH_4 deficiency or impaired BH_4 synthesis.

4.4.3. Role of ascorbate in scavenging reactive species

Several studies have reported that ASC can improve NO bioavailability by scavenging reactive species including $O_2^{\bullet-}$ and $ONOO^-$ [147, 257, 280]. Study by Meade *et al.* [281] reported local infusion of ASC augmented NO-dependent cutaneous vasodilation, due to the sensitivity of ROS to ASC, in patients experiencing increased oxidative stress conditions. Study by Jackson *et al.* [145] on isolated rabbit arterial segments reported that ASC is not as effective as using SOD for scavenging $O_2^{\bullet-}$ radical. ASC is reported to decrease cellular ROS by inhibiting expression of NADPH oxidase subunit p47^{phox} induced by inflammatory insults [282] or by inhibiting the expression of inducible NOS [283]. However, it is suggested that reduced expression of these enzymes by ASC most likely results from its modulation of cellular redox signaling [264]. Our model results confirmed these observation by showing no decrease in $[O_2^{\bullet-}]$ at $Q_{supcell}$ of 1000 nM.s^{-1} for ASC supplementation of 50 µM and above, while only 17% and 13% decrease in $[O_2^{\bullet-}]$ at $Q_{supcell}$ of 10 and 100 nM.s^{-1} respectively. Further our model results showed that ASC supplementation under oxidative stress conditions led to 10 – 40 fold increase in $[ONOO^-]$ levels. The increase in $ONOO^-$ levels was attributed to increase in NO production rate due to ASC supplementation. Reaction between increased NO production from eNOS and $O_2^{\bullet-}$ from cellular oxidative stress leads to increased $ONOO^-$ levels [284]. When we modeled reactions of GPX and Prx for $ONOO^-$ and H_2O_2 clearance, considerable decrease in the levels of $ONOO^-$ and H_2O_2, as well as increased TBP levels were was observed in our system. This was attributed to less oxidation of BH_4 by $ONOO^-$.

4.4.4. Increasing eNOS concentration and ascorbate supplementation considerably improves NO bioavailability

ASC is reported to increase eNOS activity by changing its phosphorylation [116] and S-nitrosylation status [116]. Further, studies have reported significant increase in eNOS expression and protein concentration under oxidative stress conditions [95, 138, 222]. Hink *et al.* [285] reported increase in the expression of eNOS and its protein concentration by 3-folds in diabetic rats at higher oxidative stress conditions. Similarly, study by Dubois *et al.* [286] reported up-regulation in eNOS in the lungs of mice exposed to chronic hypoxia. The increase in eNOS protein concentration was 2-fold while mRNA expression increased by 300-fold in lungs of mice exposed to chronic hypoxia up to 21 days. However, this more eNOS led to increase in cellular oxidative stress due to eNOS uncoupling and significant reduction in NO levels. In our model, we the altered eNOS protein concentration and studied its effect on eNOS NO production rate under oxidative stress (Figure 16). Our model results suggest that concentration of eNOS played critical role in determining the NO bioavailability and higher ASC supplementation concentrations were needed at higher oxidative stress conditions. However, caution should be taken for the use of enhancing eNOS strategy, as enhancing eNOS under oxidative stress may also lead to enhanced eNOS uncoupling.

4.5. Conclusion

We investigated the role of ASC in endothelial dysfunction by integrating the putative mechanisms of ASC in improving endothelial dysfunction as suggested in individual studies. For this we extended our computational model developed in Chapter III and analyzed the interactions of endothelial cell oxidative stress, BH_4 synthesis and biopterin ratio in the presence of ASC and GSH. Our model results showed that ASC supplementation improved NO production rate, TBP

levels and biopterin ratio in oxidative stress conditions. Our results indicate that the important mechanisms by which ASC improved NO bioavailability is by improving biopterin ratio and stabilizing eNOS. Our results further showed that enhancing eNOS with higher ASC supplementation resulted in considerable increase in NO production rates. The model results showed the effect of ASC on scavenging of $O_2^{\bullet-}$ is not considerable. ASC supplementation also increased $ONOO^-$ levels, which can be kept in control in the presence of physiological GPX and Prx. Our model results for simultaneous increase in ASC and BH_4 synthesis showed that higher Q_{BH4} was required to maintain elevated NO production rates in the absence of ASC. Higher NO production rates can be attained with the introduction of ASC even at low Q_{BH4}. Our results indicated that ASC supplementation can be used as an effective strategy in conditions were BH_4 is depleted.

CHAPTER V

INTERACTIONS OF GSH/GPX SYSTEM WITH ROS/RNS[3]

5.1. Introduction

Glutathione (GSH) is one of the most abundant low molecular weight non-protein thiols synthesized in cells, functionally involved in variety of cellular antioxidant systems. It is a tripeptide formed of glutamine, glycine and cysteine amino acids of which the cysteine amino acid gives GSH its reducing capacity [152, 287]. GSH is considered as a potent antioxidant due to its ability to reduce reactive species, predominantly present in the reduced form, its abundance inside the cell and ability to reversibly oxidize. The GSH imbalance of has been reported in many disease states including atherosclerosis, cancer, neurodegenerative disease, and aging [40, 288, 289]. GSH depletion can lead to an increase in the ROS and RNS generation, an increase in mitochondrial complex I activity and NADPH oxidation, a decrease in cell viability, and an impairment of ATP generation [155-157, 290].

Glutathione peroxidase (GPX) catalyzes consumption of GSH to reduce many oxidative species including H_2O_2, organic hydro-peroxides, $ONOO^-$, and lipid hydro-peroxide [105, 158]. However, GPX can remove ROS only in a certain range. When ROS production overtakes the GPX capability beyond this range, ROS levels would increase [165]. Depletion in GPX has also been implicated in several pathophysiological conditions [37, 38, 106]. Thus, GSH and GPX play an important role in modulating ROS and RNS levels in biological systems.

---

[3] Manuscript submitted

Several experimental and computational studies (as discussed in the literature review section 2.5.3) have demonstrated that GSH/GPX system interacts with ROS/RNS. However, it is not clear how this cross talk affects these reactive species and GSH/GPX enzyme system, under physiologic and oxidative/nitrosative stress conditions. In the present study, we developed a detailed endothelial cell kinetic model to understand the relationship amongst the key enzyme systems including GSH, GPX, Prx and reactive species, such as H_2O_2, $ONOO^-$, and dinitrogen trioxide (N_2O_3). The analysis presented in this study would help us interpret the complex interactions amongst reactive species and enzyme systems under physiologic and oxidative/nitrosative stress conditions.

5.2. Materials and Method

5.2.1. Model description

Figure 19 shows the schematics of the reaction pathways showing interactions of $O_2^{\bullet-}$ and NO, and their derivative products including H_2O_2, N_2O_3, and $ONOO^-$ with GSH and GPX system in an endothelial cell. The reaction rate constants used in building the model are also depicted in Figure 19 and detailed reactions and rate constants are shown in Table 9. In brief; (i) NO reacts with $O_2^{\bullet-}$ to generate $ONOO^-$ (k_4); (ii) $O_2^{\bullet-}$ undergoes self-dismutation (k_{18}) or by action of superoxide dismutase (SOD) (k_5) into H_2O_2; (iii) $ONOO^-$ (k_7) and H_2O_2 (k_{14}) oxidizes GPXr (reduced GPX) into GPXo (oxidized GPX); (iv) oxidized GPX is recycled to GPXr by GSH through two steps: first GSH combines GPXo to form a complex, GSGPX (k_{15}), then a second GSH converts GSGPX to regenerate GPXr and form GSSG (k_{16}); (v) catalase (k_{19}) and Prx (k_{20}) hydrolyzes H_2O_2; (vi) NO reacts with O_2 (multiple steps as shown in Table 1) to generate N_2O_3 (k_{12}), which hydrolyzes (k_{13}) or reacts with GSH to generate GSNO (k_{11}); (vi) GSNO reacts slowly with $O_2^{\bullet-}$ to generate GSSG (k_{10}); (vii) $ONOO^-$ reacts with GSH to generate GSNO and a small

amount of GSSG (k_6); (viii) GSNO reacts with GSH to generate NO (k_{17}); (ix) GSSG is reduced into GSH by NADPH (k_9). (x) ONOO$^-$ reacts with CO_2 (k_8) and is dismutated by Prx (k_{21}).
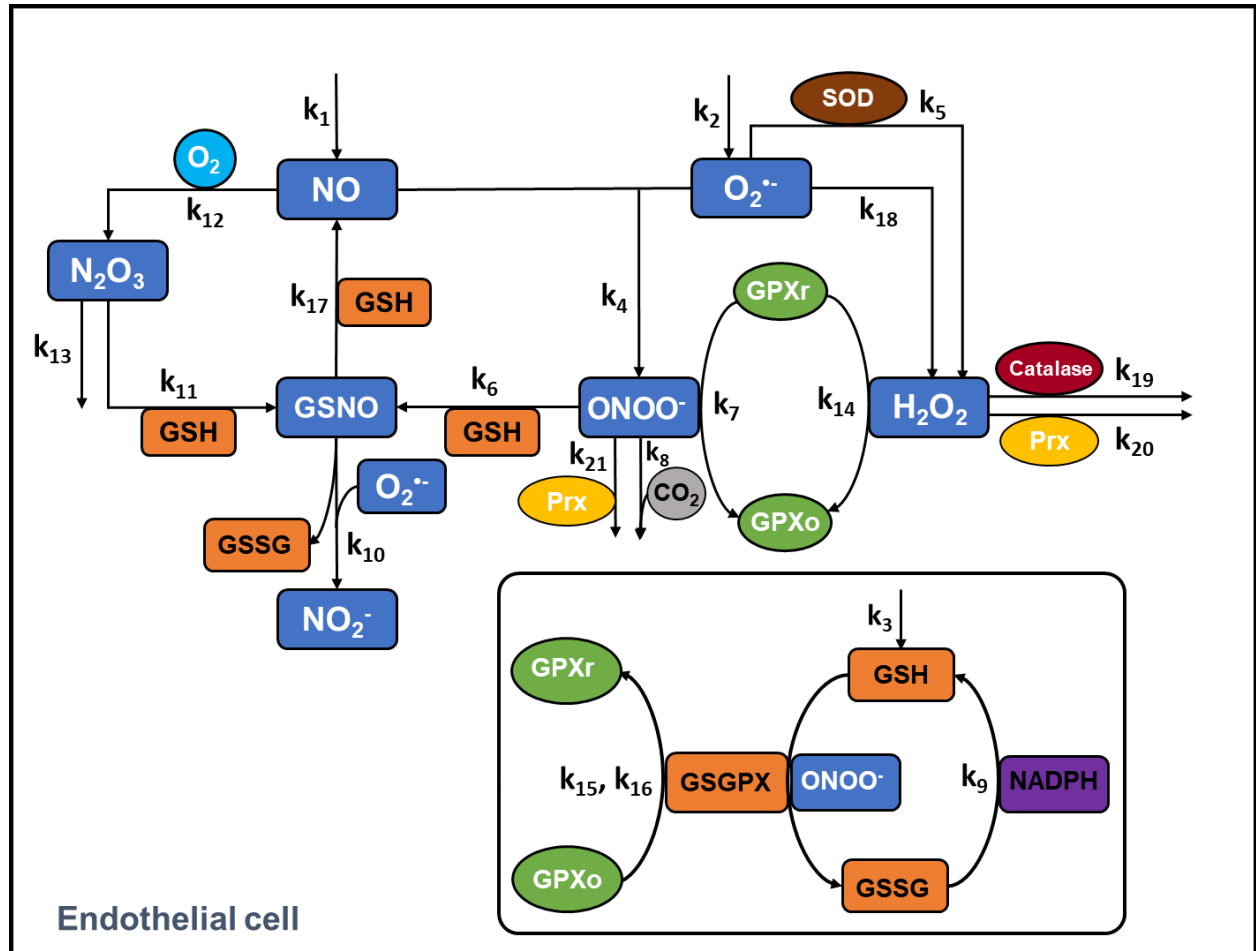
Figure 19: Schematics for reactions pathways showing interactions of $O_2^{•-}$/NO with GSH/GPX system in endothelial cell. Various species are represented inside round edged boxes, while the enzymes are represented in oval shaped boxes. Species such as O_2 and CO_2 are represented inside circles. The k values represent the rate constants for respective reactions and are detailed in Table 9.

5.2.2. Model Formulation

We developed a computational model to understand the dynamics of the interaction of ROS/RNS with GSH/GPX system in an endothelial cell. The modeled reaction kinetics network

is shown in the Figure 19. The kinetic model consisted of 12 mass balance algebraic-differential equations 1-12 for NO, $O_2^{\cdot-}$, $ONOO^-$, H_2O_2, GPXr, GPXo, GSGPX, GSH, GSSG, GSNO, nitrite (NO_2^-) and N_2O_3, respectively, as shown below. The initial condition for these 12 species was set at zero except or GSH and GPXr, as mentioned in the respective figure legends.

$$\frac{d[NO]}{dt} = k_1 - k_4[NO][O_2^-] - 4k_{12}[NO]^2[O_2] + k_{17}[GSNO][GSH] \tag{1}$$

$$\frac{d[O_2^{\cdot-}]}{dt} = k_2 - k_4[NO][O_2^-] - k_5[SOD][O_2^-] - k_{10}[GSNO]^2[O_2^-]$$

$$- k_{18}[HO_2^{\cdot}][O_2^-] \text{ (where, } [HO_2^{\cdot}] = 0.0025[O_2^-]) \tag{2}$$

$$\frac{d[ONOO^-]}{dt} = k_4[NO][O_2^-] - k_6[GSH][ONOO^-] - k_7[GPXr][ONOO^-] - k_8[ONOO^-][CO_2]$$

$$- k_{21}[Prx][ONOOH] \text{ (where, } [ONOOH]$$

$$= 0.5625[ONOO^-]) \tag{3}$$

$$\frac{d[H_2O_2]}{dt} = \frac{k_5[SOD][O_2^-]}{2} - k_{14}[H_2O_2][GPXr] + k_{18}[HO_2^{\cdot}][O_2^-] - 0.01k_{19}[H_2O_2][catalase]$$

$$- k_{20}[H_2O_2][Prx] \tag{4}$$

$$\frac{d[GPXr]}{dt} = -k_7[GPXr][ONOO^-] - k_{14}[H_2O_2][GPXr] + k_{16}[GSGPX][GSH] \tag{5}$$

$$\frac{d[GPXo]}{dt} = k_7[GPXr][ONOO^-] + k_{14}[H_2O_2][GPXr] - k_{15}[GSH][GPXo] \tag{6}$$

$$[GSGPX] = [GPXr]_i - [GPXr] - [GPXo] \tag{7}$$

$$\frac{d[GSH]}{dt} = k_3 - k_6[GSH][ONOO^-] + 2k_9[GSSG][NADPH] - k_{11}[N_2O_3][GSH] - k_{15}[GSH][GPXo]$$

$$- k_{16}[GSH][GSGPX] - k_{17}[GSNO][GSH] \tag{8}$$

$$\frac{d[GSSG]}{dt} = \frac{0.998k_6[GSH][ONOO^-]}{2} - k_9[NADPH][GSSG] + k_{10}[GSNO]^2[O_2^{\cdot-}]$$

$$+ k_{16}[GSGPX][GSH] + k_{17}[GSNO][GSH] \tag{9}$$

$$[GSNO] = [GSH]_i - [GSH] - 2[GSSG] - [GSGPX] \tag{10}$$

$$\frac{d[NO_2^-]}{dt} = k_7[GPXr][ONOO^-] + k_{10}[GSNO]^2[O_2^{\cdot-}] + k_{11}[N_2O_3][GSH] + k_{17}[GSNO][GSH] \tag{11}$$

$$\frac{d[N_2O_3]}{dt} = -k_{11}[N_2O_3][GSH] + 2k_{12}[NO]^2[O_2] - k_{13}[N_2O_3] \tag{12}$$

5.2.3. Model parameters

We assumed a homogeneous reaction model to account for the overall changes in the species concentration for the interactions of ROS/RNS with GSH/GPX system. The model parameters for NO and $O_2^{\cdot-}$ generation rates and reaction rate constants are summarized in Table 9. The generation rate of NO is denoted by 'k_1' and the generation rate of $O_2^{\cdot-}$ is denoted by 'k_2'. The value of k_1 was obtained from the previous modeling studies [93, 175, 291] and was fixed either at 1×10^{-6} $M^{-1}.s^{-1}$ or 1×10^{-7} $M^{-1}.s^{-1}$. The value of k_2 was varied such that ratio of generation rate of $O_2^{\cdot-}$ to that of NO (k_2/k_1) would be in the range of 0.01 to 10 based on the reported endothelial cell $O_2^{\cdot-}$ and NO production rates [93]. A low k_2/k_1 represents high generation rate of NO compared to that of $O_2^{\cdot-}$, which may represent nitrosative stress, and a high k_2/k_1 may represent oxidative stress.

Table 9: Reactions and rate constant used to develop the GSH/GPX computational model.

Rate constant	Value	Reaction	Reference
k_1	1×10^{-6} and 1×10^{-7} $M.s^{-1}$	Formation of NO	Hu *et al.* [175] Kar *et al.* [93] Vaughn *et al.* [291]

k_2	varied M.s^{-1} 1×10^{-8} - 10×10^{-6}	Formation of $O_2^{\bullet-}$	Kar *et al.* [93, 255]
k_3	0	Formation of GSH	Assumed
k_4	6.7×10^9 M^{-1}.s^{-1}	$O_2^{\cdot-} + NO \xrightarrow{k_4} ONOO^-$	Huie *et al.* [292]
k_5	1.6×10^9 M^{-1}.s^{-1}	$H_2O + O_2^{\cdot-} \xrightarrow{SOD,k_5} \frac{1}{2}O_2 + \frac{1}{2}H_2O_2 + OH^-$	Fielden *et al.* [293]
k_6	1.5×10^3 M^{-1}.s^{-1}	$ONOO^- + GSH \xrightarrow{k_6} GSNO + GSSG$	van der Vilet *et al.* [294]
k_7	2×10^6 M^{-1}.s^{-1}	$GPXr + ONOO^- \xrightarrow{k_7} GPXo + NO_2^-$	Sies *et al.* [105]
k_8	5.8×10^4 M^{-1}.s^{-1}	$ONOO^- + CO_2 \xrightarrow{k_8} ONOOCO_2^-$	Denicola *et al.* [295]
k_9	3.2×10^6 M^{-1}.s^{-1}	$GSSG + NADPH + H^+ \xrightarrow{k_9} 2GSH + NADP^+$	Henderson *et al.* [118]
k_{10}	9×10^8 M^{-2}.s^{-1}	$O_2^{\bullet-} + 2GSNO + H_2O \xrightarrow{k_{10}} GSSG + NO_2^- + NO_3^- + 2H^+$	Jourd'heuil *et al.* [263]
k_{11}	6.6×10^7 M^{-1}.s^{-1}	$N_2O_3 + GSH \xrightarrow{k_{11}} GSNO + H^+ + NO_2^-$	Keshive *et al.* [262]
k_{12}	2.4×10^6 M^{-2}.s^{-1}	$2NO + O_2 \rightarrow 2NO_2$ $NO + NO_2 \leftrightarrow N_2O_3$ $\underline{N_2O_3 + H_2O \rightarrow 2NO_2^- + 2H^+}$ $4NO + O_2 + H_2O \xrightarrow{k_{12}} 4NO_2^- + 4H^+$	Potdar *et al.* [199]
k_{13}	1.6×10^3 M^{-1}.s^{-1}	$N_2O_3 + H_2O \xrightarrow{k_{13}} 2NO_2^- + 2H^+$	Licht *et al.* [259]
k_{14}	2.1×10^7 M^{-1}.s^{-1}	$GPXr + H_2O_2 \xrightarrow{k_{14}} GPXo + H_2O$	Antunes *et al.* [296]
k_{15}	4×10^4 M^{-1}.s^{-1}	$GPXo + GSH \xrightarrow{k_{15}} GSGPX + H_2O$	Antunes *et al.* [296]
k_{16}	1×10^7 M^{-1}.s^{-1}	$GSGPX + GSH \xrightarrow{k_{16}} GPXr + GSSG + H^+$	Antunes *et al.* [296]
k_{17}	5.5×10^{-3} M^{-1}.s^{-1}	$GSNO + GSH \xrightarrow{k_{17}} GSSG + NH_3 + N_2O + NO_2^- + NO$	Hogg *et al.* [297] Dicks *et al.* [298]
k_{18}	8.0×10^7 M^{-1}.s^{-1}	$HO_2^{\cdot} + O_2^{\cdot-} + H^+ \xrightarrow{k_{18}} O_2 + H_2O_2$	Potdar *et al.* [199]
k_{19}	3.4×10^7 M^{-1}.s^{-1}	$H_2O_2 + H_2O_2 \xrightarrow{catalase,k_{19}} O_2 + 2H_2O$	Aebi *et al.* [260]

k_{20}	1.3×10^7 M^{-1}.s^{-1}	$H_2O_2 + \text{Prx-(SH}_2) \xrightarrow{k_{20}} H_2O + \text{Prx-SOH}$	Huang *et al.* [299], Winterbourne *et al.* [166]
k_{21}	1×10^7 M^{-1}.s^{-1}	$ONOOH + \text{Prx-(SH}_2) \xrightarrow{k_{21}} NO_2$ $+ \text{Prx-SOH} + 2H^+$	De Armas *et al.* [109], Text

Table 10 shows the initial concentration of species used in the model. The interaction between GSH and oxidative stress is complex. GSH depletion can increase oxidative stress and an increase in oxidative stress can decrease GSH levels [300]. In addition to GSH consumption through oxidative stress, GSH concentration can also be affected through regulation of GSH synthesis via r-glutamyl cysteine ligase and glutathione synthetase enzymes [301]. GSH can be oxidized or nitrosated to GSSG or GSNO by multiple oxidative species or nitrosative species [302]. Physiological concentrations of GSH range from 0.5 to 10 mM in cells and 2 to 20 µM in plasma with GSH accounting for ~85-90% of the total glutathione pool [266, 270]. To investigate the role of GSH in physiologic and pathologic conditions, we varied the initial concentration of GSH ([GSH]$_i$) from 1 µM to 100 mM [178, 270]. GSH is maintained in its reduced form by NADPH-dependent glutathione reductase, such that one molecule of GSSG can recycle 2 molecules of GSH by NADPH [118]. We used the NADPH concentration of 30 µM, which was obtained from a human umbilical vein endothelial cells (HUVECs) [303]. The rate constant for the reaction used was 3.2×10^6 M^{-1}s^{-1} (k_9) [118]. GPXr is involved in the removal of H_2O_2 and ONOO$^-$. We assumed GPXr concentration of 5 µM [304]. When GPXr concentration is less than H_2O_2 concentration, H_2O_2 removal is dependent on GPX and GSH concentration [176]. GPX knockout mice have a very short survival time (4 hours) under acute oxidative stress [305]. To understand the effect of GPX deficiency, the initial concentration of GPXr ([GPXr]$_i$) was varied from a low level of 5 pM to normal physiologic level of 5 µM and supplementation of upto 50

μM [176, 305]. The peroxisome volume to the total cell volume ratio is 1%. Based on this we calculated the removal of H_2O_2 via catalase at the rate of 3.4×10^7 $M^{-1} s^{-1}$ [260, 303]. Recently, Prx was reported to be involved in detoxifying H_2O_2 and $ONOO^-$ [130, 179]. We analyzed the presence of Prx on our model system and Prx concentration of 20 μM was used [166]. The kinetic parameters for dismutation of H_2O_2 and $ONOO^-$ by Prx are in Table 1. The fraction of total peroxynitrite ($ONOOH+ONOO^-$) present in anion form ($ONOO^-$) was calculated as described by Kavdia [226]. The ratio of $ONOO^-$ with total peroxynitrite calculated was 0.64 resulting in [ONOOH] = 0.5625[$ONOO^-$] and is incorporated in equation 3.

Table 10: Species/enzyme concentrations used in GSH/GPX model

Species	Concentration	Reference
SOD	10 μM	Beckman *et al.* [306]
CO_2	1.14 mM	Radi *et al.* [307]
O_2	35 μM	Antunes *et al.* [296]
Catalase	0.9 μM	Aebi *et al.* [260]
$[GPXr]_i$	5 μM	Jacobson *et al.* [304]
$[GSH]_i$	0.1, 1, 10 mM	Griffith *et al.* [308]
NADPH	30 μM	Adimora [179] and Sasaki [303] *et al.*
Prx	20 μM	Winterbourne *et al.* [166]

We simulated two scenarios in our modeling study; i) to provide a wide range of RNS and ROS and analyze the temporal behavior of the species in the model, we varied the generation rates of $O_2^{\bullet-}$ and NO and ii) to quantitatively understand the significance of interactions of GSH and

GPX system with ROS and RNS, we explored steady-state concentrations of species at various k_2/k_1 ratios, at varying $[GSH]_i$, $[GPXr]_i$ and NADPH concentration. For both these scenarios the NO generation rate (k_1) was fixed at either 1×10^{-6} M.s^{-1} or 1×10^{-7} M.s^{-1} and the $O_2^{\bullet-}$ generation rate was changed to represent the cellular level of oxidative or nitrosative stress. Apart from this, we also analyzed the presence of Prx on the overall interactions of ROS/RNS with GSH/GPX system.

5.2.4. Numerical Simulations

The system of algebraic- and differential- equations (1 – 12) were solved numerically using MATLAB 2017b (Mathworks Inc., Natick, MA) stiff solver ode15s. The relative error and absolute error were set at 1×10^{-10} and 1×10^{-15}, respectively for all simulated cases. The simulations were run long enough for all participating species to reach steady state. This was achieved with a time span of 2000 min.

5.3. Results

5.3.1. N_2O_3 acts as a mediator of GSH nitrosation and GPXr recycling in nitrosative stress

The simulations were performed for the ratio of generation rate of $O_2^{\bullet-}$ to that of NO (k_2/k_1) of 0.01, 0.1, 0.5, 1, and 2. The initial concentration of GSH and GPXr was 1 mM and 5 µM, respectively. Figure 20 and Figure 21 show the species profiles for the NO generation rate of 1×10^{-6} and 1×10^{-7} M.s^{-1}, respectively. As seen in Figure 20, the concentration of NO and N_2O_3 decreased whereas the concentration of $O_2^{\bullet-}$, ONOO$^-$ and H_2O_2 increased for the ratio of k_2/k_1 from 0.01 to 2, (i.e. the $O_2^{\bullet-}$ generation rate range of 0.01 to 2×10^{-6} M.s^{-1}, respectively). When $k_2/k_1 \leq 1$, GSH was converted into GSNO because of higher concentration of NO and N_2O_3. The recycling of GPXr by GSH was affected because of GSH depletion and resulted in higher GPXo (oxidized form of GPXr) under these conditions. For k_2/k_1 of 2, the concentration of $O_2^{\bullet-}$, H_2O_2 and ONOO$^-$ increased and the concentration of NO and N_2O_3 decreased. GSH and GPXr remained in their

reduced forms for k_2/k_1 of 2. The recycling capacity of GSH and GPXr improved when the $O_2^{\bullet-}$ generation rate was greater than the NO generation rate.
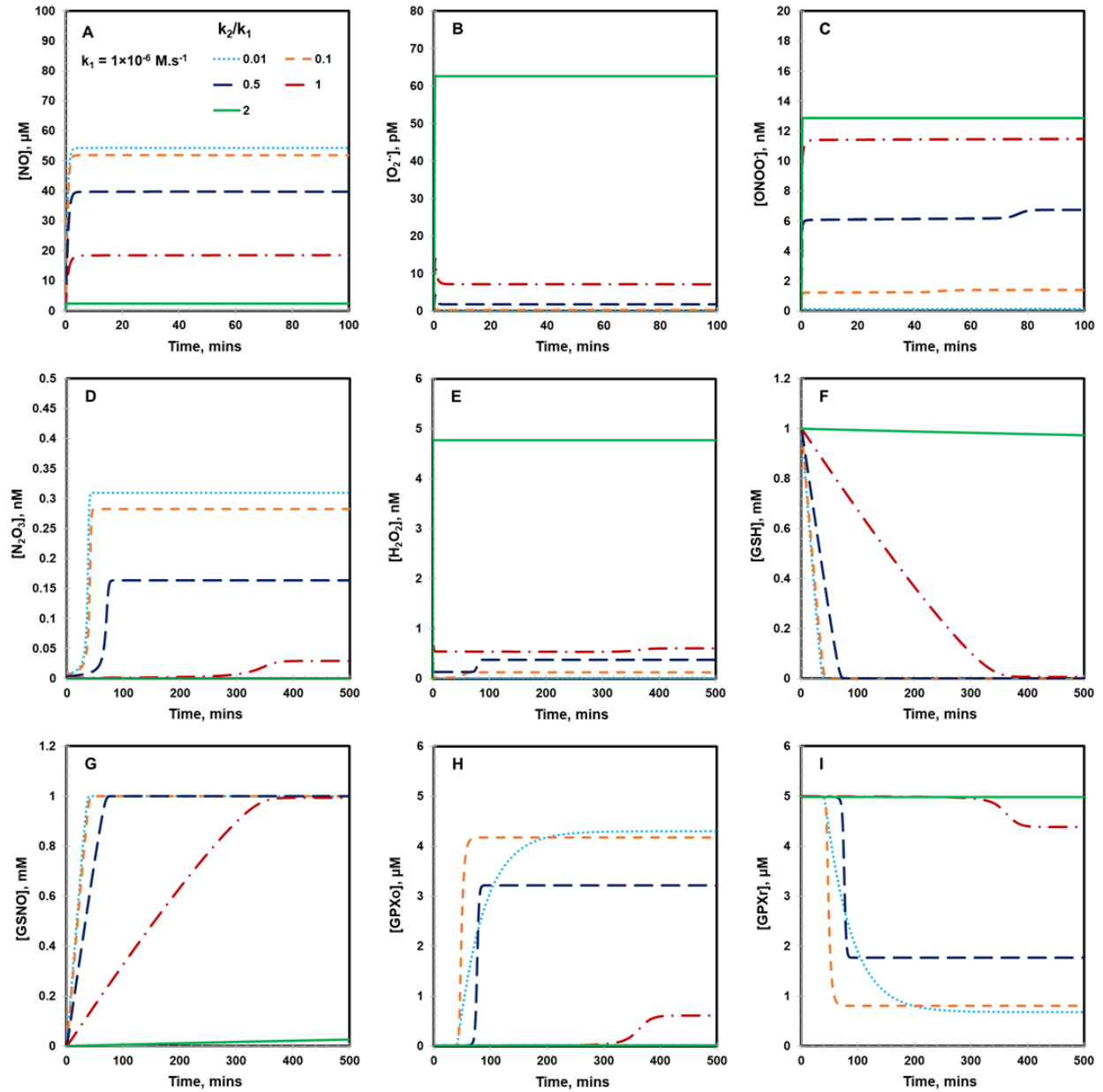
Figure 20: Concentration profiles of species for NO generation rate (k_1) of 1×10^{-6} $M.s^{-1}$. Panels A-I show temporal concentration profiles for species with a change in the ratio of the generation rate of $O_2^{\bullet-}$ to that of NO (k_2/k_1). The initial concentration of GSH, GPXr, SOD, catalase, NADPH, O_2 and CO_2 concentrations were set at 1mM, 5 µM, 10 µM, 0.9 µM, 30 µM, 35 µM and 1.14 mM respectively.
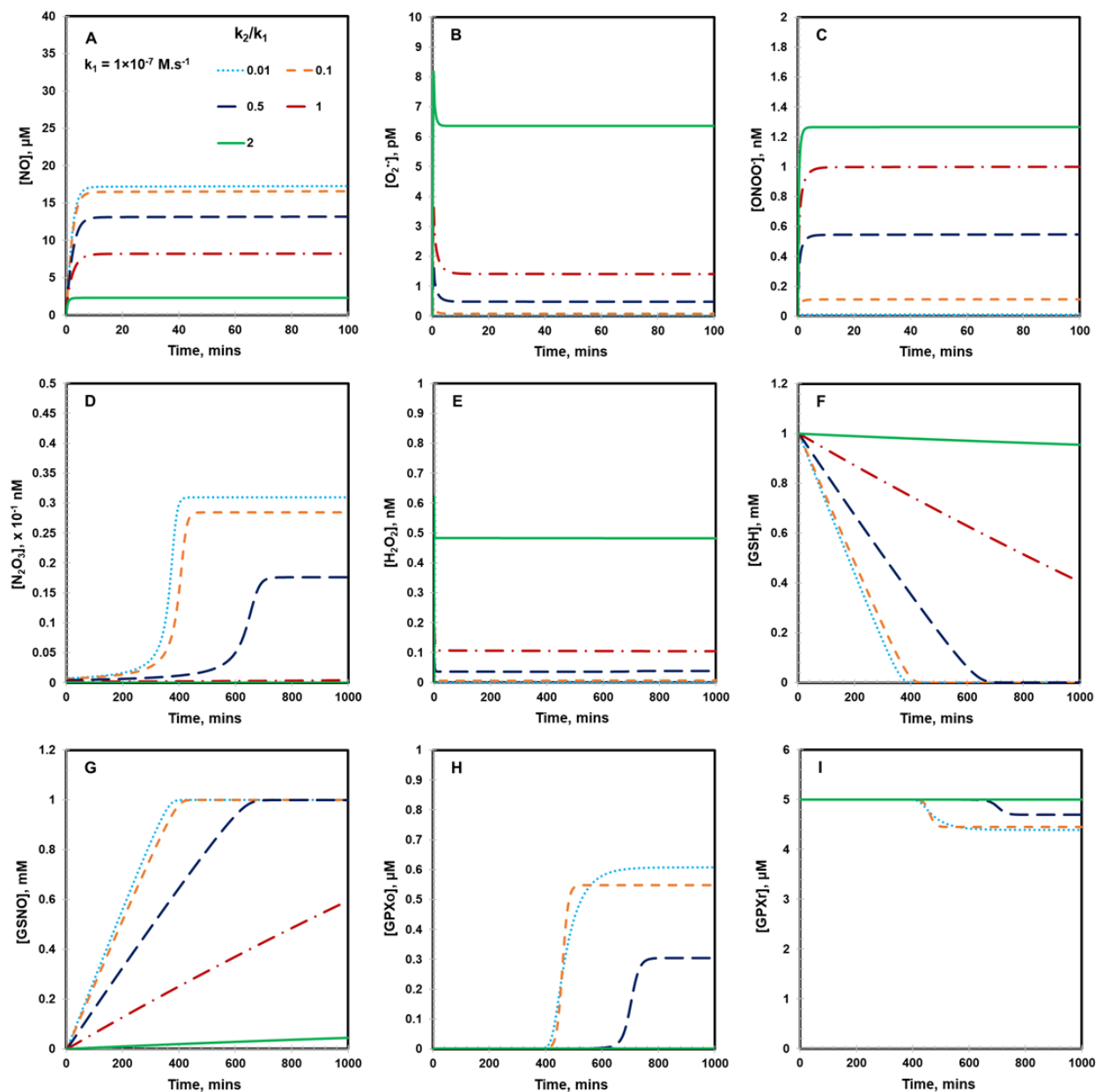
Figure 21: Concentration profiles of species for NO generation rate (k₁) of 1×10⁻⁷ M.s⁻¹. Panels A-I show temporal concentration profiles for species with a change in the ratio of the generation rate of $O_2^{\bullet-}$ to that of NO (k_2/k_1). The initial concentration of GSH, GPXr, SOD, catalase, NADPH, O_2 and CO_2 concentrations were set at 1mM, 5 µM, 10 µM, 0.9 µM, 30 µM, 35 µM and 1.14 mM respectively.

For the NO generation rate of 1×10^{-7}, Figure 21 showed that the NO and N_2O_3 concentrations decreased by 55-68% and 90%, respectively for k_2/k_1 of $0.01 - 1$. For k_2/k_1 of 2, there was no change in the concentration of NO and N_2O_3 because of low levels of NO. For both NO generation rates, the concentration of NO and N_2O_3 were 2.3 µM and 0.1 pM, respectively at k_2/k_1 of 2. The concentration of $O_2^{\bullet-}$, $ONOO^-$ and H_2O_2 decreased by almost $71 - 90$ % at k_1 of 1×10^{-7} $M.s^{-1}$ as compared to that of $k_1 = 1\times10^{-6}$ $M.s^{-1}$ (please refer Panels B, C and E in Figure 20 and Figure 21) for all k_2/k_1 ratios. Most of GSH and GPXr remained in reduced state at k_2/k_1 of 2 for both NO generation rates.

The above results showed that the GPX recycling is dependent on GSH availability and can be attributed to N_2O_3 but not to H_2O_2 and $ONOO^-$ levels under nitrosative stress (i.e. k_2/k_1 of <1). N_2O_3 is the mediating factor for GSH consumption through its nitrosation. A negligible concentration of N_2O_3 results in GSH to be maintained in its reduced form, whereas an increase in the concentration of N_2O_3 promotes conversion of GSH to GSNO. N_2O_3 mediation remained consistent in the presence of Prx, even though the H_2O_2 and $ONOO^-$ levels were reduced considerably as shown later in the Section 6.3.4. The GSH and GPX may remain in reduced state due to low availability of NO and N_2O_3 under oxidative stress conditions (i.e. k_2/k_1 equal to 2).

5.3.2. Effect of oxidative and nitrosative stress on the steady state concentrations of species

The effect of oxidative and nitrosative stress were simulated by varying the generation rate of $O_2^{\bullet-}$ to provide a range of k_2/k_1 from 0.001 to 10 for the NO generation rate of 1×10^{-6} and 1×10^{-7} M s^{-1}. The $[GSH]_i$ and $[GPXr]_i$ was 1 mM and 5 µM, respectively. As seen in Figure 22, the steady state concentrations of NO and N_2O_3 decreased for the change in k_2/k_1 from 0.1 to 3 for k_1 of 1×10^{-6} $M.s^{-1}$. GSH nitrosation to GSNO occurred for $k_2/k_1 \leq 1$, which can be attributed to N_2O_3 for both NO generation rates.
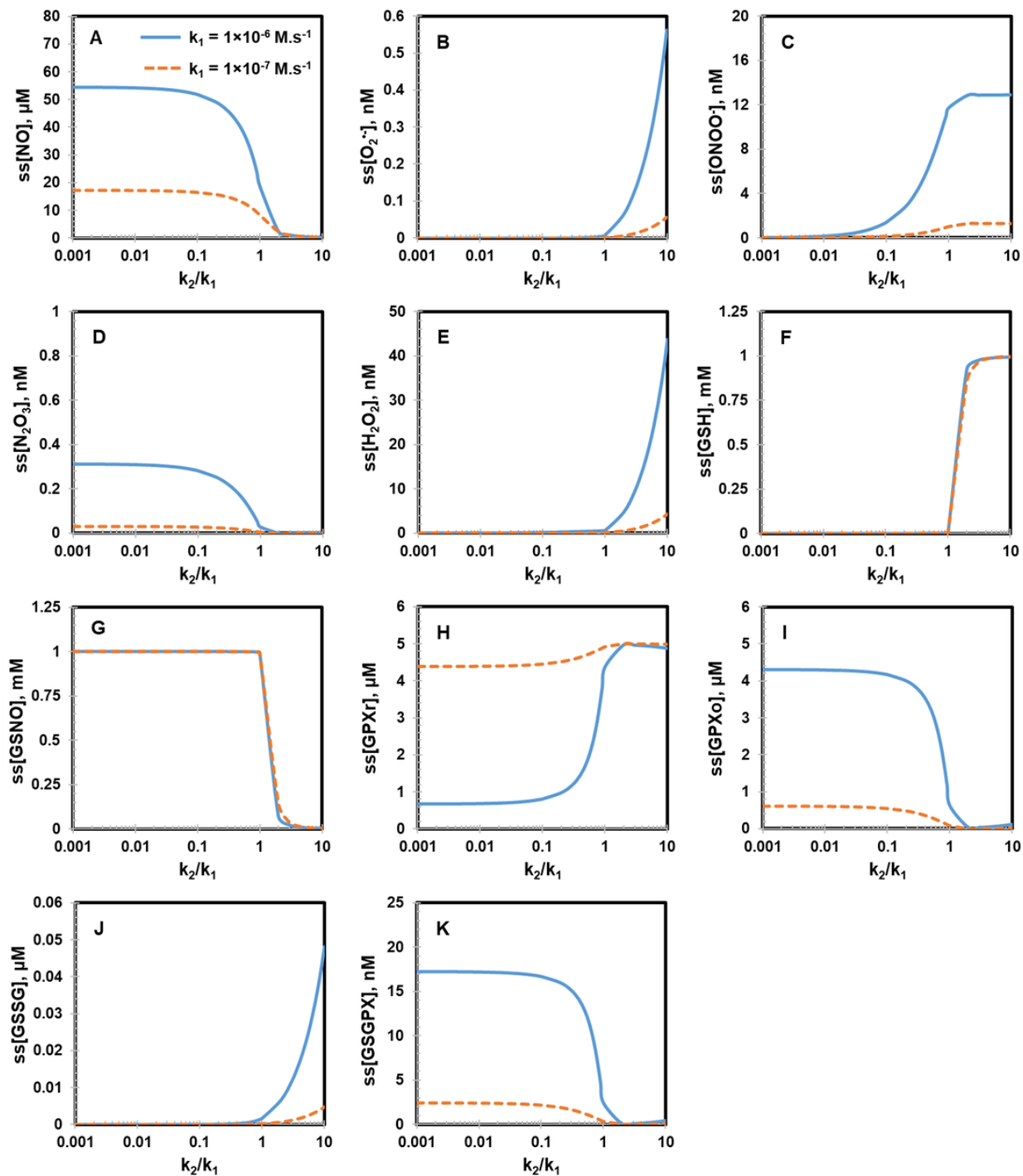
Figure 22: Steady-state concentrations profiles of species as a function of k_2/k_1. Panels A-K show semi log plots of steady state (ss) concentration for different species at NO generation rates (k_1) of 1×10^{-6} M.s^{-1} and 1×10^{-7} M.s^{-1}, respectively with respect to varied k_2/k_1 ratio on a logarithmic scale to the base 10. The initial concentration of GSH, GPXr, SOD, catalase, NADPH, O_2 and CO_2 concentrations were set at 1mM, 5 µM, 10 µM, 0.9 µM, 30 µM, 35 µM and 1.14 mM respectively.

For k_2/k_1 above 1, the $O_2^{•-}$ and H_2O_2 increased, the NO and N_2O_3 became negligible, and the GSH and GPXr remained in reduced form for both NO generation rates. GPXr remained primarily in the reduced state for lower NO generation rate (k_1 of 1×10^{-7} M.s^{-1}). These results indicate that the reducing capacity of GPX was dependent on GSH availability and on the level of oxidative/nitrosative stress.

5.3.3. Effect of varying GSH and GPXr on the steady state concentrations of species

Figure 23 and Figure 24 shows the species concentration profiles for initial concentrations of GSH and GPXr from 1 µM to 100 mM and from 5 pM to 50 µM, respectively. The NO generation rate was 1×10^{-6} and 1×10^{-7} M.s^{-1} and the k_2/k_1 ratio was kept constant at 1. The results showed that the steady state (ss) concentrations of NO and $O_2^{•-}$ were not affected by increasing $[GSH]_i$ from 0.001 to 1 mM. However, the ss[NO] increased and ss[$O_2^{•-}$] decreased for $[GSH]_i$ above 1 mM. The ss[ONOO$^-$] was 13.4 nM at k_1 of 1×10^{-6} M.s^{-1} and 1.2 nM for k_1 of 1×10^{-7} M.s^{-1} at all $[GSH]_i$ below 0.1mM. The ss[ONOO$^-$] decreased for $[GSH]_i$ above 0.1 mM. N_2O_3 concentration decreased for $[GSH]_i$ above 0.3 mM for both NO generation rates. The GSNO concentration reached a peak and decreased once N_2O_3 concentration became negligible at higher $[GSH]_i$. H_2O_2 concentration decreased considerably (Figure 23E) for $[GSH]_i$ below 0.3 and 0.1 mM for k_1 of 1×10^{-6} and 1×10^{-7} M.s^{-1}, respectively. GPXo reduced to GPXr for $[GSH]_i$ above 0.2 and 0.02 mM for k_1 of 1×10^{-6} and 1×10^{-7} M.s^{-1}, respectively.
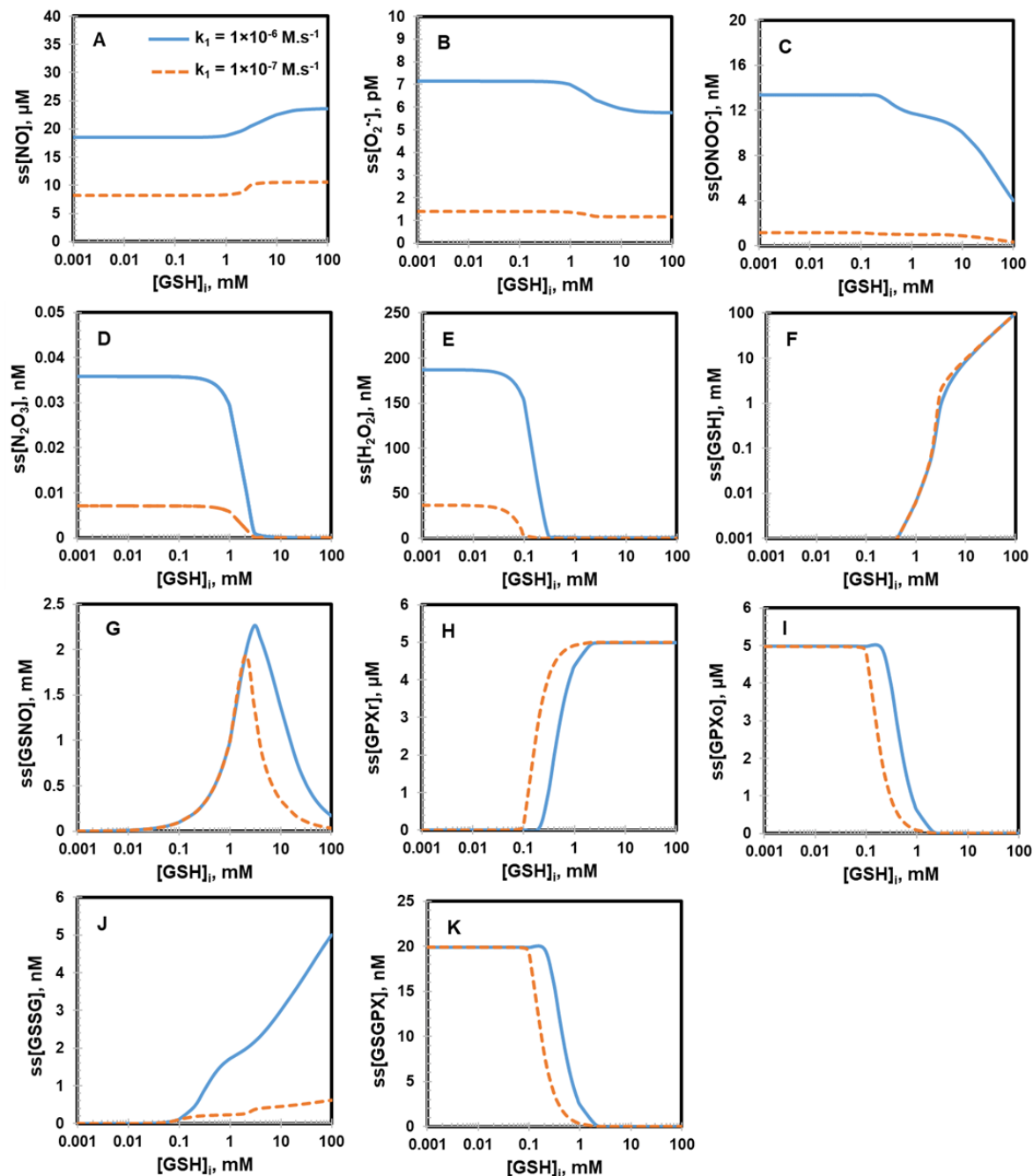
Figure 23: Steady-state concentrations profiles of species as a function of initial GSH concentration. Panels A-K, except for Panel F, show semi log plots for steady state (ss) concentration for different species at NO generation rates (k_1) of 1×10^{-6} M.s-1 and 1×10^{-7} M.s^{-1}, respectively, with respect to initial concentration of GSH on a logarithmic scale to the base 10. Panel F shows a log-log plot of ss[GSH] with respect to varied $[GSH]_i$. The NO and $O_2^{\bullet-}$ generation rates were kept equal (i.e. $k_2/k_1 = 1$). The GPXr, SOD, catalase, NADPH, O_2 and CO_2 concentrations were set at 5 µM, 10 µM, 0.9 µM, 30 µM, 35 µM and 1.14 mM respectively.
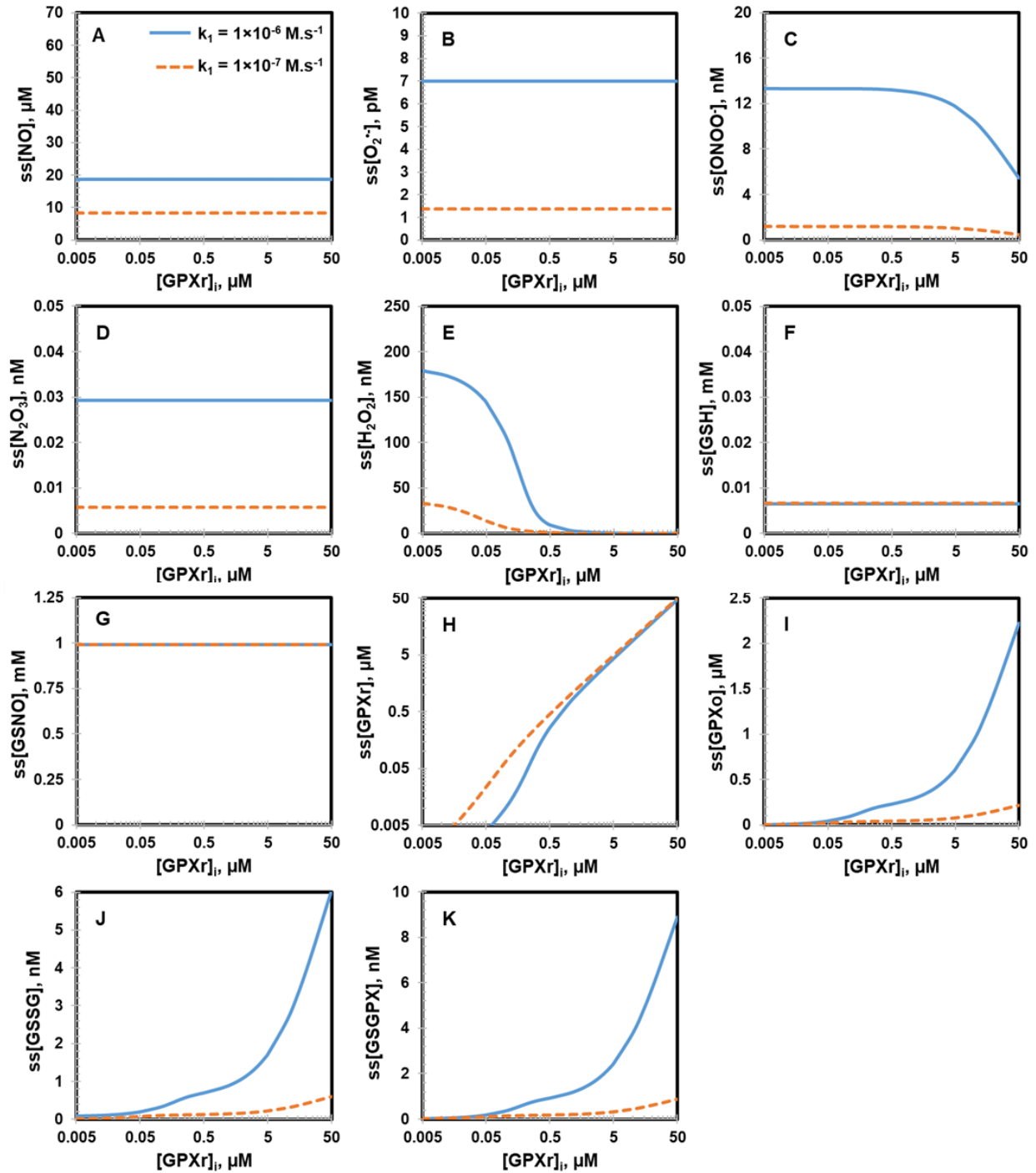
Figure 24: Steady-state concentrations profiles of species as a function of initial GPXr concentration. Panels A-K, except for Panel H, show semi log plots for steady state (ss) concentration for different species at NO generation rates (k_1) of 1×10^{-6} M.s^{-1} and 1×10^{-7} M.s^{-1}, respectively with respect to initial concentration of GPXr on a logarithmic scale to the base 10. Panel H shows a log-log plot of ss[GPXr] with respect to varied [GPXr]$_i$. The NO and $O_2^{\bullet-}$ generation rates were kept equal (i.e. $k_2/k_1 = 1$). The GSH, SOD, catalase, NADPH, O_2 and CO_2 concentrations were set at 1mM, 10 µM, 0.9 µM, 30 µM, 35 µM and 1.14 mM respectively.

Increasing GPXr level from 0.005 to 50 µM did not affect the steady state concentration of NO, $O_2^{\bullet-}$, N_2O_3, GSH, and GSNO as seen in Figure 24. H_2O_2 concentration decreased with an increase in $[GPXr]_i$ and deceased considerably for $[GPXr]_i$ above 0.3 and 3µM for k_1 of 1×10^{-7} and 1×10^{-6} $M.s^{-1}$, respectively (Figure 24E). These results showed that both GSH and GPXr are critical for removal of H_2O_2 in the absence of Prx. In the presence of Prx, the removal of H_2O_2 is primarily dependent on Prx as described in the next Section.

5.3.4. Effect of presence of Prx

Figure 25 and Figure 26 show the overall species profile in the presence of Prx for the NO generation rate of 1×10^{-6} and 1×10^{-7} $M.s^{-1}$, respectively. The $[GSH]_i$, $[GPXr]_i$, and Prx was 1 mM, 5 µM and 20 µM, respectively. These results were compared with the respective results in the absence of Prx that are presented in Section 6.3.1 (Figure 20 and Figure 21). As compared to the respective levels when Prx was not present, the presence of Prx did not change the levels of NO, $O_2^{\bullet-}$, N_2O_3, GSH and GSNO by more than 1 %, whereas the presence of Prx decreased the levels of $ONOO^-$ and H_2O_2 by 59 – 63 % and 71 – 95 %, respectively for both NO generation rates for all k_2/k_1 levels. The presence of Prx increased GPXr levels.

We further analyzed levels of $ONOO^-$ and H_2O_2 in the presence of both GPXr and Prx, and only GPXr or Prx. The results are summarized in Table 11. The respective concentrations for $ONOO^-$ and H_2O_2 were provided in the presence of both GPXr and Prx (GPXr + Prx) and % increase from these levels are presented when only GPXr or only Prx was present. We observed that $ONOO^-$ concentration increased by 5 – 6 %, and H_2O_2 concentration increased by 38 – 40% in the case of only Prx, except for k_2/k_1 of 0.1 for the NO generation rate of 1×10^{-6} $M.s^{-1}$. This % increase indicates GPXr contribution in $ONOO^-$ and H_2O_2 removal. Thus, Prx was more effective than GPXr to remove $ONOO^-$, whereas GPXr and Prx both contributed towards H_2O_2 removal.
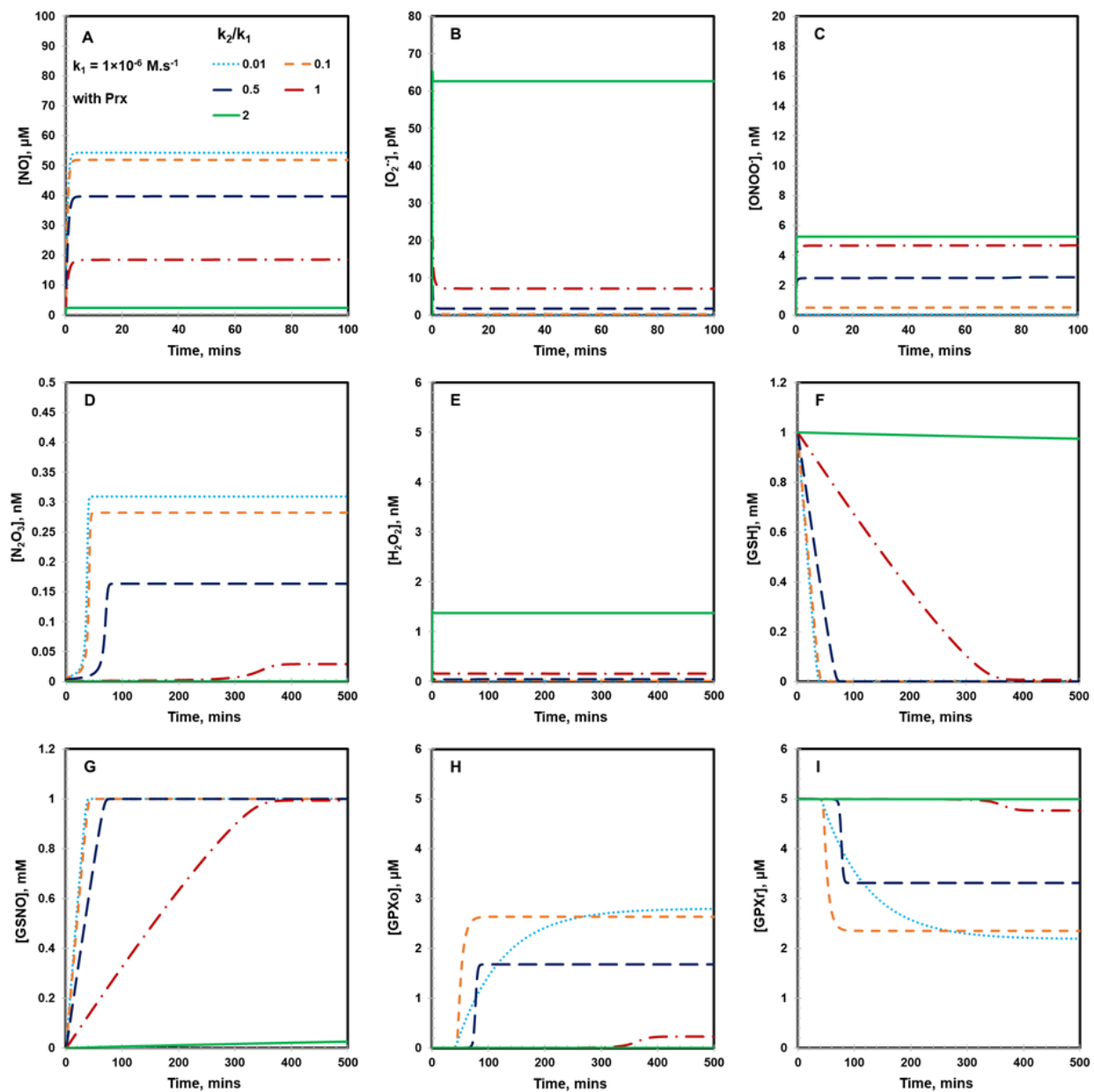
Figure 25: Concentration profiles of species with Prx for NO generation rate (k_1) of 1×10^{-6} M.s^{-1}. Panels A-I show temporal concentration profiles for species with a change in the ratio of the generation rate of $O_2^{\bullet-}$ to that of NO (k_2/k_1). The initial concentration of GSH, GPXr, Prx, SOD, catalase, NADPH, O_2 and CO_2 concentrations were set at 1mM, 5 µM, 20 µM, 10 µM, 0.9 µM, 30 µM, 35 µM and 1.14 mM respectively.
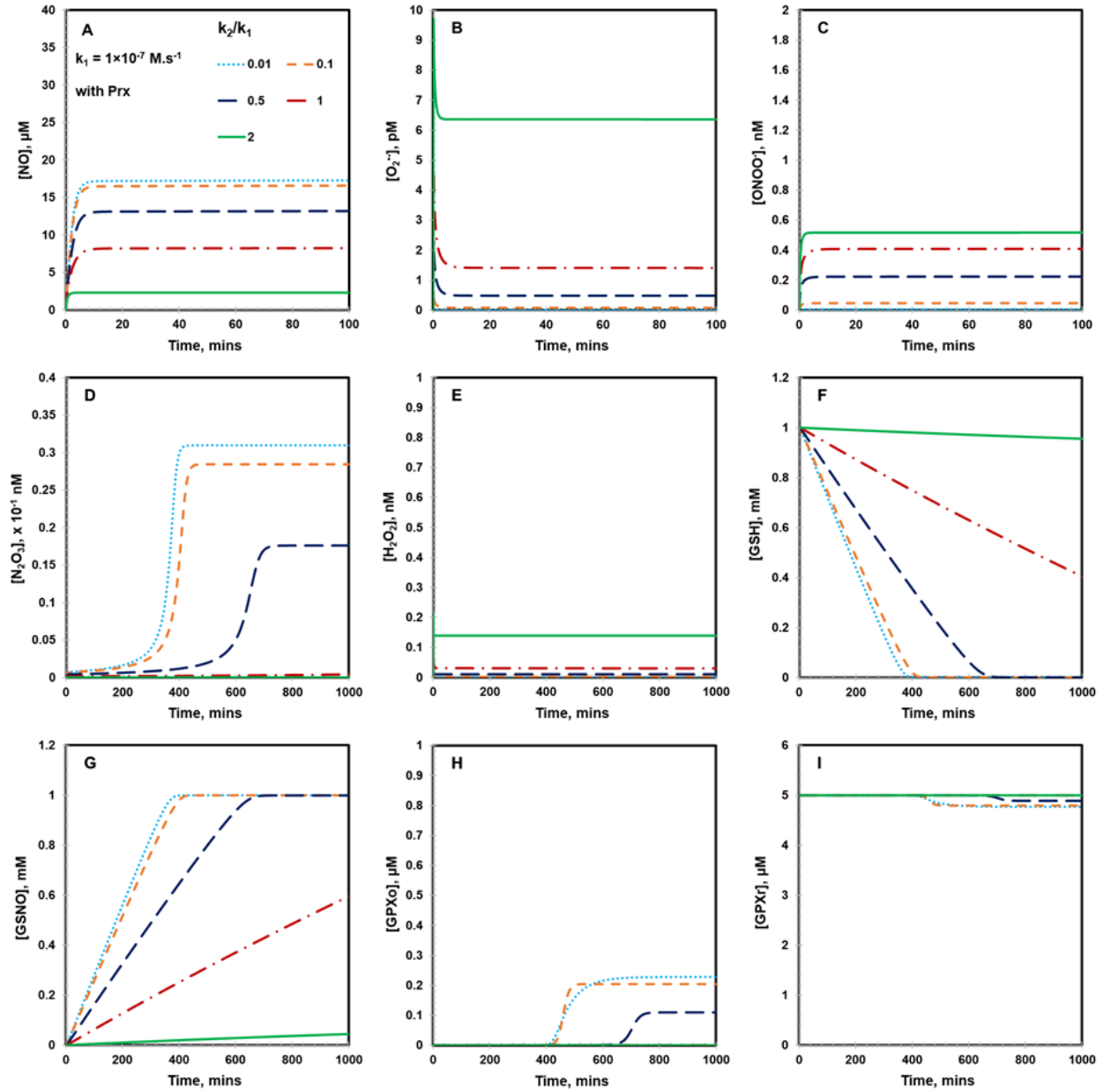
Figure 26: Concentration profiles of species with Prx for NO generation rate (k₁) of 1×10⁻⁷ M.s⁻¹. Panels A-I show temporal concentration profiles for species with a change in the ratio of the generation rate of $O_2^{\bullet-}$ to that of NO (k_2/k_1). The initial concentration of GSH, GPXr, Prx, SOD, catalase, NADPH, O_2 and CO_2 concentrations were set at 1mM, 5 µM, 20 µM,10 µM, 0.9 µM, 30 µM, 35 µM and 1.14 mM respectively.

Table 11: Effect of GPXr and Prx on the levels of ONOO⁻ and H₂O₂

Simulated cases *	NO generation rate (k_1), M.s^{-1}					
	1×10^{-6}			1×10^{-7}		
	k_2/k_1			k_2/k_1		
	0.1	1	10	0.1	1	10
$[ONOO^-]_{(GPXr+Prx)}$, nM	0.52	4.69	5.26	0.046	0.41	0.53
$\dfrac{[ONOO^-]_{only\ GPXr}}{[ONOO^-]_{(GPXr+Prx)}}$, % increase	171 %	151 %	146 %	151 %	147 %	145 %
$\dfrac{[ONOO^-]_{only\ Prx}}{[ONOO^-]_{(GPXr+Prx)}}$, % increase	2.6 %	5.3 %	5.5 %	5.4 %	5.6 %	5.6 %
$[H_2O_2]_{(GPXr+Prx)}$, nM	7.1×10^{-3}	0.16	12.34	1.7×10^{-3}	0.03	1.23
$\dfrac{[H_2O_2]_{only\ GPXr}}{[H_2O_2]_{(GPXr+Prx)}}$, % increase	1696 %	290 %	254 %	285 %	247 %	247 %
$\dfrac{[H_2O_2]_{only\ Prx}}{[H_2O_2]_{(GPXr+Prx)}}$, % increase	19 %	38.4 %	40.1 %	39%	40%	40%

* % increase for ONOO⁻ and H₂O₂ were calculated when only GPXr or only Prx were present with respect to the concentration when both GPXr and Prx were present in the system.

5.3.5. Effect of NADPH concentration on GSH recycling

Glucose 6-phosphate dehydrogenase (G6PD) deficiency depletes NADPH, which is essential for recycling GSH from its oxidized product GSSG [309, 310]. As previously seen in Figure 4J, the majority of GSSG was reduced to GSH for $k_2/k_1 \geq 1$ because sufficient amount of NADPH was available for reduction of GSSG. In order to understand the relationship of NADPH on GSH recycling in oxidative stress conditions, we varied NADPH concentration from 0.00003 to 3.0 μM and k_2/k_1 of 5.
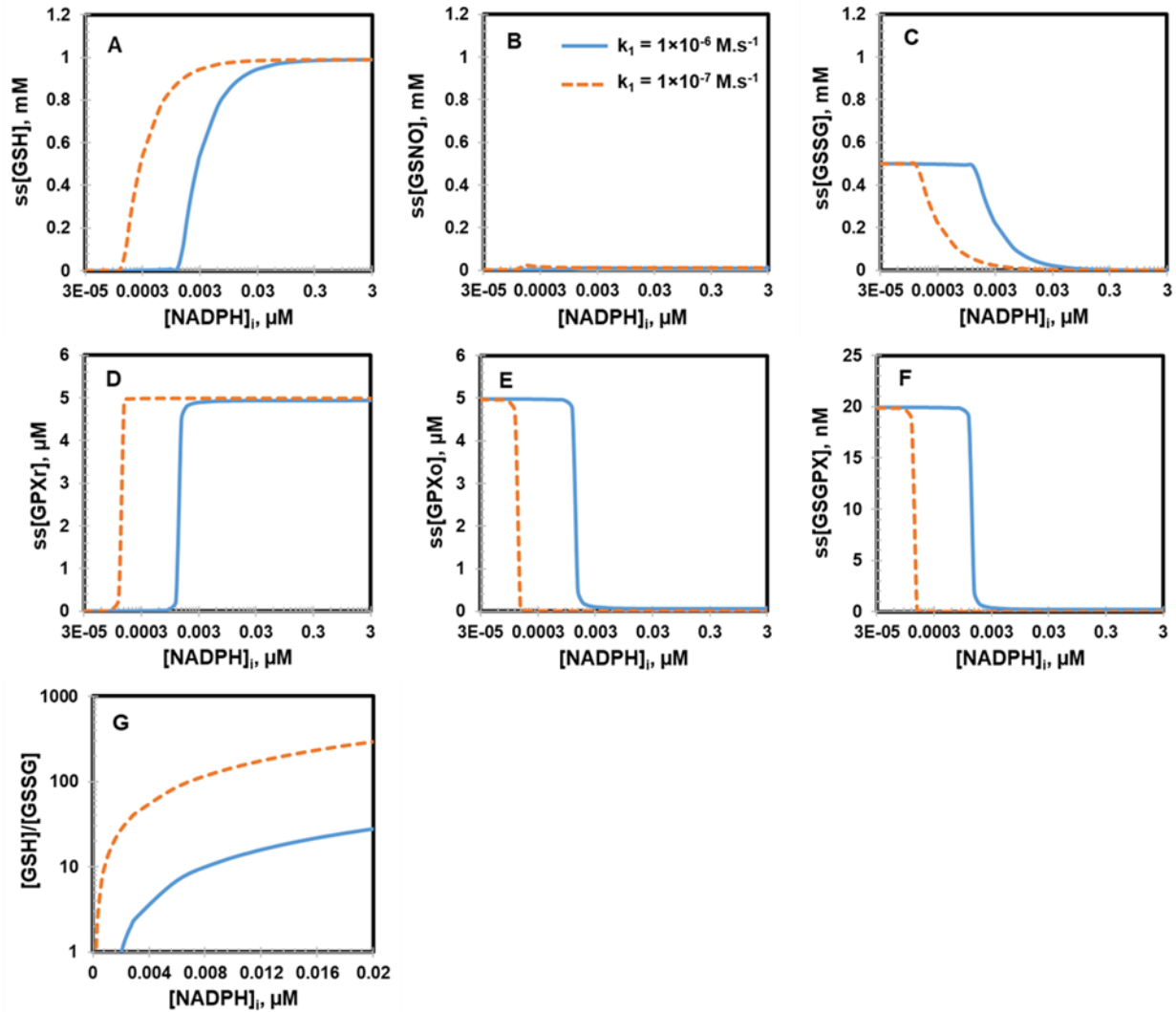
Figure 27: Steady-state GSH/GPX concentration profiles as a function of NADPH concentration. Panels A-F show the semi-log plots for steady state (ss) concentration profiles for various GSH/GPX species, at the NO generation rates (k_1) of 1×10^{-6} M.s^{-1} and 1×10^{-7} M.s^{-1}, respectively, plotted with respect to varied initial concentration of NADPH on a log scale. Panel G shows a semi-log plot for [GSH]/[GSSG] ratio (plotted on log scale), with respect to lower range of [NADPH]$_i$. The ratio of k_2/k_1 was kept constant at 5. The initial concentrations of GSH, GPXr, SOD, catalase, O_2 and CO_2 concentrations were set at 1mM, 5 µM, 10 µM, 0.9 µM, 35 µM and 1.14 mM respectively.

Figure 27 shows that [NADPH] above 0.15 and 0.015 µM reduced GSSG and GPXo for k_1 of 1×10^{-6} M.s^{-1} and 1×10^{-7} M.s^{-1}, respectively and maintained GSH and GPXr levels. GSSG and GPXo were not reduced below 0.03 µM of [NADPH]. We also calculated the redox ratio,

[GSH]/[GSSG] and saw that this ratio decreased with a decrease in [NADPH] in Figure 9G. The [GSH]/[GSSG] ratio decreased below 10 when [NADPH] decreased below 0.009 and 0.0009 µM for k_1 of 1×10^{-6} M.s^{-1} and 1×10^{-7} M.s^{-1}, respectively. These results implicate that the recycling of GSH and GPX was dependent on NADPH only at low levels.

5.4. Discussions

In this study, we performed interactions of GSH/GPX enzyme system under oxidative/nitrosative stress using a detailed reaction kinetic computational model in endothelial cells. Major results from our mechanistic analysis were (i) the oxidative and nitrosative stress related species were dependent on the ratio of generation rates of $O_2^{\bullet-}$ and NO, (ii) N_2O_3 mediated depletion of GSH in a switch-like manner, (iii) GSH, GPXr and Prx were critical for the removal of H_2O_2, (iv) Prx removed $ONOO^-$ effectively than GPXr, however, Prx did not play major role in the overall cross-talk of ROS/RNS with the GSH/GPX system, and (v) the cellular reduction ability of GSH/GPX system was independent of physiologic NADPH levels.

5.4.1. The ratio of generation rates of $O_2^{\bullet-}$ to NO determines the cellular levels of ROS and RNS

The alterations in $O_2^{\bullet-}$ and NO generation play a critical role under physiological and pathophysiological conditions [130]. Our results showed that the variation in the generation rate of $O_2^{\bullet-}$ and NO led to a wide range of levels of ROS and RNS. The model results showed that the NO, N_2O_3 and $ONOO^-$ were high when the NO generation rate was higher than the $O_2^{\bullet-}$ generation rate, whereas the H_2O_2 was high when the $O_2^{\bullet-}$ generation rate was equal to or greater than the NO generation rate. Low NO levels are protective, whereas high NO levels are cytotoxic [311]. Joshi *et al.* [255] reported that oxidative stress led to the uncoupling of endothelial NO synthase (eNOS) and resulted in the imbalance of NO and $O_2^{\bullet-}$ generation. Ali *et al.* [312] reported that high NO

levels yield high N_2O_3 and $ONOO^-$ levels. Excess N_2O_3 is reported to cause S-nitrosylation of proteins [313]. Excess $ONOO^-$ can form toxic NO_2 and $^\bullet OH$ radicals and may exacerbate the irreversible nitrosation and nitrosylation of proteins, lipids, and DNA [131]. High intracellular concentrations of H_2O_2 leads to cellular apoptosis due to mitochondrial membrane hyperpolarization and causes membrane lipid peroxidation [314].

5.4.2. N_2O_3 mediates switch-like depletion in GSH

High fluxes of NO under pathological condition enables N_2O_3 formation, which in the presence of thiols such as GSH leads to the formation of S-nitrosylated proteins [315]. Ali *et al.* [312] reported that N_2O_3, and not $ONOO^-$, acts as an intermediate for NO-mediated cytotoxicity in the presence of GSH. We predict that the depletion of GSH is dependent on the N_2O_3. Our modeling results showed that N_2O_3 mediated GSH depletion in a switch-like manner and a lower N_2O_3 maintained GSH levels. These results agree with previous studies [175, 178]. Bagci *et al.* [178] suggested that the probable reason for GSH depletion, as seen in NO-mediated toxicity, may due to the switch-like increase in N_2O_3 concentration. Hu *et al.* [175] showed that the N_2O_3, GSNO and GSH were sensitive to the initial GSH concentrations. Hu *et al.* suggested that GSH acts as a dynamic switch for N_2O_3 levels and cause a step-like increase in N_2O_3 when GSH decreased below a critical value. However, our results showed that the presence of N_2O_3 depleted GSH, whereas GSH was maintained when N_2O_3 was negligible as seen Figure 22D and F. This holds also true even in the presence of Prx (Figure 25D and F), which reduced levels of $ONOO^-$ and H_2O_2. This indicates that the depletion in N_2O_3 would maintain the levels of GSH under nitrosative stress conditions.

5.4.3. Mechanism of GSNO formation

GSNO has been widely used in research studies as a NO donor [316, 317]. However, other studies have reported that GSNO decomposition is a reductive process and is dependent on GSH and thiols, and NO is a minor product of GSNO decay [318, 319]. Therefore, GSNO cannot be used as a NO donor. Studies also suggested that the formation of GSNO is dependent on the NO concentration and GSNO can be formed via the reaction between $^\bullet NO_2$, N_2O_3 and $ONOO^-$ and GSH [320, 321]. Our results showed that the majority of GSNO formation occurred through the interactions of N_2O_3 and GSH. This indicates that GSNO formation is related to the nitrosative stress and suggests that GSNO decomposition leads to only a small fraction of the total NO generation. Our model included the reaction of GSNO with $O_2^{\bullet-}$ to form NO, however, there are other cysteine residues that may decompose GSNO to form GSSG and GSH, and release NO [322, 323]. Deficiency of GPX is directly linked to endothelial dysfunction due to decrease in NO availability and increased oxidative stress [38]

5.4.4. Contribution of GSH/GPX and Prx in H_2O_2 removal

The removal of H_2O_2 is mainly dependent on GPX, GSH and catalase activity [176, 324]. The GSH/GPX redox system is attributed to 80 to 90% of intracellular H_2O_2 removal [325, 326]. Recently, Prx is reported to be a dominant clearance pathway for H_2O_2 [327, 328]. Johnson *et al.* [328] reported that both GPX and Prx participated in removing endogenous H_2O_2. They reported that the absence of Prx increased the intracellular H_2O_2 by 400 % (to 1 nM) and the absence of GPX increased the intracellular H_2O_2 by 20 % (to 0.32 nM). Our model predictions showed similar trends. Our model predicted that the absence of Prx increased H_2O_2 levels by 247 to 290 % (0.1 to 44 nM) whereas the absence of GPX increased H_2O_2 by 38.4 to 40.3 % (0.04 to 17.3 nM) under oxidative stress conditions (for k_2/k_1 of 1 to 10) as compared to when both GPX and Prx were

present in the system. Further, both GSH and GPX were critical for H_2O_2 removal in the absence of Prx. Since, H_2O_2 levels were high at low levels of GSH and/or GPXr (Figure 23E and Figure 24E) and decreased when levels of GSH and/or GPXr increased above 0.1 mM and 0.5 µM, respectively. This model results are in agreement with the study by Ng *et al.* [176] that reported that the removal of H_2O_2 is a function of both GSH and GPXr. In our model, Prx and GPXr have comparable rate constants for their reaction with H_2O_2, however, the intracellular concentration of Prx was 4 times more than the concentration of GPXr. Winterbourn *et al.* [166] suggested that Prx removes more H_2O_2 as compared to GPXr, because of its abundance. The relative effectiveness of Prx versus GPX may also depend on the availability of its reducing equivalent thioredoxin and GSH, respectively [106, 329].

5.4.5. Contribution of GSH/GPX and Prx in the removal of ONOO⁻

GPX and Prx may act as ONOO⁻ reductase thereby modulating ONOO⁻-induced signaling pathways *in vivo* [105, 130]. Forgione *et al.* [38] reported increased ONOO⁻ levels and nitrosative stress in GPX⁻ᐟ⁻ mice than that of in wild type mice. Increasing GSH concentration reduced ONOO⁻ toxicity in these GPX⁻ᐟ⁻ mice. GSH has been shown to be dependent on GPX to defend against ONOO⁻ toxicity *in vitro* [105]. Studies have also reported that endothelial cells were protected against ONOO⁻-mediated damages because of an increase in Prx expression [110], and cellular GSH content and GPX activity [330], following exposure to an organic selenium compound. Our model results showed that Prx removed ONOO⁻ efficiently than GSH/GPX system. As compared to when both GPX and Prx were present in the system, the ONOO⁻ levels increased 3 – 6 % and 145 – 171 % for only GPXr and only Prx, respectively. GSH and GPXr, above concentrations of 0.1 mM and 0.5 µM, respectively, complemented each other in removing ONOO⁻ in the absence of Prx.

5.4.6. Recycling of GSH/GPX system is independent of physiologic NADPH concentration

G6PD deficiency is implicated in vascular diseases [331]. G6PD deficiency has been shown to deplete NADPH, increase oxidative stress, reduce NO bioactivity, and perturb cellular redox homeostasis [14, 309, 332] and increasing levels of G6PD showed an improvement in these conditions [333]. Other studies reported that G6PD derived NADPH may increase NADPH oxidase activity and lead to an increase in oxidative stress [334]. Our model results showed that GSH/GPX activity was independent of NADPH concentration under oxidative stress conditions. The redox ratio, [GSH]/[GSSG], which is used as a measure of the extent of oxidative stress, is normally greater than 100:1 under physiological conditions and can decrease to as low as 4:1, under oxidative stress conditions [335]. Enough NADPH was available for GSH recycling in our model system. Thus, the [GSH]/[GSSG] ratio always remained above 500 in all our model simulations, except for very low NADPH concentrations. We predict that elevated G6PD does not affect the cellular reduction ability of GSH/GPX system in NADPH dependent manner.

5.5. Conclusion

In this study, a detailed endothelial cell kinetic model was developed to analyze the interactions of ROS/RNS with the GSH/GPX system in oxidative/nitrosative stress conditions. With this computational model, we showed that the ratio of generation rates of $O_2^{\bullet-}$ and NO produced a wide range of outcomes for ROS/RNS levels and determined the cellular levels of oxidative and nitrosative stress. The nitrosative stress from N_2O_3 became important for cases where the NO generation was higher than the $O_2^{\bullet-}$ generation. The oxidative stress from H_2O_2 became important for the generation of $O_2^{\bullet-}$ higher than the generation of NO. We observed that GPX recycling was dependent on GSH availability and can be attributed to N_2O_3 but not to H_2O_2 and $ONOO^-$ levels under nitrosative stress. Prx removed $ONOO^-$ efficiently than GSH/GPX

system. Prx and GSH/GPX complemented each other for H_2O_2 detoxification. We propose that a decrease in N_2O_3 may maintain GSH levels under nitrosative stress and an increase in the NADPH levels may not affect the reduction ability of GSH/GPX system.

CHAPTER VI

CONCLUSIONS AND FUTURE DIRECTIONS

6.1. Conclusions

The body of work presented in this dissertation thesis advances the knowledge on the quantitative understanding of the oxidative stress mediated endothelial dysfunction in terms of therapeutic potential of cofactor BH_4 and antioxidants including ASC and GSH enzyme system for improving endothelial dysfunction. Complex interactions amongst the reactive species and antioxidant system underlay endothelial cell dysfunction. Since ROS and RNS are thought to cause or aggravate several pathologies which leads to endothelial dysfunction, a systems perspective should be employed to study these complex interactions and gain quantitative understanding about the underlying mechanisms. Computational modeling approaches based on mass balances and reaction kinetics were used in this study to overcome the limitations of measurements of reactive species using traditional and still evolving experimental approaches.

Oxidative stress has been reported to cause eNOS uncoupling by decreasing the bioavailability of BH_4. In Chapter III, we were able to develop the most comprehensive computational model to date of eNOS biochemical pathway and used it to analyze complex interactions of oxidative stress and essential cofactor for eNOS, BH_4. Using this model, we were able to investigate the dynamic interactions reactive species, antioxidants, oxidative stress coming from eNOS uncoupling as well as non-eNOS based sources and BH_4 synthesis. Our model results indicated that eNOS remains coupled under normal physiologic conditions because of a minimal amount of oxidative stress, which is necessary for the normal signaling by ROS. eNOS uncoupling has been reported in several diseases and targeting this enzyme, in its uncoupled state, has been

proposed as an attractive therapeutic option [5, 336]. There have been attempts on developing eNOS-directed pharmaceutical, so-called eNOS enhancers, compounds that up-regulate the expression of eNOS at the mRNA and protein level [337, 338]. Preclinical studies have provided quite favorable results; however, no clinical data are available to establish the efficacy of eNOS enhancers in patients with CVD. Our model results suggest that the eNOS uncoupling alone contributes negligibly towards the cellular oxidative stress while, the ROS coming from sources such as NOX, XO and mitochondrial electron transport chain may further worsen the overall oxidative stress experienced by the cell and may lead to eNOS uncoupling. Further, sole overexpression of eNOS without up-regulation of its cofactor BH_4 (maintained in reduced form) will ultimately lead to its uncoupling and worsen disease conditions rather than improving them. Also, to keep BH_4 in its reduced state the overall cellular oxidative stress needs to be lessened. More computational based studies on products used for scavenging ROS and RNS including uric acid [339], SOD mimetics [340, 341] and others are needed to deepen our understanding on their beneficial roles.

In Chapter IV, we analyzed the role of ASC in endothelial dysfunction. For this study we developed a computational model that integrated the proposed mechanisms of ASC for its beneficial effect in endothelial dysfunction, as suggested in individual studies, and analyzed its interaction with our model of eNOS biochemical pathway and its downstream reactions (presented in Chapter III). We also incorporated reaction kinetics of GSH and catalase in this model. From our analysis we were able to identify the most important mechanism for the protective role of ASC in endothelial dysfunction - ASC stabilizes eNOS by increasing BH_4 bioavailability. Also, based on our analysis of increasing/decreasing eNOS activity/concentration, we propose increasing eNOS concentration or activity (using eNOS enhancers) along with combination therapy of BH_4

and ASC supplementation would be beneficial in improving endothelial dysfunction. Our model results also showed that ASC supplementation increased ONOO$^-$ levels. Elevated ONOO$^-$ levels can have deleterious effect on the cells and more nitrosative stress is experienced by the cells. Presence of GPX and Prx in their physiological range can effectively keep the levels of ONOO$^-$ as well H$_2$O$_2$ in check and ensure decreased BH$_4$ oxidation. Use of ebselen (GPX mimetic) or Prx mimetic are reported to protect endothelial cells from oxidative damage [119, 342]. More studies (both experimental and computational) are needed to evaluate the effect of ASC supplementation on the expression and activity of antioxidant enzymes.

In Chapter V, we developed a detailed endothelial cell kinetic model to analyze the interactions of ROS/RNS with the GSH/GPX system in oxidative/nitrosative stress conditions. This is one of the few models developed for NO and O$_2^{\bullet-}$ coexisting systems, as researchers most often focus on either ROS or RNS, but not both. Mathematical modeling studies using reaction kinetics are often used to evaluate the dynamics of H$_2$O$_2$ [176, 179, 299, 343] or ONOO$^-$ [344, 345] generation and clearance in terms of their concentrations. The cross-talk amongst species can provide the overall behavior of the system, which remain to be evaluated. There is a need to integrate knowledge from both kinds of studies and move towards models that consider ROS, RNS, which we were able to perform in the present study. Our model analysis showed that the ratio of generation rates of O$_2^{\bullet-}$ and NO is an important determinant for the cellular levels of oxidative and nitrosative stress. At higher NO generation rate, higher levels of N$_2$O$_3$ can lead to nitrosative stress, while at higher O$_2^{\bullet-}$ generation rates, higher levels of H$_2$O$_2$ exerts oxidative stress. The contribution of N$_2$O$_3$ to the NO donor mediated cytotoxicity with respect to S-nitrosylation has been proposed recently [312]. Our model results show, Prx removed ONOO$^-$ efficiently than GSH/GPX system. Prx and GSH/GPX complemented each other for H$_2$O$_2$

detoxification. Based on our model predictions we propose that a decrease in N_2O_3 may maintain GSH levels under nitrosative stress and an increase in the NADPH levels may not affect the reduction ability of GSH/GPX system. Analyses from computational modeling provides new insights into the current understanding of endothelial dysfunction and can be used as guidelines for designing future experiments.

6.2. Future Work Recommendations

(i) Therapeutic potential of L-arginine (substrate of eNOS) and L-citrulline (can be converted to L-arginine) to increase NO bioavailability has been reported to generate mixed results [346]. The mathematical modeling of eNOS biochemical pathway and its interactions with oxidative stress and BH_4 synthesis can be modified developed in Chapter II can be modified to understand the effect of these substrates the NO bioavailability in oxidative stress conditions.

(ii) Computational model developed in Chapter IV to analyze the role of ASC in endothelial dysfunction does not consider the dynamics of ASC. Introducing the ASC dynamics may provide useful information on the generation and consumption of ASC and its optimal intracellular concentrations in endothelial cells in health and disease.

(iii) The homeostasis and health of the brain is maintained by neurovascular units that comprises of different cell types. Endothelial cells in these neurovascular units are considered to play commander-in-chief role. Recent findings indicate that oxidative stress and vascular dysfunction underlies the development of neurodegenerative diseases [44]. The computational modeling approaches presented in this dissertation can be used to understand the dynamics of ROS/RNS and antioxidant interactions in the endothelia cells of the neurovascular units.

APPENDIX - Listings of MATLAB sample codes

A1 - Model to analyze for interactions of oxidative stress and tetrahydrobiopterin synthesis in eNOS coupling

```matlab
function enos34
close all
clear all
clc

%----------------------------------------------------------------

%Defining Mass matrix
M=zeros(38,38);
M(1,1)=1;
M(2,2)=1;
M(3,3)=1;
M(4,4)=1;
M(5,5)=1;
M(6,6)=1;
M(7,7)=1;
M(8,8)=1;
M(9,9)=1;
M(10,10)=1;
M(11,11)=0;
M(12,12)=1;
M(13,13)=1;
M(14,14)=1;
M(15,15)=1;
M(16,16)=1;
M(17,17)=1;
M(18,18)=1;
M(19,19)=1;
M(20,20)=1;
M(21,21)=1;
M(22,22)=1;
M(23,23)=1;
M(24,24)=1;
M(25,25)=1;
M(26,26)=1;
M(27,27)=0;
M(28,28)=1;
M(29,29)=1;
M(30,30)=1;
```

```
M(31,31)=1;
M(32,32)=1;
M(33,33)=1;
M(34,34)=1;
M(35,35)=1;
M(36,36)=1;
M(37,37)=1;
M(38,38)=0;

%----------------------------------------------------------------

% Defining the ODE parameters and solver
tspan = [0 10000];

x0=[0.097e-06 0e-8 0e-8 0e-8 0e-8 0e-8 0e-8 0e-8 0e-8 0e-8 0e-8 0e-8 0e-8 0e-8 0e-8 0e-8 0 0e-8
0e-8 0e-8 0e-8 0e-8 0e-8 0e-8 0e-8 0.035e-6 0.035e-6 0e-8 0e-8 0e-8 0e-8 0e-8 0e-8 0e-8 0e-8 0e-
8 0.1e-3 0e-8];

options=odeset('Mass',M,'MstateDependence','strong','RelTol',1e-10,'AbsTol',[1e-15 1e-15 1e-15
1e-15 1e-15 1e-15 1e-15 1e-15 1e-15 1e-15 1e-15 1e-15 1e-15 1e-15 1e-15 1e-15 1e-15 1e-15 1e-
15 1e-15 1e-15 1e-15 1e-15 1e-15 1e-15 1e-15 1e-15 1e-15 1e-15 1e-15 1e-15 1e-15 1e-15 1e-15
1e-15],'Vectorized','off');

sol=ode15s(@grant2,tspan,x0,options);
x1=linspace(0,10000,100);
[y,z] = deval(sol,x1);
[y1,z1]=deval(sol,x1,20); % NO
[y2,z2]=deval(sol,x1,24); % Superoxide
[y3,z3]=deval(sol,x1,28); % Peroxynitrite
[y4,z4]=deval(sol,x1,29); % NO Production
[y5,z5]=deval(sol,x1,30);  % Superoxide Production
figure (1)
plot(x1,y*1e6) % Concentration profiles all
figure (2)
plot(x1,y1*1e6) % NO Concentration profile
figure (3)
plot(x1,z1*1e6) % NO rate
figure (4)
plot(x1,y2*1e6) % Superoxide Concentration profiles
figure (5)
plot(x1,y3*1e6) % Peroxynitrite Concentration profiles
figure (6)
plot (x1,z4*1e6) % NO Production rate
figure (7)
plot (x1,z5*1e6) % Superoxide Production rate
p=xlswrite('b4DEPGSH.xls',[x1' y' z4' z5' z1']);
```

```
%--------------------------------------------------------------

function dx = grant2(t,x)
dx=zeros(38,1);

% Defining the rate constants
nosi=0.097e-06;
tbpi=7e-6;
GSHi=0.1e-3;
carg=100e-6;
cBH4=6.93e-6;   % Introduce BH4 Concentration Here
co2=140e-6;  % Oxygen Concentration
cco2=1.1e-3; % Carbon Dioxide concentration
Qsupcell=0;
casc=0e-6;
csod=10e-6;
ka1=1.19e6;
ka_1=3.77;
ka2=0.474;
ka3=8.2e5;
ka_3=48.3;
ka5=7.68;
ka6=7.68;
ka7=6.85;
ka8=3.62;
kb1=0.1;
kb_1=1e5;
kb2=0.474;
kb3=9.19e5;
kb_3=40.5;
kb5=36.6;
kb6=9.45;
kb7=11;
kb9=0.033e6;
kb_7=1.7e6;
kb8=7.8e-3;
kb10=1.76e-3;
kb_10=3.07e6;
kb12=3.77;
kb_12=1.19e6;
k13=1.19e6;
k_13=3.77;
kc2=2.2e4;
kc_2=5e-3;
kc3=2.2e4;
kc_3=4.7e-2;
```

```
kc4=1.19e6;
kc_4=3.77;
kc5=0.474;
kc6=1.73e6;
kc_6=14.2;
kc8=0.375;
k14=6.7e9;
k15=2.40e6;
k16=3.85e9;
k17=0.60;
k18=3.9e5;
k19=4.65e4;
k20=1.7e5;
k21=3.62;
k22=6e3;
k23=364;
k24=5.09e5;
k25=0.981;
k26=0.401;
k27=9.10e4;
k28=3.57e5;
k29=3.89e4;
k30=1.91e4;
k31=6.65e8;
k32=5.82e9;
k33=8.8e9;
k34=9.4e8;
k35=4.6e9;
k36=3.2e3;
k37=6e8;
k38=1.35e3;
k39=6.6e7;
vm1=3.2e-4;
km1=50e-6;
%----------------------------------------------------------------
% Defining the rate equations
%( x1=E-1; x2=Ec1; x3=Ec2; x4=Ec3;
%x5=Ec4;  x6=E; x7=Ea1;
%x8=Ea2; x9=Ea3; X10=Ea4;
%x11=Ea5; x12=Ea6, X13=Eb1; X14=Eb2; X15=Eb3; X(16)=Eb4;
%X(17)=Eb5; X(18)=Eb6; X(19)=Eb7; X20=NO; X21=NHA; x22=Citrulline; cBH4=BH4;
x23=NO3-; x24=O2-; x25=H2O2; x26=BH3; x27=BH2; x28=ONOO-; x29=NO Production;
x30=O2- Production;
%  x31=NO2-;  x32=.OH;  x33=.NO2;  x34=CO3.-;  x35=GSNO;  x36=N2O3;  x37=GSH;
x38=GSSG )
```

dx(1)=kc_3*x(2)+kc_2*x(6)-kc3*x(27)*x(1)-kc2*x(1)*cBH4;

dx(2)=kc_4*x(3)+kc3*x(27)*x(1)-kc4*x(2)*carg-kc_3*x(2);

dx(3)=kc4*x(2)*carg+kc8*x(5)-kc_4*x(3)-kc5*x(3);

dx(4)=kc5*x(3)+kc_6*x(5)-kc6*x(4)*co2;

dx(5)=kc6*x(4)*co2-kc_6*x(5)-kc8*x(5);

dx(6)=kc2*x(1)*cBH4+ka_1*x(7)+kb1*x(13)+kb7*x(17)+kb9*x(18)*co2-kc_2*x(6)-ka1*x(6)*carg-kb_1*x(21)*x(6)-kb_7*x(20)*x(6);

dx(7)=ka1*x(6)*carg-ka_1*x(7)-ka2*x(7);

dx(8)=ka2*x(7)+ka_3*x(9)-ka3*x(8)*co2+k13*carg*x(19)-k_13*x(8);

dx(9)=ka3*co2*x(8)-ka_3*x(9)-ka5*x(9);

dx(10)=ka5*x(9)-ka6*x(10);

dx(11)=x(1)+x(2)+x(3)+x(4)+x(5)+x(6)+x(7)+x(8)+x(9)+x(10)+x(11)+x(12)+x(13)+x(14)+x(15)+x(16)+x(17)+x(18)+x(19)-nosi;

dx(12)=ka7*x(11)-ka8*x(12);

dx(13)=ka8*x(12)+kb_1*x(21)*x(6)-kb2*x(13)-kb1*x(13);

dx(14)=kb2*x(13)+kb_3*x(15)+kb_12*x(19)*x(21)-kb3*x(14)*co2-kb12*x(14);

dx(15)=kb3*x(14)*co2-kb_3*x(15)-kb5*x(15);

dx(16)=kb5*x(15)-kb6*x(16);

dx(17)=kb6*x(16)+kb_7*x(6)*x(20)-kb8*x(17)-kb7*x(17);

dx(18)=kb8*x(17)+kb_10*x(20)*x(19)-kb10*x(18)-kb9*x(18)*co2;

dx(19)=kb10*x(18)+k_13*x(8)+kb12*x(14)-kb_10*x(19)*x(20)-kb_12*x(19)*x(21)-k13*x(19)*carg;

dx(20)=kb7*x(17)+kb10*x(18)-kb_7*x(20)*x(6)-kb_10*x(20)*x(19)-(4*k15*((x(20))^2)*co2)-k14*x(20)*x(24)-k27*0.22*x(28)*x(20)-k32*x(20)*x(34)+k37*(x(35)^2)*x(24);%ok

dx(21)=kb1*x(13)+kb12*x(14)-kb_1*x(21)*x(6)-kb_12*x(19)*x(21);

```
dx(22)=kb6*x(16);

dx(23)=kb9*x(18)*co2+k25*x(28)+k29*x(28)*cco2;

dx(24)=kc8*x(5)+Qsupcell-k14*x(20)*x(24)-k16*csod*x(24)-k28*0.0025*x(24)*x(24)-
k31*x(24)*x(34)-k24*casc*x(24)-k18*cBH4*x(24)-k37*(x(35)^2)*x(24);

dx(25)=k16*csod*x(24)+k28*0.0025*x(24)*x(24)+k18*cBH4*x(24);

dx(26)=k33*x(32)*cBH4+k34*x(33)*cBH4+k35*x(34)*cBH4+k22*cBH4*x(28)+k18*cBH4*x
(24)-2*k19*((x(26))^2)-k20*x(26)*casc-k36*x(26)*co2;

dx(27)=tbpi-cBH4-x(26)-x(27);

dx(28)=k14*x(20)*x(24)-k25*x(28)-k26*x(28)-k29*x(28)*cco2-k30*x(28)*cco2-
k27*0.22*x(28)*x(20)-k23*casc*0.22*x(28)-k22*cBH4*x(28)-k38*x(28)*x(37);

dx(29)=kb7*x(17)+kb10*x(18)+k37*(x(35)^2)*x(24);

dx(30)=kc8*x(5)+Qsupcell;
 dx(31)=4*k15*((x(20))^2)*co2+k27*x(20)*0.22*x(28)+k32*x(34)*x(20)+k34*x(33)*cBH4;

dx(32)=k26*x(28)-k33*x(32)*cBH4;

dx(33)=k26*x(28)+k30*x(28)*cco2+k27*0.22*x(28)*x(20)-k34*x(33)*cBH4;

dx(34)=k30*x(28)*cco2-k31*x(34)*x(24)-k32*x(34)*x(20)-k35*x(34)*cBH4;

dx(35)=k38*x(28)*x(37)+k39*x(36)*x(37)-k37*(x(35)^2)*x(24);

dx(36)=(4*k15*((x(20))^2)*co2)-k39*x(36)*x(37);

dx(37)=((vm1*x(38))/(km1+x(38)))-k38*x(28)*x(37)-k39*x(36)*x(37);

dx(38)=-GSHi-(-x(37)-x(35)-x(38));
%-------------------------------------------------------------
```

A-2 Model to analyze role of ascorbate in endothelial dysfunction

```
function enos34newasc
close all
clear all
clc

%Defining Mass matrix
M=zeros(39,39);
M(1,1)=1;
M(2,2)=1;
M(3,3)=1;
M(4,4)=1;
M(5,5)=1;
M(6,6)=1;
M(7,7)=1;
M(8,8)=1;
M(9,9)=1;
M(10,10)=1;
M(11,11)=0;
M(12,12)=1;
M(13,13)=1;
M(14,14)=1;
M(15,15)=1;
M(16,16)=1;
M(17,17)=1;
M(18,18)=1;
M(19,19)=1;
M(20,20)=1;
M(21,21)=1;
M(22,22)=1;
M(23,23)=1;
M(24,24)=1;
M(25,25)=1;
M(26,26)=1;
M(27,27)=1;
M(28,28)=1;
M(29,29)=1;
M(30,30)=1;
M(31,31)=1;
M(32,32)=1;
M(33,33)=1;
M(34,34)=1;
M(35,35)=1;
M(36,36)=1;
M(37,37)=1;
```

```
M(38,38)=1;
M(39,39)=0;
%--------------------------------------------------------------------

% Defining the ODE parameters and solver
tspan = [0 1000000];
%0.05 at TBP = 7 uM
x0=[0.097e-6 0e-8 0e-8 0e-8 0e-8 0e-8 0e-8 0e-8 0e-8 0e-8 0e-8 0e-8 0e-8 0e-8 0e-8 0e-8 0 0e-8
0e-8 0e-8 0e-8 0e-8 0e-8 0e-8 0e-8 3.325e-6 3.325e-6 0e-8 0e-9 0e-8 0e-8 0e-8 0e-8 0e-8 0.35e-6
0e-8 0e-8 0.01e-3 0e-8];

options=odeset('Mass',M,'MstateDependence','strong','RelTol',1e-10,'AbsTol',[1e-15 1e-15 1e-15
1e-15 1e-15 1e-15 1e-15 1e-15 1e-15 1e-15 1e-15 1e-15 1e-15 1e-15 1e-15 1e-15 1e-15 1e-15
1e-15 1e-15 1e-15 1e-15 1e-15 1e-15 1e-15 1e-15 1e-15 1e-15 1e-15 1e-15 1e-15 1e-15 1e-15
1e-15 1e-15 1e-15 1e-15 1e-15 1e-15],'Vectorized','off');
sol=ode15s(@grant2,tspan,x0,options);
x1=linspace(0,1000000,10000);
[y,z] = deval(sol,x1);
[y1,z1]=deval(sol,x1,20); % NO
[y2,z2]=deval(sol,x1,24); % Superoxide
[y3,z3]=deval(sol,x1,28); % Peroxynitrite
[y4,z4]=deval(sol,x1,29); % NO Production
[y5,z5]=deval(sol,x1,30);  % Superoxide Production
[y6,z6]=deval(sol,x1,26); % BH3
[y7,z7]=deval(sol,x1,27); % BH2
[y8,z8]=deval(sol,x1,35); % BH4
[y9,z9]=deval(sol,x1,25); % H2O2
figure (1)
plot(x1,y*1e6) % Concentration profiles all
figure (2)
plot(x1,y1*1e6) % NO Concentration profile
figure (3)
plot(x1,z1*1e6) % NO rate
figure (4)
plot(x1,y2*1e6) % Superoxide Concentration profiles
figure (5)
plot(x1,y3*1e6) % Peroxynitrite Concentration profiles
figure (6)
plot (x1,z4*1e6) % NO Production rate
figure (7)
plot (x1,z5*1e6) % Superoxide Production rate
p=xlswrite('ResultsASCnew.xls',[x1' y' z4' z5' z1']);

%--------------------------------------------------------------------
function dx = grant2(t,x)
dx=zeros(39,1);
```

```
%-------------------------------------------------------------------
% Defining the rate constants

nosi=0.097e-6;
% nosi=0.048e-6;
% nosi=0.144e-6;
tbpi=7e-6;
carg=100e-6;
GSHi=0.01e-3;
co2=140e-6;  % Oxygen Concentration
cco2=1.1e-3; % Carbon Dioxide concentration
Qsupcell=1e-9; %   Other Sources of Superoxide Production
QBH4=0.5e-9; % BH4 production rate
casc=5e-6; % Ascorbate Concentration
csod=10e-6; % SOD concentration
ccat=9e-7; % Catalase conc. peroxisomes
ka1=1.19e6;
ka_1=3.77;
ka2=0.474;
ka3=8.2e5;
ka_3=48.3;
ka5=7.68;
ka6=7.68;
ka7=6.85;
ka8=3.62;
kb1=0.1;
kb_1=1e5;
kb2=0.474;
kb3=9.19e5;
kb_3=40.5;
kb5=36.6;
kb6=9.45;
kb7=11;
kb9=0.0133e6;
kb_7=1.7e6;
kb8=7.8e-3;
kb10=1.76e-3;
kb_10=3.07e6;
kb12=3.77;
kb_12=1.19e6;
k13=1.19e6;
k_13=3.77;
kc2= 2.2e4;
kc_2=5e-3;
kc3=2.2e4;
```

```
kc_3=4.7e-2;
kc4=1.19e6;
kc_4=3.77;
kc5=0.474;
kc6=1.73e6;
kc_6=14.2;
kc8=0.375;
k14=6.7e9;
k15=2.4e6;
k16=3.85e9;
k17=0.6; % BH4 auto-oxidation
k18=3.9e5;
k19=4.65e4;
k20=1.7e5;
k22=6e3;
k23=361.7;
k24=5.1e5;
k25=0.981;
k26=0.401;
k27=9.1e4;
k28=3.57e5;
k29=3.89e4;
k30=1.91e4;
k31=6.65e8;
k32=5.82e9;
k33=8.8e9;
k34=9.4e8;
k35=4.6e9;
k36=3.2e3;
k37=3.4e7; % rate constanst for catalase
k38=152.5; % BH2 extracellular diffusion rate constant
k39=1.35e3;
k40=6.6e7;
vm1=3.2e-4;
km1=50e-6;
k41=1.6e3;
k42=9e8;
cPer=10e-6; %20e-6;
cGPXR=2.5e-6; %5e-6;
k43=2e6; %Hydrolysis of ONOO- by GPXr
k44=2.1e7; % Hydrolysis of H2O2 by GPXr
k45=1.3e7; % Rate constant for H2O2 hydrolysis with peroxiredoxin
k46=1e7; %Rate constant for ONOO- hydrolysis by peroxyredoxin

%-----------------------------------------------------------------
```

% Defining the rate equations

%(x1=E-1; x2=Ec1; x3=Ec2; x4=Ec3; x5=Ec4; x6=E; x7=Ea1; x8=Ea2; x9=Ea3; x10=Ea4; x11=Ea5; x12=Ea6, x13=Eb1; x14=Eb2; x15=Eb3; x16=Eb4; x17=Eb5; x18=Eb6; x19=Eb7; x20=NO; x21=NHA; x22=Citrulline; x23=NO3-; x24=O2-; x25=H2O2; x26=BH3; x27=BH2; x28=ONOO-; x29=NO Production; x30=O2- Production; x31=NO2-; x32=.OH; x33=.NO2; x34=CO3.-; x35=BH4; x36=GSNO; x37=N2O3; x38=GSH; x39=GSSG) Taken out --> x40=GS.)

dx(1)=kc_3*x(2)+kc_2*x(6)-kc3*x(27)*x(1)-kc2*x(1)*x(35);

dx(2)=kc_4*x(3)+kc3*x(27)*x(1)-kc4*x(2)*carg-kc_3*x(2);

dx(3)=kc4*x(2)*carg+kc8*x(5)-kc_4*x(3)-kc5*x(3);

dx(4)=kc5*x(3)+kc_6*x(5)-kc6*x(4)*co2;

dx(5)=kc6*x(4)*co2-kc_6*x(5)-kc8*x(5);

dx(6)=kc2*x(1)*x(35)+ka_1*x(7)+kb1*x(13)+kb7*x(17)+kb9*x(18)*co2-kc_2*x(6)-ka1*x(6)*carg-kb_1*x(21)*x(6)-kb_7*x(20)*x(6);

dx(7)=ka1*x(6)*carg-ka_1*x(7)-ka2*x(7);

dx(8)=ka2*x(7)+ka_3*x(9)-ka3*x(8)*co2+k13*carg*x(19)-k_13*x(8);

dx(9)=ka3*co2*x(8)-ka_3*x(9)-ka5*x(9);

dx(10)=ka5*x(9)-ka6*x(10);

dx(11)=x(1)+x(2)+x(3)+x(4)+x(5)+x(6)+x(7)+x(8)+x(9)+x(10)+x(11)+x(12)+x(13)+x(14)+x(15)+x(16)+x(17)+x(18)+x(19)-nosi;

dx(12)=ka7*x(11)-ka8*x(12);

dx(13)=ka8*x(12)+kb_1*x(21)*x(6)-kb2*x(13)-kb1*x(13);

dx(14)=kb2*x(13)+kb_3*x(15)+kb_12*x(19)*x(21)-kb3*x(14)*co2-kb12*x(14);

dx(15)=kb3*x(14)*co2-kb_3*x(15)-kb5*x(15);

dx(16)=kb5*x(15)-kb6*x(16);

dx(17)=kb6*x(16)+kb_7*x(6)*x(20)-kb8*x(17)-kb7*x(17);

dx(18)=kb8*x(17)+kb_10*x(20)*x(19)-kb10*x(18)-kb9*x(18)*co2;

dx(19)=kb10*x(18)+k_13*x(8)+kb12*x(14)-kb_10*x(19)*x(20)-kb_12*x(19)*x(21)-k13*x(19)*carg;

dx(20)=kb7*x(17)+kb10*x(18)-kb_7*x(20)*x(6)-kb_10*x(20)*x(19)-k14*x(20)*x(24)-(4*k15*((x(20))^2)*co2)-k27*0.22*x(28)*x(20)-k32*x(20)*x(34)+k42*((x(36))^2)*x(24); % X20=NO

dx(21)=kb1*x(13)+kb12*x(14)-kb_1*x(21)*x(6)-kb_12*x(19)*x(21);% X21=NHA

dx(22)=kb6*x(16);%x22=Citrulline

dx(23)=kb9*x(18)*co2+k25*x(28)+k29*x(28)*cco2; % x23=NO3-

dx(24)=Qsupcell+kc8*x(5)-k14*x(20)*x(24)-k16*csod*x(24)-k18*x(35)*x(24)-k24*casc*x(24)-k28*0.0025*x(24)*x(24)-k31*x(24)*x(34)-k42*(x(36)^2)*x(24); %x24=O2-

dx(25)=k16*csod*x(24)+k18*x(35)*x(24)+k28*0.0025*x(24)*x(24)-k37*ccat*x(25)-k45*cPer*x(24)-k44*x(24)*cGPXR; %x25=H2O2

dx(26)=k18*x(35)*x(24)-2*k19*((x(26))^2)-k20*x(26)*casc+k22*x(35)*x(28)+k33*x(32)*x(35)+k34*x(33)*x(35)+k35*x(34)*x(35)-k36*x(26)*co2; %x26=BH3

dx(27)= kc_3*x(2)-kc3*x(27)*x(1)+k17*x(35)*co2+k19*((x(26))^2) +k36*x(26)*co2-k38*x(27); %x27=BH2

dx(28)= k14*x(20)*x(24)-k22*x(35)*x(28)-k23*casc*x(28)-k25*x(28)-k26*x(28)-k27*0.22*x(28)*x(20)-k29*x(28)*cco2-k30*x(28)*cco2-k39*x(28)*x(38)-0.5625*k46*cPer*x(28)-k43*x(28)*cGPXR; %x28=ONOO-

dx(29)=kb7*x(17)+kb10*x(18)+k42*((x(36))^2)*x(24); %x29=NO Production;

dx(30)=kc8*x(5)+Qsupcell; %x30=O2- Production;

dx(31)=(2*k15*((x(20))^2)*co2)+k27*0.22*x(20)*x(28)+k32*x(34)*x(20)+k34*x(33)*x(35)+k40*x(37)*x(38)+k41*x(37); %x31=NO2-;

dx(32)=k26*x(28)-k33*x(32)*x(35); % x32=.OH;

dx(33)=k26*x(28)+k27*0.22*x(28)*x(20)+k30*x(28)*cco2-k34*x(33)*x(35); %x33=.NO2;
dx(34)=k30*x(28)*cco2-k31*x(34)*x(24)-k32*x(34)*x(20)-k35*x(34)*x(35); %x34=CO3.-;

dx(35)=QBH4+kc_2*x(6)-kc2*x(35)*x(1)-k17*x(35)*co2-k18*x(35)*x(24)+k19*((x(26))^2)+k20*x(26)*casc-k22*x(35)*x(28)-k33*x(32)*x(35)-k34*x(33)*x(35)-k35*x(34)*x(35); %x35=BH4;

```
dx(36)=k39*x(28)*x(38)+k40*x(37)*x(38)-k42*((x(36))^2)*x(24); % x36=GSNO;

dx(37)=(4*k15*((x(20))^2)*co2)-k40*x(37)*x(38)-k41*x(37); % x37=N2O3;

dx(38)=((vm1*x(39))/(km1+x(39)))-k39*x(28)*x(38)-k40*x(37)*x(38); %x38=GSH;

dx(39)=GSHi-x(38)-x(36)-x(39); %x39=GSSG

%---------------------------------------------------------------
```

A-3 Model to analyze interactions of GSH/GPX with ROS/RNS

```
function gshuirevisedkper
%Defining Mass matrix because we have al
M=zeros(14,14);
M(1,1)=1;
M(2,2)=1;
M(3,3)=1;
M(4,4)=0;%Mass Balance
M(5,5)=1;
M(6,6)=1;
M(7,7)=1;
M(8,8)=1;
M(9,9)=0;%Mass Balance
M(10,10)=1;
M(11,11)=1;
M(12,12)=1;
M(13,13)=1;
M(14,14)=1;

%-------------------------------------------------------------------

% Defining the ODE parameters and solver
tspan = [0 100000];

%Initial Concentration x0=[x1=NO; x2=O2-; x3=ONOO-; x4=GSNO; x5=N2O3; x6=GSH;
x7=H2O2; x8=GPXo; x9=GSGPX; x10=GPXr; x11=ONO-; x12=[GSSG]; x13=NO Production;
x14=O2- Production ]

x0=[0 0 0 0 0 1e-3 0 0 0 5e-6 0 0 0 0];
options=odeset('Mass',M,'MstateDependence','strong','RelTol',1e-10,'AbsTol',[1e-15 1e-15 1e-15
1e-15 1e-15 1e-15 1e-15 1e-15 1e-15 1e-15 1e-15 1e-15 1e-15 1e-15],'Vectorized','off');
sol=ode15s(@gshoder,tspan,x0,options);
x1=linspace(0,100000,10000);

[y,z] = deval(sol,x1);
[y1,z1]=deval(sol,x1,6); % gsh conc
[y2,z2]=deval(sol,x1,2); %  Superoxide conc
[y3,z3]=deval(sol,x1,5); % N2O3 conc
[y4,z4]=deval(sol,x1,13); % NO Production
[y5,z5]=deval(sol,x1,14);  % Superoxide Production
[y6,z6]=deval(sol,x1,1);%NO Concentration
[y7,z7]=deval(sol,x1,7);%H2O2 Conc
[y8,z8]=deval(sol,x1,4);%GSNO Conc
[y9,z9]=deval(sol,x1,3);%ONOO- Conc
```

```matlab
figure (1)
plot(x1,y*1e6) % Concentration profiles all
figure (2)
plot(x1,y1*1e3) % Gsh Concentration
figure (3)
plot(x1,y2*1e6) % O2- Conc
figure (4)
plot(x1,y3*1e6) % N2O3 Conc
figure (5)
plot (x1,z4*1e6) % NO Production Rate
figure (6)
plot (x1,z5*1e6) % Superoxide Production Rate
figure (7)
plot (x1,y6*1e6) %NO Conc
figure(8)
plot (x1,y8*1e3) %GSNO Conc
figure(9)
plot (x1,y9*1e6) %ONOO- Conc
figure (10)
plot (x1,y7*1e6)%h2o2 conc
p=xlswrite('gsh_valueschanging.xls',[x1' y' z4' z5']);

function dx = gshoder(t,x)
dx=zeros(14,1);
% Defining the rate constants and Concentration Values
cSOD=10e-6;
cco2=1.14e-3;
cO2=35e-6;
cCAT=9e-7;
cPer=20e-6;
cGSHi=1e-3;% introduce initial Gsh here
cGPXRi=5e-6;
cNADPH=30e-6;
k1=1e-6;
k2=10e-6;
k3=0e-5;%Rate constant of gsh formation
k4=6.7e9;
k5=1.6e9;
k6=1.5e3;%k6=1.35e3;
k7=2e6; %Hydrolysis of ONOO- by GPXr
k8=5.8e4;
k9=3.2e6;
k10=9e8;%k10=3e8;
k11=6.6e7;
k12=2.4e6;
k13=1.6e3;
```

k14=2.1e7; % Hydrolysis of H2O2 by GPXr
k15=4e4;
k16=1e7;
k17=5.5e-3;
k18=8e7;
k19=3.4e7;
k20=1.3e7; % Rate constant for H2O2 hydrolysis with peroxiredoxin
k21=1e7; %Rate constant for ONOO- hydrolysis by peroxyredoxin
%--
% Defining the rate equations

dx(1)=k1+k17*x(4)*x(6)-k4*(x(1))*x(2)-4*k12*cO2*((x(1))^2);%Rate of change of NO
dx(2)=k2-k4*x(1)*x(2)-k5*cSOD*x(2)-k10*x(2)*((x(4))^2)-(k18*((x(2))^2)*0.0025);%Rate   of change of O2-

dx(3)=k4*x(1)*x(2)-k6*x(6)*x(3)-k7*x(10)*x(3)-k8*cco2*x(3)-0.5625*k21*cPer*x(3);%Rate of Change of ONOO-

dx(4)=cGSHi-x(6)-2*x(12)-x(9)-x(4);%Rate of Change of GSNO

dx(5)=2*k12*cO2*((x(1))^2)-k11*x(5)*x(6)-k13*x(5);%Rate of Change of N2O3

dx(6)=k3+2*k9*x(12)*cNADPH-k11*x(5)*x(6)-k6*x(6)*x(3)-k15*x(6)*x(8)-k16*x(6)*x(9)-k17*x(4)*x(6);%Rate of Change of GSH

dx(7)=k5*(1/2)*cSOD*x(2)-k14*x(7)*x(10)+(k18*((x(2))^2)*0.0025)-(0.01*k19*x(7)*cCAT)-k20*cPer*x(7);%Rate of Change of H2O2

dx(8)=k14*x(7)*x(10)-k15*x(6)*x(8)+k7*x(10)*x(3);%Rate of Change of GPXo

dx(9)=cGPXRi-x(10)-x(8)-x(9);

dx(10)=k16*x(9)*x(6)-k14*x(7)*x(10)-k7*x(10)*x(3);%Rate of Change of GPXr
 dx(11)=k7*x(3)*x(10)+k10*x(2)*((x(4))^2)+k11*x(5)*x(6)+k17*x(4)*x(6);%Rate of Change of ONO-
 dx(12)=0.499*k6*x(6)*x(3)+k16*x(9)*x(6)+k17*x(4)*x(6)+k10*((x(4)^2))*x(2)-k9*cNADPH*x(12); %Rate of Change of GSSG

dx(13)=k1+k17*x(5)*x(6);%NO production

dx(14)=k2;%O2- Production
%--

REFERENCES

1. *World Health Organization*. Cardiovascular diseases (CVDs) Fact Sheet 2016 September 2016]; Available from: http://www.who.int/mediacentre/factsheets/fs317/en/.

2. Karbach, S., et al., *eNOS uncoupling in cardiovascular diseases--the role of oxidative stress and inflammation.* Curr Pharm Des, 2014. **20**(22): p. 3579-94.

3. Vanhoutte, P.M., et al., *Endothelial dysfunction and vascular disease - a 30th anniversary update.* Acta Physiol (Oxf), 2017. **219**(1): p. 22-96.

4. Incalza, M.A., et al., *Oxidative stress and reactive oxygen species in endothelial dysfunction associated with cardiovascular and metabolic diseases.* Vascul Pharmacol, 2018. **100**: p. 1-19.

5. Daiber, A., et al., *Targeting vascular (endothelial) dysfunction.* Br J Pharmacol, 2017. **174**(12): p. 1591-1619.

6. Salisbury, D. and U. Bronas, *Reactive oxygen and nitrogen species: impact on endothelial dysfunction.* Nurs Res, 2015. **64**(1): p. 53-66.

7. Daiber, A., et al., *Crosstalk of mitochondria with NADPH oxidase via reactive oxygen and nitrogen species signalling and its role for vascular function.* Br J Pharmacol, 2017. **174**(12): p. 1670-1689.

8. Di Meo, S., et al., *Role of ROS and RNS Sources in Physiological and Pathological Conditions.* Oxid Med Cell Longev, 2016. **2016**: p. 1245049.

9. Li, H., S. Horke, and U. Forstermann, *Oxidative stress in vascular disease and its pharmacological prevention.* Trends Pharmacol Sci, 2013. **34**(6): p. 313-9.

10. Finkel, T. and N.J. Holbrook, *Oxidants, oxidative stress and the biology of ageing.* Nature, 2000. **408**(6809): p. 239-47.

11. Angelova, P.R. and A.Y. Abramov, *Functional role of mitochondrial reactive oxygen species in physiology.* Free Radic Biol Med, 2016. **100**: p. 81-85.

12. Zuo, L., et al., *Biological and physiological role of reactive oxygen species--the good, the bad and the ugly.* Acta Physiol (Oxf), 2015. **214**(3): p. 329-48.

13. He, L., et al., *Antioxidants Maintain Cellular Redox Homeostasis by Elimination of Reactive Oxygen Species.* Cell Physiol Biochem, 2017. **44**(2): p. 532-553.

14. Espinosa-Diez, C., et al., *Antioxidant responses and cellular adjustments to oxidative stress.* Redox Biol, 2015. **6**: p. 183-197.

15. Cahill, P.A. and E.M. Redmond, *Vascular endothelium - Gatekeeper of vessel health.* Atherosclerosis, 2016. **248**: p. 97-109.

16. Starr, A., D. Hussein, and M. Nandi, *The regulation of vascular tetrahydrobiopterin bioavailability.* Vascul Pharmacol, 2013. **58**(3): p. 219-30.

17. Desjardins, F. and J.L. Balligand, *Nitric oxide-dependent endothelial function and cardiovascular disease.* Acta Clin Belg, 2006. **61**(6): p. 326-34.

18.   Pastore, A., et al., *Analysis of glutathione: implication in redox and detoxification.* Clin Chim Acta, 2003. **333**(1): p. 19-39.

19.   Landmesser, U., et al., *Oxidation of tetrahydrobiopterin leads to uncoupling of endothelial cell nitric oxide synthase in hypertension.* J Clin Invest, 2003. **111**(8): p. 1201-9.

20.   Higashi, Y., et al., *Oxidative stress and endothelial dysfunction: clinical evidence and therapeutic implications.* Trends Cardiovasc Med, 2014. **24**(4): p. 165-9.

21.   Griendling, K.K., et al., *Measurement of Reactive Oxygen Species, Reactive Nitrogen Species, and Redox-Dependent Signaling in the Cardiovascular System: A Scientific Statement From the American Heart Association.* Circ Res, 2016. **119**(5): p. e39-75.

22.   Alon, U., *An introduction to systems biology : design principles of biological circuits.* Chapman & Hall/CRC mathematical and computational biology series. 2007, Boca Raton, FL: Chapman & Hall/CRC. xvi, 301 p., 4 p. of plates.

23.   Forstermann, U. and T. Munzel, *Endothelial nitric oxide synthase in vascular disease: from marvel to menace.* Circulation, 2006. **113**(13): p. 1708-14.

24.   Alderton, W.K., C.E. Cooper, and R.G. Knowles, *Nitric oxide synthases: structure, function and inhibition.* Biochem J, 2001. **357**(Pt 3): p. 593-615.

25.   Bendall, J.K., et al., *Tetrahydrobiopterin in cardiovascular health and disease.* Antioxid Redox Signal, 2014. **20**(18): p. 3040-77.

26.   Chen, D.D., et al., *Tetrahydrobiopterin regulation of eNOS redox function.* Curr Pharm Des, 2014. **20**(22): p. 3554-62.

27.   Santhanam, A.V., et al., *Uncoupling of endothelial nitric oxide synthase in cerebral vasculature of Tg2576 mice.* J Neurochem, 2015.

28.   Wang, Q., et al., *Tetrahydrobiopterin improves endothelial function in cardiovascular disease: a systematic review.* Evid Based Complement Alternat Med, 2014. **2014**: p. 850312.

29.   Cai, S., J. Khoo, and K.M. Channon, *Augmented BH4 by gene transfer restores nitric oxide synthase function in hyperglycemic human endothelial cells.* Cardiovasc Res, 2005. **65**(4): p. 823-31.

30.   Cunnington, C., et al., *Systemic and vascular oxidation limits the efficacy of oral tetrahydrobiopterin treatment in patients with coronary artery disease.* Circulation, 2012. **125**(11): p. 1356-66.

31.   Nystrom, T., A. Nygren, and A. Sjoholm, *Tetrahydrobiopterin increases insulin sensitivity in patients with type 2 diabetes and coronary heart disease.* Am J Physiol Endocrinol Metab, 2004. **287**(5): p. E919-25.

32.   Worthley, M.I., et al., *Effects of tetrahydrobiopterin on coronary vascular reactivity in atherosclerotic human coronary arteries.* Cardiovasc Res, 2007. **76**(3): p. 539-46.

33.   Padayatty, S.J., et al., *Vitamin C as an antioxidant: evaluation of its role in disease prevention.* J Am Coll Nutr, 2003. **22**(1): p. 18-35.

34. Tyml, K., *Vitamin C and Microvascular Dysfunction in Systemic Inflammation.* Antioxidants (Basel), 2017. **6**(3).

35. Grebe, M., et al., *Antioxidant vitamin C improves endothelial function in obstructive sleep apnea.* Am J Respir Crit Care Med, 2006. **173**(8): p. 897-901.

36. May, J.M., *How does ascorbic acid prevent endothelial dysfunction?* Free Radic Biol Med, 2000. **28**(9): p. 1421-9.

37. Robaczewska, J., et al., *Role of glutathione metabolism and glutathione-related antioxidant defense systems in hypertension.* J Physiol Pharmacol, 2016. **67**(3): p. 331-7.

38. Forgione, M.A., et al., *Cellular glutathione peroxidase deficiency and endothelial dysfunction.* Am J Physiol Heart Circ Physiol, 2002. **282**(4): p. H1255-61.

39. Son, S.M., *Reactive oxygen and nitrogen species in pathogenesis of vascular complications of diabetes.* Diabetes Metab J, 2012. **36**(3): p. 190-8.

40. Townsend, D.M., K.D. Tew, and H. Tapiero, *The importance of glutathione in human disease.* Biomed Pharmacother, 2003. **57**(3-4): p. 145-55.

41. McClellan, M., et al., *Call to Action: Urgent Challenges in Cardiovascular Disease: A Presidential Advisory From the American Heart Association.* Circulation, 2019. **139**(9): p. e44-e54.

42. Cai, H. and D.G. Harrison, *Endothelial dysfunction in cardiovascular diseases: the role of oxidant stress.* Circ Res, 2000. **87**(10): p. 840-4.

43. Koene, R.J., et al., *Shared Risk Factors in Cardiovascular Disease and Cancer.* Circulation, 2016. **133**(11): p. 1104-14.

44. Carvalho, C. and P.I. Moreira, *Oxidative Stress: A Major Player in Cerebrovascular Alterations Associated to Neurodegenerative Events.* Front Physiol, 2018. **9**: p. 806.

45. Bryk, D., W. Olejarz, and D. Zapolska-Downar, *The role of oxidative stress and NADPH oxidase in the pathogenesis of atherosclerosis.* Postepy Hig Med Dosw (Online), 2017. **71**(0): p. 57-68.

46. Jha, J.C., et al., *Diabetes and Kidney Disease: Role of Oxidative Stress.* Antioxid Redox Signal, 2016. **25**(12): p. 657-684.

47. Melo, A., et al., *Oxidative stress in neurodegenerative diseases: mechanisms and therapeutic perspectives.* Oxid Med Cell Longev, 2011. **2011**: p. 467180.

48. Sosa, V., et al., *Oxidative stress and cancer: an overview.* Ageing Res Rev, 2013. **12**(1): p. 376-90.

49. Shaw, P.X., G. Werstuck, and Y. Chen, *Oxidative stress and aging diseases.* Oxid Med Cell Longev, 2014. **2014**: p. 569146.

50. Sies, H., *Oxidative stress: a concept in redox biology and medicine.* Redox Biol, 2015. **4**: p. 180-3.

51. Sena, C.M., et al., *Vascular Oxidative Stress: Impact and Therapeutic Approaches.* Front Physiol, 2018. **9**: p. 1668.

52.   Santilli, F., D. D'Ardes, and G. Davi, *Oxidative stress in chronic vascular disease: From prediction to prevention.* Vascul Pharmacol, 2015.

53.   Siti, H.N., Y. Kamisah, and J. Kamsiah, *The role of oxidative stress, antioxidants and vascular inflammation in cardiovascular disease (a review).* Vascul Pharmacol, 2015. **71**: p. 40-56.

54.   Ferrer-Sueta, G., et al., *Biochemistry of Peroxynitrite and Protein Tyrosine Nitration.* Chem Rev, 2018. **118**(3): p. 1338-1408.

55.   Halliwell, B. and J. Gutteridge, *Oxidative stress and redox regulations:adaptation, damage, repair, senescence, and death*. Free Radicals in Biology and Medicine. 2015, Oxford, London: Oxford University Place. 84.

56.   Godo, S. and H. Shimokawa, *Endothelial Functions.* Arterioscler Thromb Vasc Biol, 2017. **37**(9): p. e108-e114.

57.   Konukoglu, D. and H. Uzun, *Endothelial Dysfunction and Hypertension.* Adv Exp Med Biol, 2017. **956**: p. 511-540.

58.   Rajendran, P., et al., *The vascular endothelium and human diseases.* Int J Biol Sci, 2013. **9**(10): p. 1057-69.

59.   Chiu, J.J. and S. Chien, *Effects of disturbed flow on vascular endothelium: pathophysiological basis and clinical perspectives.* Physiol Rev, 2011. **91**(1): p. 327-87.

60.   Domingueti, C.P., et al., *Diabetes mellitus: The linkage between oxidative stress, inflammation, hypercoagulability and vascular complications.* J Diabetes Complications, 2015.

61.   Golbidi, S., L. Edvinsson, and I. Laher, *Smoking and Endothelial Dysfunction.* Curr Vasc Pharmacol, 2018.

62.   Lai, W.K. and M.Y. Kan, *Homocysteine-Induced Endothelial Dysfunction.* Ann Nutr Metab, 2015. **67**(1): p. 1-12.

63.   Ungvari, Z., et al., *Endothelial dysfunction and angiogenesis impairment in the ageing vasculature.* Nat Rev Cardiol, 2018. **15**(9): p. 555-565.

64.   Engin, A., *Endothelial Dysfunction in Obesity.* Adv Exp Med Biol, 2017. **960**: p. 345-379.

65.   Vara, D. and G. Pula, *Reactive oxygen species: physiological roles in the regulation of vascular cells.* Curr Mol Med, 2014. **14**(9): p. 1103-25.

66.   Chen, Q., et al., *Reactive oxygen species: key regulators in vascular health and diseases.* Br J Pharmacol, 2018. **175**(8): p. 1279-1292.

67.   Fridovich, I., *Superoxide radical: an endogenous toxicant.* Annu Rev Pharmacol Toxicol, 1983. **23**: p. 239-57.

68.   D'Autreaux, B. and M.B. Toledano, *ROS as signalling molecules: mechanisms that generate specificity in ROS homeostasis.* Nat Rev Mol Cell Biol, 2007. **8**(10): p. 813-24.

69.   Fisher, A.B., *Redox signaling across cell membranes.* Antioxid Redox Signal, 2009. **11**(6): p. 1349-56.

70. Thomas, C., et al., *Hydroxyl radical is produced via the Fenton reaction in submitochondrial particles under oxidative stress: implications for diseases associated with iron accumulation.* Redox Rep, 2009. **14**(3): p. 102-8.

71. Blanco, S., et al., *Melatonin influences NO/NOS pathway and reduces oxidative and nitrosative stress in a model of hypoxic-ischemic brain damage.* Nitric Oxide, 2017. **62**: p. 32-43.

72. Speckmann, B., et al., *Peroxynitrite: From interception to signaling.* Arch Biochem Biophys, 2016. **595**: p. 153-60.

73. Lassegue, B., A. San Martin, and K.K. Griendling, *Biochemistry, physiology, and pathophysiology of NADPH oxidases in the cardiovascular system.* Circ Res, 2012. **110**(10): p. 1364-90.

74. Montezano, A.C. and R.M. Touyz, *Reactive oxygen species, vascular Noxs, and hypertension: focus on translational and clinical research.* Antioxid Redox Signal, 2014. **20**(1): p. 164-82.

75. Bedard, K. and K.H. Krause, *The NOX family of ROS-generating NADPH oxidases: physiology and pathophysiology.* Physiol Rev, 2007. **87**(1): p. 245-313.

76. Petry, A., M. Weitnauer, and A. Gorlach, *Receptor activation of NADPH oxidases.* Antioxid Redox Signal, 2010. **13**(4): p. 467-87.

77. Dikalov, S.I., et al., *Distinct roles of Nox1 and Nox4 in basal and angiotensin II-stimulated superoxide and hydrogen peroxide production.* Free Radic Biol Med, 2008. **45**(9): p. 1340-51.

78. Helmcke, I., et al., *Identification of structural elements in Nox1 and Nox4 controlling localization and activity.* Antioxid Redox Signal, 2009. **11**(6): p. 1279-87.

79. Judkins, C.P., et al., *Direct evidence of a role for Nox2 in superoxide production, reduced nitric oxide bioavailability, and early atherosclerotic plaque formation in ApoE-/- mice.* Am J Physiol Heart Circ Physiol, 2010. **298**(1): p. H24-32.

80. Drummond, G.R. and C.G. Sobey, *Endothelial NADPH oxidases: which NOX to target in vascular disease?* Trends Endocrinol Metab, 2014. **25**(9): p. 452-63.

81. Lener, B., et al., *The NADPH oxidase Nox4 restricts the replicative lifespan of human endothelial cells.* Biochem J, 2009. **423**(3): p. 363-74.

82. Montezano, A.C., et al., *NADPH Oxidase 5 Is a Pro-Contractile Nox Isoform and a Point of Cross-Talk for Calcium and Redox Signaling-Implications in Vascular Function.* J Am Heart Assoc, 2018. **7**(12).

83. Choi, D.H. and J. Lee, *A Mini-Review of the NADPH oxidases in Vascular Dementia: Correlation with NOXs and Risk Factors for VaD.* Int J Mol Sci, 2017. **18**(11).

84. Loffredo, L., et al., *Obesity and hypercholesterolemia are associated with NOX2 generated oxidative stress and arterial dysfunction.* J Pediatr, 2012. **161**(6): p. 1004-9.

85. Schulz, R., et al., *Arterial hypertension in a murine model of sleep apnea: role of NADPH oxidase 2.* J Hypertens, 2014. **32**(2): p. 300-5.

86.   Bayir, H., *Reactive oxygen species.* Crit Care Med, 2005. **33**(12 Suppl): p. S498-501.

87.   Berry, C.E. and J.M. Hare, *Xanthine oxidoreductase and cardiovascular disease: molecular mechanisms and pathophysiological implications.* J Physiol, 2004. **555**(Pt 3): p. 589-606.

88.   Landmesser, U., et al., *Angiotensin II induces endothelial xanthine oxidase activation: role for endothelial dysfunction in patients with coronary disease.* Arterioscler Thromb Vasc Biol, 2007. **27**(4): p. 943-8.

89.   Guthikonda, S., et al., *Xanthine oxidase inhibition reverses endothelial dysfunction in heavy smokers.* Circulation, 2003. **107**(3): p. 416-21.

90.   Schroder, K., et al., *Xanthine oxidase inhibitor tungsten prevents the development of atherosclerosis in ApoE knockout mice fed a Western-type diet.* Free Radic Biol Med, 2006. **41**(9): p. 1353-60.

91.   Nomura, J., et al., *Xanthine oxidase inhibition by febuxostat attenuates experimental atherosclerosis in mice.* Sci Rep, 2014. **4**: p. 4554.

92.   Forstermann, U. and W.C. Sessa, *Nitric oxide synthases: regulation and function.* Eur Heart J, 2012. **33**(7): p. 829-37, 837a-837d.

93.   Kar, S. and M. Kavdia, *Modeling of biopterin-dependent pathways of eNOS for nitric oxide and superoxide production.* Free Radic Biol Med, 2011. **51**(7): p. 1411-27.

94.   Katusic, Z.S., L.V. d'Uscio, and K.A. Nath, *Vascular protection by tetrahydrobiopterin: progress and therapeutic prospects.* Trends in Pharmacological Sciences, 2009. **30**(1): p. 48-54.

95.   Crabtree, M.J., et al., *Ratio of 5,6,7,8-tetrahydrobiopterin to 7,8-dihydrobiopterin in endothelial cells determines glucose-elicited changes in NO vs. superoxide production by eNOS.* Am J Physiol Heart Circ Physiol, 2008. **294**(4): p. H1530-40.

96.   Presta, A., et al., *Comparative functioning of dihydro- and tetrahydropterins in supporting electron transfer, catalysis, and subunit dimerization in inducible nitric oxide synthase.* Biochemistry, 1998. **37**(1): p. 298-310.

97.   Marchal, S., et al., *Evidence of two distinct oxygen complexes of reduced endothelial nitric oxide synthase.* J Biol Chem, 2004. **279**(19): p. 19824-31.

98.   Dromparis, P. and E.D. Michelakis, *Mitochondria in vascular health and disease.* Annu Rev Physiol, 2013. **75**: p. 95-126.

99.   Andreyev, A.Y., et al., *Mitochondrial ROS Metabolism: 10 Years Later.* Biochemistry (Mosc), 2015. **80**(5): p. 517-31.

100.   Sturza, A., et al., *Monoamine oxidases are novel sources of cardiovascular oxidative stress in experimental diabetes.* Can J Physiol Pharmacol, 2015. **93**(7): p. 555-61.

101.   Zorov, D.B., M. Juhaszova, and S.J. Sollott, *Mitochondrial reactive oxygen species (ROS) and ROS-induced ROS release.* Physiol Rev, 2014. **94**(3): p. 909-50.

102. Rocha, S., et al., *Peroxiredoxin 2, glutathione peroxidase, and catalase in the cytosol and membrane of erythrocytes under H2O2-induced oxidative stress.* Free Radic Res, 2015. **49**(8): p. 990-1003.

103. Kurutas, E.B., *The importance of antioxidants which play the role in cellular response against oxidative/nitrosative stress: current state.* Nutr J, 2016. **15**(1): p. 71.

104. Benhar, M., *Roles of mammalian glutathione peroxidase and thioredoxin reductase enzymes in the cellular response to nitrosative stress.* Free Radic Biol Med, 2018. **127**: p. 160-164.

105. Sies, H., et al., *Glutathione peroxidase protects against peroxynitrite-mediated oxidations. A new function for selenoproteins as peroxynitrite reductase.* J Biol Chem, 1997. **272**(44): p. 27812-7.

106. Lubos, E., J. Loscalzo, and D.E. Handy, *Glutathione peroxidase-1 in health and disease: from molecular mechanisms to therapeutic opportunities.* Antioxid Redox Signal, 2011. **15**(7): p. 1957-97.

107. Sharma, A., et al., *Lack of glutathione peroxidase-1 facilitates a pro-inflammatory and activated vascular endothelium.* Vascul Pharmacol, 2016. **79**: p. 32-42.

108. Patel, P. and S. Chatterjee, *Peroxiredoxin6 in Endothelial Signaling.* Antioxidants (Basel), 2019. **8**(3).

109. De Armas, M.I., et al., *Rapid peroxynitrite reduction by human peroxiredoxin 3: Implications for the fate of oxidants in mitochondria.* Free Radic Biol Med, 2019. **130**: p. 369-378.

110. Fiuza, B., et al., *Impact of SIN-1-derived peroxynitrite flux on endothelial cell redox homeostasis and bioenergetics: protective role of diphenyl diselenide via induction of peroxiredoxins.* Free Radic Res, 2015. **49**(2): p. 122-32.

111. Kisucka, J., et al., *Peroxiredoxin1 prevents excessive endothelial activation and early atherosclerosis.* Circ Res, 2008. **103**(6): p. 598-605.

112. Qiao, H. and J.M. May, *Development of ascorbate transporters in brain cortical capillary endothelial cells in culture.* Brain Res, 2008. **1208**: p. 79-86.

113. Padayatty, S.J. and M. Levine, *Vitamin C: the known and the unknown and Goldilocks.* Oral Dis, 2016. **22**(6): p. 463-93.

114. Wilson, J.X., *Mechanism of action of vitamin C in sepsis: ascorbate modulates redox signaling in endothelium.* Biofactors, 2009. **35**(1): p. 5-13.

115. Sanchez-Moreno, C., et al., *Decreased levels of plasma vitamin C and increased concentrations of inflammatory and oxidative stress markers after stroke.* Stroke, 2004. **35**(1): p. 163-8.

116. Ladurner, A., et al., *Ascorbate stimulates endothelial nitric oxide synthase enzyme activity by rapid modulation of its phosphorylation status.* Free Radic Biol Med, 2012. **52**(10): p. 2082-90.

117. May, J.M. and F.E. Harrison, *Role of vitamin C in the function of the vascular endothelium.* Antioxid Redox Signal, 2013. **19**(17): p. 2068-83.

118. Henderson, G.B., et al., *Engineering the Substrate-Specificity of Glutathione-Reductase toward That of Trypanothione Reduction.* Proceedings of the National Academy of Sciences of the United States of America, 1991. **88**(19): p. 8769-8773.

119. Vera, M., et al., *Antioxidant and Anti-Inflammatory Strategies Based on the Potentiation of Glutathione Peroxidase Activity Prevent Endothelial Dysfunction in Chronic Kidney Disease.* Cell Physiol Biochem, 2018. **51**(3): p. 1287-1300.

120. Channon, K.M., *Tetrahydrobiopterin: a vascular redox target to improve endothelial function.* Curr Vasc Pharmacol, 2012. **10**(6): p. 705-8.

121. Deponte, M., *Glutathione catalysis and the reaction mechanisms of glutathione-dependent enzymes.* Biochim Biophys Acta, 2013. **1830**(5): p. 3217-66.

122. Lewin, M.H., et al., *Selenium supplementation acting through the induction of thioredoxin reductase and glutathione peroxidase protects the human endothelial cell line EAhy926 from damage by lipid hydroperoxides.* Biochim Biophys Acta, 2002. **1593**(1): p. 85-92.

123. Campolo, J., et al., *Medium-term effect of sublingual l-glutathione supplementation on flow-mediated dilation in subjects with cardiovascular risk factors.* Nutrition, 2017. **38**: p. 41-47.

124. Chen, J., et al., *Glutathione Supplementation Attenuates Oxidative Stress and Improves Vascular Hyporesponsiveness in Experimental Obstructive Jaundice.* Oxid Med Cell Longev, 2015. **2015**: p. 486148.

125. Chen, J.Y., et al., *Nitric oxide bioavailability dysfunction involves in atherosclerosis.* Biomed Pharmacother, 2018. **97**: p. 423-428.

126. Satitthummanid, S., et al., *Depleted nitric oxide and prostaglandin E2 levels are correlated with endothelial dysfunction in beta-thalassemia/HbE patients.* Int J Hematol, 2017. **106**(3): p. 366-374.

127. Gabryel, B., et al., *Superoxide dismutase 1 and glutathione peroxidase 1 are involved in the protective effect of sulodexide on vascular endothelial cells exposed to oxygen-glucose deprivation.* Microvasc Res, 2016. **103**: p. 26-35.

128. Likidlilid, A., et al., *Glutathione and glutathione peroxidase in type 1 diabetic patients.* J Med Assoc Thai, 2007. **90**(9): p. 1759-67.

129. Chen, L., et al., *Impaired Endothelial Repair Capacity of Early Endothelial Progenitor Cells in Hypertensive Patients With Primary Hyperaldosteronemia: Role of 5,6,7,8-Tetrahydrobiopterin Oxidation and Endothelial Nitric Oxide Synthase Uncoupling.* Hypertension, 2016. **67**(2): p. 430-9.

130. Radi, R., *Oxygen radicals, nitric oxide, and peroxynitrite: Redox pathways in molecular medicine.* Proc Natl Acad Sci U S A, 2018. **115**(23): p. 5839-5848.

131. Pacher, P., J.S. Beckman, and L. Liaudet, *Nitric oxide and peroxynitrite in health and disease.* Physiol Rev, 2007. **87**(1): p. 315-424.

132. Nurkiewicz, T.R., et al., *Decreased arteriolar tetrahydrobiopterin is linked to superoxide generation from nitric oxide synthase in mice fed high salt.* Microcirculation, 2010. **17**(2): p. 147-57.

133. Crabtree, M.J., et al., *Critical role for tetrahydrobiopterin recycling by dihydrofolate reductase in regulation of endothelial nitric-oxide synthase coupling: relative importance of the de novo biopterin synthesis versus salvage pathways.* J Biol Chem, 2009. **284**(41): p. 28128-36.

134. Shimizu, S., et al., *Hydrogen peroxide stimulates tetrahydrobiopterin synthesis through the induction of GTP-cyclohydrolase I and increases nitric oxidesynthase activity in vascular endothelial cells.* Free Radical Biology and Medicine, 2003. **34**(10): p. 1343-1352.

135. Shimizu, S., et al., *Possible involvement of hydroxyl radical on the stimulation of tetrahydrobiopterin synthesis by hydrogen peroxide and peroxynitrite in vascular endothelial cells.* Int J Biochem Cell Biol, 2005. **37**(4): p. 864-75.

136. Meininger, C.J., et al., *Impaired nitric oxide production in coronary endothelial cells of the spontaneously diabetic BB rat is due to tetrahydrobiopterin deficiency.* Biochemical Journal, 2000. **349**: p. 353-356.

137. Sasaki, N., et al., *Augmentation of vascular remodeling by uncoupled endothelial nitric oxide synthase in a mouse model of diabetes mellitus.* Arterioscler Thromb Vasc Biol, 2008. **28**(6): p. 1068-76.

138. Alp, N.J., et al., *Tetrahydrobiopterin-dependent preservation of nitric oxide-mediated endothelial function in diabetes by targeted transgenic GTP-cyclohydrolase I overexpression.* J Clin Invest, 2003. **112**(5): p. 725-35.

139. Aouacheri, O., et al., *The investigation of the oxidative stress-related parameters in type 2 diabetes mellitus.* Can J Diabetes, 2015. **39**(1): p. 44-9.

140. Li, H., S. Horke, and U. Forstermann, *Vascular oxidative stress, nitric oxide and atherosclerosis.* Atherosclerosis, 2014. **237**(1): p. 208-19.

141. Wang, W., et al., *Superoxide production and reactive oxygen species signaling by endothelial nitric-oxide synthase.* J Biol Chem, 2000. **275**(22): p. 16899-903.

142. Huang, A., et al., *Ascorbic acid enhances endothelial nitric-oxide synthase activity by increasing intracellular tetrahydrobiopterin.* J Biol Chem, 2000. **275**(23): p. 17399-406.

143. Mortensen, A., et al., *Guinea pig ascorbate status predicts tetrahydrobiopterin plasma concentration and oxidation ratio in vivo.* Nutr Res, 2013. **33**(10): p. 859-67.

144. Patel, K.B., et al., *Oxidation of tetrahydrobiopterin by biological radicals and scavenging of the trihydrobiopterin radical by ascorbate.* Free Radic Biol Med, 2002. **32**(3): p. 203-11.

145. Jackson, T.S., et al., *Ascorbate prevents the interaction of superoxide and nitric oxide only at very high physiological concentrations.* Circ Res, 1998. **83**(9): p. 916-22.

146. Mortensen, A. and J. Lykkesfeldt, *Does vitamin C enhance nitric oxide bioavailability in a tetrahydrobiopterin-dependent manner? In vitro, in vivo and clinical studies.* Nitric Oxide, 2014. **36**: p. 51-7.

147.   Akolkar, G., et al., *Vitamin C mitigates oxidative/nitrosative stress and inflammation in doxorubicin-induced cardiomyopathy.* Am J Physiol Heart Circ Physiol, 2017. **313**(4): p. H795-H809.

148.   Mullan, B.A., et al., *Ascorbic acid reduces blood pressure and arterial stiffness in type 2 diabetes.* Hypertension, 2002. **40**(6): p. 804-9.

149.   Gokce, N., et al., *Long-term ascorbic acid administration reverses endothelial vasomotor dysfunction in patients with coronary artery disease.* Circulation, 1999. **99**(25): p. 3234-40.

150.   Hornig, B., et al., *Vitamin C improves endothelial function of conduit arteries in patients with chronic heart failure.* Circulation, 1998. **97**(4): p. 363-8.

151.   Varadharaj, S., et al., *Vitamin C-induced loss of redox-dependent viability in lung microvascular endothelial cells.* Antioxid Redox Signal, 2005. **7**(1-2): p. 287-300.

152.   Forman, H.J., H. Zhang, and A. Rinna, *Glutathione: overview of its protective roles, measurement, and biosynthesis.* Mol Aspects Med, 2009. **30**(1-2): p. 1-12.

153.   Friesen, C., Y. Kiess, and K.M. Debatin, *A critical role of glutathione in determining apoptosis sensitivity and resistance in leukemia cells.* Cell Death Differ, 2004. **11 Suppl 1**: p. S73-85.

154.   Ray, P.D., B.W. Huang, and Y. Tsuji, *Reactive oxygen species (ROS) homeostasis and redox regulation in cellular signaling.* Cell Signal, 2012. **24**(5): p. 981-90.

155.   Chi, L., et al., *Depletion of reduced glutathione enhances motor neuron degeneration in vitro and in vivo.* Neuroscience, 2007. **144**(3): p. 991-1003.

156.   Rizzardini, M., et al., *Mitochondrial dysfunction and death in motor neurons exposed to the glutathione-depleting agent ethacrynic acid.* Journal of the Neurological Sciences, 2003. **207**(1-2): p. 51-58.

157.   Armstrong, J.S., et al., *Role of glutathione depletion and reactive oxygen species generation in apoptotic signaling in a human B lymphoma cell line.* Cell Death Differ, 2002. **9**(3): p. 252-263.

158.   Flohe, L., et al., *A comparison of thiol peroxidase mechanisms.* Antioxid Redox Signal, 2011. **15**(3): p. 763-80.

159.   Mai, H.N., et al., *Genetic depletion of glutathione peroxidase-1 potentiates nephrotoxicity induced by multiple doses of cocaine via activation of angiotensin II AT1 receptor.* Free Radic Res, 2016. **50**(4): p. 467-83.

160.   Ehrhart, J. and G.D. Zeevalk, *Hydrogen peroxide removal and glutathione mixed disulfide formation during metabolic inhibition in mesencephalic cultures.* J Neurochem, 2001. **77**(6): p. 1496-507.

161.   Canals, S., et al., *Glutathione depletion switches nitric oxide neurotrophic effects to cell death in midbrain cultures: implications for Parkinson's disease.* J Neurochem, 2001. **79**(6): p. 1183-1195.

162. Yeh, E.L., et al., *A higher glutathione demand may be necessary for assisting hemodialysis patients to cope with increased oxidative stress.* Nephrology (Carlton), 2019.

163. Prasai, P.K., et al., *Decreases in GSH:GSSG activate vascular endothelial growth factor receptor 2 (VEGFR2) in human aortic endothelial cells.* Redox Biol, 2018. **19**: p. 22-27.

164. Fu, Y.X., J.M. Porres, and X.G. Lei, *Comparative impacts of glutathione peroxidase-1 gene knockout on oxidative stress induced by reactive oxygen and nitrogen species in mouse hepatocytes.* Biochemical Journal, 2001. **359**: p. 687-695.

165. Maraldi, T., et al., *Low levels of selenium compounds are selectively toxic for a human neuron cell line through ROS/RNS increase and apoptotic process activation.* Neurotoxicology, 2011. **32**(2): p. 180-187.

166. Winterbourn, C.C. and M.B. Hampton, *Thiol chemistry and specificity in redox signaling.* Free Radic Biol Med, 2008. **45**(5): p. 549-61.

167. Perkins, A., et al., *Peroxiredoxins: guardians against oxidative stress and modulators of peroxide signaling.* Trends Biochem Sci, 2015. **40**(8): p. 435-45.

168. Kang, D.H., et al., *Peroxiredoxin II is an essential antioxidant enzyme that prevents the oxidative inactivation of VEGF receptor-2 in vascular endothelial cells.* Mol Cell, 2011. **44**(4): p. 545-58.

169. Bartocci, E. and P. Lio, *Computational Modeling, Formal Analysis, and Tools for Systems Biology.* PLoS Comput Biol, 2016. **12**(1): p. e1004591.

170. Kar, S., B. Bhandar, and M. Kavdia, *Impact of SOD in eNOS uncoupling: a two-edged sword between hydrogen peroxide and peroxynitrite.* Free Radic Res, 2012. **46**(12): p. 1496-513.

171. Kuiper, C., M.C. Vissers, and K.O. Hicks, *Pharmacokinetic modeling of ascorbate diffusion through normal and tumor tissue.* Free Radic Biol Med, 2014. **77**: p. 340-52.

172. Ponte, F., N. Russo, and E. Sicilia, *Insights from Computations on the Mechanism of Reduction by Ascorbic Acid of Pt(IV) Prodrugs with Asplatin and Its Chlorido and Bromido Analogues as Model Systems.* Chemistry, 2018. **24**(38): p. 9572-9580.

173. Hu, T.M. and Y.J. Chen, *Nitrosation-modulating effect of ascorbate in a model dynamic system of coexisting nitric oxide and superoxide.* Free Radic Res, 2010. **44**(5): p. 552-62.

174. Presnell, C.E., et al., *Computational insights into the role of glutathione in oxidative stress.* Curr Neurovasc Res, 2013. **10**(2): p. 185-94.

175. Hu, T.M., W.L. Hayton, and S.R. Mallery, *Kinetic modeling of nitric-oxide-associated reaction network.* Pharm Res, 2006. **23**(8): p. 1702-11.

176. Ng, C.F., et al., *The rate of cellular hydrogen peroxide removal shows dependency on GSH: mathematical insight into in vivo H2O2 and GPx concentrations.* Free Radic Res, 2007. **41**(11): p. 1201-11.

177. Keszler, A., Y.H. Zhang, and N. Hogg, *Reaction between nitric oxide, glutathione, and oxygen in the presence and absence of protein: How are S-nitrosothiols formed?* Free Radical Biology and Medicine, 2010. **48**(1): p. 55-64.

178. Bagci, E.Z., et al., *Computational insights on the competing effects of nitric oxide in regulating apoptosis.* PLoS One, 2008. **3**(5): p. e2249.

179. Adimora, N.J., D.P. Jones, and M.L. Kemp, *A Model of Redox Kinetics Implicates the Thiol Proteome in Cellular Hydrogen Peroxide Responses.* Antioxid Redox Signal, 2010. **13**(6): p. 731-743.

180. Vasquez-Vivar, J., *Tetrahydrobiopterin, superoxide, and vascular dysfunction.* Free Radic Biol Med, 2009. **47**(8): p. 1108-19.

181. Dikalov, S., *Cross talk between mitochondria and NADPH oxidases.* Free Radic Biol Med, 2011. **51**(7): p. 1289-301.

182. Brown, D.I. and K.K. Griendling, *Nox proteins in signal transduction.* Free Radic Biol Med, 2009. **47**(9): p. 1239-53.

183. Quijano, C., et al., *Enhanced mitochondrial superoxide in hyperglycemic endothelial cells: direct measurements and formation of hydrogen peroxide and peroxynitrite.* Am J Physiol Heart Circ Physiol, 2007. **293**(6): p. H3404-14.

184. Quinlan, C.L., et al., *Native rates of superoxide production from multiple sites in isolated mitochondria measured using endogenous reporters.* Free Radic Biol Med, 2012. **53**(9): p. 1807-17.

185. Spiekermann, S., et al., *Electron spin resonance characterization of vascular xanthine and NAD(P)H oxidase activity in patients with coronary artery disease: relation to endothelium-dependent vasodilation.* Circulation, 2003. **107**(10): p. 1383-9.

186. Dikalova, A.E., et al., *Therapeutic targeting of mitochondrial superoxide in hypertension.* Circ Res, 2010. **107**(1): p. 106-16.

187. Chen, K. and A.S. Popel, *Theoretical analysis of biochemical pathways of nitric oxide release from vascular endothelial cells.* Free Radic Biol Med, 2006. **41**(4): p. 668-80.

188. Klatt, P., et al., *The pteridine binding site of brain nitric oxide synthase. Tetrahydrobiopterin binding kinetics, specificity, and allosteric interaction with the substrate domain.* J Biol Chem, 1994. **269**(19): p. 13861-6.

189. Berka, V. and A.L. Tsai, *Characterization of interactions among the heme center, tetrahydrobiopterin, and L-arginine binding sites of ferric eNOS using imidazole, cyanide, and nitric oxide as probes.* Biochemistry, 2000. **39**(31): p. 9373-83.

190. Berka, V., et al., *Redox function of tetrahydrobiopterin and effect of L-arginine on oxygen binding in endothelial nitric oxide synthase.* Biochemistry, 2004. **43**(41): p. 13137-48.

191. Berka, V., P.F. Chen, and A.L. Tsai, *Spatial relationship between L-arginine and heme binding sites of endothelial nitric-oxide synthase.* J Biol Chem, 1996. **271**(52): p. 33293-300.

192. Santolini, J., A.L. Meade, and D.J. Stuehr, *Differences in three kinetic parameters underpin the unique catalytic profiles of nitric-oxide synthases I, II, and III.* J Biol Chem, 2001. **276**(52): p. 48887-98.

193. Wei, C.C., et al., *Structure of tetrahydrobiopterin tunes its electron transfer to the heme-dioxy intermediate in nitric oxide synthase.* Biochemistry, 2003. **42**(7): p. 1969-77.

194. Wei, C.C., et al., *The three nitric-oxide synthases differ in their kinetics of tetrahydrobiopterin radical formation, heme-dioxy reduction, and arginine hydroxylation.* J Biol Chem, 2005. **280**(10): p. 8929-35.

195. Wei, C.C., et al., *Catalytic reduction of a tetrahydrobiopterin radical within nitric-oxide synthase.* J Biol Chem, 2008. **283**(17): p. 11734-42.

196. Wei, C.C., et al., *A tetrahydrobiopterin radical forms and then becomes reduced during Nomega-hydroxyarginine oxidation by nitric-oxide synthase.* J Biol Chem, 2003. **278**(47): p. 46668-73.

197. Abu-Soud, H.M., et al., *Electron transfer, oxygen binding, and nitric oxide feedback inhibition in endothelial nitric-oxide synthase.* J Biol Chem, 2000. **275**(23): p. 17349-57.

198. Wei, C.C., et al., *Rapid kinetic studies link tetrahydrobiopterin radical formation to heme-dioxy reduction and arginine hydroxylation in inducible nitric-oxide synthase.* J Biol Chem, 2001. **276**(1): p. 315-9.

199. Potdar, S. and M. Kavdia, *NO/peroxynitrite dynamics of high glucose-exposed HUVECs: chemiluminescent measurement and computational model.* Microvasc Res, 2009. **78**(2): p. 191-8.

200. Lancaster, J.R., Jr., *Nitroxidative, nitrosative, and nitrative stress: kinetic predictions of reactive nitrogen species chemistry under biological conditions.* Chem Res Toxicol, 2006. **19**(9): p. 1160-74.

201. Kirsch, M., et al., *The autoxidation of tetrahydrobiopterin revisited. Proof of superoxide formation from reaction of tetrahydrobiopterin with molecular oxygen.* J Biol Chem, 2003. **278**(27): p. 24481-90.

202. Kuzkaya, N., et al., *Interactions of peroxynitrite, tetrahydrobiopterin, ascorbic acid, and thiols: implications for uncoupling endothelial nitric-oxide synthase.* J Biol Chem, 2003. **278**(25): p. 22546-54.

203. Quijano, C., N. Romero, and R. Radi, *Tyrosine nitration by superoxide and nitric oxide fluxes in biological systems: modeling the impact of superoxide dismutase and nitric oxide diffusion.* Free Radic Biol Med, 2005. **39**(6): p. 728-41.

204. Ohashi, A., et al., *Asymmetric uptake of sepiapterin and 7,8-dihydrobiopterin as a gateway of the salvage pathway of tetrahydrobiopterin biosynthesis from the lumenal surface of rat endothelial cells.* Mol Genet Metab, 2011. **104**(3): p. 404-6.

205. Sawabe, K., et al., *Cellular uptake of sepiapterin and push-pull accumulation of tetrahydrobiopterin.* Mol Genet Metab, 2008. **94**(4): p. 410-6.

206. Shiraishi, H., et al., *Cilostazol inhibits cytokine-induced tetrahydrobiopterin biosynthesis in human umbilical vein endothelial cells.* J Atheroscler Thromb, 2011. **18**(4): p. 312-7.

207. Quinlan, C.L., et al., *Mitochondrial complex II can generate reactive oxygen species at high rates in both the forward and reverse reactions.* J Biol Chem, 2012. **287**(32): p. 27255-64.

208. Nalwaya, N. and W.M. Deen, *Nitric oxide, oxygen, and superoxide formation and consumption in macrophage cultures.* Chem Res Toxicol, 2005. **18**(3): p. 486-93.

209. Schmidt, T.S. and N.J. Alp, *Mechanisms for the role of tetrahydrobiopterin in endothelial function and vascular disease.* Clin Sci (Lond), 2007. **113**(2): p. 47-63.

210. Benson, M.A., et al., *A pivotal role for tryptophan 447 in enzymatic coupling of human endothelial nitric oxide synthase (eNOS): effects on tetrahydrobiopterin-dependent catalysis and eNOS dimerization.* J Biol Chem, 2013. **288**(41): p. 29836-45.

211. Luo, S., et al., *Molecular Mechanisms of Endothelial NO Synthase Uncoupling.* Curr Pharm Des, 2014. **20**(22): p. 3548-53.

212. Werner-Felmayer, G., et al., *Pteridine biosynthesis in human endothelial cells. Impact on nitric oxide-mediated formation of cyclic GMP.* J Biol Chem, 1993. **268**(3): p. 1842-6.

213. Liu, J., G. Garcia-Cardena, and W.C. Sessa, *Palmitoylation of endothelial nitric oxide synthase is necessary for optimal stimulated release of nitric oxide: implications for caveolae localization.* Biochemistry, 1996. **35**(41): p. 13277-81.

214. Meininger, C.J., et al., *Impaired nitric oxide production in coronary endothelial cells of the spontaneously diabetic BB rat is due to tetrahydrobiopterin deficiency.* Biochem J, 2000. **349**(Pt 1): p. 353-6.

215. Persechini, A. and P.M. Stemmer, *Calmodulin is a limiting factor in the cell.* Trends Cardiovasc Med, 2002. **12**(1): p. 32-7.

216. Wickham, N.W., et al., *Measurement of intracellular calcium concentration in intact monolayers of human endothelial cells.* J Lab Clin Med, 1988. **112**(2): p. 157-67.

217. Rengasamy, A. and R.A. Johns, *Determination of Km for oxygen of nitric oxide synthase isoforms.* J Pharmacol Exp Ther, 1996. **276**(1): p. 30-3.

218. Hasegawa, H., et al., *Delivery of exogenous tetrahydrobiopterin (BH4) to cells of target organs: role of salvage pathway and uptake of its precursor in effective elevation of tissue BH4.* Mol Genet Metab, 2005. **86 Suppl 1**: p. S2-10.

219. Murphy, M.P., *How mitochondria produce reactive oxygen species.* Biochemical Journal, 2009. **417**: p. 1-13.

220. Arnal, J.F., et al., *Ethinylestradiol does not enhance the expression of nitric oxide synthase in bovine endothelial cells but increases the release of bioactive nitric oxide by inhibiting superoxide anion production.* Proc Natl Acad Sci U S A, 1996. **93**(9): p. 4108-13.

221. Vasquez-Vivar, J., et al., *The ratio between tetrahydrobiopterin and oxidized tetrahydrobiopterin analogues controls superoxide release from endothelial nitric oxide synthase: an EPR spin trapping study.* Biochem J, 2002. **362**(Pt 3): p. 733-9.

222. Channon, K.M., *Tetrahydrobiopterin: regulator of endothelial nitric oxide synthase in vascular disease.* Trends Cardiovasc Med, 2004. **14**(8): p. 323-7.

223. An, H., et al., *Metformin attenuates fluctuating glucose-induced endothelial dysfunction through enhancing GTPCH1-mediated eNOS recoupling and inhibiting NADPH oxidase.* J Diabetes Complications, 2016. **30**(6): p. 1017-24.

224. Cai, H., *Hydrogen peroxide regulation of endothelial function: origins, mechanisms, and consequences.* Cardiovasc Res, 2005. **68**(1): p. 26-36.

225. Zou, M.H., *Peroxynitrite and protein tyrosine nitration of prostacyclin synthase.* Prostaglandins Other Lipid Mediat, 2007. **82**(1-4): p. 119-27.

226. Kavdia, M., *A computational model for free radicals transport in the microcirculation.* Antioxid Redox Signal, 2006. **8**(7-8): p. 1103-11.

227. Buettner, G.R., B.A. Wagner, and V.G. Rodgers, *Quantitative redox biology: an approach to understand the role of reactive species in defining the cellular redox environment.* Cell Biochem Biophys, 2013. **67**(2): p. 477-83.

228. Li, J.M. and A.M. Shah, *Endothelial cell superoxide generation: regulation and relevance for cardiovascular pathophysiology.* Am J Physiol Regul Integr Comp Physiol, 2004. **287**(5): p. R1014-30.

229. Zimmet, J.M. and J.M. Hare, *Nitroso-redox interactions in the cardiovascular system.* Circulation, 2006. **114**(14): p. 1531-44.

230. Jerkic, M. and M. Letarte, *Contribution of oxidative stress to endothelial dysfunction in hereditary hemorrhagic telangiectasia.* Front Genet, 2015. **6**: p. 34.

231. Sugiyama, T., B.D. Levy, and T. Michel, *Tetrahydrobiopterin recycling, a key determinant of endothelial nitric-oxide synthase-dependent signaling pathways in cultured vascular endothelial cells.* J Biol Chem, 2009. **284**(19): p. 12691-700.

232. Xu, J., et al., *Proteasome-dependent degradation of guanosine 5'-triphosphate cyclohydrolase I causes tetrahydrobiopterin deficiency in diabetes mellitus.* Circulation, 2007. **116**(8): p. 944-53.

233. Li, H.G. and U. Foerstermann, *Uncoupling of endothelial NO synthase in atherosclerosis and vascular disease.* Current Opinion in Pharmacology, 2013. **13**(2): p. 161-167.

234. Zhou, Z.W., et al., *Mechanism of reversal of high glucose-induced endothelial nitric oxide synthase uncoupling by tanshinone IIA in human endothelial cell line EA.hy926.* Eur J Pharmacol, 2012. **697**(1-3): p. 97-105.

235. Francis, B.N., et al., *Effects of tetrahydrobiopterin oral treatment in hypoxia-induced pulmonary hypertension in rat.* Pulm Circ, 2014. **4**(3): p. 462-70.

236. Shinozaki, K., et al., *Abnormal biopterin metabolism is a major cause of impaired endothelium-dependent relaxation through nitric oxide/O2- imbalance in insulin-resistant rat aorta.* Diabetes, 1999. **48**(12): p. 2437-45.

237. Schmidt, K., et al., *Evidence against tetrahydrobiopterin depletion of vascular tissue exposed to nitric oxide/superoxide or nitroglycerin.* Free Radic Biol Med, 2010. **48**(1): p. 145-52.

238. Kinoshita, H. and Z.S. Katusic, *Exogenous tetrahydrobiopterin causes endothelium-dependent contractions in isolated canine basilar artery.* Am J Physiol, 1996. **271**(2 Pt 2): p. H738-43.

239. Cai, S., et al., *GTP cyclohydrolase I gene transfer augments intracellular tetrahydrobiopterin in human endothelial cells: effects on nitric oxide synthase activity, protein levels and dimerisation.* Cardiovasc Res, 2002. **55**(4): p. 838-49.

240. Alp, N.J., et al., *Increased endothelial tetrahydrobiopterin synthesis by targeted transgenic GTP-cyclohydrolase I overexpression reduces endothelial dysfunction and atherosclerosis in ApoE-knockout mice.* Arterioscler Thromb Vasc Biol, 2004. **24**(3): p. 445-50.

241. Sawabe, K., et al., *Accumulated BH4 in mouse liver caused by administration of either 6R- or 6SBH4 consisted solely of the 6R-diastereomer: evidence of oxidation to BH2 and enzymic reduction.* Mol Genet Metab, 2005. **86 Suppl 1**: p. S145-7.

242. Shinozaki, K., et al., *Supplement of tetrahydrobiopterin by a gene transfer of GTP cyclohydrolase I cDNA improves vascular dysfunction in insulin-resistant rats.* J Cardiovasc Pharmacol, 2005. **46**(4): p. 505-12.

243. Antoniades, C., et al., *Induction of vascular GTP-cyclohydrolase I and endogenous tetrahydrobiopterin synthesis protect against inflammation-induced endothelial dysfunction in human atherosclerosis.* Circulation, 2011. **124**(17): p. 1860-70.

244. Shinde, S.N., V.N. Dhadke, and A.N. Suryakar, *Evaluation of Oxidative Stress in Type 2 Diabetes Mellitus and Follow-up Along with Vitamin E Supplementation.* Indian J Clin Biochem, 2011. **26**(1): p. 74-7.

245. Plantinga, Y., et al., *Supplementation with vitamins C and E improves arterial stiffness and endothelial function in essential hypertensive patients.* Am J Hypertens, 2007. **20**(4): p. 392-7.

246. Baumgardt, S.L., et al., *Chronic Co-Administration of Sepiapterin and L-Citrulline Ameliorates Diabetic Cardiomyopathy and Myocardial Ischemia/Reperfusion Injury in Obese Type 2 Diabetic Mice.* Circ Heart Fail, 2016. **9**(1): p. e002424.

247. Coronel, I., et al., *L-arginine and antioxidant diet supplementation partially restores nitric oxide-dependent regulation of phenylephrine renal vasoconstriction in diabetics rats.* J Ren Nutr, 2010. **20**(3): p. 158-68.

248. Jacob, R.A. and G. Sotoudeh, *Vitamin C function and status in chronic disease.* Nutr Clin Care, 2002. **5**(2): p. 66-74.

249. Lykkesfeldt, J. and H.E. Poulsen, *Is vitamin C supplementation beneficial? Lessons learned from randomised controlled trials.* Br J Nutr, 2010. **103**(9): p. 1251-9.

250. Heller, R., et al., *L-ascorbic acid potentiates endothelial nitric oxide synthesis via a chemical stabilization of tetrahydrobiopterin.* J Biol Chem, 2001. **276**(1): p. 40-7.

251. Baker, T.A., S. Milstien, and Z.S. Katusic, *Effect of vitamin C on the availability of tetrahydrobiopterin in human endothelial cells.* J Cardiovasc Pharmacol, 2001. **37**(3): p. 333-8.

252. Erwin, P.A., et al., *Receptor-regulated dynamic S-nitrosylation of endothelial nitric-oxide synthase in vascular endothelial cells.* J Biol Chem, 2005. **280**(20): p. 19888-94.

253. Bendall, J.K., et al., *Stoichiometric relationships between endothelial tetrahydrobiopterin, endothelial NO synthase (eNOS) activity, and eNOS coupling in vivo: insights from*

transgenic mice with endothelial-targeted GTP cyclohydrolase 1 and eNOS overexpression. Circ Res, 2005. **97**(9): p. 864-71.

254. Shi, W., et al., *Regulation of tetrahydrobiopterin synthesis and bioavailability in endothelial cells.* Cell Biochem Biophys, 2004. **41**(3): p. 415-34.

255. Joshi, S., S. Kar, and M. Kavdia, *Computational analysis of interactions of oxidative stress and tetrahydrobiopterin reveals instability in eNOS coupling.* Microvasc Res, 2017. **114**: p. 114-128.

256. Gotoh, N. and E. Niki, *Rates of interactions of superoxide with vitamin E, vitamin C and related compounds as measured by chemiluminescence.* Biochim Biophys Acta, 1992. **1115**(3): p. 201-7.

257. Squadrito, G.L., X. Jin, and W.A. Pryor, *Stopped-flow kinetic study of the reaction of ascorbic acid with peroxynitrite.* Arch Biochem Biophys, 1995. **322**(1): p. 53-9.

258. Wink, D.A., et al., *Reactions of the bioregulatory agent nitric oxide in oxygenated aqueous media: determination of the kinetics for oxidation and nitrosation by intermediates generated in the NO/O2 reaction.* Chem Res Toxicol, 1993. **6**(1): p. 23-7.

259. Licht, W.R., S.R. Tannenbaum, and W.M. Deen, *Use of Ascorbic-Acid to Inhibit Nitrosation - Kinetic and Mass-Transfer Considerations for an Invitro System.* Carcinogenesis, 1988. **9**(3): p. 365-372.

260. Aebi, H., *Catalase in vitro.* Methods Enzymol, 1984. **105**: p. 121-6.

261. Koppenol, W.H., et al., *Peroxynitrite, a cloaked oxidant formed by nitric oxide and superoxide.* Chem Res Toxicol, 1992. **5**(6): p. 834-42.

262. Keshive, M., et al., *Kinetics of S-nitrosation of thiols in nitric oxide solutions.* Chem Res Toxicol, 1996. **9**(6): p. 988-93.

263. Jourd'heuil, D., et al., *The reaction of S-nitrosoglutathione with superoxide.* Biochem Biophys Res Commun, 1998. **244**(2): p. 525-30.

264. Li, R., *Vitamin C, a Multi-Tasking Molecule, Finds a Molecular Target in Killing Cancer Cells.* React Oxyg Species (Apex), 2016. **1**(2): p. 141-156.

265. Meister, A., *Glutathione-ascorbic acid antioxidant system in animals.* J Biol Chem, 1994. **269**(13): p. 9397-400.

266. Franco, R., et al., *The central role of glutathione in the pathophysiology of human diseases.* Arch Physiol Biochem, 2007. **113**(4-5): p. 234-58.

267. Kavdia, M., *Mathematical and computational models of oxidative and nitrosative stress.* Crit Rev Biomed Eng, 2011. **39**(5): p. 461-72.

268. Montecinos, V., et al., *Vitamin C is an essential antioxidant that enhances survival of oxidatively stressed human vascular endothelial cells in the presence of a vast molar excess of glutathione.* J Biol Chem, 2007. **282**(21): p. 15506-15.

269. May, J.M. and Z.C. Qu, *Transport and intracellular accumulation of vitamin C in endothelial cells: relevance to collagen synthesis.* Arch Biochem Biophys, 2005. **434**(1): p. 178-86.

270. Reed, M.C., et al., *A mathematical model of glutathione metabolism.* Theor Biol Med Model, 2008. **5**: p. 8.

271. Berger, M.M. and H.M. Oudemans-van Straaten, *Vitamin C supplementation in the critically ill patient.* Curr Opin Clin Nutr Metab Care, 2015. **18**(2): p. 193-201.

272. Edgar, K.S., et al., *BH4-Mediated Enhancement of Endothelial Nitric Oxide Synthase Activity Reduces Hyperoxia-Induced Endothelial Damage and Preserves Vascular Integrity in the Neonate.* Invest Ophthalmol Vis Sci, 2017. **58**(1): p. 230-241.

273. Solzbach, U., et al., *Vitamin C improves endothelial dysfunction of epicardial coronary arteries in hypertensive patients.* Circulation, 1997. **96**(5): p. 1513-9.

274. Ceriello, A., et al., *Vitamin C further improves the protective effect of glucagon-like peptide-1 on acute hypoglycemia-induced oxidative stress, inflammation, and endothelial dysfunction in type 1 diabetes.* Diabetes Care, 2013. **36**(12): p. 4104-8.

275. El-Aal, A.A., et al., *The effect of vitamin C and/or E supplementations on type 2 diabetic adult males under metformin treatment: A single-blinded randomized controlled clinical trial.* Diabetes Metab Syndr, 2018.

276. Boyacioglu, M., et al., *The protective effects of vitamin C on the DNA damage, antioxidant defenses and aorta histopathology in chronic hyperhomocysteinemia induced rats.* Exp Toxicol Pathol, 2014. **66**(9-10): p. 407-13.

277. Heller, R., et al., *L-Ascorbic acid potentiates nitric oxide synthesis in endothelial cells.* J Biol Chem, 1999. **274**(12): p. 8254-60.

278. Valent, S. and M. Toth, *Spectrophotometric analysis of the protective effect of ascorbate against spontaneous oxidation of tetrahydrobiopterin in aqueous solution: kinetic characteristics and potentiation by catalase of ascorbate action.* Int J Biochem Cell Biol, 2004. **36**(7): p. 1266-80.

279. Vasquez-Vivar, J., et al., *Reaction of tetrahydrobiopterin with superoxide: EPR-kinetic analysis and characterization of the pteridine radical.* Free Radic Biol Med, 2001. **31**(8): p. 975-85.

280. Smith, A.R., F. Visioli, and T.M. Hagen, *Vitamin C matters: increased oxidative stress in cultured human aortic endothelial cells without supplemental ascorbic acid.* FASEB J, 2002. **16**(9): p. 1102-4.

281. Meade, R.D., et al., *Local infusion of ascorbate augments NO-dependent cutaneous vasodilatation during intense exercise in the heat.* J Physiol, 2015. **593**(17): p. 4055-65.

282. Wu, F., et al., *Ascorbate inhibits NADPH oxidase subunit p47phox expression in microvascular endothelial cells.* Free Radic Biol Med, 2007. **42**(1): p. 124-31.

283. Wu, F., J.X. Wilson, and K. Tyml, *Ascorbate inhibits iNOS expression and preserves vasoconstrictor responsiveness in skeletal muscle of septic mice.* Am J Physiol Regul Integr Comp Physiol, 2003. **285**(1): p. R50-6.

284. Kelm, M., et al., *The nitric oxide/superoxide assay. Insights into the biological chemistry of the NO/O-2. interaction.* J Biol Chem, 1997. **272**(15): p. 9922-32.

285. Hink, U., et al., *Mechanisms underlying endothelial dysfunction in diabetes mellitus.* Circ Res, 2001. **88**(2): p. E14-22.

286. Dubois, M., et al., *Biopterin metabolism and eNOS expression during hypoxic pulmonary hypertension in mice.* PLoS One, 2013. **8**(11): p. e82594.

287. Meister, A. and M.E. Anderson, *Glutathione.* Annu Rev Biochem, 1983. **52**: p. 711-60.

288. Reid, M. and F. Jahoor, *Glutathione in disease.* Curr Opin Clin Nutr Metab Care, 2001. **4**(1): p. 65-71.

289. Callegari, A., et al., *Gain and loss of function for glutathione synthesis: impact on advanced atherosclerosis in apolipoprotein E-deficient mice.* Arterioscler Thromb Vasc Biol, 2011. **31**(11): p. 2473-82.

290. Vali, S., et al., *Integrating glutathione metabolism and mitochondrial dysfunction with implications for Parkinson's disease: A dynamic model.* Neuroscience, 2007. **149**(4): p. 917-930.

291. Vaughn, M.W., L. Kuo, and J.C. Liao, *Estimation of nitric oxide production and reaction rates in tissue by use of a mathematical model.* Am J Physiol, 1998. **274**(6 Pt 2): p. H2163-76.

292. Huie, R.E. and S. Padmaja, *The reaction of no with superoxide.* Free Radic Res Commun, 1993. **18**(4): p. 195-9.

293. Fielden, E.M., et al., *Mechanism of action of superoxide dismutase from pulse radiolysis and electron paramagnetic resonance. Evidence that only half the active sites function in catalysis.* Biochem J, 1974. **139**(1): p. 49-60.

294. van der Vliet, A., et al., *Formation of S-nitrosothiols via direct nucleophilic nitrosation of thiols by peroxynitrite with elimination of hydrogen peroxide.* J Biol Chem, 1998. **273**(46): p. 30255-62.

295. Denicola, A., et al., *Peroxynitrite reaction with carbon dioxide/bicarbonate: kinetics and influence on peroxynitrite-mediated oxidations.* Arch Biochem Biophys, 1996. **333**(1): p. 49-58.

296. Antunes, F., A. Salvador, and R.E. Pinto, *PHGPx and phospholipase A2/GPx: comparative importance on the reduction of hydroperoxides in rat liver mitochondria.* Free Radic Biol Med, 1995. **19**(5): p. 669-77.

297. Hogg, N., R.J. Singh, and B. Kalyanaraman, *The role of glutathione in the transport and catabolism of nitric oxide.* FEBS Lett, 1996. **382**(3): p. 223-8.

298. Dicks, A.P., et al., *The reaction of S-nitrosothiols with thiols at high thiol concentration.* Canadian Journal of Chemistry-Revue Canadienne De Chimie, 1998. **76**(6): p. 789-794.

299. Huang, B.K. and H.D. Sikes, *Quantifying intracellular hydrogen peroxide perturbations in terms of concentration.* Redox Biol, 2014. **2**: p. 955-62.

300. Schulz, J.B., et al., *Glutathione, oxidative stress and neurodegeneration.* Eur J Biochem, 2000. **267**(16): p. 4904-11.

301. Lu, S.C., *Glutathione synthesis.* Biochim Biophys Acta, 2013. **1830**(5): p. 3143-53.

302. Singh, S.P., et al., *The chemistry of the S-nitrosoglutathione/glutathione system.* Proc Natl Acad Sci U S A, 1996. **93**(25): p. 14428-33.

303. Sasaki, K., S. Bannai, and N. Makino, *Kinetics of hydrogen peroxide elimination by human umbilical vein endothelial cells in culture.* Biochim Biophys Acta, 1998. **1380**(2): p. 275-88.

304. Jacobson, G.A., K.C. Yee, and C.H. Ng, *Elevated plasma glutathione peroxidase concentration in acute severe asthma: comparison with plasma glutathione peroxidase activity, selenium and malondialdehyde.* Scand J Clin Lab Invest, 2007. **67**(4): p. 423-30.

305. Fu, Y.X., et al., *Knockout of cellular glutathione peroxidase gene renders mice susceptible to diquat-induced oxidative stress.* Free Radical Biology and Medicine, 1999. **27**(5-6): p. 605-611.

306. Beckman, J.S. and W.H. Koppenol, *Nitric oxide, superoxide, and peroxynitrite: The good, the bad, and the ugly.* American Journal of Physiology-Cell Physiology, 1996. **271**(5): p. C1424-C1437.

307. Radi, R., et al., *The biological chemistry of peroxynitrite.* In Ignarro, L.J. (ed.), Nitric Oxide Biology and Pathobiology. Academic Press, San Diego, USA., 2000.

308. Griffith, O.W., *Biologic and pharmacologic regulation of mammalian glutathione synthesis.* Free Radic Biol Med, 1999. **27**(9-10): p. 922-35.

309. Matsui, R., et al., *Glucose-6-phosphate dehydrogenase deficiency decreases vascular superoxide and atherosclerotic lesions in apolipoprotein E(-/-) mice.* Arterioscler Thromb Vasc Biol, 2006. **26**(4): p. 910-6.

310. Leopold, J.A., et al., *Glucose-6-phosphate dehydrogenase overexpression decreases endothelial cell oxidant stress and increases bioavailable nitric oxide.* Arterioscler Thromb Vasc Biol, 2003. **23**(3): p. 411-7.

311. Laurent, M., M. Lepoivre, and J.P. Tenu, *Kinetic modelling of the nitric oxide gradient generated in vitro by adherent cells expressing inducible nitric oxide synthase.* Biochem J, 1996. **314 (Pt 1)**: p. 109-13.

312. Ali, A.A., et al., *The contribution of N(2)O(3) to the cytotoxicity of the nitric oxide donor DETA/NO: an emerging role for S-nitrosylation.* Biosci Rep, 2013. **33**(2).

313. Gobert, A.P., et al., *Mechanism of extracellular thiol nitrosylation by N(2)O(3) produced by activated macrophages.* Nitric Oxide, 1999. **3**(6): p. 467-72.

314. Ito, J.I., et al., *Biochemical properties in membrane of rat astrocytes under oxidative stress.* Brain Res, 2015. **1615**: p. 1-11.

315. Jourd'heuil, D., F.L. Jourd'heuil, and M. Feelisch, *Oxidation and nitrosation of thiols at low micromolar exposure to nitric oxide - Evidence for a free radical mechanism.* Journal of Biological Chemistry, 2003. **278**(18): p. 15720-15726.

316. Berenyiova, A., et al., *The reaction products of sulfide and S-nitrosoglutathione are potent vasorelaxants.* Nitric Oxide, 2015. **46**: p. 123-30.

317.   Hornyak, I., et al., *Current developments in the therapeutic potential of S-nitrosoglutathione, an endogenous NO-donor molecule.* Curr Pharm Biotechnol, 2011. **12**(9): p. 1368-74.

318.   Zeng, H., N.Y. Spencer, and N. Hogg, *Metabolism of S-nitrosoglutathione by endothelial cells.* Am J Physiol Heart Circ Physiol, 2001. **281**(1): p. H432-9.

319.   Broniowska, K.A., A.R. Diers, and N. Hogg, *S-nitrosoglutathione.* Biochim Biophys Acta, 2013. **1830**(5): p. 3173-81.

320.   Madrasi, K., et al., *Glutathiyl radical as an intermediate in glutathione nitrosation.* Free Radic Biol Med, 2012. **53**(10): p. 1968-76.

321.   Shin, H.Y. and S.C. George, *Microscopic modeling of NO and S-nitrosoglutathione kinetics and transport in human airways.* J Appl Physiol (1985), 2001. **90**(3): p. 777-88.

322.   Barglow, K.T., et al., *Site-specific and redox-controlled S-nitrosation of thioredoxin.* Proc Natl Acad Sci U S A, 2011. **108**(35): p. E600-6.

323.   Zhang, Y. and N. Hogg, *The mechanism of transmembrane S-nitrosothiol transport.* Proc Natl Acad Sci U S A, 2004. **101**(21): p. 7891-6.

324.   Vergauwen, B., F. Pauwels, and J.J. Van Beeumen, *Glutathione and catalase provide overlapping defenses for protection against respiration-generated hydrogen peroxide in Haemophilus influenzae.* J Bacteriol, 2003. **185**(18): p. 5555-62.

325.   Pannala, V.R., et al., *A mechanistic mathematical model for the catalytic action of glutathione peroxidase.* Free Radic Res, 2014. **48**(4): p. 487-502.

326.   Makino, N., et al., *Kinetic studies on the removal of extracellular hydrogen peroxide by cultured fibroblasts.* J Biol Chem, 1994. **269**(2): p. 1020-5.

327.   Peskin, A.V., et al., *The high reactivity of peroxiredoxin 2 with H(2)O(2) is not reflected in its reaction with other oxidants and thiol reagents.* J Biol Chem, 2007. **282**(16): p. 11885-92.

328.   Johnson, R.M., et al., *The effects of disruption of genes for peroxiredoxin-2, glutathione peroxidase-1, and catalase on erythrocyte oxidative metabolism.* Free Radic Biol Med, 2010. **48**(4): p. 519-25.

329.   Low, F.M., et al., *Peroxiredoxin 2 functions as a noncatalytic scavenger of low-level hydrogen peroxide in the erythrocyte.* Blood, 2007. **109**(6): p. 2611-7.

330.   de Bem, A.F., et al., *Protective effect of diphenyl diselenide against peroxynitrite-mediated endothelial cell death: a comparison with ebselen.* Nitric Oxide, 2013. **31**: p. 20-30.

331.   Thomas, J.E., et al., *Glucose-6-Phosphate Dehydrogenase Deficiency is Associated with Cardiovascular Disease in U.S. Military Centers.* Tex Heart Inst J, 2018. **45**(3): p. 144-150.

332.   Hecker, P.A., et al., *Glucose 6-phosphate dehydrogenase deficiency increases redox stress and moderately accelerates the development of heart failure.* Circ Heart Fail, 2013. **6**(1): p. 118-26.

333. Zhang, Z., et al., *Increasing glucose 6-phosphate dehydrogenase activity restores redox balance in vascular endothelial cells exposed to high glucose.* PLoS One, 2012. **7**(11): p. e49128.

334. Gupte, R.S., et al., *Upregulation of glucose-6-phosphate dehydrogenase and NAD(P)H oxidase activity increases oxidative stress in failing human heart.* J Card Fail, 2007. **13**(6): p. 497-506.

335. Han, D., et al., *Mechanisms of liver injury. III. Role of glutathione redox status in liver injury.* Am J Physiol Gastrointest Liver Physiol, 2006. **291**(1): p. G1-7.

336. Daiber, A., et al., *New Therapeutic Implications of Endothelial Nitric Oxide Synthase (eNOS) Function/Dysfunction in Cardiovascular Disease.* Int J Mol Sci, 2019. **20**(1).

337. Fraccarollo, D., et al., *Improvement in left ventricular remodeling by the endothelial nitric oxide synthase enhancer AVE9488 after experimental myocardial infarction.* Circulation, 2008. **118**(8): p. 818-27.

338. Miao, Y., et al., *Enhancer-associated long non-coding RNA LEENE regulates endothelial nitric oxide synthase and endothelial function.* Nat Commun, 2018. **9**(1): p. 292.

339. Amaro, S., F. Jimenez-Altayo, and A. Chamorro, *Uric acid therapy for vasculoprotection in acute ischemic stroke.* Brain Circ, 2019. **5**(2): p. 55-61.

340. Salvemini, D. and S. Cuzzocrea, *Therapeutic potential of superoxide dismutase mimetics as therapeutic agents in critical care medicine.* Crit Care Med, 2003. **31**(1 Suppl): p. S29-38.

341. Bonetta, R., *Potential Therapeutic Applications of MnSODs and SOD-Mimetics.* Chemistry, 2018. **24**(20): p. 5032-5041.

342. Bhowmick, D., et al., *Highly Efficient Glutathione Peroxidase and Peroxiredoxin Mimetics Protect Mammalian Cells against Oxidative Damage.* Angew Chem Int Ed Engl, 2015. **54**(29): p. 8449-53.

343. Lim, J.B., et al., *A reaction-diffusion model of cytosolic hydrogen peroxide.* Free Radic Biol Med, 2016. **90**: p. 85-90.

344. Carballal, S., S. Bartesaghi, and R. Radi, *Kinetic and mechanistic considerations to assess the biological fate of peroxynitrite.* Biochim Biophys Acta, 2014. **1840**(2): p. 768-80.

345. Manta, B., et al., *The peroxidase and peroxynitrite reductase activity of human erythrocyte peroxiredoxin 2.* Arch Biochem Biophys, 2009. **484**(2): p. 146-54.

346. Allerton, T.D., et al., *l-Citrulline Supplementation: Impact on Cardiometabolic Health.* Nutrients, 2018. **10**(7).

ABSTRACT

COMPUTATIONAL ANALYSIS OF OXIDATIVE STRESS MEDIATED ENDOTHELIAL DYSFUNCTION: INSIGHTS ON THE ROLE OF TETRAHYDROBIOPTERIN, ASCORBATE AND GLUTATHIONE

by

SHEETAL KEDAR PANDAY

May 2020

Advisor: Dr. Mahendra Kavdia

Major: Biomedical Engineering

Degree: Doctor of Philosophy

Oxidative stress and endothelial dysfunction are reported in the cardiovascular and neurovascular diseases. Oxidative stress is caused due to an increase in the generation of reactive oxygen (ROS) and nitrogen species (RNS) and incapacity of antioxidant systems to eliminate ROS and RNS. Endothelial dysfunction is characterized by a reduction in nitric oxide (NO) bioavailability. NO is constitutively produced by enzyme endothelial nitric oxide synthase (eNOS). A reduction in tetrahydrobiopterin (BH_4), which is an essential cofactor of eNOS, can lead to eNOS uncoupling. There is complex interplay between the ROS/RNS and antioxidant system underlying pathophysiologies of vascular diseases, however our quantitative understanding of the oxidative stress and these biochemical species in endothelial cell is not complete. The overall objective of this dissertation is to investigate mechanistically the complex interactions of eNOS uncoupling, cellular oxidative stress, BH_4 bioavailability and antioxidant levels in endothelial cells. We developed a series of mathematical models for eNOS biochemical pathway and downstream reactions involving interactions of ROS/RNS with antioxidant systems. Using these models, we investigated the effects of BH_4 synthesis, ascorbate (ASC) and glutathione (GSH) on

cellular ROS and RNS. Our model results showed that variations in the generation rates of superoxide ($O_2^{\bullet-}$) and NO produces a wide range of outcomes for ROS/RNS levels that determines the cellular levels of oxidative stress. Variation in endothelial cell oxidative stress levels increases the extent of eNOS uncoupling and introduces instabilities in the eNOS based NO/ $O_2^{\bullet-}$ production rate. ASC supplementation removed these instabilities and resulted in improved NO and BH_4 bioavailability. Enhancement of BH_4 synthesis also showed improvement in eNOS uncoupling and NO production rate. ASC supplementation also resulted in increasing RNS level such as peroxynitrite ($ONOO^-$). The GSH and glutathione peroxidase (GPX) kept in check the levels of ROS/RNS including $ONOO^-$ and hydrogen peroxide (H_2O_2) and resulted in decreasing cellular oxidative stress. Collectively, these models provide qualitative information about ROS/RNS levels in endothelial dysfunction. In addition, the therapeutic potential of cofactors, substrates and antioxidants can be analyzed using these models for effective treatments as well as earlier intervention in treating cardiovascular and neurovascular diseases.

AUTOBIOGRAPHICAL STATEMENT

Sheetal Kedar Panday came to the US in 2014 from India to pursue doctoral studies in Biomedical Engineering at Wayne State University. She was admitted at WSU with her maiden name as **Sheetal Srikant Joshi**, which she changed to her current married name in August 2018.

EDUCATION

PhD, Biomedical Engineering, Wayne State University, Detroit, MI. USA	2014 – 2019
Masters in Biochemical Engineering, Shivaji University, India	2012
Bachelors in Biochemical Engineering, Shivaji University, India	2006

ACADEMIC AND PROFESSIONAL EXPERIENCE

Graduate Teaching Assistant, Basic Engineering, Wayne State University	2017 – 2018
Graduate Teaching Assistant, BME Design Labs, Wayne State University	2014 – 2016
Assistant Manager, Sales and Support at KNF German multinational, Pune, India	2010 – 2012
Project trainee, TATA Chemical Limited, Innovation Centre, Pune, India	2009 – 2010
Executive Business Development, Distributor for Accelrys, Inc, Pune, India	2007 – 2009

PEER – REVIEWED PUBLICATION

Joshi, S., S. Kar, and M. Kavdia, Computational analysis of interactions of oxidative stress and tetrahydro-biopterin reveals instability in eNOS coupling. Microvasc Res, 2017. 114: p. 114-128.

HONORS AND MERITS

Outstanding Graduate Teaching Assistant Award, BME, WSU	2016
Graduate Student Professional Travel Award (GSPTA), WSU – 4 awards	2014 – 2018
Cardiovascular Research Institute (CVRI) Travel Award, WSU – 2 awards	2014 and 2018
Availed cash award of INR 100,000 for qualifying highly competitive entrance exam in Engineering (GATE), India	2010